



Mag. Thomas Stoisser, Bakk. rer. nat.

L-LACTATE OXIDASE
The Effects and Interpretation of LOX Mutants from *Aerococcus viridans*

DISSERTATION

zur Erlangung des akademischen Grades

Doktor der Naturwissenschaften

eingereicht an der

Technischen Universität Graz

Betreuer

Univ.-Prof. Dipl.-Ing. Dr.techn. Bernd Nidetzky

Institut für Biotechnologie und Bioprozesstechnik

EIDESSTATTLICHE ERKLÄRUNG

AFFIDAVIT

Ich erkläre an Eides statt, dass ich die vorliegende Arbeit selbstständig verfasst, andere als die angegebenen Quellen/Hilfsmittel nicht benutzt, und die den benutzten Quellen wörtlich und inhaltlich entnommenen Stellen als solche kenntlich gemacht habe. Das in TUGRAZonline hochgeladene Textdokument ist mit der vorliegenden Dissertation identisch.

I declare that I have authored this thesis independently, that I have not used other than the declared sources/resources, and that I have explicitly indicated all material which has been quoted either literally or by content from the sources used. The text document uploaded to TUGRAZonline is identical to the present doctoral dissertation.

Datum / Date

Unterschrift / Signature

SUMMARY

This PhD thesis mainly deals with the flavoprotein L-lactate oxidase (LOX), an enzyme, which converts L-lactate into pyruvate and H_2O_2 when molecular oxygen is present. It possesses a cofactor named flavin mononucleotide (FMN), which is essential for the redox reaction. The reaction is divided into two half-reactions, the reductive half-reaction, where FMN is reduced, pyruvate is produced and released from the active site, and the oxidative half-reaction, where the cofactor is re-oxidized by O_2 , and H_2O_2 is produced as by-product. The reaction is also called ping-pong-mechanism. Further, FMN is responsible for the yellow appearance of the enzyme and a 2 electron transfer – so it can either be reduced or oxidized - the (re-)oxidized enzyme shows two absorbance maxima (373 nm and 455 nm), whereas the reduced form lacks both peaks; such a change from an oxidized into an reduced enzyme can thereof be followed in an stopped flow experiment.

Within this thesis various mutation studies have been performed. The generated active site mutants were tested with either an oxygen consumption measurement or an enzyme (peroxidase) coupled assay. Further, the mutants were generated by a PCR strategy and all proteins harvested from *E. coli* cells were purified in the same manner with a FPLC system (see mutation protocol, growing conditions and purification protocol in Unterweger *et al.*). We also considered the possibility of alternated substrate specificity and thereof tested a set of various substrates for all mutants. Besides the primary substrates, we wanted to examine alternative electron acceptors other than O_2 . To test alternative electron acceptors, we chose a so called DCIP-assay. DCIP, several quinones and the usual acceptor O_2 were also used to investigate the oxidative half-reaction of the LOX mutants. We yielded steady state data of LOX variants and consequently tested differences

between the oxidative and reductive half-reaction in pre-steady state experiments (also known as stopped flow analysis). Further, we wanted to shed light onto the reaction mechanism of LOX. Utilizing pre-steady state results of the reductive half-reaction and Berkeley Madonna software, we could demonstrate a mechanism for each single mutant, which was described in previous publications. For three single mutants we were also able to solve the crystal structure and induced new insights into the active site of these variants in terms of substrate binding and catalysis.

ZUSAMMENFASSUNG

Diese Doktorarbeit beschäftigt sich mit dem Flavoprotein L-Laktat Oxidase (abgekürzt LOX), einem Enzym, welches Laktat (Milchsäure) in Pyruvat und H_2O_2 (Wasserstoffperoxid) umwandelt wenn Sauerstoff vorhanden ist. Das Enzym besitzt als Co-Faktor FMN (Flavomononukleotid) welches essentiell für die Redoxreaktion ist. Die Reaktion selbst ist in zwei Halbreaktionen aufgeteilt, zum einen gibt es die reduktive Halbreaktion, in welcher FMN und somit das Enzym reduziert wird und wo Pyruvat gebildet und vom aktiven Zentrum des Proteins wieder entlassen wird. Auf der anderen Seite gibt es die oxidative Halbreaktion, in welcher der Co-Faktor wieder re-oxidiert wird durch O_2 - Wasserstoffperoxid entsteht dabei als Nebenprodukt. Man nennt diese Reaktion auch Ping-Pong-Mechanismus. FMN ist auch für die gelbe Farbe des Enzyms und für den 2-Elektronentransfer verantwortlich, es kann also entweder in reduzierter oder oxidiert Form vorliegen, wobei die (re-)oxidierte Form zwei Absorptionsmaxima (bei 373 und 455 nm) im sichtbaren Licht aufweist, während hingegen die reduzierte Form keines dieser beiden Peaks zeigt. Ein Wechsel von oxidiertem zu reduziertem Enzym kann deshalb in sogenannten Stopped Flow Experimenten verfolgt werden und dieser Umstand stellte einen wesentlichen Bestandteil für die Erkenntnisse dieser Doktorarbeit bereit.

In der vorliegenden Dissertation wurden mehrere Punktmutationen im aktiven Zentrum auf genetischer Ebene durchgeführt. Diese generierten Mutanten wurden mit einer Sauerstoffsverbrauchsmessung und einem gekoppelten enzymatischen (Peroxidase-)Test auf ihre Aktivität mit diversen Substraten inklusive dem Hauptsubstrat Laktat getestet. Alle Mutanten wurden mit einem speziellen PCR-Verfahren generiert. Die Proteine wurden in *Escherichia coli* Zellen exprimiert und die Enzyme wurden alle auf dieselbe Weise mit einem FPLC-System gereinigt. Da es

nicht ausgeschlossen war, dass die generierten Enzyme auch mit anderen Substraten reagieren, wurden sämtliche Mutanten auf mehrere unterschiedliche Hydroxy-Säuren getestet. Zusätzlich zu Sauerstoff wurden noch weitere künstliche Elektronenakzeptoren benutzt, um den Einfluss der Mutation zu analysieren. Für die Untersuchung wurde ein sogenannter DCIP-Assay verwendet. Zu den gewählten Akzeptoren zählten neben DCIP auch unterschiedliche Quinone, die allesamt 2 Elektronen aufnehmen können, und mit welchen in Abwesenheit von O₂ die oxidative Halbreaktion des Enzyms erforscht wurde. Für die LOX-Varianten wurden ‚Steady-State‘-Daten ermittelt und Unterschiede zwischen der oxidativen und reduktiven Halbreaktion in ‚Pre-Steady-State‘-Experimenten (auch bekannt als Stopped-Flow-Analyse) beobachtet. Ein Ziel war es, den Reaktionsmechanismus dieses Enzyms aufzuklären. Mittels der vorhandenen ‚Pre-Steady-State‘-Resultaten der reduktiven Halbreaktion sowie der Simulationssoftware Berkeley Madonna konnte ein Mechanismus für jede einzelne LOX-Mutante demonstriert werden, der bereits in früheren Veröffentlichungen diskutiert worden ist. Des Weiteren konnte die Kristallstruktur von 3 beschriebenen Enzymvarianten gelöst werden, ein nützliches Tool, welches in Hinsicht auf Substratbindung und Substratumsetzung neue Einblicke und Erkenntnisse über das aktive Zentrum gewährleistet.

DANKSAGUNG

Normalerweise würde man vermuten, dass man die Danksagung erst am Ende schreibt, wenn die Einreichung der Doktorarbeit kurz bevorsteht, bei mir ist das ein wenig anders. Als Dissertant erlebt man einige Höhen und Tiefen, vor allem, wenn manchmal nicht alles nach Plan läuft, weiß man, dass es immer wieder Menschen in seinem Leben gibt, die einem den nötigen Halt geben, weiter zu machen und gute Arbeit zu leisten. Iris, Petra und Vid, ihr seid oft eine große Hilfe gewesen, danke dafür. In den letzten Jahren habe ich neue Freunde gewonnen, die mir stets zur Seite standen, die meisten davon waren in meinem Büro - Johanna, Kathi, Mareike, Patricia, Sarah, Alex, Ulrich - danke, dass wir gemeinsam eine tolle Zeit verbringen durften als Dissertanten. Gefreut habe ich mich über 4 Diplomandinnen (Dani und Dani, Stephi und Birgit), die in meinem Projekt waren, ich hoffe auch ihr hattet eine schöne Zeit. Besonderer Dank gilt Dr. Stephan Leitgeb, der in diesem Projekt viel bewegt hat und mich vor allem am Anfang und am Ende (natürlich auch während des Projekts) viel unterstützt hat. Außerordentlicher Dank gebührt meinem Betreuer, Prof. Bernd Nidetzky, der mit seinem Fachwissen und seiner Beratung mir bei dieser Arbeit immens weitergeholfen hat und ich behaupte, dass diese Dissertation gerade deshalb eine besondere Qualität aufweist. Doch es sind 2 Menschen, bei denen ich mich gar nicht oft genug bedanken kann. Meine Eltern waren die letzten Jahre meine wohl größte mentale Unterstützung, denn ich weiß, dass ich mich immer auf sie verlassen kann - danke, dass es euch gibt und ihr immer an mich geglaubt habt!

Tausend Dank!!!

CONTENTS

1	Structure and function of the α -hydroxy acid oxidase family.....	10
2	Engineering of <i>Aerococcus viridans</i> L-lactate oxidase for site-specific PEGYLATION: characterization and chemical modification of a S218C mutant.....	58
3	Probing the substrate specificity of L-lactate oxidase from <i>Aerococcus viridans</i> : analysis with different electron acceptors and crystallographic study of A95G mutant at 1.65 Angstrom resolution.....	77
4	Characterization of <i>Aerococcus viridans</i> L-lactate oxidase Y215F and Y215H mutants.....	135
5	Clarifying the influence of a hydrogen bond network on the substrate binding in the active site of <i>Aerococcus viridans</i> L-lactate oxidase by substitution of residue Tyr 191.....	183
6	Appendix.....	225

1 Structure and function of the α -hydroxy acid oxidase family

Stefan Leitgeb †, Thomas Stoisser †, Bernd Nidetzky *†

† Research Center Pharmaceutical Engineering, and Institute of Biotechnology and Biochemical Engineering, Graz University of Technology, Petersgasse 12, A-8010 Graz, Austria

* Corresponding author

Institute of Biotechnology and Biochemical Engineering, Graz University of Technology, Petersgasse 12/1, A-8010 Graz

Phone: +43-316-873-8400; Fax: +43-316-873-8434

Email: bernd.nidetzky@tugraz.at

ABBREVIATIONS

ChDH: choline dehydrogenase, DAO: D-amino acid oxidase, DCIP: 2,6 dichloroindophenol, FCB2: flavocytochrome b_2 , FMN: flavomononucleotide, GIDH: glucose dehydrogenase, GIOX: glucose oxidase, GOX: glycolate oxidase, LCHAO: long chain hydroxy acid oxidase, LMO: L-lactate monooxygenase, LOX: L-lactate oxidase, MDH: L-mandelate dehydrogenase, PDB: protein database, WT: wild-type

ABSTRACT

This review provides an overview of the L-lactate oxidase (LOX) belonging to α -hydroxy acid oxidizing family, which catalyze a variety of different reactions. The reviewed flavoproteins are biotechnologically very useful and interesting enzymes due to their applications as biocatalysts and contributors in biosensors. Survey of 3D structures pointed out that the hydroxy acid oxidases share a lot of common features in terms of their substrate binding site and catalysis, but also indicate a large variety of folding topologies. Many active site residues are highly conserved within the family and therefore lead to a similar first half-reaction in catalysis, where the flavin cofactor is reduced. In terms of the oxidative half-reaction, where the cofactor is re-oxidized, there are distinctions: still, the reactivity towards oxygen remains an unsolved problem, because oxidases, monooxygenases and dehydrogenases react differently with O_2 , although they have similar substrate binding pockets. For so far, no structural rules exist that might explain, if a flavoenzyme is able to react with oxygen or not. On the other hand, some of the reviewed flavoenzymes turned out to react with alternative electron acceptors.

1. INTRODUCTION

History

The first investigations of lactate conversion by α -hydroxy acid oxidases date back to the late 1940s (1). Back then, the oxidation of lactate by acetone-extracts of crushed cells from *Mycobacterium phlei* was followed by oxygen consumption

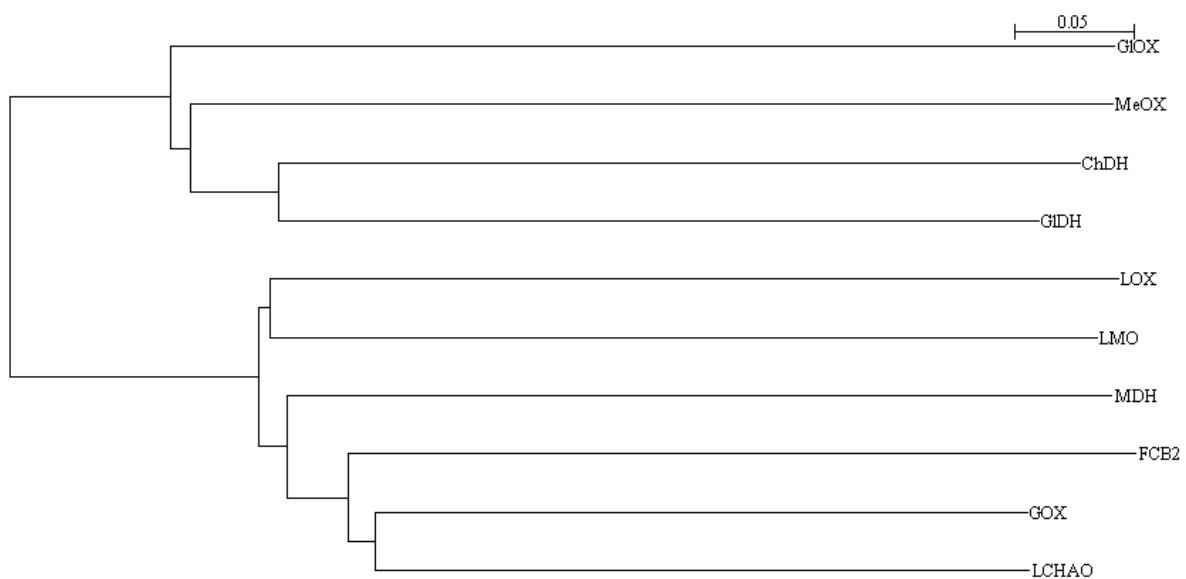
measurements. It was already described that the extracted enzyme was specific for L-lactate as substrate, but did not convert D-lactate (1). The interest in this enzyme class lasted for decades. Starting in the 70s, thorough mechanistic studies were done with the main focus on lactate monooxygenase (formerly called lactate oxidase) from *Mycobacterium smegmatis* (2-6) and flavocytochrome b_2 (7). Nowadays, e.g. lactate oxidase from *Aerococcus viridans* is still a prominent enzyme being used in lactate biosensors (8-10).

Definition and family members

Members of the family of α -hydroxy acid oxidizing enzymes are able to convert 2-hydroxy acids with varying chain lengths from C=2 (glycolate) to C=16 (2-hydroxypalmitate). The enzymes all contain FMN as redox-active co-substrate. The reaction mechanism is similar for all family members with a reductive half-reaction, where the substrate is initially oxidized with the FMN being reduced. After product release, the co-substrate is re-oxidized again by either a simple electron transfer to oxygen (oxidases, oxygenases) or a more complex electron transfer to an external electron acceptor (dehydrogenases). Enzymes, using molecular oxygen as acceptor, follow a common reaction scheme of a ping-pong mechanism (11). The family of FMN-dependent α -hydroxy acid oxidizing enzymes consists only of a small group of proteins; nevertheless, they have important practical use. So far, 6 distinct members have been characterized: lactate monooxygenase (LMO; EC 1.13.12.4), flavocytochrome b_2 (FCB2; L-lactate dehydrogenase, EC 1.1.2.3), L-mandelate dehydrogenase (MDH; EC 1.1.99.31) are classified as individual enzyme families, while lactate oxidase (LOX), glycolate oxidase (GOX) and long chain α -hydroxy acid oxidase (LCHAO) are classified under EC 1.1.3.15. The classification has been changed recently, and LOX was managed under the same EC number as LMO,

despite having a different product spectrum. Older literature can be confusing, using the expression lactate oxidase for both the oxidase and monooxygenase.

A comparison of the members of α -hydroxy acid oxidizing enzymes with members of the GMC oxidoreductases superfamily (**12**) shows the different clustering of the families. The latter family includes glucose oxidase (GLOX), methanol oxidase (MeOX), choline dehydrogenase (ChDH) or glucose dehydrogenase (GIDH).



For a better overview of this family we do want to introduce you the members in short

Long-chain α -hydroxy acid oxidase

The peroxisomal long-chain α -hydroxy acid oxidase (LCHAO, EC 1.1.3.15, isozyme B) is classified as isoenzyme of glycolate oxidase. The structure of the tetrameric enzyme has been solved recently. While the reductive half-reaction is believed to be identical in all enzymes of this family, there are differences in the

oxidative half-reaction. LCHAO is re-oxidized in a 2-electron step using molecular oxygen as electron acceptor. The cDNA was originally cloned from rat kidney, and 2 different variants were identified with a difference of 3 base pairs with the shorter variant forming 90% of rat kidney proteins (**13, 14**). Up to now the physiological substrate for LCHAO is not known, the highest activity could be obtained with L-mandelate. However, its efficiency decreases together with the substrate chain length for substrates L-2-hydroxyisocaproate, L-phenyllactate and DL-2-hydroxy-4-methylthiobutanoate (**13**). Despite reacting with some other substrates (**15-17**), LCHAO even catalyzes the conversion of creatol, which is not a 2-hydroxy carboxylic acid to methylguanidine (**18, 19**).

Glycolate oxidase

The best characterized glycolate oxidase (GOX, EC 1.1.3.15, isozyme A) is the one from spinach (**20-24**). The enzyme also occurs in plants, animals and mammals, with the human liver glycolate oxidase as most prominent enzyme (**25**). The native substrate for GOX is glycolate, the shortest possible 2-hydroxy acid, which is converted into glyoxylate. The latter one is itself a substrate for the enzyme and is further metabolized to yield oxalate with ~250-fold weaker catalytic efficiency (**25**). However, oxalate is a strong inhibitor of GOX (**20**).

Mandelate dehydrogenase

(S)-Mandelate dehydrogenase (EC 1.1.99.31) catalyzes the conversion of (S)-mandelate to benzoylformate in the metabolic pathway of mandelate in *Pseudomonas putida*. The enzyme differs from other members of the family of α -hydroxy acid oxidases, as the ultimate electron acceptor in the oxidative half-reaction is not molecular oxygen. Since it is a membrane-associated enzyme, the electrons

are transferred from the reduced flavin to a component of the electron transfer chain. The reductive half-reaction, however, is proposed to share the same mechanism as the other members of the family (26, 27).

Flavocytochrome b_2

FCB2 (also known as L-lactate dehydrogenase, EC 1.1.2.3) from *Saccharomyces cerevisiae* has been the most studied member of this family. Each subunit contains one FMN and a heme b_2 cofactor. The enzyme catalyzes the oxidation of L-lactate to pyruvate at the expense of cytochrome *c* in the yeast mitochondrial intermembrane space (28). FMN is reduced by the substrate in a two-electron reaction; then, the prosthetic group reduces heme b_2 in two successive one-electron transfer steps and in turn heme b_2 reduces cytochrome *c*. Besides L-lactate, FCB is able to utilize several other L-2-hydroxy acids, and mutagenesis studies could increase the substrate selectivity for substrates, such as L-mandelate or 2-hydroxyoctanoate (29). FCB2 has successfully been tested with artificial electron acceptors like ferricyanide or 2,6-dichloroindophenol (DCIP) (30.). Known inhibitors of the enzyme are sulfite, D-lactate, propionate and L-lactate and oxalate at high concentrations (30-32).

Activities

The enzymes of this family act on the hydroxyl-groups of α -hydroxy acids and accept substrates of different sizes and chain lengths. LOX and LMO both catalyze the oxidative cleavage of L-lactate, however, their reaction products differ. The reaction with LOX provides the products pyruvate and H_2O_2 , whilst the LMO-catalysed reaction yields acetate, CO_2 and H_2O . The reaction pathways are identical

in the initial phase, but split up on the level of an intermediate (*vide infra*) **(11)**. GOX catalyzes the oxidation of glycolate to glyoxylate **(20)**, whilst LCHAO oxidizes long-chain α -hydroxy acid substrates to the corresponding keto-acids **(33)**. FCB2 catalyzes the oxidation of L-lactate to pyruvate with intramolecular electron transfer from the flavin group to heme b_2 followed by the reduction of cytochrome c **(34)**. The last member of the family, membrane-bound MDH, uses ubiquinone of an electron transport chain in the membrane as physiological electron acceptor for the oxidation of (S)-mandelate to benzoylformate **(35, 36)**.

α -Hydroxy acid oxidases catalyze the conversion of 2-hydroxy acids to 2-keto acids. In the reductive half-reaction, two electrons of the substrate are transferred to the flavin to reduce it to its semiquinone form. Concomitantly, the α -hydroxy acid is oxidized to the respective keto-acid and released from the enzyme. In the oxidative half-reaction, the semiquinone is re-oxidized to the flavin. The electron acceptor for this step is either molecular oxygen, a heme group or an external group from the respiratory chain.

Structure

With the exception of LMO, all members of the family have been structurally characterized. They all share a common structure of 8 α -helices and 8 β -sheets in a $(\beta/\alpha)_8$ -barrel arrangement with alternating β -sheets and α -helices. The inner core is formed by the β -sheets (**Figure 2**). The quaternary structures of LOX **(37)**, FCB2 **(38)**, GOX **(39)**, LCHAO **(40)** and MDH **(41)** are tetramers.

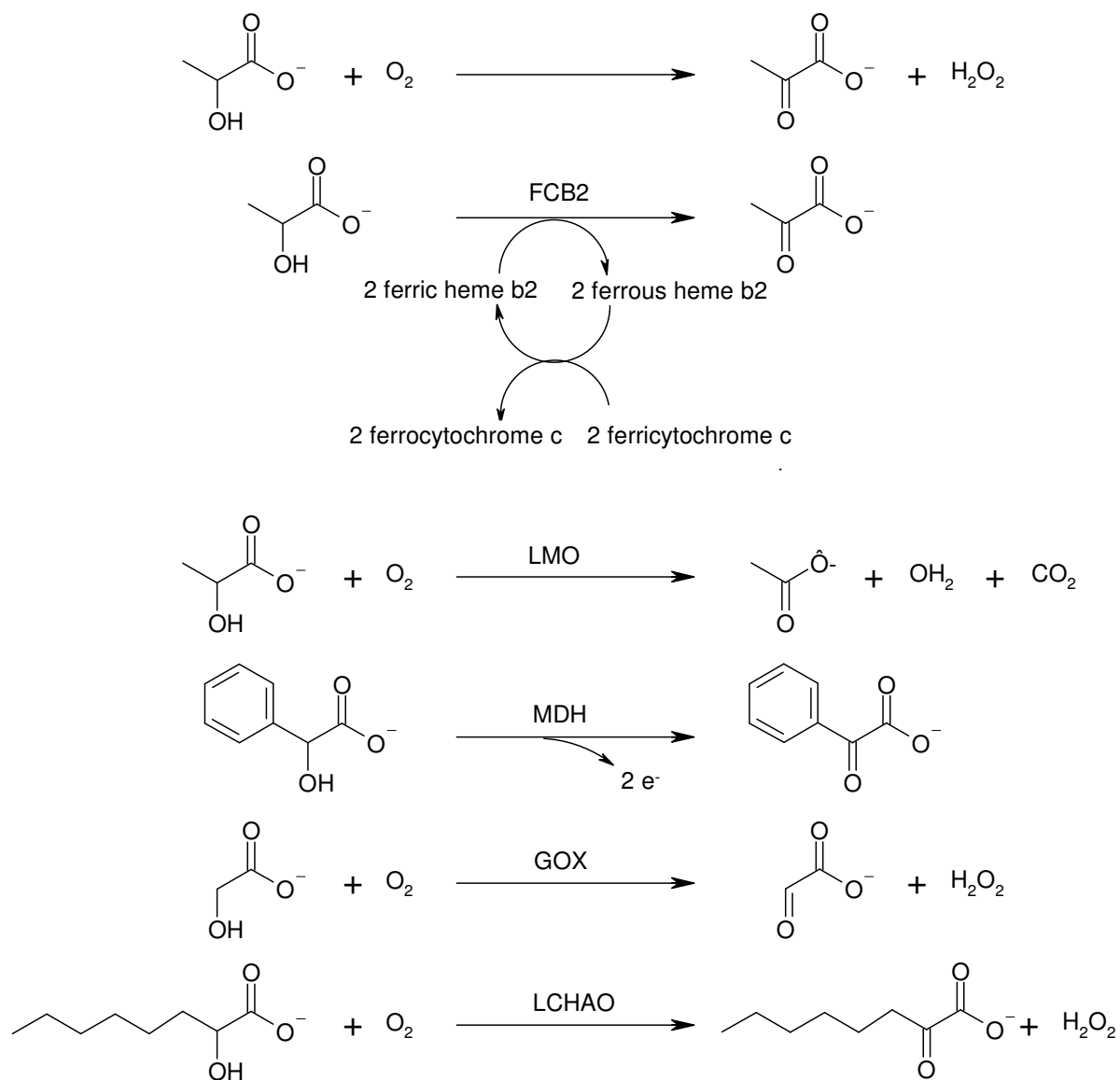


Figure 1

Reactions catalyzed by members of the α -hydroxy acid oxidizing enzymes

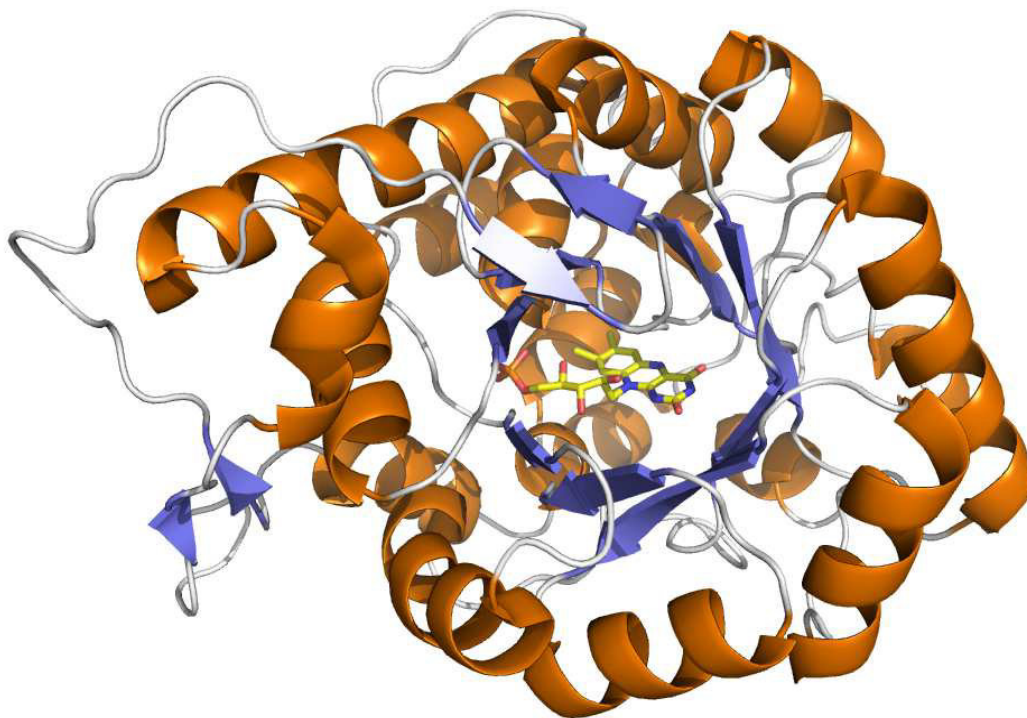


Figure 2

Monomer-structure of LOX (PDB 2DU2). FMN is shown in yellow.

Each subunit contains 1 FMN prosthetic group that is located close to the C-terminus. The FMN cofactor is bound in the inner core and essential for the reactivity.

Scope

The interest in the enzymes of this family is mainly focused on two applications. The first one is the use of LOX in biosensors for the surveillance of lactate in the blood of intensive care patients. Lactate biosensors were first used in the middle of the 80s in the last century and are still developed further for better and more robust performance **(9, 40)**. LOX is also used in test strips for lactate monitoring. The strip consists of the enzyme and a redox mediator that reversibly accepts electrons from lactate and transfers it to the working electrode. The current between working and reference electrode is measured amperometrically **(41)**.

The second application of α -hydroxy acid oxidases is their use as biocatalysts. These reactions make complex 2-ketoacids available in a cheap and alternative route compared to classical chemical synthesis. Racemic mixtures can be separated by the highly specific enzymes (**42**, **43**). These enzymes offer large flexibility in terms of substrate acceptance and can be used for the production of a broad range of compounds.

Residue numbers in this review are for L-lactate oxidase (LOX), if not indicated differently.

2. STRUCTURE

Overall

The crystal structures of five out of the six enzymes are available in the Protein Data Bank. All members share a common fold with a $(\beta/\alpha)_8$ -barrel core with the FMN being bound close to the C-terminus. The quaternary structures of LOX (**37**), FCB2 (**38**), GOX (**13**), LCHAO (**33**) and MDH (**39**) are tetramers. Overlaying the monomers of all proteins to subunit A of LOX leads to r.m.s.d. values between 0.959 and 1.474 (**Figure 3**). The core of the proteins is virtually identical, differences occur in the outer regions; especially FCB2 shows an extended C-terminus and an N-terminal cytochrome *c* domain. The small N-terminal domain contains protoheme IX and consists of residues 1-99 while the flavin-binding domain spans from residue 100 to 486 with a C-terminal tail from residues 487-511. The cytochrome domain consists of 6 β -sheets with 5 of them being ordered parallel. Adjacent is a single helix at the one side and 2 pairs of antiparallel helices on the other side forming the heme

binding pocket. The structure of the cytochrome domain resembles cytochrome b_2 (38).

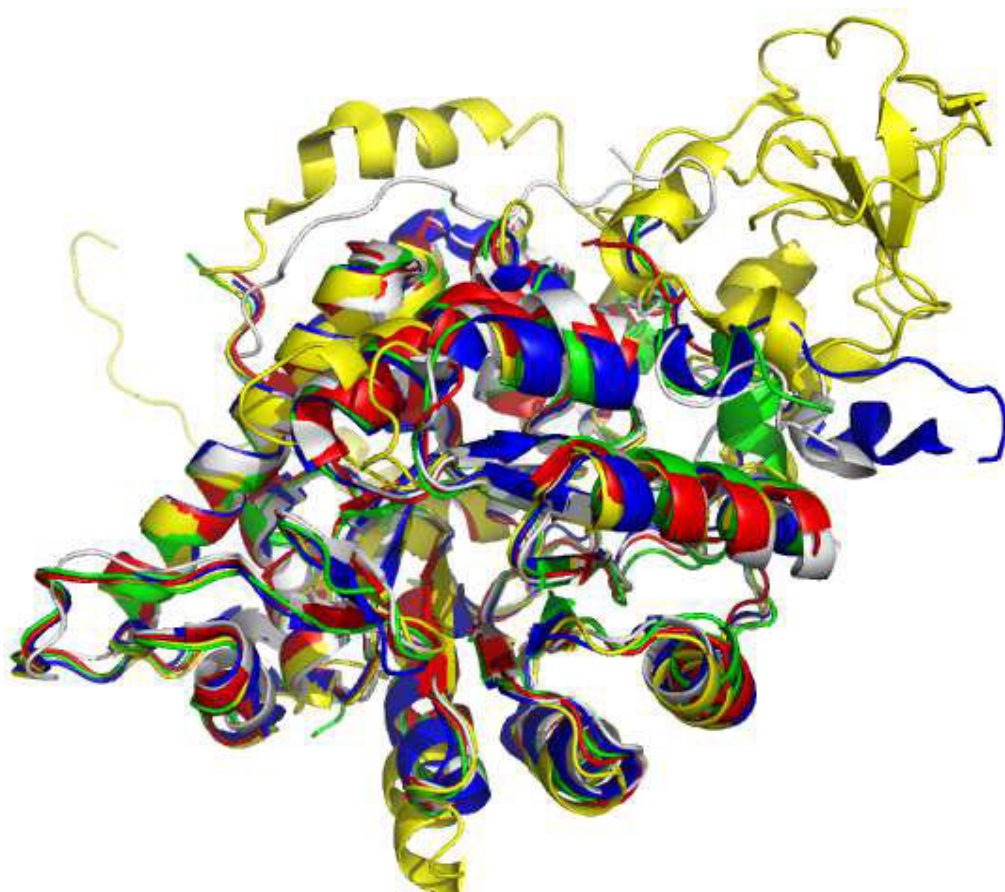


Figure 3

Overlay of the structures of LOX (white), FCB2 (yellow), GOX (green), MDH (red) and LCHAO (blue)

FMN binding site

The FMN is located towards the C-terminus of the proteins, and its binding pocket is defined by well-conserved residues (LOX numbering: Arg-320, Arg-300, Asp-296, Ser-263, Thr-172, Gln-144, Ser-122) and is shown in **Figure 4**. The FMN phosphate group is tightly fixed in position by 2 salt bridges to the guanidinium group of Arg-300, and a strong interaction each to the backbone and functional group of Arg-320. Lys-241, which is proposed to stabilize the anionic form of the semiquinone,

forms direct interactions with O(2) and O(2') of the flavin (**44**). The O(3') directly interacts with the side chains of Asp-296 and Ser-263. The O(2) and O(4) are additionally bound to Thr-172 and Ser-122 by strong hydrogen bonds, respectively. Gln-144 and Tyr-146, which has been proposed to stabilize the transition state (vide supra), are in direct contact with the flavin N(3) (**45**).

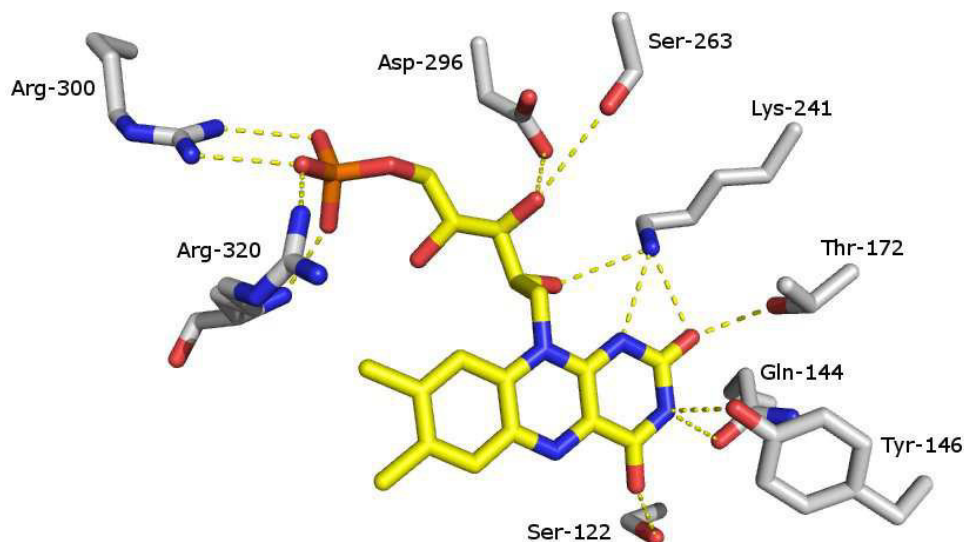


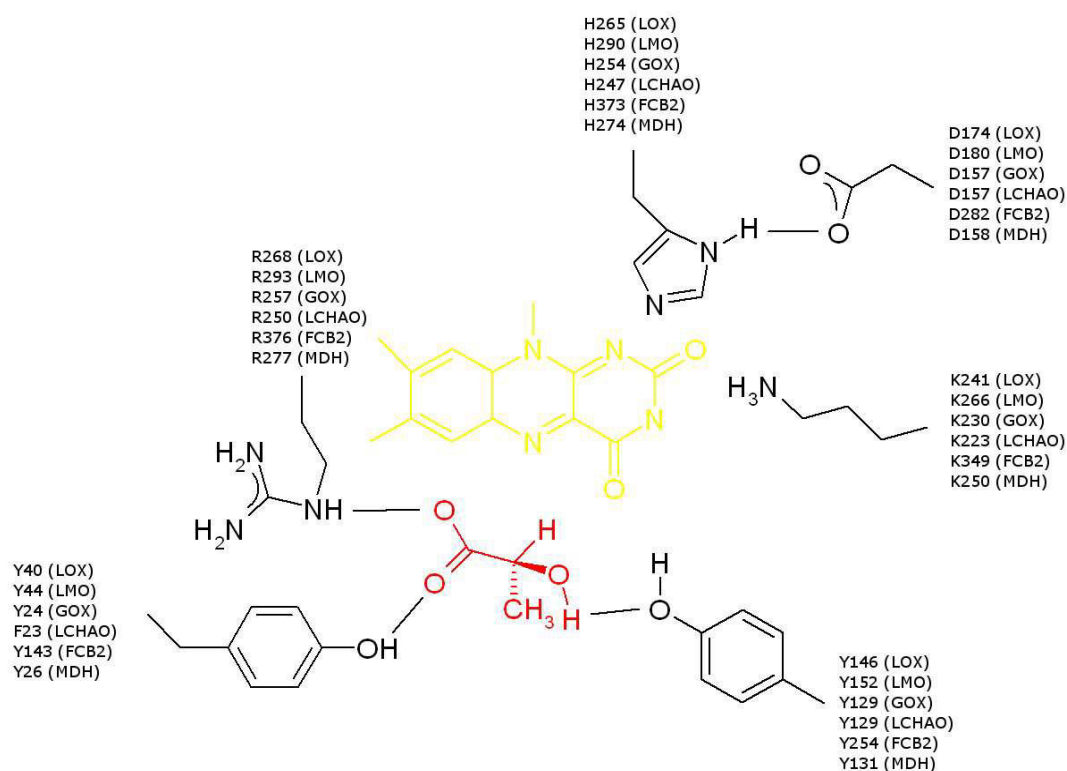
Figure 4

FMN binding site in LOX

In GIOX from *Aspergillus niger*, a member of the GMC superfamily, FAD is used as cofactor. The binding there is governed by the nucleotide binding $\beta\alpha\beta$ -motif attaching the ribose and pyrophosphate group (**46**). The flavin group itself is rigidly fixed between loops rather close to the N-terminus, and the start of the C-terminal helix (**47**). FAD binding is similar in D-amino acid oxidase (DAO) that also adopts the $\beta\alpha\beta$ -motif compensating for the negative charge of the ribityl phosphate group. The flavin group is held in place by several interactions with the protein and is buried in the protein (**48**).

Catalytic site

The active site of all members of this family is strictly conserved and is shown in **Scheme 1** and **Figure 5**. The only difference in these enzymes is the replacement of Tyr-40, which is binding the carboxyl function on the substrate, by a phenylalanine in LCHAO.



Scheme 1: Conserved residues in the active site of α -hydroxy acid oxidases.

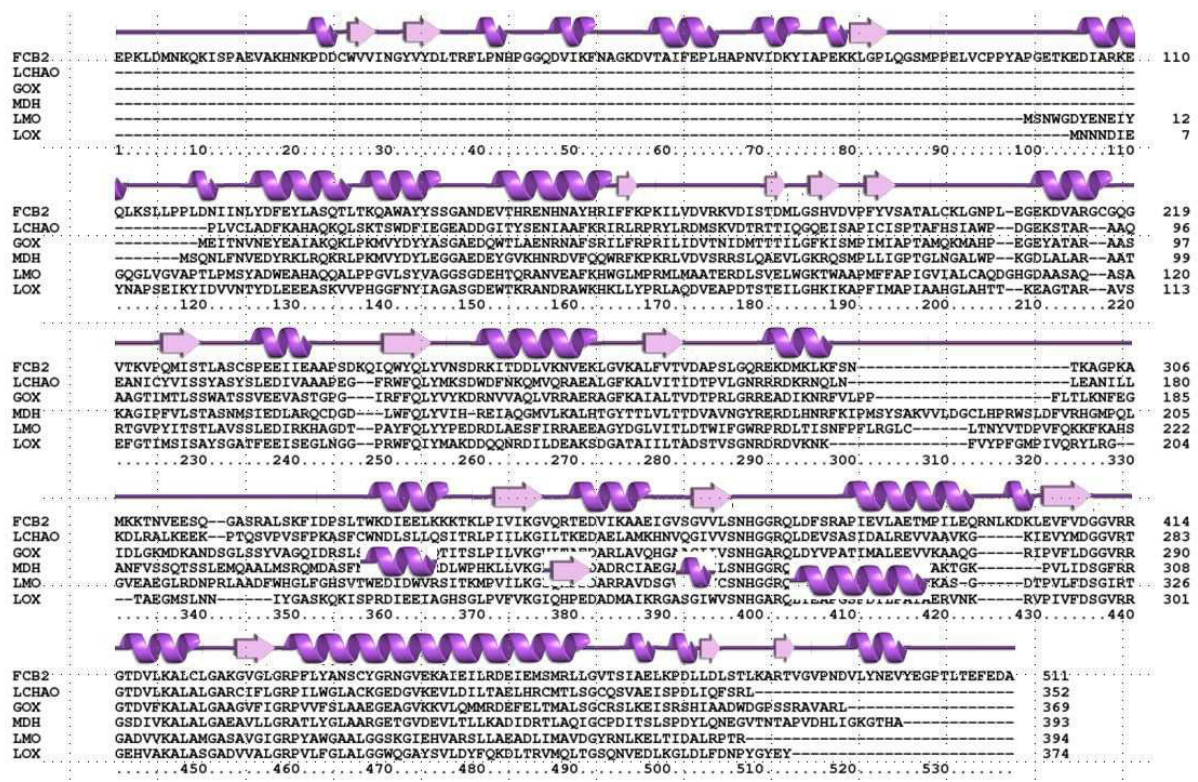


Figure 5

Sequence alignment of the family of 2-hydroxy acid oxidizing enzymes. Secondary structure assignment was based on the structure of FCB2.

His-265 (LOX numbering) is the active site base abstracting the α -proton of the substrate. In the crystal structure of LOX at pH 4.5 the histidine is flipped away from the active site forming a hydrogen bond network with Asp-174 to Lys-221, which is located close to the surface. It is argued that this conformation reflects an intermediate state of the enzyme after proton abstraction from the substrate, since His-265 is most likely fully protonated at pH 4.5 (49). The proposed role for the adjacent aspartate 174 is the stabilization of the protonated form of the histidine (37). Crystal structures of LOX at pH 8.0 (37) and 4.5 (49) revealed a flip of Asp-174 (together with His-165 and Lys-221) to adopt a hydrogen bonding network that is reaching from the active site to the surface of the protein. Due to the flip the hydrogen bonding partner for the carboxyl oxygen atom is switched from N δ 1 (pH 8.0) to N ϵ 2 (pH 4.5). Lys-241 is proposed to stabilize the anionic form of the flavin as has been

shown by mutagenesis studies (vide infra). Two residues have been found to bind to the carboxylate group of the substrate; one is a strictly conserved Arg-268, the other one Tyr-40 that is replaced by a phenylalanine in LCHAO. The last of the six conserved residues in the active site is Tyr-146 that is proposed to be involved in substrate binding and catalysis. This position is of particular interest, since it may play different roles in a carbanion and hydride transfer mechanism.

Substrate binding site

Subtle differences can be found around the substrate binding sites of the different members of the enzyme family. **Figure 6** shows the substrate binding site of LOX with pyruvate bound (PDB 2E77). Both oxygen atoms of the carboxylate function form H-bonds with Arg-181 and Arg-268. Additionally, Tyr-40 is in hydrogen bonding distance of O1 and His-265 of O2 (**50**). Tyr-40, His-265 and Arg-268 were discussed before and are strictly conserved. Arg-181 is conserved in all members as well, and it has been reported to be involved in hydrogen bonding to the substrate (**33, 36, 51**). However, LOX structure was solved at pH 4.5 in the presence of the inhibitor D-lactate, and in that case Arg-181 was not involved in substrate binding showing the flexibility of the side chain (**46**). The equivalent arginine residue in FCB2 (Arg-289) is also not involved in the binding of pyruvate, but flipped away (**38**).

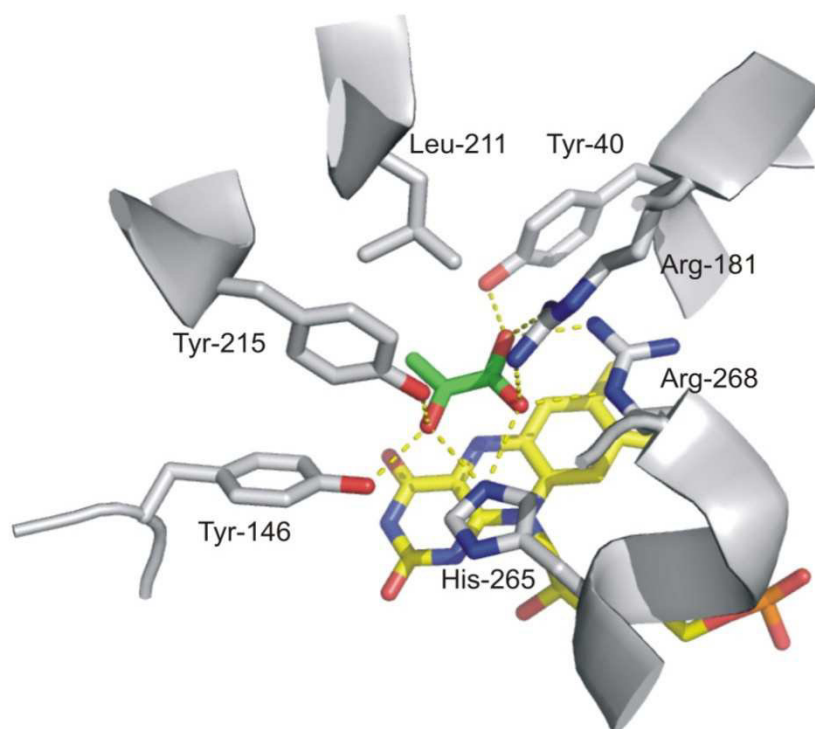


Figure 6

Substrate binding site in LOX

Tyr-215 and Tyr-146 form strong H-bonds with the α -hydroxy function of pyruvate in LOX. Tyr-146 is strictly conserved and adopts a similar position and orientation in all structures solved so far for this family. Tyr-215, however, which is part of loop 4, is in a unique position in LOX. Loop 4 has been proposed to play a prominent role for substrate binding. The main chain in all other crystal structures of the family is located further away from the substrate. In GOX, the equivalent residue is located on a helix, but a part of the loop 4 (residues 189-198) is not visible in the crystal structure **(21)**. For LCHAO, the electron density in this region was partially missing as well (residues 176-202) **(33)**. In MDH and FCB2, the loop adopts a different orientation. However, in MDH, loop 4 was derived from GOX for crystal preparation **(52)**. The crystal structure of FCB2 was solved in different variations. In the first structure solved, residues 300-316 were unordered **(38)**, later crystal

structures showed similar results (53-56). This loop has been reported to influence the activity of LCHAO by possible interactions with the active site (13), in MDH it forms a domain that is responsible for the attachment to the bacterial membrane (57), and in FCB2 it forms a subdomain interface (58).

In a recent work of Murray et al. loop 4, residues 169-212, was clearly showing electron density for all residues in human glycolate oxidase (GO). A structural comparison with GOX, where a part of the loop is missing, showed that loop 4 was in a different orientation suggesting a flexible region. It is proposed that the loop 4 orientation shifts upon substrate binding, as it occludes the active site (59). This region shows only low sequence homology within the family.

3. CATALYTIC MECHANISM

Half-reactions

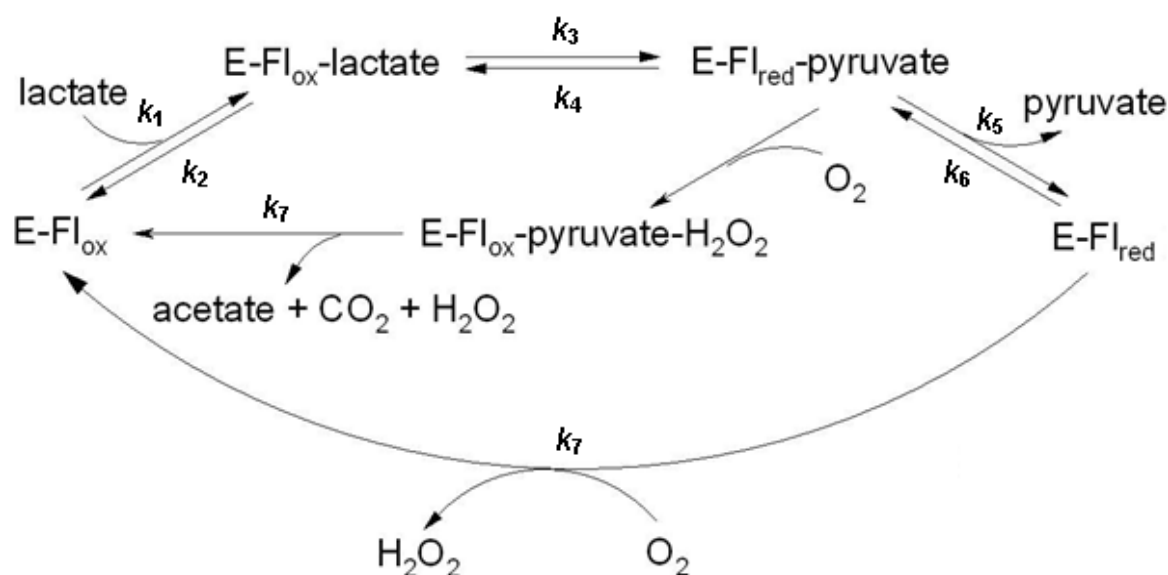
The reaction mechanisms can be divided in 2 half-reactions. In the first part of the ping-pong reaction mechanism the α -hydroxy acid enters the active site and is oxidized to the respective keto-acid. The flavin cofactor itself is reduced to its semiquinone form. In the second part of the reaction cycle - the oxidative half-reaction - the electrons are transferred to an electron acceptor, which can differ among the enzymes of this family.

Reductive half-reaction

Catalysis

The initial reaction steps are identical in all members of the family as depicted in **Scheme 2** for LOX and LMO. The first step of the reductive half-reaction is the binding of the α -hydroxy acid substrate to the active site to form a binary oxidized enzyme-substrate complex (**11**). The dissociation constants for L-lactate are $K_{d,L-lactate} \sim 5 \times 10^{-4}$ M for LOX (**11**) and $K_{d,L-lactate} = 5 \times 10^{-2}$ M for LMO (**4**). In MDH, a distinctive transient intermediate could be identified, which has been annotated as charge-transfer complex of an electron-rich donor and oxidized FMN (**60**). The next step is the oxidation of the α -hydroxy acid to the keto-acid resulting in a reduced enzyme-product complex, as it has been observed in all members. The presence of this intermediate was proven by photometric studies of LOX showing a biphasic behavior of the traces observed from 340 to 550. This species has been identified as a complex of reduced enzyme and pyruvate by titration of reduced enzyme with pyruvate and in stopped flow experiments by mixing different concentrations of pyruvate with the reduced enzyme (**11**). In GOX, the ping-pong reaction mechanism doesn't differ from LOX or LCHAO. In the reductive half-reaction, first an intermediate complex of oxidized enzyme and substrate is formed, before the flavin is reduced and glycolate oxidized to glyoxylate in an irreversible step. After product release, the second substrate, which is molecular oxygen, enters and acts as electron acceptor (**20**). This concomitant oxidation of the substrate and reduction of the flavin is the rate limiting step ($k_{cat} = 25 \text{ s}^{-1}$) (**20**). LCHAO, which is an isomer of GOX, is reported to follow the identical pathway (**33**). Interestingly, the MDH reaction features 2 rate-limiting steps, both of them in the reductive half-reaction. The formation and disappearance of the intermediate proceed at rates in a similar range (398 s^{-1} and 121 s^{-1} , respectively) (**60**). The reductive half-reaction is completed by the release of

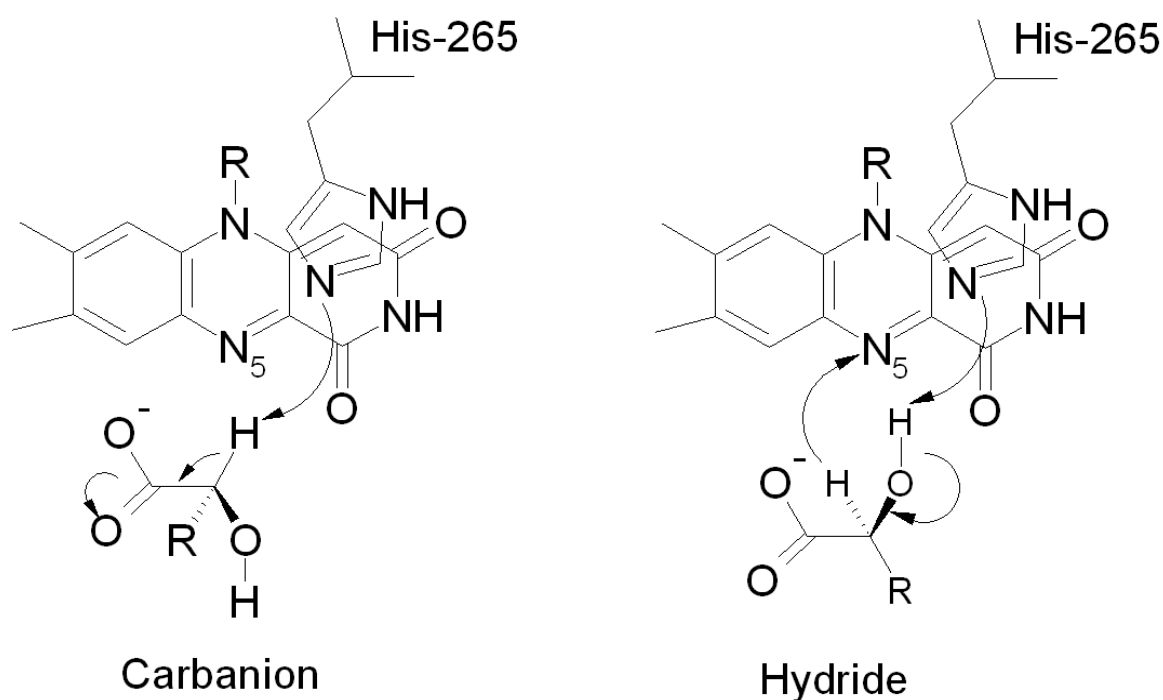
product and the reduced enzyme is available for the binding of the second substrate - the electron acceptor - in the ping-pong mechanism **(26)**. This intermediate decays into free pyruvate and oxidized enzyme at a rate of 500 s^{-1} at $25 \text{ }^\circ\text{C}$ in LOX **(11)**. In LMO, the rate of pyruvate dissociation is 0.042 s^{-1} and therefore $>10^4$ -fold slower **(4)**. This discrepancy is the cause for the different product spectrum of LOX and LMO. In LMO, the reaction quantitatively yields acetate, CO_2 and H_2O , whereas LOX converts L-lactate to pyruvate and H_2O_2 exclusively **(Scheme 2)**. However, under anaerobic conditions the reductive half-reaction is identical in both enzymes proceeding via a binary complex of reduced enzyme and pyruvate (E-FI_{red} -pyruvate) to yield the free enzyme with the reduced hydroquinone form of the flavin and pyruvate as product **(11)**. In FCB2, the discrimination of reductive and oxidative half-reaction is not possible so easily, since an intramolecular electron transfer from FMN to heme takes place immediately (see below). However, the reductive half-reaction is similar to LOX with an overall k_{cat} of 600 s^{-1} **(61)**.



Scheme 2

The reaction cycles of LOX (outer cycle) and LMO (inner cycle)

There have been ongoing discussions, on whether the first step of the reaction, the substrate oxidation, involves carbanion formation or follows a hydride transfer mechanism. The mechanism involving the carbanion requires the deprotonation of the α -carbon of L-lactate by the active site His-265. Subsequently, the electron equivalents are transferred to the flavin cofactor. In the hydride transfer mechanism the catalytic histidine deprotonates the α -hydroxyl group and the α -hydrogen is transferred as hydride to the FMN. Both possible mechanisms are shown in **Scheme 3**. A common mechanism for all enzymes of this family is assumed and both variants have been discussed in detail in the past (22, 26, 49, 62-66).



Scheme 3

Schematic representation of the possible reaction mechanism

Mechanistic studies with LMO from the early 80s suggest a carbanion mechanism for the catalytic reaction of LMO (62, 63). Therefore, the first step of the

reaction cascade would be the rate-limiting abstraction of the α -carbon of lactate by the catalytic histidine. The following step would be the fast electron transfer to the flavin to form the binary enzyme-pyruvate complex. Molecular oxygen reacts with the intermediate to form a ternary complex, where the turnover of pyruvate to acetate, carbon dioxide and water takes place **(4)**. Lehoux and Mitra showed for MDH that the catalytic base has to be unprotonated for activity and abstraction of the substrate α -proton. The unchanged substrate isotope effect was related to a carbanion mechanism **(26)**.

Recent studies with LOX indicate a hydride transfer mechanism for this family of enzymes **(49)**. In either of the 2 possible reaction mechanism the first step has to be the abstraction of a proton by His-265. The crystal structure of LOX at pH 4.5 was solved in the presence of the inhibitor D-lactate. The reason for its inactivity with this substrate is explained by a hydride transfer mechanism. In the structure with D-lactate the C_{α} -atom is 3.8 Å away of the flavin N5. In this orientation the C_{α} -H is pointing away from FMN while the C_{α} -OH group is facing His-265. However, with the native substrate L-lactate the C_{α} -H would be oriented closer to the flavin N5 facilitating a possible hydride transfer. Attempts to model the substrate L-mandelate into the active site of the LCHAO crystal structure also led to a reasonable model for a hydride transfer, but not for a carbanion mechanism **(33)**. In a recent molecular dynamics study of FCB2 the simulation was in favor of a hydride transfer mechanism. The complexes obtained at room temperature could only be explained by this reaction mechanism. The lactate dehydrogenation reaction was calculated as asynchronous hydride transfer mechanism with proton transfer from the substrate α -hydroxyl group to His373 (FCB2 numbering) followed by the hydride transfer of the α -H to the flavin. No intermediate has been observed in this step **(68)**. The free

activation energy is similar in both the calculation ($12.1 \text{ kcal mol}^{-1}$) **(68)** and experiments ($13.5\text{-}13.6 \text{ kcal mol}^{-1}$) **(69, 70)**.

His-265 is the active site base abstracting either the α -proton in a possible carbanion mechanisms or the proton of the α -hydroxyl group of the substrate in a hydride transfer mechanism. In LMO, the active site His-290 was mutated to Gln and activity was virtually abolished. The reductive half-reaction was $\sim 10^7\text{-}10^8$ times slower than in the wild-type, while the oxidative half-reaction proceeded at a similar rate. L-lactate had similar affinities in both enzymes **(67)**. Similar results have been found for FCB2 with a $\sim 10^5$ -fold reduction of reactivity **(71)**. In MDH, despite complete loss of activity, the replacement of the catalytic histidine by Gly, Ala and Asn also affected substrate binding. Binding of (S)-mandelate was estimated to be ~ 65 -fold weaker in H274G compared to the wild-type. Partial rescue of activity was possible by adding external imidazole to the H274G and H274A. However, the extent of recovery of catalytic activity was 0.1% of that of the wild-type **(27)**. Earlier studies for MDH determined that one residue with a pK_a of ~ 5.5 (5.1 in the enzyme-substrate complex) has to be unprotonated and another residue with a pK_a of ~ 8.9 has to be protonated. The residue with the lower pK_a was assigned to be the catalytic histidine. In the rescue studies this assumption was confirmed, since the pK_a values measured there resembled the ones for imidazole in solution. Therefore, the unprotonated form of the histidine is the active species **(26)**.

Auxiliary residues

In the crystal structure of LOX at pH 4.5 His-265 is flipped away from the active site forming a hydrogen bond network with Asp-174 to Lys-221, which is

located close to the surface. It is argued that this conformation reflects an intermediate state of the enzyme after proton abstraction from the substrate, since His-265 is most likely fully protonated at pH 4.5 (49). The proposed role for the adjacent aspartate 174 is the stabilization of the protonated form of the histidine (37). Crystal structures of LOX at pH 8.0 (37) and 4.5 (49) revealed a flip of Asp-174 (together with His-265 and Lys-221) to adopt a hydrogen bonding network that is reaching from the active site to the surface of the protein. Due to the flip the hydrogen bonding partner for the carboxyl oxygen atom is switched from N δ 1 (pH 8.0) to N ϵ 2 (pH 4.5). D174A and D174N mutants that were created lost all its activity (49). This strictly conserved residue hasn't been addressed yet by site-directed mutagenesis in the other family members. Lys-221 is not conserved in this class of enzymes. Based on sequence analysis and homology modeling, the His-Asp-Lys network found in LOX cannot be formed due to the absence of a lysine at a homologous position to Lys-221 in LOX. The mechanism of the proton shuttle in other family members therefore remains elusive.

Lys-241 is proposed to stabilize the anionic form of the flavin. In LMO, the lysine (266) was exchanged by a methionine (K266M) essentially removing the positive charge from the side-chain. In contrast to the wild-type enzyme, the semiquinone was thermodynamically unstable in the mutant enzyme. The mutation also perturbed the properties of the enzyme for reactions, where the negative charge at the flavin N(1)-position is involved (sulfite binding, stabilization of the benzoquinoid form of 8-mercapto-FMN). The k_{cat} value was lowered 104-fold and the K_{d} value 50-fold in the K266M mutant. Taking all these data together with the observation of changed flavin spectra that indicate a different environment, it was shown that this lysine residue is responsible for the stabilization of anionic FMN

forms (**72**, **73**). In FCB2, the appropriate lysine was replaced by an arginine (K349R). However, this replacement led to total loss of activity, which is consistent with the proposal of a stabilizing function (**56**).

Tyr-146 is proposed to be involved in substrate binding and catalysis. This position is of particular interest, since it may play different roles in a carbanion and hydride transfer mechanism. Over the last couple of years several groups addressed the role of this particular residue. In GOX a Y129F mutant has been prepared exhibiting 3.5% of wild-type activity with mainly unaffected glycolate binding. Interestingly, the mutant enzyme had a 30-fold higher affinity for molecular oxygen, however, the rate of re-oxidation remained the same. The lower K_M value for molecular oxygen was explained by the reduced reduction rate that is incorporated in the equation for K_M (**22**). In the wild-type enzyme the pK_a value of the N(3) of FMN is shifted to 6.4 (**20**), while in Y129F the pK_a is above pH 9.0 resembling closely the pK_a of free FMN (10.3). In contrast to the wild-type, the GOX mutant enzyme was not able to bind oxalate and therefore also was not inhibited by it. It was suggested earlier that oxalate acts as transition state analogue in a carbanion mechanism (**2**), and the result of the mutation study indicates that Tyr-129 has no influence on substrate binding, but does stabilize the transition state. The tyrosine was proposed to form a hydrogen bond from the hydroxyl group to the C(4=O) of FMN in the oxidized state. Upon substrate binding, a weak hydrogen bond to the substrate hydroxyl is formed and a negative charge is stabilized upon reaction (**22**). The same mutation (Y152F) was introduced into LMO and led to ~100-fold reduction of catalytic turnover. During the reaction the enzyme remained fully oxidized, which is indicating a low K_M for oxygen and is in full agreement with the observations made in GOX. The K_d for lactate was 10-fold lower than for the wild-type enzyme. Y152F followed mainly

the LMO pathway, even though a small portion (20-30%) of the reaction proceeded via the LOX mechanism and released pyruvate and H₂O₂. While the mutant was still able to bind oxalate, even though with a 60-fold increased dissociation constant, it was postulated that the tyrosine plays an important role in the stabilization of a potential carbanion transition state **(73)**.

The role of Tyr-254 in FCB2 has been addressed in several papers. The first mutational study has been performed by Dubois et al., where Y254F mutant was prepared and characterized. K_M was unaffected, however, k_{cat} was reduced ~40-fold. Deuterium isotope effects confirmed that the rate-limiting step is still the same, which was postulated to be the α -hydrogen abstraction. It was argued that, despite a missing change in K_M , the tyrosine hydroxyl group of the wild-type hydrogen bonds to lactate, but the missing interaction is compensated in the mutant due to small rearrangements in the phenylalanine side-chain to form weak electrostatic interactions between the negatively polarized oxygen atoms and the positively charged aromatic ring edge. It was postulated that the tyrosine residue plays a critical role in both Michaelis bond formation and transition state stabilization (2.3 kcal/mol) with the main function being to force the substrate in the proper orientation for α -hydrogen abstraction by His-373 **(74)**.

Upon replacing tyrosine with a leucine (Y254L), the activity was reduced >500-fold, while there was little effect on substrate binding. The similar K_M value to the wild-type contradicts the proposed role of Tyr-254 in substrate binding. The destabilization of the transition state is increased to 3.6 kcal/mol. Interestingly, the mutant enzyme showed sub-stoichiometric incorporation of FMN. It was argued that the mutation might influence proper protein folding in the expression strain **(30)**. Further, kinetic characterizations of the 2 mutant enzymes (Y254L, Y254F) indicated

that the first step of the reaction, which would be hydrogen abstraction from carbon, is rate-limiting. The data confirm the significance of the tyrosine in transition state stabilization, while no influence on substrate binding could be found. Upon changing the substrate to phenyllactate, the mutant enzymes showed higher affinities, and the K_M values decreased ~3-fold (Y254F) and 10-fold (Y254L), while k_{cat} became smaller. However, for Y254L phenyllactate was the preferred substrate over lactate in terms of catalytic efficiency. The cause for this effect remains elusive, but speculations have been made about the origin. One possibility are hydrophobic interactions of the aromatic substrate with the leucine side chain, other effects could be the larger substrate cavity, which would allow the phenyllactate to adopt a more favorable orientation, but could also lead to a more loosely oriented lactate. The authors are positive about the participation of Tyr-254 in a hydrogen bond to the L-lactate hydroxyl group and even more in the transition state. Based on modeling studies of the alternative substrates, a hydride transfer mechanism is ruled out. It is proposed that, since mandelate can't bind in a proper orientation for the carbanion mechanism, it is a poor substrate **(30)**.

However, the latest work dealing with Y254F in FCB2 proposes a hydride transfer mechanism. Deuterium isotope effects were measured for both the wild-type and Y254F indicating an important role of Tyr-254 in catalysis. Primary isotope effects for the wild-type of 3 for V_{max} and V/K_M are consistent with CH bond cleavage being partially rate limiting. In the mutant enzyme both values are raised to 5 making this step even more rate-limiting. The solvent isotope effect has been shown to arise from a different step in the wild-type enzyme, but from the same step as the primary isotope effect in the Y254F mutant variant. The explanation for this is that cleavage of the α -CH and the lactate hydroxyl bond occur at the same time in a concerted

reaction. This is fully consistent with a hydride transfer mechanism, but can hardly be explained by a carbanion mechanism. In the mutant enzyme the lactate hydroxyl proton is removed by His-373, while the α -hydrogen is abstracted as hydride by the flavin. The authors also applied this model to the wild-type enzyme. They argued that in the hydride transfer mechanism, opposite to the carbanion mechanism, the OH bond cleavage occurs before CH bond cleavage (64). Tyr-254 has been proposed to stabilize the transition state of the lactate oxidation reaction, and the mutations at that position showed decreased affinities for anionic inhibitors (30). This is also in accordance with a hydrogen bond that has been observed between the hydroxyl group of tyrosine and a sulfite oxygen atom (75). The pH profiles of wild-type and mutant enzyme were similar to each other leading to the assumption that the pK_a for the tyrosine OH group must be either below 5 or above 11. Since such a pK_a below 5 is very unlikely, Tyr-254 is assumed to be protonated in its active form. This is consistent with the neutral tyrosine side chain stabilizing the lactate alkoxide in the intermediate state. The loss of this interaction in the Y254F mutant would lead to a destabilization of the alkoxide, which would make its formation slower. This is in full agreement with a hydride transfer mechanism, since the 2 distinct steps in the wild-type enzyme (OH and CH bond cleavage) would merge into a concerted reaction. In a carbanion mechanism, however, the two steps would be even more discrete, which should lead to a more rate-limiting OH bond cleavage, which has not been observed in the deuterium isotope effect studies. It was concluded that these results can be explained by a concerted cleavage of the lactate O-H bond and the α -CH bond. This scenario strongly favors a hydride mechanism for the mutant enzyme, while a carbanion mechanism for the wild-type cannot be ruled out (64).

The following reaction mechanism has been proposed for LOX based on the hydride transfer mechanism, which is favored in recent literature. In a first step, both the C_α-H and C_α-OH bonds are disrupted concomitant with reduction of FMN. His-265 gets protonated in this step abstracting the hydroxyl proton of the substrate, while a hydride is transferred to the cofactor. The histidine flips out of the active site creating space for dioxygen to enter, while the product pyruvate gets released. This intermediate structure is stabilized by a network of His-265, Asp-174 and Lys-221 in LOX. After the completion of the reductive half-reaction, molecular oxygen can enter the substrate binding site to start the oxidative half-reaction. His-265 flips back, in order to accommodate dioxygen in the same manner as the C_α and keto-oxygen atoms of lactate **(49)**.

Oxidative half-reaction

In the oxidative half-reaction the flavin cofactor gets re-oxidized to finish the catalytic cycle. The enzymes of the family can be divided in 2 groups, one of them using molecular oxygen for re-oxidation and the other one using other electron acceptors.

Molecular oxygen

The reaction starts by electron transfer from the reduced flavin to O₂ yielding a caged radical pair between the flavin semiquinone and superoxide anion **(76, 77)**. In the case of oxidases, a second electron transfer takes place generating oxidized flavin and H₂O₂. For monooxygenases the radical pair collapses to form the intermediate C4a-(hydro)peroxyflavin. Due to its instability the radical pair has not

been characterized and could only be observed for one single enzyme, glycolate oxidase (78).

LOX, LMO, LCHAO and GOX use dioxygen as electron acceptor in a 2-electron reaction to yield hydrogen peroxide. In a recent crystallographic study of LOX at pH 4.5 electron density for molecular oxygen has been identified. Dioxygen was bound above the *si*-face of the flavin ring. It was proposed that due to the flipping of His-265 space for the entrance of dioxygen is created (49). However, crystal structures of LOX at pH 7.5 (79) and 8.0 (37, 50) did not show bound dioxygen, therefore the flipping of His-265 is mandatory. **Figure 7** shows a surface representation of the LOX at pH 4.5 (PDB: 2NLI) with the putative entry channel for molecular oxygen. His-265 of a crystal structure solved at pH 8.0 (PDB: 2DU2) is shown in blue, after overlaying both structures. The figure shows that dioxygen (shown in red) is occupying the space liberated by the flip of His-265. Based on analysis of the crystal structures, it can be assumed that both the substrate as well as dioxygen enter and leave the enzyme through the same channel.

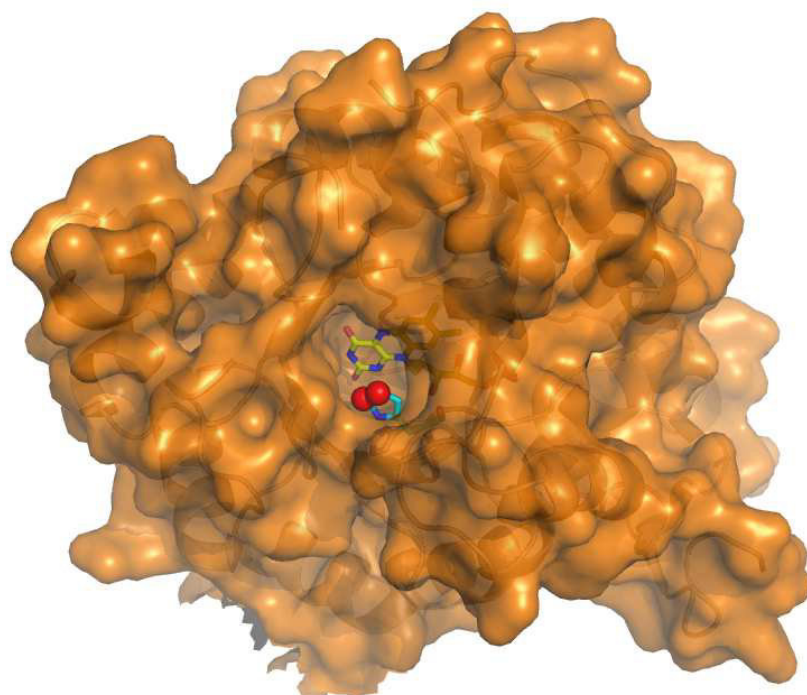


Figure 7

Surface of LOX at pH 4.5 looking down the substrate channel. Dioxygen is shown in **red**, FMN in **yellow** and His265 of LOX at pH 8.0 is shown in **blue**.

Molecular oxygen is accepted as electron acceptor by the flavin domain in FCB2 to form superoxide, but the reaction is slow and therefore cannot compete with artificial electron acceptors. It was shown that superoxide is formed during the conversion with oxygen. Superoxide is expected to be dismutated to yield hydrogen peroxide. A coupled assay with horseradish peroxidase as reporter for hydrogen peroxide showed a turnover of 15 - 19 min⁻¹ dependent on the presence or absence of superoxide dismutase. In contrast, the catalytic turnover with ferricyanide is ~ 250 s⁻¹ (**80**). Re-oxidation of reduced MDH by dioxygen proceeds only slowly as well (**26**, **60**).

LMO is a special case within these members of the family, since oxygen already binds to the enzyme, before the product dissociates. It was mentioned above

that pyruvate dissociation is much slower, and therefore a ternary complex EFl_{ox} -pyruvate- H_2O_2 is formed. Re-oxidation of the flavin cofactor takes place in this ternary complex leading to the release of CO_2 , H_2O and pyruvate. Additionally, the reduced enzyme - pyruvate intermediate reacts ~ 200 -fold faster with O_2 than the free reduced enzyme. Taking together the slow dissociation of pyruvate from the intermediate and the reduced reaction rate of free reduced enzyme with oxygen, this pathway for catalysis is highly favorable over the LOX pathway. This is a unique reaction in this family, since the other enzymes using dioxygen as electron acceptor yield hydrogen peroxide as co-product (**4, 11**).

LMO, LOX and FCB2 have a highly conserved active site, but their reactivity towards oxygen varies drastically, with rate constants of almost 0 for FCB2 and 1×10^6 for LOX and LMO (**11, 38**). Mutagenesis studies on LMO showed that small changes in the cofactor environment especially next to N5-C4a position of FMN can have dramatic effect on oxygen reactivity. Substitution of Gly99 by Ala alters the reactivity with $\text{O}_2 \sim 10^5$ -fold (**101**).

Alternative electron acceptors

The dehydrogenases in this family, MDH and FCB2, use monoelectric acceptors for 1-electron transfer steps in contrast to the 2-electron transfers to dioxygen. The native electron acceptor for membrane-bound MDH is unknown, but it is assumed that it is a component of the electron transport chain (**26, 60**). In FCB2, the reducing equivalents are transferred from the flavin to heme b_2 , which is located in the heme-binding domain. During the transfer a flavin semiquinone is formed. Subsequently, the electrons are shuttled to cytochrome c for the recycling of heme b_2 (**80**).

The question was raised in literature, whether different electron acceptors can be used as electron sinks. Most work has been done on FCB2, where the transfer reaction to selected alternative electron acceptors has been studied. The electron transfer cascade shuttles the reducing equivalents from the flavin domain to the heme b_2 domain and finally to cytochrome c , which are both one-electron steps **(34)**. Ferricyanide is used as non-physiological electron acceptor and can accept electrons from both the flavin semiquinone and the heme group, while cytochrome c does only react with FMN with a 10^6 -fold reduced rate compared to the transfer from heme b_2 . The transfer of electrons from the reduced form of FMN to ferricyanide is only working, if the intramolecular electron transfer to heme b_2 is slowed down or eliminated **(81-83)**. Dichloroindophenol (DCIP), which is generally known as 2-electron acceptor, only reacts with the heme b_2 -group, but does not show significant activity with the FMN group. This indicates 1-electron steps for the DCIP reduction compared to the expected 2-electron step **(71)**. However, there are precedent reports of DCIP acting as 1-electron acceptor as well **(84-86)**.

MDH is able to use DCIP, cytochrome c and ferricyanide as electron acceptors with relative activities of 1:1.18:3.03, respectively. MDH is also able to transfer the reducing equivalents to molecular oxygen, even though the rate is much slower **(39)**. The catalytic turnover in the presence of DCIP was 360 s^{-1} , while the rate was reduced to 1.2 s^{-1} with oxygen as sole electron acceptor under otherwise similar conditions **(87)**.

In the 1950s it was already reported that a lactate monooxygenase from *Mycobacterium phlei* transfers its electrons to several artificial electron acceptors. DCIP, ferricyanide, cytochrome c and methylene blue could all serve as electron sinks for the uptake of electrons of the flavin group **(88, 89)**. The glycolate oxidase

assay is also based on either the reduction of ferricyanide or DCIP. The catalytic turnover with DCIP was twice the value that was obtained by using molecular oxygen as electron acceptor (90). DCIP is also used as routine electron acceptor for LCHAO. It has been demonstrated that DCIP and ferricyanide gave similar reactivities, the rate with molecular oxygen was only slightly lower (13, 91). LOX has already been shown to work with ferricyanide in a disposable biosensor for the determination of lactate levels in whole blood. In this setup the electrons are finally shuttled from ferricyanide to modified carbon nanotubes (92). As investigated for LOX from *Pediococcus sp.* DCIP and other electron transfer mediators based on indophenols derivatives worked for lactate sensor and showed good sensor performance including a high sensitivity and good durability (93, 94).

4. SUBSTRATE BINDING AND SPECIFICITY

Table 1 provides an overview of substrates used by the members of the α -hydroxy acid oxidase family. Catalytic efficiencies (k_{cat}/K_M) showed that glycolate is preferred ~20-fold over L-lactate in GOX. For LOX, LMO and FCB2 L-lactate is the preferred substrate with FCB2 being the most effective enzyme ($k_{cat}/K_M = 2.3 \times 10^6$). MDH is very specific for L-mandelate and shows only weak catalytic efficiency for other substrates. LCHAO has a very broad substrate spectrum ranging from chain lengths of 2 C to 16 C.

Several structures of α -hydroxy acid oxidases in the presence of substrate analogues and inhibitors have been solved and assist in better understanding of the factors governing the selectivity. The residues Tyr-40, Tyr-146 and Arg-268 (LOX

numbering) are strictly conserved with the exception of the introduction of a Phe in LCHAO to replace the residue analogue to Tyr-40.

Table 1. Substrate specificities of α -hydroxy acid oxidase family

K_M [mM]	Glycolate	L-lactate	L-mandelate	DL-2-hydroxy-butyrates	L-2-hydroxy octanoate	L-2-hydroxy palmitate	Glyoxylate	DL-glycerate
LOX		0.94 (11)	0.3 (100)	18 (100)				5.0 (100)
LMO		22 (11)						
FCB2	0.34 (29)	0.16 (64)		0.59 (29)	0.11 (29)			
MDH			0.12 (97)	32 (26)	0.75 (97)			
GOX	1 (20)	11.5 (23)	58 (23)	3 (23)				
LCHAO		6.1 (33)	0.11 (33)	0.6 (105)	0.046 (33)	1.36 (33)		
k_{cat} [s^{-1}]	Glycolate	L-lactate	L-mandelate	DL-2-hydroxy-butyrates	L-2-hydroxy octanoate	L-2-hydroxy palmitate	Glyoxylate	DL-glycerate
LOX		280 (11)	0.003 (100)	11 (100)				0.87 (100)
LMO	1.17 (63)	105 (11)						
FCB2	7 (29)	372 (64)	0.02 (99)	82 (29)	45 (29)			
MDH			270 (97)	0.1 (87)	0.51 (97)			
GOX	20 (20)	11 (23)	0.09 (23)	13.2 (23)				
LCHAO		0.26 (33)	1.16 (33)		0.99 (33)	0.34 (33)		
k_{cat}/K_M [$M^{-1}s^{-1}$]	Glycolate	L-lactate	L-mandelate	DL-2-hydroxy-butyrates	L-2-hydroxy octanoate	L-2-hydroxy palmitate	Glyoxylate	DL-glycerate
LOX		298000	10	610				174
LMO		4770						
FCB2	20000	2325000		140000	410000 (97)			
MDH			2250000 (97)	3.4 (87)	630			
GOX	20000 (20)	960 (23)	1.5 (23)	4400 (23)				
LCHAO		40 (33)	10500 (33)		21400 (33)	250 (33)		

Two residues have been found to bind to the carboxylate group of the substrate, one is a strictly conserved Arg-268, the other one Tyr-40 that is replaced by a phenylalanine in LCHAO. In the latter enzyme the conserved motif was remodeled by site-directed mutagenesis (F23Y). However, mandelate, which is the best known substrate for LCHAO, showed a ~10-fold reduced turnover in the mutant variant compared to the wild-type enzyme. Since the K_M value was reduced 10-fold as well the catalytic efficiency remained unaffected (**95**). The reverse mutation was made in GOX (Y24F) and led to higher K_M values, but unchanged substrate specificities. The K_M value for glycolate, the best substrate for GOX, was ~10-fold higher with a 3-fold decrease of k_{cat} . The amino acid exchange also led to a presence of an unidentified N(5)-flavin adduct that compromised 50-80% of total FMN present. The presence of the adduct was explained by an alteration of the water network close to the hydroxyl group of Tyr-24 in the wild-type enzyme. The rate of reduction of the flavin cofactor was hardly influenced by the mutation, and therefore the main purpose of the tyrosine has been appointed to substrate binding and not to a catalytic step (**23**). The results obtained for the Y24F mutant are in full accordance with mutant enzymes from FCB2 (Y143F) and LMO (Y44F). Using isotope effects for the wild-type and mutant form of FCB2, it was shown that Tyr-143 stabilizes the enzyme-substrate complex by forming a hydrogen bond to a substrate carboxylate. However, it was postulated that the transition state is not stabilized by this tyrosine residue (**70**). In a different work with the same mutant enzyme it has been shown that Tyr-143 plays a prominent role in electron transfer from FMN to the heme prosthetic group as this was the rate-determining step for the overall reaction. For the wild-type it was the proton abstraction from the substrate. That step was 20-fold slower compared to the wild-type enzyme (**69**). The Y44F variant of LMO showed a ~1000-fold reduction of k_{cat} and a ~50-fold lower K_M value for lactate. Interestingly, it was also shown that a

significant amount of H_2O_2 was produced leading to the assumption that part of the reaction proceeds via the LOX-pathway (73).

The second residue interacting with the substrate carboxylate group is the strictly conserved Arg-268. This position has been probed by a conservative mutation to lysine in 4 of the 6 enzymes. In LOX, the R268K mutant showed little effect on the oxidative half-reaction, but the reductive half-reaction showed second order behavior. This indicated a more complex reaction together with very weak substrate binding, as no Michaelis complex has been observed. It has also been found that the FMN cofactor slowly was converted to 8-formyl-FMN in the mutant variant (96). In the appropriate mutation in LMO (R293K) spectra changes were appointed to a (N)5 adduct with a protein cysteine residue. k_{cat} in this mutant was reduced almost 4000-fold, and - similar to Y44F - the reaction was partially uncoupled and did proceed partially via the LOX pathway. Interestingly, the enzyme remained in the oxidized state during catalysis, which indicated a high K_M value for oxygen, whereas the affinity constant for D-lactate was mainly unaffected. It is argued that in this mutation the lysine can take over the role of arginine in substrate binding (73).

In MDH more distinct effects on substrate binding have been found. In the charge-conserved mutation R277K k_{cat} was only lowered 4-fold, while its K_M value was 40-fold higher. Mutations that also changed the charge of the side-chain (R277H, R277L and R277G) had a more sophisticated effect on catalytic turnover (400- to 1000-fold decrease) and substrate binding (160- to 600-fold). The oxidative half-reactions of the mutant enzymes were not affected. A combination of rescue experiments and isotope effect measurements led to the conclusion that a positive charge at this specific position is important for catalysis. It was concluded that the reduced activity in the R277L mutant was due to a decrease in the rate of the α -C-H bond breaking step.

Calculation of binding energy differences led to a specific arginine-substrate interaction with an energy of 2.1 kcal/mol, which was appointed to a hydrogen bond between the arginine ϵ -H and a substrate carboxylate oxygen. However, the differences in activation energies between wild-type and mutant enzymes indicated a stabilization of the transition state by a positive charge and a hydrogen bond as main contribution by the arginine residue. The authors argued that these results are in good agreement with a carbanion mechanism, where the negatively charged intermediate is stabilized by the positively charged arginine residue (97). In a study with mandelic esters as substrates it was also found that Arg-277 plays a critical role for transition state stabilization, but not for binding affinity (98).

Figure 8 illustrates the substrate binding site of FCB2 with the product pyruvate modeled in the active site, where the residues Ala-198 and Leu-230 are indicated, which are in close proximity to the methyl group of the substrate L-lactate.

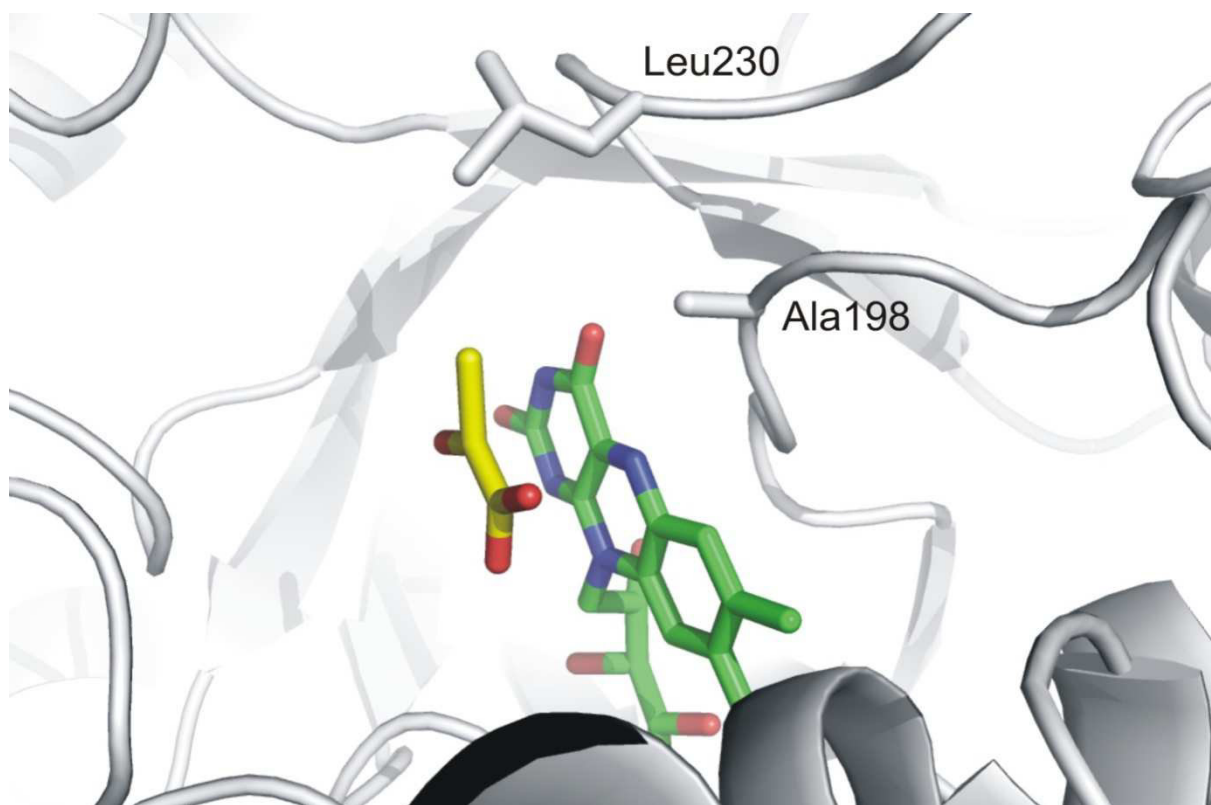


Figure 8

Substrate binding in FCB2. The product pyruvate is shown in yellow, the cofactor FMN in green.

In a work by Daff et al. those 2 residues have been shown to play an important role in governing substrate specificity. A198G and L230A mutants were created together with a A198G/L230A double mutant. In the wild-type enzyme the ratio of catalytic efficiencies (k_{cat}/K_M) for L-lactate over (S)-2-Hydroxyoctanoate was 2.00, whereas in the double mutant it was reversed to 0.03. Therefore the C-8 substrate was preferred ~65-fold over the C-3 substrate. Activity with glycolate was completely lost (29). The double mutant showed a ~6-fold preference of L-mandelate over L-lactate, whereas the wild-type enzyme showed low mandelate activity (0.02 s^{-1}) (99).

The sequence alignment in **Figure 5** evidences that Ala-198 is replaced by Leu in MDH and LMO, for the rest of the family Ala is conserved. Leu-230 is not conserved and even replaced by bulky residues like Tyr (LCHAO, LOX) or Trp

(GOX). Only MDH has Ala as native amino acid at this particular position. In LOX, the same Ala→Gly mutation has been introduced (A95G) with the consequence of improved conversion of long-chain α -hydroxy acids. In the wild-type enzyme L-lactate is preferred 2.9×10^4 -fold over L-mandelate, in A95G the ratio was reduced dramatically to 46. The turnover number for mandelate was increased almost 5000-fold. A comparison of the substrates L-lactate with the longer DL- α -OH-*n*-butyrate showed a 533-fold preference for the native substrate in the wild-type, while in the mutant variant this value shrank to 2. Catalytic turnover was even twice as fast for the alternative substrate in A95G. Even though the amino acid replacement resembles the LMO sequence, the reaction pathway for lactate conversion was not altered and still followed the LOX-circle **(100)**. The reverse mutation was made in LMO leading to a G99A mutant enzyme. The efficiency for bulkier substrates was not tested, however, the catalytic turnover of L-lactate was ~1000-fold reduced accompanied by ~1000-fold tighter binding of the substrate. The most interesting result though is that the catalytic pathway had been switched, and the LMO mutant enzyme followed the LOX reaction cycle, where pyruvate is released before oxygen enters the active site to form a ternary complex. This reflects that the highest impact of the mutation is on the oxidative half-reaction. This is in very good agreement with the observed reduced affinity for oxygen (~100-fold) **(101)**.

MDH is one of the 2 members of the family that have a Gly at this particular position in the native structure. Increasing of the side chain size by introducing a mutation to Ala (G81A) led to a 19-fold decreased turnover for L-mandelate while the substrate affinity remained unaffected. The insertion of a hydroxy or carboxylic functional group (Ser, Asp) led to ~15-fold weaker substrate binding while further, reducing the turnover number as well (130- and 3300-fold, respectively). The biggest

impact on k_{cat} was found for a G81V mutant, where the activity was 7200 times less than in the wild-type enzyme. The influence of these mutations was mainly on the reductive half-reaction. For G81A, however, modest improvement of oxygen reactivity was observed as well. The impact of the G81A was also evaluated with longer substrates, and while catalytic efficiency with L-mandelate decreased, it increased with longer substrates. MDH wild-type prefers for example L-mandelate 4.3×10^3 -fold over (S)-2-Hydroxyoctanoate, while for G81A the preference was reduced to 67-fold **(87)**.

The residue at the position of Leu-230 (FCB2) is not conserved throughout the family, and it's not possible to draw conclusions for the substrate specificity by the side chain size. LMO, which also has L-lactate as preferred substrate, has a leucine as well at this particular position, whereas LOX features a bulky tyrosine. However, also LCHAO, which is expected to have a smaller side-chain to accommodate the larger substrates in the active site, has a tyrosine at this particular position. GOX features a tryptophan excluding bulkier substrates from binding to the active site, whereas in MDH the alanine creates enough space for mandelate. The influence of Trp-108 in GOX on substrate specificity was investigated by removing the bulky side-chain and creating a W108S mutant enzyme. The ratio in catalytic efficiency between glycolate and mandelate was completely reverted from 1.3×10^4 in the wild-type enzyme to 4.4×10^{-3} in the mutant form. A single amino acid mutation therefore led to a dramatic 3.0×10^6 -fold change in substrate specificity. The row of K_M values for the W108S mutant was L-mandelate < DL-2-hydroxy butyrate < L-lactate < glycolate, making glycolate, the native substrate for GOX, the least favorable one **(23)**.

The crystal structure of human GO, which is 57% identical to GOX, was solved with sulphate, glyoxylate and the inhibitor 4-carboxy-5-dodecylsulfanyl-1,2,3-triazole

(CDST), respectively. A comparison of the complexes showed that Trp-110 (structural homologue to Trp-108 in GOX) is able to rotate its side-chain to make room for large and bulky substrates. However, the conformation of the Trp differs between GOX and human GO, and GOX is not able to accommodate larger substrates. Movement of Trp-110 in human GO also initiates the disruption of a hydrogen bond network that holds loop 4 in place. Loop 4 was visible in the sulphate complex, but unordered in the CDST complex (59). All these examples illustrate that small changes inside the active site can influence the substrate specificity, and that loop 4 plays a key role in catalysis.

Concluding remarks

The reviewed members of the oxidase family oxidize aromatic or aliphatic 2-hydroxy acids. The solved structures of the highlighted flavoproteins (with the exception of LMO) provide insights into the fold and the catalytically important residues. All proteins have a $\beta 8/\alpha 8$ TIM barrel structure. Regarding the catalytic mechanism, the reductive half-reaction of the mentioned oxidases is still controversial. Studies support both the ideas of a hydride transfer mechanism or the formation of a carbanion, where the catalytic histidine is involved (His-265 in LOX). Furthermore, this review has pointed out that a similar active site is no guarantee for similar substrate specificity and quite often auxiliary amino residues are important for substrate binding or product release.

On the other hand, the reaction of molecular oxygen with the reduced flavoprotein is still the most discussed task in research of oxidases, monooxygenases and dehydrogenases. For instance, there are only few predictions, why FCB2 reacts poorly with oxygen, but better with other electron acceptors (80). Recent

computational and structural studies suggested a direct contact between the flavin N5-C4a locus and oxygen to be responsible for the oxygen reaction, and residues around this locus can therefore control the accessibility and the reactivity. Nevertheless, for many systems (FCB2 **(80)**), the reasons for inefficient reactivity with oxygen remain unclear. Future prospects include the investigation of structural features of the active site of flavin dependent enzymes, which might facilitate the reaction of reduced enzyme and oxygen **(102)**. Apart from that, the question arises, if special gas diffusion paths for oxygen exist to get into the active sites of oxidases and monooxygenases. Many mechanisms are possible for oxygen activation by flavoproteins. In the last decades scientists tried to turn oxidases into monooxygenases or dehydrogenases into oxygen reacting enzymes or vice versa. The group of Winter and Fraaije, for instance, have introduced peroxidase activity into an oxidase, and Liferink *et al.* altered a dehydrogenase into an oxidase **(103, 104)**. Finding clues to the aforementioned questions could facilitate such alterations and be a milestone for biochemical engineering and the development of oxidase-based biotechnological applications.

REFERENCES

- 1 Edson NL (1947) The oxidation of lactic acid by *Mycobacterium phlei*. *Biochemical journal* **41**, 145-151.
- 2 Ghisla S & Massey V (1975) Mechanism of inactivation of the flavoenzyme lactate oxidase by oxalate. *The Journal of biological chemistry* **250**, 577-584.
- 3 Ghisla S, Massey V & Choong YS (1979) Covalent adducts of lactate oxidase. Photochemical formation and structure identification. *The Journal of biological chemistry* **254**, 10662-10669.
- 4 Lockridge O, Massey V & Sullivan PA (1972) Mechanism of action of the flavoenzyme lactate oxidase. *The Journal of biological chemistry* **247**, 8097-8106.
- 5 Averill BA, Schonbrunn A & Abeles RH (1976) Studies on the mechanism of *Mycobacterium smegmatis* L-lactate oxidase. 5-deazaflavin mononucleotide as a coenzyme analogue. *The Journal of biological chemistry* **250**, 1603-1605.
- 6 Ghisla S, Massey V (1977) Studies on the mechanism of action of the flavoenzyme lactate oxidase: Proton uptake and release during the binding of transition state analogs *The Journal of biological chemistry* **252**, 6729-6735.
- 7 Fitzpatrick PF (2004) Carbanion versus hydride transfer mechanisms in flavoprotein-catalyzed dehydrogenations. *Bioorganic chemistry* **32**, 125-139.
- 8 Schuvailo O, Soldatkin O, Lefebvre A, Cespuglio R & Soldatkin A (2006) Highly selective microbiosensors for in vivo measurement of glucose, lactate and glutamate. *Analytica chimica acta* **573-574**, 110-116.
- 9 Mehrvar M & Abdi M (2004) Recent developments, characteristics, and potential applications of electrochemical Biosensors. *Analytical sciences* **20**, 1113-1126.
- 10 Ghamouss F, Ledru S, Ruillé N, Lantier F, Boujtita M. (2006) Bulk-modified screen-printing carbon electrodes with both lactate oxidase (lod) and horseradish peroxidase (hrp) for the determination of L-lactate in flow injection analysis mode. *Analytica chimica acta* **570**, 158-164.
- 11 Maeda-Yorita K, Aki K, Sagai H, Misaki H & Massey V (1995) L-lactate oxidase and L-lactate monooxygenase: Mechanistic variations on a common structural theme. *Biochimie* **77**, 631-642.
- 12 Cavener DR (1992) GMC Oxidoreductases. A newly defined family of homologous proteins with diverse catalytic activities. *Journal of molecular biology* **223**, 811-814.
- 13 Belmouden A & Lederer F (1996) The role of a p barrel loop 4 extension in modulating the physical and functional properties of long-chain 2-hydroxy-acid oxidase isozymes. *European journal of biochemistry* **238**, 790-798.
- 14 Belmouden A, Lê KH, Lederer F, Garchon HJ. (1993) Molecular cloning and nucleotide sequence of cDNA encoding rat kidney long-chain L-2-hydroxy acid oxidase. *European journal of biochemistry* **214**, 17-25.
- 15 Stevens JL, Robbins JD & Byrd RA (1986) A purified cysteine conjugate beta-lyase from rat kidney cytosol. Requirement for an alpha-keto acid or an amino acid oxidase for activity and identity with soluble glutamine transaminase K. *The Journal of biological chemistry* **261**, 15529-15537.
- 16 Gunshore S, Brush EJ & Hamilton GA (1985) Equilibrium constants for the formation of glyoxylate thiohemiacetals and kinetic constants for their oxidation by O₂ catalyzed by L-hydroxy acid oxidase. *Bioorganic chemistry* **13**, 1-13.
- 17 Brush EJ & Hamilton GA (1981) Thiol-glyoxylate adducts as substrates for rat kidney. *Biochemical and biophysical research communications* **103**, 1194-1200.
- 18 Yokozawa T, Fujitsuka N, Oura H, Akao T, Kobashi K, Ienaga K, Nakamura K & Hattori M (1993) Purification of methylguanidine synthase from the rat kidney. *Nephron* **63**, 452-457.
- 19 Ozasa H, Horikawa S & Ota K (1994) Methylguanidine synthase from rat kidney is identical to long-chain L-2-hydroxy acid oxidase. *Nephron* **68**, 279.

- 20 Macheroux P, Massey V & Thiele DJ (1991) Expression of spinach glycolate oxidase in *Saccharomyces cerevisiae*: Purification and characterization. *Biochemistry* **30**, 4612-4619.
- 21 Lindqvist Y (1989) Refined structure of, spinach glycolate oxidase at 2 Å Resolution. *Journal of molecular biology* **209**, 151-166.
- 22 Macheroux P, Kieweg V, Massey V, Söderlind E, Stenberg K & Lindqvist Y (1993) Role of tyrosine 129 in the active site of spinach glycolate oxidase. *European journal of biochemistry* **213**, 1047-1054.
- 23 Stenberg K, Clausen T, Lindqvist Y & Macheroux P (1995) Involvement of Tyr24 and Trp108 in substrate binding and substrate specificity of glycolate oxidase. *European journal of biochemistry* **228**, 408-416.
- 24 Stenberg K & Lindqvist Y (1997) Three-dimensional structures of glycolate oxidase with bound active-site inhibitors. *Protein science* **6**, 1009-1015.
- 25 Vignaud C, Pietrancosta N, Williams EL, Rumsby G & Lederer F (2007) Purification and characterization of recombinant human liver glycolate oxidase. *Archives of biochemistry and biophysics* **465**, 410-416.
- 26 Lehoux IE & Mitra B (1999) (S)-mandelate dehydrogenase from *Pseudomonas putida*: mechanistic studies with alternate substrates and pH and kinetic isotope effects. *Biochemistry* **38**, 5836-5848.
- 27 Lehoux IE & Mitra B (1999) (S)-Mandelate dehydrogenase from *Pseudomonas putida*: mutations of the catalytic base histidine-274 and chemical rescue of activity. *Biochemistry* **38**, 9948-9955.
- 28 Pajot AP & Claisse ML (1974) Utilization by yeast of D-lactate and L-lactate as sources of energy in the presence of antimycin. *European journal of biochemistry* **49**, 275-285.
- 29 Daff S, Manson FD, Reid GA & Chapman SK (1994) Strategic manipulation of the substrate specificity of *Saccharomyces cerevisiae* flavocytochrome *b₂*. *Biochemical journal* **301**, 829-834.
- 30 Lederer F. (1991) Flavocytochrome *b₂*. Chemistry and biochemistry of flavoenzymes (Mueller F. ed.) pp. 153-242. CRC Press, Boca Raton, FL, USA.
- 31 Gondry M, Terrier M & Lederer F (2001) The catalytic role of tyrosine 254 in flavocytochrome *b₂* (L-lactate dehydrogenase from baker's yeast). Comparison between the Y254F and Y254L mutant proteins. *European journal of biochemistry* **268**, 4918-4927.
- 32 Somlo M, Slonimski PP (1966) Differences between the properties of physiological L-lactate dehydrogenase and L-lactate dehydrogenase crystallized from yeast. *Biochimie* **48**, 1221-1249.
- 33 Cunane LM, Barton JD, Chen Z, Lê KH, Amar D, Lederer F & Mathews FS (2005) Crystal structure analysis of recombinant rat kidney long chain hydroxy acid oxidase. *Biochemistry* **44**, 1521-1531.
- 34 Labeyrie F, Baudras A & Lederer F (1978) Flavocytochrome *b₂* or L-lactate cytochrome *c* reductase from yeast. *Methods in enzymology* **53**, 238-256.
- 35 Mitra B, Gerlt JA, Babbitt PC, Koo CW, Kenyon GL, Joseph D & Petsko GA (1993) A novel structural basis for membrane association of a protein: construction of a chimeric soluble mutant of (S)-mandelate dehydrogenase from *Pseudomonas putida*. *Biochemistry* **32**, 12959-12967.
- 36 Sukumar N (2003) High Resolution Structures of an Oxidized and Reduced Flavoprotein: The Water Switch in a Soluble Form of (S)-Mandelate Dehydrogenase. *The Journal of biological chemistry* **279**, 3749-3757.
- 37 Umena Y, Yorita K, Matsuoka T, Kita A, Fukui K & Morimoto Y (2006) The crystal structure of L-lactate oxidase from *Aerococcus viridans* at 2.1 Å resolution reveals the mechanism of strict substrate recognition. *Biochemical and biophysical research communications* **350**, 249-256.
- 38 Xia Z & Mathews FS (1990) Molecular structure of flavocytochrome *b₂* at 2.4 Å resolution. *Journal of molecular biology* **212**, 837-863.

- 39 Yasin M & Fewson CA (1993) L(+)-mandelate dehydrogenase from *Rhodotorula graminis*: purification, partial characterization and identification as a flavocytochrome b. *Biochemical journal* **293**, 455-460.
- 40 Racek J & Musil J (1987) Biosensor for lactate determination in biological fluids. I. Construction and properties of the biosensor. *Yeast* **162**, 129-139.
- 41 Wang J & Chen Q (1994) Enzyme microelectrode array strips for glucose and lactate. *Scanning* **66**, 1007-1011.
- 42 Das S, Glenn JH & Subramanian M (2010) Enantioselective oxidation of 2-hydroxy carboxylic acids by glycolate oxidase and catalase coexpressed in methylotrophic *Pichia pastoris*. *Biotechnology progress* **26**, 607-615.
- 43 Adam W, Lazarus M, Boss B, Saha-Möller CR, Humpf H & Schreier P (1997) Enzymatic resolution of chiral 2-hydroxy carboxylic acids by enantioselective oxidation with molecular oxygen catalyzed by the glycolate oxidase from spinach (*Spinacia oleracea*). *The Journal of organic chemistry* **62**, 7841-7843.
- 44 Müh U, Massey V & Williams CH (1994) Lactate Monooxygenase. I. Expression of the mycobacterial gene in *Escherichia coli* and site-directed mutagenesis of lysine 266. *The Journal of biological chemistry* **269**, 7982-7988.
- 45 Müh U, Williams CH & Massey V (1994) Lactate monooxygenase. III. Additive contributions of active site residues to catalytic efficiency and stabilization of an anionic transition state. *The Journal of biological chemistry* **269**, 7994-8000.
- 46 Wierenga RK, Drenth J, Schulz GE (1983) Comparison of the three-dimensional protein and nucleotide structure of the FAD-binding domain of p-hydroxybenzoate hydroxylase with the FAD- as well as NADPH-binding domains of glutathione reductase. *Journal of molecular biology* **167**, 725-739.
- 47 Hecht HJ, Kalisz HM, Hendle J, Schmid RD, Schomburg D. (1993) Crystal structure of glucose oxidase from *Aspergillus niger* refined at 2.3 Å resolution. *Journal of molecular biology* **229**, 153-172.
- 48 Mattevi A, Vanoni MA, Todone F, Rizzi M, Teplyakov A, Coda A, Bolognesi M, Curti B. (1996) Crystal structure of D-amino acid oxidase: a case of active site mirror-image convergent evolution with flavocytochrome *b₂*. *Proceedings of the National Academy of Sciences of the United States of America* **93**, 7496-7501.
- 49 Furuichi M, Suzuki N, Dhakshnamoorthy B, Minagawa H, Yamagishi R, Watanabe Y, Goto Y, Kaneko H, Yoshida Y & Yagi H (2008) X-Ray structures of *Aerococcus viridans* lactate oxidase and its complex with D-lactate at pH 4.5 show an α -hydroxyacid oxidation mechanism. *Journal of molecular biology* **378**, 436-446.
- 50 Li S, Umena Y, Yorita K, Matsuoka T, Kita A, Fukui K & Morimoto Y (2007) Crystallographic study on the interaction of L-lactate oxidase with pyruvate at 1.9 Angstrom resolution. *Biochemical and biophysical research communications* **358**, 1002-1007.
- 51 Lindqvist Y, Branden C, Mathews FS & Lederer F (1991) Spinach glycolate oxidase and yeast flavocytochrome *b₂* are structurally homologous and evolutionarily related enzymes with distinctly different function and flavin mononucleotide binding. *The Journal of biological chemistry* **266**, 3198-3207.
- 52 Sukumar N, Xu Y, Gatti DL, Mitra B & Mathews FS (2001) Structure of an active soluble mutant of the membrane-associated (S)-mandelate dehydrogenase. *Biochemistry* **40**, 9870-9878.
- 53 Tegoni M, Begotti S, Cambillad C, Aiguier CJ, Cedex M, Biochimiche S & Parma U (1995) X-ray structure of two complexes of the Y143F flavocytochrome. *Biochemistry* **34**, 9840-9850.
- 54 Cunane LM, Barton JD, Chen Z, Welsh FE, Chapman SK, Reid Ga & Mathews FS (2002) Crystallographic study of the recombinant flavin-binding domain of baker's yeast flavocytochrome b(2): Comparison with the intact wild-type enzyme. *Biochemistry* **41**, 4264-4272.

- 55 Mowat CG, Beaudoin I, Durley RC, Barton JD, Pike AD, Chen Z, Reid GA, Chapman SK, Mathews FS & Lederer F (2000) Kinetic and crystallographic studies on the active Site Arg289Lys mutant of flavocytochrome b_2 (yeast L-lactate dehydrogenase). *Biochemistry* **39**, 3266-3275.
- 56 Mowat CG, Wehenkel A, Green AJ, Walkinshaw MD, Reid Ga & Chapman SK (2004) Altered substrate specificity in flavocytochrome b_2 : structural insights into the mechanism of L-lactate dehydrogenation. *Biochemistry* **43**, 9519-9526.
- 57 Xu Y & Mitra B (1999) A highly active, soluble mutant of the membrane-associated (S)-mandelate dehydrogenase from *Pseudomonas putida*. *Biochemistry* **38**, 12367-12376.
- 58 Ghir R & Lederer F (1981) Study of a zone highly sensitive to proteases in flavocytochrome b_2 from *Saccharomyces cerevisiae*. *European journal of biochemistry* **120**, 279-287.
- 59 Murray MS, Holmes RP & Lowther WT (2008) Active site and loop 4 movements within human glycolate oxidase: implications for substrate specificity and drug design. *Biochemistry* **47**, 2439-2449.
- 60 Dewanti AR & Mitra B (2003) A transient intermediate in the reaction catalyzed by (S)-mandelate dehydrogenase from *Pseudomonas putida*. *Biochemistry* **42**, 12893-12901.
- 61 Miles CS, Rouvière-Fourmy N, Lederer F, Mathews FS, Reid GA, Black MT, Chapman SK (1992) Tyr-143 facilitates interdomain electron transfer in flavocytochrome b_2 . *Biochemical journal* **285**, 187-192.
- 62 Massey V, Ghisla S & Kischke K (1980) Studies on the reaction mechanism of lactate oxidase. Formation of two covalent flavin-substrate adducts on reaction with glycolate. *The Journal of biological chemistry* **255**, 2796-2806.
- 63 Ghisla S & Massey V (1980) Studies on the catalytic mechanism of lactate oxidase. Formation of enantiomeric flavin-N(5)-glycolyl adducts via carbanion intermediates. *The Journal of biological chemistry* **255**, 5688-5696.
- 64 Sobrado P & Fitzpatrick PF (2003) Solvent and primary deuterium isotope effects show That lactate CH and OH Bond cleavages are concerted in Y254F flavocytochrome b_2 , consistent with a hydride transfer mechanism. *Biochemistry* **42**, 15208-15214.
- 65 Walsh C, Lockridge O, Massey V & Abeles R (1973) Studies on the mechanism of action of the flavoenzyme lactate oxidase. Oxidation and elimination with beta-chlorolactate. *The Journal of biological chemistry* **248**, 7049-7054.
- 66 Fitzpatrick PF (2001) Substrate dehydrogenation by flavoproteins. *Accounts of chemical research* **34**, 299-307.
- 67 Müh U, Williams CH & Massey V (1994) Lactate monooxygenase II: Site-directed mutagenesis of the postulated active site base histidine 290. *The Journal of biological chemistry* **269**, 7989-7993.
- 68 Tabacchi G, Zucchini D, Caprini G, Gamba A, Lederer F, Vanoni MA & Fois E (2009) L-lactate dehydrogenation in flavocytochrome b_2 . A first principles molecular dynamics study. *FEBS Journal* **276**, 2368-2380.
- 69 Miles CS, Rouvière-fourmy N, Lederer F, Mathews FS, Reid GA, Black MT & Chapman SK (1992) Tyr-143 facilitates interdomain electron transfer in flavocytochrome b_2 . *Biochemical Journal* **285**, 187-192.
- 70 Rouvière-Fourmy N, Capeillère-Blandin C, Lederer F. (1994) Role of Tyrosine 143 in lactate dehydrogenation by flavocytochrome. Primary kinetic isotope effect studies with a phenylalanine mutant. *Biochemistry* **33**, 798-806.
- 71 Gaume B, Sharp R, Manson F, Chapman S, Reid G & Lederer F (1995) Mutation to glutamine of histidine 373, the catalytic base of flavocytochrome b_2 (L-lactate dehydrogenase). *Biochimie* **77** 621-630.

- 72 Müh U, Massey V & Williams CH (1994) Lactate monooxygenase: I. Expression of the mycobacterial gene in *Escherichia coli* and site-directed mutagenesis of lysine 266. *The Journal of biological chemistry* **269**, 7982-7988.
- 73 Müh U, Williams CH & MASSEY V (1994) Lactate Monooxygenase: III. Additive contributions of active site residues to catalytic efficiency and stabilization of an anionic transition state. *The Journal of biological chemistry* **269**, 7994-8000.
- 74 Dubois J, Chapman SK, Mathews FS, Reid GA & Lederer F (1990) Substitution of Tyr254 with Phe at the active site of flavocytochrome b_2 : consequences on catalysis of lactate dehydrogenation. *Biochemistry* **29**, 6393-6400.
- 75 Tegoni M & Cambillau C (1994) Structural studies on recombinant and point mutants of flavocytochrome b_2 . *Biochimie* **76**, 501-14.
- 76 Massey V (1994) Activation of molecular oxygen by flavins and flavoproteins. *The Journal of biological chemistry*. **269**, 22459-22462.
- 77 Eberlein G, Bruice TC (1983) The chemistry of a 1,5-diblocked flavin. 2. Proton and electron transfer steps in the reaction of dihydroflavins with oxygen. *Journal of the american chemical society* **105**, 6685-6697.
- 78 Pennati A, Gadda G (2011) Stabilization of an intermediate in the oxidative half-reaction of human liver glycolate oxidase. *Biochemistry* **50**, 1-3.
- 79 Leiros I, Wang E, Rasmussen T, Oksanen E, Repo H, Petersen SB, Heikinheimo P & Hough E (2006) The 2.1 Å structure of *Aerococcus viridans* L-lactate oxidase (LOX). *Acta crystallographica section F structural biology and crystallization communications* **62**, 1185-1190.
- 80 Boubacar aK, Pethe S, Mahy J & Lederer F (2007) Flavocytochrome b_2 : reactivity of its flavin with molecular oxygen. *Biochemistry* **46**, 13080-13088.
- 81 Balme A, Brunt CE, Pallister RL, Chapman SK & Reid GA (1995) Isolation and characterization of the flavin-binding domain of flavocytochrome b_2 expressed independently in *Escherichia coli*. *Biochemical journal* **309**, 601-605.
- 82 Iwatsubo V & Labeyrie F (1975) Rapid kinetic studies of partial reactions in the heme free derivative of L-lactate cytochrome. *Biochemistry* **16**, 3558-3566.
- 83 Rouviere N, Mayer M, Tegoni M, Capeille C & Lederer F (1997) Molecular interpretation of inhibition by excess substrate in flavocytochrome b_2 : A Study with wild-type and Y143F mutant enzymes. *Biochemistry* **36**, 7126-7135.
- 84 Barber M & Solomonson L Assimilatory nitrate reductase. In *Biochemistry of Flavoenzymes* (Müller F), vol III, pp. 319-329. CRC Press, Boca Raton, Fl.
- 85 Le KH & Lederer F (1983) On the presence of a heme-binding domain homologous to cytochrome b_5 in *Neurospora crasse* assimilatory nitrate reductase. *EMBO Journal* **2**, 1909-1914.
- 86 Reinsch J, Feinberg B & Mc Farland J (1980) Intermediates during the fatty acid acyl CoA dehydrogenase catalyzed reduction of electron transfer flavoprotein by fatty acyl CoA esters. *Biochemical and biophysical research communications* **94**, 1409-1416.
- 87 Dewanti AR, Xu Y & Mitra B (2004) Role of glycine 81 in (S)-mandelate dehydrogenase from *Pseudomonas putida* in substrate specificity and oxidase activity. *Biochemistry* **43**, 10692-10700.
- 88 Sutton WB (1957) Mechanism of action and crystallization of lactic oxidative decarboxylase from *Mycobacterium phlei*. *The Journal of biological chemistry* **226**, 395-405.
- 89 Dixon M (1971) The acceptor specificity of flavins and flavoproteins, III. Flavoproteins. *Biochimica et biophysica acta* **226**, 269-284.
- 90 Schuman M & Massey V (1971) Effect of anions on the catalytic activity of pig liver glycolic acid oxidase. *Biochimica biophysica acta* **227**, 521-37.

- 91 Cromartie TH & Walsh CT (1975) Rat kidney L-alpha-hydroxy acid oxidase: Isolation of enzyme with one flavine coenzyme per two subunits. *Biochemistry* **14**, 2588-2596.
- 92 Jijun T, Jie H, Zhongchao H, Min P, Yuquan C (2005) A novel lactate biosensor. *Annual international conference of the IEEE engineering in medicine and biology - Proceedings* **7**, 252-254.
- 93 Hirano K, Yamato H, Kunimoto K, Ohwa M (2002) Design of novel electron mediators based on indophenol derivatives for lactate sensor. *Biosensors and bioelectronics* **17**, 315-322.
- 94 Hirano K, Yamato H, Kunimoto K, Ohwa M (2001) Novel electron transfer mediators based on dichloroindophenol derivatives for lactate oxidase. *Journal of electroanalytical chemistry* **510**, 149-152.
- 95 Filipe A, Belmouden A, Lacombe J & Lederer F (1997) Long-chain α -hydroxy acid oxidase: Substitution of the active site Phe23 with tyrosine. In *Flavins and Flavoproteins 1996* (Stevenson L, Massey V, & Williams C), pp. 559-562. University of Calgary Press, Calgary.
- 96 Yorita K, Matsuoka T, Misaki H & Massey V (2000) Interaction of two arginine residues in lactate oxidase with the enzyme flavin: Conversion of FMN to 8-formyl-FMN. *Proceedings of the National Academy of Sciences of the United States of America* **97**, 13039-13044.
- 97 Lehoux IE & Mitra B (2000) Role of arginine 277 in (S)-mandelate dehydrogenase from *Pseudomonas putida* in substrate binding and transition state stabilization. *Biochemistry* **39**, 10055-10065.
- 98 Dewanti AR, Xu Y & Mitra B (2004) Esters of mandelic acid as substrates for (S)-mandelate dehydrogenase from *Pseudomonas putida*: Implications for the reaction mechanism. *Biochemistry* **43**, 1883-1890.
- 99 Sinclair R, Reid GA & Chapman SK (1998) Re-design of *Saccharomyces cerevisiae* flavocytochrome b_2 : introduction of L-mandelate dehydrogenase activity. *Biochemical journal* **120**, 117-120.
- 100 Yorita K, Aki K, Ohkuma-Soyejima T, Kokubo T, Misaki H & Massey V (1996) Conversion of L-lactate oxidase to a long chain α -hydroxyacid oxidase by site-directed mutagenesis of alanine 95 to glycine. *The Journal of biological chemistry* **271**, 28300-28305.
- 101 Sun W, Williams CH & Massey V (1996) Site-directed Mutagenesis of Glycine 99 to alanine in L-lactate monooxygenase from *Mycobacterium smegmatis*. *The Journal of biological chemistry* **271**, 17226-17233.
- 102 Chaiyen P, Fraaije MW, Mattevi A (2012) The enigmatic reaction of flavins with oxygen. *Trends in biochemical sciences* **37**, 373-380.
- 103 Winter RT, Fraaije MW (2012) Applications of flavoprotein oxidases in organic synthesis: novel reactivities that go beyond amine and alcohol oxidation. *Current organic chemistry* **16**, 2542-2550.
- 104 Leferink NGH, Fraaije MW, Joosten HJ, Schaap PJ, Mattevi A, van Berkel WJH (2009) Identification of a gatekeeper residue that prevents dehydrogenases from acting as oxidases. *The Journal of biological chemistry* **284**, 4392-4397.
- 105 Urban P, Chirat I, Lederer F (1988) Rat kidney L-2-hydroxyacid oxidase. Structural and mechanistic comparison with flavocytochrome b_2 from baker's yeast. *Biochemistry* **27**, 7365-7371.

- 2 Engineering of *Aerococcus viridans* L-lactate oxidase for site-specific PEGYLATION: characterization and chemical modification of a S218C mutant**

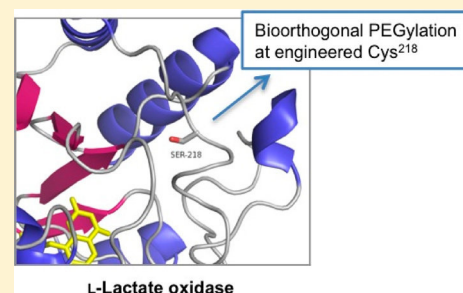
Engineering of *Aerococcus viridans* L-Lactate Oxidase for Site-Specific PEGylation: Characterization and Selective Bioorthogonal Modification of a S218C Mutant

 Birgit Unterweger,[†] Thomas Stoisser,[†] Stefan Leitgeb,[†] Ruth Birner-Grünberger,[‡] and Bernd Nidetzky^{*†}
[†]Research Center Pharmaceutical Engineering, and Institute of Biotechnology and Biochemical Engineering, Graz University of Technology, Petersgasse 12, A-8010 Graz, Austria

[‡]Institute of Pathology and Center for Medical Research, Medical University of Graz, Stiftingtalstraße 24, A-8010 Graz, Austria

S Supporting Information

ABSTRACT: A defined bioconjugate of *Aerococcus viridans* L-lactate oxidase and poly(ethylene glycol) 5000 was prepared and characterized in its structural and functional properties in comparison to the unmodified enzyme. Because the L-lactate oxidase in the native form does not contain cysteines, we introduced a new site for chemical modification via thiol chemistry by substituting the presumably surface-exposed serine-218, a nonconserved residue in the amino acid sequence, with cysteine. The resulting S218C mutant was isolated from *Escherichia coli* and shown in kinetic assays to be similarly (i.e., about half as) active as the native enzyme, thus validating the structure-guided design of the mutation. Using maleimide-activated methoxypoly(ethylene glycol) 5000 in about 10-fold molar excess over protein, the S218C mutant was converted in high yield (94%) into PEGylated derivative, while the native enzyme was totally unreactive under equivalent conditions. PEGylation caused only a relatively small decrease (30%) in the specific activity of the S218C mutant, and it did not change the protein stability. PEGylation went along with enhancement of the apparent size of the homotetrameric L-lactate oxidase in gel permeation chromatography, from 170 kDa to 250 kDa. The protein hydrodynamic diameter determined by dynamic light scattering increased from 11.9 nm in unmodified S218C mutant to 16.4 nm in the PEGylated form. Site-selective PEGylation of the mutated L-lactate oxidase, using orthogonal maleimide–thiol coupling, could therefore facilitate incorporation of the enzyme into biosensors currently employed for determination of blood L-lactate levels, and it could also support different applications of the enzyme in applied biocatalysis.



■ INTRODUCTION

Covalent grafting of poly(ethylene glycol) chains on proteins, in short, “PEGylation”, is a powerful technique to optimize the structure and function of a given protein for a destined application.^{1–4} One major use of PEGylation is in the development of protein biopharmaceuticals for human therapy where PEGylated proteins often display longer in vivo circulating half-lives than the native (unPEGylated) counterparts.⁵ PEGylation has also been used widely in the preparation of apt molecular sensors for diagnostic assays.^{6–9} Moreover, it has been employed to enhance activity and stability of enzymes, particularly for biocatalysis in nonaqueous solvents.^{3,10–12} Recent studies emphasize another interesting effect of PEGylation that is in fine-tuning of protein interactions with surfaces.^{13,14} PEGylated lysozyme, for example, showed attenuated adsorption and aggregation on solid surfaces as compared to the unconjugated protein.¹⁴ In addition, PEGylation increased the reversibility of adsorption of lysozyme on solid supports.¹⁴

PEG–protein conjugates are often prepared by reaction of the protein with PEG molecules having amine-reactive end-groups.⁴ Because it is typical for most proteins to contain a

variety of internal amine groups from lysine residues in addition to the N-terminal amine, the resulting PEGylation is normally quite heterogeneous in the number and placement of the PEG chains. Heterogeneity in the structure may hinder the biological activity, and separation of the individual PEGylated forms is usually not practical.⁴ It is therefore important to generate well-defined PEG–protein conjugates, and site-selective derivatization is probably the best way to obtain such biomolecules.^{2,4,15,16} Cysteine residues are often the targets for site-specific modification using thiol chemistry.^{2,17–20} Proteins lacking a cysteine in their native structure can be genetically engineered to incorporate one or more cysteines in specific positions, which are usually chosen away from the protein functional site to minimize possible interference of chemical modification with the biological activity. Even though the literature gives a few examples of site-specific PEGylation of proteins at newly introduced cysteines,^{21–23} it is also clear from these studies that the overall approach remains a difficult

Received: January 2, 2012

Revised: May 11, 2012

Published: May 31, 2012

challenge that necessitates useful coordination of protein design with cysteine-directed conjugation.

L-Lactate oxidase (EC 1.13.12.4; LOX) is a flavin mononucleotide (FMN)-dependent enzyme that catalyzes oxidation of L-lactate into pyruvate.²⁴ O₂ serves as the terminal electron acceptor of the enzymatic reaction that gives H₂O₂ as its second product. LOX has its major uses in medical analytics where the enzyme is applied widely as biological transducer of different biosensors and test strips.^{25–27} LOX from the bacterium *Aerococcus viridans* has been well-characterized biochemically,²⁴ and a high-resolution crystal structure has been determined for this homotetrameric enzyme.^{28,29} Each subunit of about 41 kDa size contains one FMN that is bound noncovalently. The *A. viridans* LOX does not contain cysteine residues. Here, a potentially useful concept of bioconjugation by design is proposed for this LOX that exploits cysteine-directed chemical modification of a mutated LOX (having residue Ser²¹⁸ replaced by Cys; S218C mutant) with PEG molecule containing maleimide end-group. The modification is shown to proceed selectively and in quantitative yields. About 30% of original biological activity of the wild-type enzyme is retained in PEGylated S218C mutant.

The enzymatically active part of the lactate biosensor is usually a thin solid film in which the used LOX is immobilized through the combined physical effects of adsorption to and entrapment within the matrix materials.^{30–32} Of note, the often irreversible adsorption to the film can result in substantial activity loss, and controlled PEGylation of the enzyme might help preventing it (see ref 14 for the case of lysozyme). In the absence of covalent fixation, strength of retention of the enzyme in the matrix can present another problem. Even though chemical cross-linking with a bifunctional reagent such as glutardialdehyde presents a possible solution, there are the clear disadvantages that the cross-linking very often results in large losses of the enzyme activity, and homogeneous distribution of the cross-linked, sometimes partly insoluble enzyme in the matrix can become a serious issue.³³ A method providing controlled size enhancement for the soluble LOX would facilitate stable embedment of the enzyme in the sensor matrix, and it should additionally be compatible with the currently used immobilization procedures. It might also have favorable effects on enzyme adsorption on the biosensor film (considering ref 14). Nonselective (random) PEGylation was previously applied to a maltose biosensor⁶ as well as glucose oxidase,^{7,8} and the resulting bioconjugates showed useful properties for sensor development. The results presented herein open up the possibility to provide selectively PEGylated LOX for biosensor applications. Other applications of the enzyme in applied biocatalysis^{34,35} could also benefit from the reported developments.

EXPERIMENTAL PROCEDURES

Materials. Monomethoxypoly(ethylene glycol) maleimide (mPEG-mal) 5000, L-(+)-lactic acid, (S)-2-hydroxybutyric acid, and (S)-2-hydroxyisocaproic acid in the highest available purity, 3,3-dimethylglutaric acid, 4-aminoantipyrine, peroxidase from horseradish, *N,N*-dimethylaniline, and dodecylbenzenesulfonic acid were all obtained from Sigma Aldrich. Lyophilized wild-type LOX from *Aerococcus viridans* (WT) was a gift of Roche Diagnostics GmbH. Enzyme was stored at –25 °C until further use. The plasmid pLO-1, which harbored the LOX gene, was kindly provided by Dr. T. Meier (Roche).

Molecular Cloning and Site-Directed Mutagenesis. Mutations leading to substitution of Ser²¹⁸ by Cys were introduced by a two-stage polymerase chain reaction, using a protocol from the literature.³⁶ Briefly, two separate primer extension reactions were carried out in which pLO-1 was used as the template and one of the two mutagenic oligonucleotide primers was also present. The two primers were 5'-GGTGCTTGCAAACAAAAAATCTCACCAAGA-GA-TATTG-3' (termed S218Cfw; melting point: 61.3 °C), and 5'-TTGTTTGCAAGCACCGTAGAT-ATTGTTTAATGACATACC-3' (termed S218Crev; melting point: 61.3 °C). DNA was amplified by Pfu DNA Polymerase (Promega) using the following conditions: heat denaturation at 95 °C for 1 min; 4 elongation cycles, each consisting of 95 °C for 50 s, 59 °C for 50 s, and 68 °C for 10 min; final extension at 68 °C for 7 min, and cooling at 4 °C. The two separate PCR mixtures were combined in a volume ratio of 1:1, and another PCR was performed under the conditions above, but with a total repeat of 18 cycles. Template DNA was digested with *DpnI* at 37 °C for 1 h. Plasmid DNA was transformed into electrocompetent *E. coli* BL21 (DE3) cells. After regeneration, the cells were cultured overnight at 37 °C on LB-amp plates (1% peptone, 0.5% yeast extract, 0.5% NaCl, 1.8% agar supplemented with 100 µg/mL ampicillin). Only transformants carrying plasmids with the mutation of interest verified by DNA sequencing were used for further steps.

Production of S218C Mutant. *Escherichia coli* BL21 (DE3) was grown overnight as starter culture in medium containing 5.5 g/L glucose monohydrate, 10 g/L peptone, 5 g/L yeast extract, 5 g/L NaCl, 1 g/L NH₄Cl, 0.25 g/L MgSO₄ monohydrate, 3 g/L K₂HPO₄, 6 g/L KH₂PO₄, 2 mg/L thiamine, 115 mg/L ampicillin, 4 mg/L FeSO₄ heptahydrate, 1 mg/L MnSO₄ monohydrate, 0.4 mg/L CoCl₂, 0.15 mg/L CuSO₄ pentahydrate, 0.1 mg/L H₃BO₃, 0.2 mg/L ZnSO₄ heptahydrate, 0.2 mg/L Na₂MoO₄ dihydrate, and 0.4 mg/L AlCl₃. About 100 µL poly(propylene glycol) was added per L medium. The main culture was prepared from the same medium except that a 4-fold higher amount of glucose monohydrate was used. It was inoculated to an OD₆₀₀ of 0.5. Cultivation was performed in B. Braun Biotech International BiostatC, Type CT5–2 bioreactor. Temperature, stirring, pH, and oxygen partial pressure were controlled and adjusted automatically. The pH was controlled at pH 7.0 using 2 M KOH and 1 M H₃PO₄; the pO₂ was fixed to a minimum of 40%. The cells were grown at 37 °C before induction. At an OD₆₀₀ of about 2, isopropyl β-D-1-thiogalactopyranoside was added to a final concentration of 0.25 mM. Upon induction, the cells were cultured at 30 °C. When the level of glucose had decreased to a level <1 g/L (Diabur Test 5000, Roche Diagnostics), the cells were harvested by centrifugation. About 33 g wet cell mass/L was obtained. The cell pellet was suspended in 50 mM potassium phosphate buffer, pH 7.0, and stored at –25 °C.

Protein Purification. All steps were performed in 50 mM potassium phosphate buffer, pH 7.0. Cells were disrupted in a French press, and the crude extract was obtained by centrifugation. Protein was precipitated in the presence of 1.5 M (NH₄)₂SO₄ at 4 °C, and precipitate was removed by centrifugation. The S218C mutant remaining in the supernatant was further purified by hydrophobic interaction chromatography using a Phenyl Sepharose 6 Fast Flow (High Sub) column (GE Healthcare Life Sciences; 64 mL) and the Äkta FPLC system (Amersham Biosciences). The protein

(about 100 mg in total) was loaded on the column equilibrated with buffer and eluted at 25 °C with a linearly decreasing gradient of $(\text{NH}_4)_2\text{SO}_4$. The flow rate was 5 mL/min, and eluted protein was detected at 280 nm. Fractions containing LOX activity were pooled. Purity was checked with SDS-PAGE, using PhastGel Gradient 8–25 (GE Healthcare Life Sciences) gels and the Pharmacia High Speed Electrophoresis System (Pharmacia Biotech). Enzyme solution was then desalted by repeated cycles of concentration and dilution using concentrator tubes (Vivaspin 20, 10 kDa cutoff, Vivascience AG) and stored in 50 mM potassium phosphate buffer, pH 7.0, at –25 °C until further use.

Assays. LOX activity was measured using a peroxidase-coupled spectrophotometric assay (Sigma) in which the H_2O_2 produced in the LOX reaction is further reacted with peroxidase in the presence of 4-aminoantipyrine and *N,N*-dimethylaniline to give a quinonediimine dye that is detected. About 5 to 10 μL of enzyme appropriately diluted in 50 mM potassium phosphate buffer, pH 7.0, was added to a solution containing 40 mM 3,3-dimethylglutaric acid, 2.5 units peroxidase, 1.5 mM 4-aminoantipyrine, 50 mM L-(+)-lactic acid, and 0.04% (v/v) *N,N*-dimethylaniline in a total volume of 0.5 mL. The pH of the solution was pH 6.5. After a reaction time of between 10 and 20 min at 37 °C, 1 mL of 0.25% (w/v) dodecylbenzenesulfonic acid was added to stop the reaction. The produced quinonediimine dye was measured spectrophotometrically at 565 nm with a Varian Cary 50 Bio UV–visible spectrophotometer at 25 °C.

Protein concentrations were measured according to the Bradford protein quantification assay (Roti-Quant, Carl Roth GmbH + Co KG) using BSA as reference. Note: the commercial preparation of LOX was not used for calibration of the protein assay. The enzyme is a solid powder that contains various substances other than target enzyme. Calibration based on solid mass is therefore not possible.

PEGylation. PEGylation was done according to a procedure adopted from the literature.²⁰ Briefly, the purified S218C mutant (8 μM) was incubated in the presence of different molar excesses of mPEG-mal 5000 in 50 mM potassium phosphate buffer, pH 7.0, at 4 °C for up to 7 h under gentle agitation (300 rpm; Eppendorf Thermomixer). The molar ratio of mPEG-mal 5000 to protein was varied in several steps in the range 1–12.5. Samples were taken and processed after 2, 4, and 7 h. To remove residual mPEG-mal 5000, repeated ultrafiltration with Vivaspin 6 centrifugal concentrator tubes (10 kDa cutoff, Vivascience AG) was performed. The PEGylated S218C mutant was used immediately for further characterization. The wild-type enzyme was treated in exactly the same manner for reference. To determine if residual free PEG that was not removed by the ultrafiltration could affect the measured enzyme activities, we performed controls in which PEG 4000 was added to the assays. The PEG 4000 was used in 12.5-fold molar excess over protein (WT; S218C mutant).

Mass Spectrometry. MALDI-TOF (time-of-flight)-MS measurements were performed on a Bruker Ultraflex-treme instrument. Protein solutions (2.4 mg/mL PEGylated enzyme; 7.2 mg/mL unPEGylated enzyme) in 50 mM potassium phosphate buffer (pH 7.0) were diluted in 50% acetonitrile and 0.1% trifluoroacetic acid 1:5 (v/v). They were mixed 1:1 (v/v) with a suspension of 5 mg super-DHB matrix (Sigma; 9:1 mixture of 2,5-dihydroxybenzoic acid and 2-hydroxy-5-methoxybenzoic acid) in 50 μL acetonitrile and 50 μL 0.1% trifluoroacetic acid. One microliter was spotted onto an 800

μm Bruker MTP Anchorchip and left to dry. Full MS spectra were obtained in positive linear mode after external calibration using an appropriate protein standard (10–70 kDa) in the mass/charge range from 550 to 73 000 by summarizing 9000 laser shots.

Internal sequence information of PEGylated LOX as confirmed by the detected mass shifts in MALDI-TOF analysis was received from LC-MS/MS. Details of the experimental protocol are given in the Supporting Information. The LC-MS/MS data were analyzed by searching the amino acid sequence of LOX of *Aerococcus viridans* (NCBI accession number ZP_06807595), with Mascot 2.2 (MatrixScience) contained in a database including known contaminants such as the enzymes used for digestion and human keratins. PEGylation with 110 and 111 monomeric units (the two most abundant masses of PEG 5000) was included as variable modification at Cys or the protein N-terminus next to carbamidomethylation on Cys as variable modification. A maximum false discovery rate of 5% using decoy database search, an ion score cutoff of 20, and a minimum of 2 identified peptides was chosen as identification criteria.

Absorbance Spectroscopy. UV–vis absorbance spectra were recorded with a Varian Cary 50 Bio UV–visible Spectrophotometer in quartz cuvettes (Hellma GmbH & Co. KG) of 10 mm light path. About 0.1 mM enzyme in potassium phosphate buffer, pH 7.0, was scanned at 25 °C, and the values were corrected for blank readings. Determination of enzyme-bound cofactor was done by spectrophotometric quantification of free FMN at 445 nm. A molar extinction coefficient of 12500 $\text{M}^{-1} \text{cm}^{-1}$ was assumed, and the FMN was released from the enzyme (typically about 25 μM) by treatment with trifluoroacetic acid.³⁷

Kinetic Analysis. Initial rates of enzymatic oxidation of L-(+)-lactic acid or an alternative α -hydroxy acid substrate were obtained at pH 6.5 and 37 °C. A 50 mM potassium phosphate buffer was used. The substrate concentration was varied, typically at 10 different levels in the range 0.1–50 mM. The rates were recorded using the peroxidase-coupled spectrophotometric assay. Kinetic constants (K_M , V_{max}) were obtained from nonlinear fit of the Michaelis–Menten equation to the measured data using *Sigma Plot*. Turnover numbers (k_{cat}) were calculated from V_{max} using the relationship, $k_{\text{cat}} = V_{\text{max}}/E$ where E is the molar enzyme concentration. E was determined from the protein concentration assuming a molecular mass of 41 kDa for the enzyme subunit.

Stability of Enzyme Activity. Irreversible inactivation at 37 °C was measured. The enzyme (WT, PEGylated, or unmodified S218C mutant) was incubated in a concentration of 0.2–0.4 μM in 40 mM HEPES buffer (pH 8.1) containing 150 mM NaCl. An Eppendorf Thermomixer was used for temperature control and slight agitation. Samples were taken at different times, and residual enzyme activity was measured. Enzyme half-life times were determined by fitting an exponential decay function to the experimental time course.

Protein Conformational Stability. Differential scanning fluorimetry was used. This was performed with a Bio-Rad C1000 Thermocycler RT-PCR machine (CFX96 system) applying a general protocol reported elsewhere.³⁸ Experiments were done in 50 mM potassium phosphate buffer (pH 7.0) using 2–10 μM enzyme (WT, PEGylated or unmodified S218C mutant). SYPRO Orange (Invitrogen) was used as fluorescence probe. It was diluted 100-fold from the commercial stock solution (in dimethylsulfoxide) using

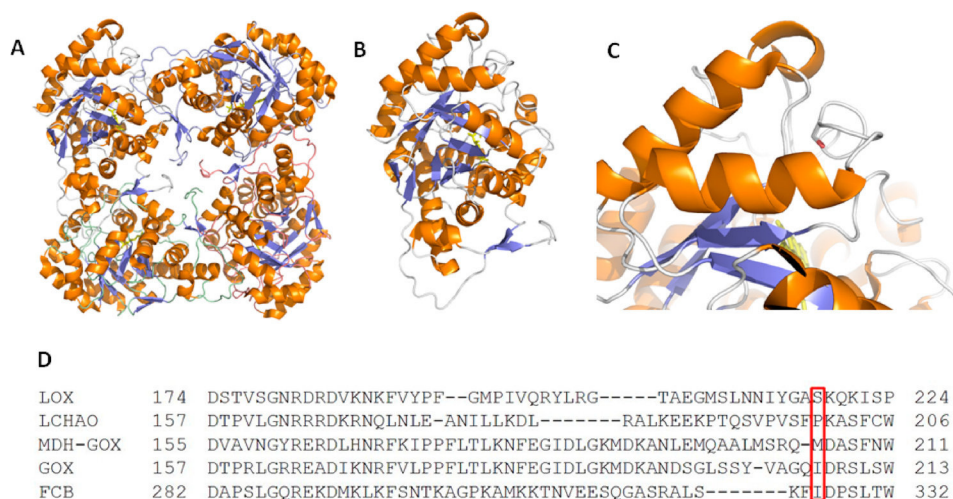


Figure 1. Structure of *A. viridans* LOX and selection of Ser²¹⁸ as site for site-directed substitution with cysteine and subsequent PEGylation via thiol chemistry: (A) the functional LOX homotetramer; (B) overall fold of monomer A of LOX; (C) loop 4 region with Ser²¹⁸ rendered as stick representation in CPK coloring. Structural data was from PDB-file 2DU2. Graphical representations were done in *Pymol 0.99*. Orange color represents helix regions, blue the sheet regions. The cofactor FMN is shown in stick representation in yellow. (D) Structure-based sequence alignment of the loop 4 between members of the family of α -hydroxy acid oxidases. LOX, L-lactate oxidase from *Aerococcus viridans*; LCHAO, rat kidney long-chain α -hydroxy acid oxidase; MDH-GOX, soluble chimeric mutant form of L-mandelate dehydrogenase from *Pseudomonas putida*, where parts of loop 4 were substituted by a corresponding GOX sequence part. GOX, glycolate oxidase from *Spinacia oleracea*; FCB, flavocytochrome b2 from *Saccharomyces cerevisiae*. The alignment was adapted from the literature.²⁸

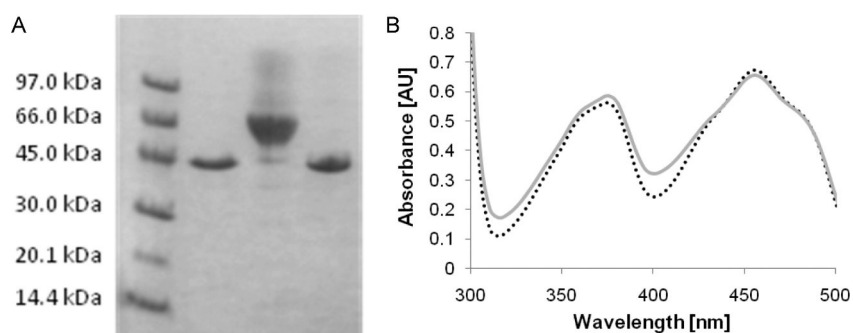


Figure 2. PEGylation of purified S218C mutant monitored by SDS-PAGE (A) and comparison of the visible absorbance spectrum of the mutated LOX with that of the wild-type enzyme. Panel A: lane 1, molecular mass markers; lane 2, unmodified WT; lane 3, PEGylated S218C; lane 4, WT LOX incubated under PEGylation conditions; about 10 μ g protein was applied on each lane. Panel B: WT (broken black line) and S218C (full light gray line). Spectra were recorded at an enzyme concentration of 0.1 mM in 50 mM potassium phosphate buffer, pH 7.0, at 25 $^{\circ}$ C. The enzyme molarity was calculated from the protein concentration, determined with the Bradford dye binding assay using BSA as reference. A molecular mass of 41 kDa was assumed. AU, arbitrary units.

phosphate buffer (50 mM; pH 7.0). Excitation and emission filters for SYPRO Orange were at 465 and 610 nm, respectively. Reactions were carried out in 96-well format using 25 μ L of total reaction volume each. Bio-Rad thin-wall PCR plates were used. Temperature was raised at 0.5 $^{\circ}$ C/min from 25 to 95 $^{\circ}$ C, and fluorescence intensity was measured every 0.5 $^{\circ}$ C. Fluorescence intensity increases when due to unfolding at elevated temperature hydrophobic surfaces are exposed in the protein, and SYPRO Orange binds to them. A control containing 25 μ M of each free FMN and wild-type enzyme was carried out in the absence of SYPRO Orange. Boltzmann sigmoid was used for data fitting, yielding a temperature of inflection of the transition curve (T_i), as shown in Figures S1 of Supporting Information. The T_i value is used here to characterize the conformational stabilities of the different protein preparations used. Reported T_i values are means of eight independent experiments.

Dynamic Light Scattering. Nanosizer ZS (Malvern) was used for measurement of particle size distribution. All samples (WT, S218C in PEGylated and unmodified form) were analyzed in triplicate. Protein concentrations of 1 mg/mL (24 μ M) were used. Proteins were dissolved in 50 mM potassium phosphate buffer (pH 7.0). The total volume of sample analyzed was 800 μ L. A DTS0012 disposable sizing cuvette was used. A temperature of 25 $^{\circ}$ C was applied, and the measurement time was 60 s. Samples were analyzed at a backscattering angle of 173 $^{\circ}$. The size distribution was automatically evaluated by the program *Zetasizer v 6.30*. Mean value and standard deviation were calculated out of the three independent measurements using the peak with the main intensity.

RESULTS AND DISCUSSION

Preparation of the S218C Mutant. The LOX from *A. viridans* that does not contain cysteines in its wild-type form

was mutated at position 218 (Figure 1) where a possibly sufficiently accessible Ser is positioned on the surface of the structure of the native protein. Ser²¹⁸ is situated on a loop that has been reported to be highly flexible in LOX,²⁸ as well as in related flavoenzymes of the α -hydroxyacid oxidase family.^{39–41} The relevant loop was seen to be disordered in several crystal structures, suggesting that Ser²¹⁸ of *A. viridans* LOX may not adopt a single defined structural position. In the crystal structure of wild-type LOX,²⁸ the inward-directed side-chain of Ser²¹⁸ would not be optimally available for reaction. However, conformational flexibility of the loop harboring Ser²¹⁸ was thought to be conducive to the intended site-directed protein modification. To further explain the choice of the mutation site, we must also emphasize that the native structure of the enzyme should be perturbed as little as possible by the site-specific substitution of a serine by cysteine. Candidate serine residues from highly conserved regions of the protein (e.g., the fully exposed Ser¹⁶³) were therefore not considered. Moreover, using Ser²¹⁸, the site for covalent attachment of a PEG molecule was considered to be sufficiently far away from the enzyme active site, as indicated by the FMN cofactor in the structure, to prevent interference with LOX function after derivatization of Cys²¹⁸. The resulting S218C mutant was obtained by expression in *E. coli*, and we show successful modification of the isolated mutant with mPEG-mal 5000.

Mutations in the native LOX gene (GenBank accession number: D50611.1) resulting in site-directed substitution of Ser²¹⁸ by Cys were introduced by a two-stage PCR employing a suitable pair of oligonucleotide primers. The mutated gene was verified by sequencing and placed into plasmid vector pLO-1 that provided target gene expression under control of the *tac* promoter. Enzyme production was done in *E. coli* BL21 (DE3) using controlled cultivation conditions in a 5 L stirred bioreactor. The S218C mutant was obtained in apparent electrophoretic homogeneity (Figure 2A) by using a two-step purification consisting of ammonium sulfate precipitation of non-LOX protein from *E. coli* cell extract followed by hydrophobic interaction chromatography. Table 1 shows a

Table 1. Purification of the S218C Mutant^a

purification step	specific activity [U/mg]	activity recovery [%]	total protein [mg] and activity [U]
Crude cell extract	15	100	1003/15000
(NH ₄) ₂ SO ₄ precipitation	24	89	564/13254
HIC pool 1	56	8	21/1193
HIC pool 2, after desalting	90 (\pm 5)	27	45/4022

^aData are based on the processing of 30 g wet biomass. HIC column chromatography was performed in 10 runs. Two pools denoted 1 and 2 were obtained. Pool 2 was used for further experiments.

summary of the purification. Figure S2 (panel A) in the Supporting Information displays the protein elution profile during hydrophobic interaction chromatography. Figure S2 (panel B) shows the different steps of the purification documented by SDS-PAGE. Note that a final step of desalting by repeated ultrafiltration, removing any residual (NH₄)₂SO₄ from the elution buffer, was important to recover mutated enzyme in a high specific activity and with good storage stability. Figure S2 shows that contaminating proteins of low molecular mass were removed by appropriate fraction collection during HIC. From a comparison of the specific

activity of the S218C mutant in the *E. coli* cell extract and the specific activity of the purified enzyme, we can estimate that the mutant was expressed to a level of 12% ($=15/90 \times 100$) of total intracellular protein. The mutated LOX was recovered in an overall yield of 27%. About 50 mg of purified enzyme was obtained from each liter of medium from the bioreactor.

Characterization of the S218C Mutant. The specific activity of the mutated LOX was measured with a standard peroxidase-coupled assay (Sigma) using 50 mM L-lactate as substrate. A value of 90 (\pm 10) units/mg was obtained. By way of comparison, the specific activity of wild-type LOX produced and purified in exactly the same way as the mutant was about 200 (\pm 25) U/mg. The commercial preparation of the wild-type enzyme (Roche Diagnostics) displayed identical specific activity (\sim 200 U/mg). Additionally, the commercial enzyme appeared to be essentially pure by the criterion of migration as single protein band in SDS-PAGE, as shown in the Supporting Information (Figure S2B). Therefore and because of convenient availability, we used the commercial LOX as a reference for the characterization of the S218C mutant. A more detailed kinetic comparison of the enzymes used in this study is shown later in Table 1.

Figure 2B shows an overlay of the visible absorbance spectra of S218C mutant and wild-type LOX, both recorded at an exactly comparable protein concentration. Each spectrum contains two prominent bands with wavelengths of maximum absorption at around 375 and 455 nm that are highly characteristic of the FMN cofactor in its oxidized form. The spectrum of the mutant was nearly superimposable on the reference spectrum, suggesting that binding of FMN to LOX was essentially unaffected by the site-directed substitution of Ser²¹⁸. The result also implies that catalytic constants for the two enzymes can be compared with the assumption of a similar occupancy of their respective FMN binding site. The saturation of both proteins with their FMN cofactor was determined to be close to 100% (WT: 0.98; S218C: 0.95).

PEGylation of the S218C Mutant. Different molar ratios of enzyme and mPEG-mal 5000 were tested for bioconjugate formation, and a 12.5-fold molar surplus of mPEG-mal 5000 was found to give exhaustive modification of the S218C mutant, as demonstrated by SDS-PAGE and MALDI-TOF MS. Figure 2A shows that the apparent molecular mass of wild-type LOX had not been affected by incubation with mPEG-mal 5000, suggesting the absence of PEGylation, as expected. The S218C mutant by contrast displayed a clear shift in apparent mass to a higher value due to the PEGylation reaction, indicating that derivatization of the mutated LOX had taken place. The absence of a prominent protein band corresponding to the unmodified mutant in the sample analyzed implies that the chemical modification of the S218C mutant had proceeded to near-completion under the conditions used. MS analysis of the S218C mutant prior to and after incubation with mPEG-mal 5000 gave more detailed information about the process of PEGylation. Figure 3 shows that the underivatized enzyme, which displayed the expected molecular mass of 41 kDa, had disappeared almost entirely from the protein sample after the PEGylation reaction, corroborating the results of SDS PAGE (Figure 2A). Two new macromolecular species were formed in the reaction, and they were present in different amounts. The by-far abundant species displayed a mass of 46 kDa, consistent with the notion that the unmodified S218C mutant had acquired the extra mass of +5 kDa resulting from attachment of one mPEG-mal 5000 to the protein at Cys²¹⁸. The second mass

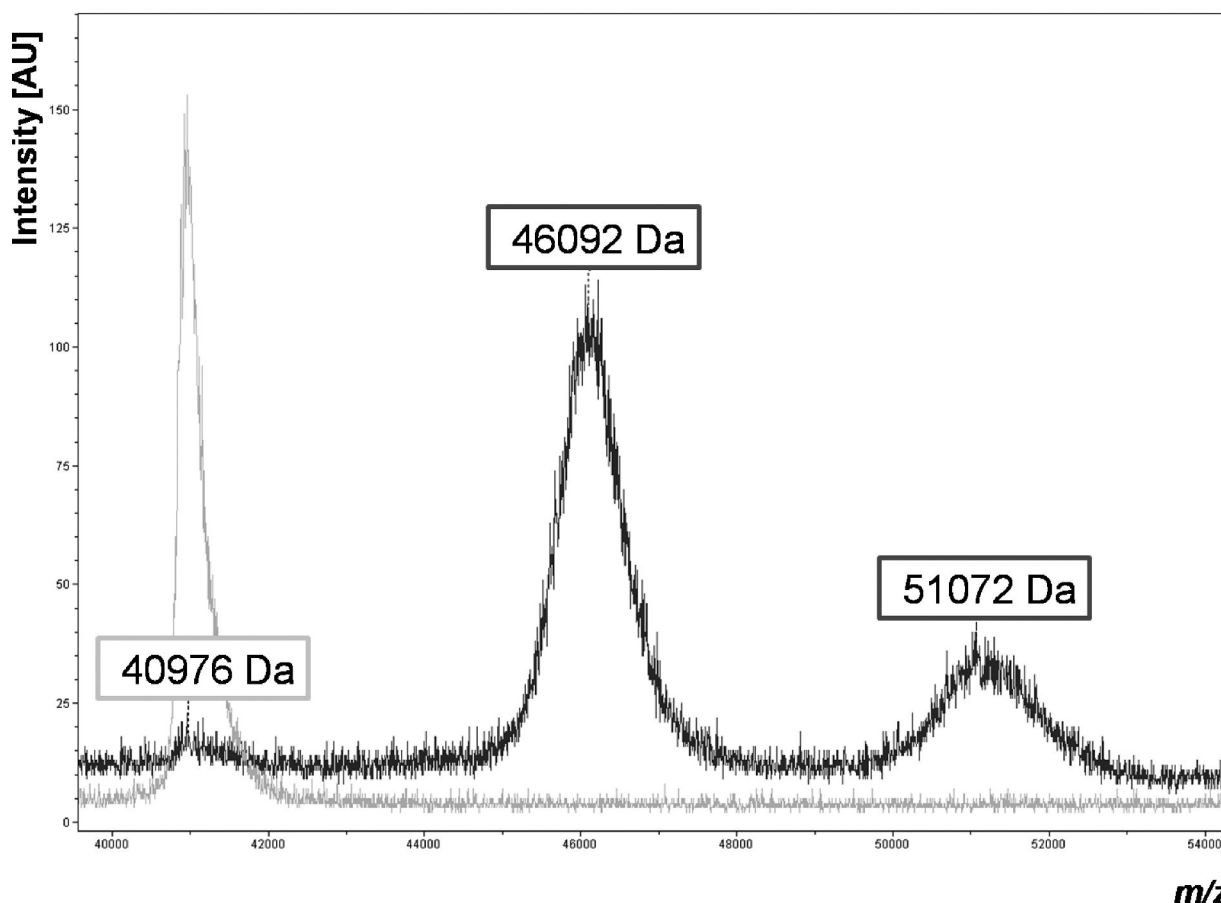


Figure 3. PEGylation of S218C mutant monitored by MS. Peaks at the indicated masses around 41 kDa, 46 kDa, and 51 kDa, respectively, represent unPEGylated (light gray line), monoPEGylated, and doubly PEGylated (dark gray line) S218C forms. AU, arbitrary units.

peak of 51 kDa could have originated from a double modification of the mutant. Assuming that the PEGylation(s) did not interfere with ionization of the protein, we estimated the relative quantities by integration of the peaks in Figure 3, which were determined to be 6% unmodified protein, 77% mono-, and 17% di-PEGylated protein.

Overall high sequence coverage was achieved by LC-MS/MS for all digested protein samples. For the PEGylated protein, 867 peptides were matched with combined 98% sequence coverage and a score of 29 407 for the 6 digests. The N-terminus was covered with 11 unmodified peptides. The Cys was covered with only 2 carbamidomethylated peptides. For the original protein without PEGylation, 735 peptides with combined sequence coverage of 97% and a score of 23 932 of the 6 digests were matched to the protein. The N-terminus was covered with 13 peptides, the Cys with 2 carbamidomethylated peptides. Detection of the PEGylation sites by this approach may have failed due to insufficient cleavage of the enzymes close to the site(s) of modification and/or the high mass of the modification, which may have hindered efficient fragmentation by collision induced dissociation. However, the aggregate data on the chemical modification of the S218C mutant (Figures 2A and 3) plus the absence detectable modification in the wild-type enzyme leave relatively little doubt that Cys²¹⁸ is in fact the major site of derivatization by mPEG-mal 5000.

The high efficiency of PEGylation of the S218C mutant is worth noting. Modification with mPEG-mal 5000 of engineered cysteines in other proteins was incomplete, even when large molar excesses (≥ 20 -fold) of reagent over target protein were

employed.^{17–23} The yields often did not exceed values around 50%, implying the need to separate the PEGylated protein from the unmodified form. Derivatization of the S218C mutant proceeded to near-completion. However, double PEGylation of the S218C mutant might be an issue.

To examine enlargement of the hydrodynamic volume of the S218C mutant resulting from PEGylation, we performed gel filtration analysis using conditions in which direct interaction of protein and PEG with the chromatographic material should have been minimized. The elution profiles of the PEGylated and underivatized forms of the mutant are superimposed in Figure 4. The results are clear in showing a marked size enhancement for the PEGylated enzyme. The elution volume for the main peak corresponded to an apparent molecular mass of approximately 250 kDa that can be compared to a native molecular mass for the homotetramer of about 170 kDa. We also analyzed our protein samples by dynamic light scattering. The WT displayed a hydrodynamic diameter of 11.67 ± 0.46 nm. The S218C mutant showed essentially the same hydrodynamic diameter (11.88 ± 0.86 nm). The PEGylated mutant was substantially larger; its hydrodynamic diameter was determined to be 16.38 ± 3.09 nm. The measurement did not detect peaks of smaller size, suggesting that PEGylation did not trigger dissociation of the protein subunits in the functional enzyme tetramer.

Functional Properties of PEGylated and unPEGylated Forms of the S218C Mutant. To obtain more detailed information about functional consequences of the site-directed replacement of Ser²¹⁸ by Cys and of the modification by

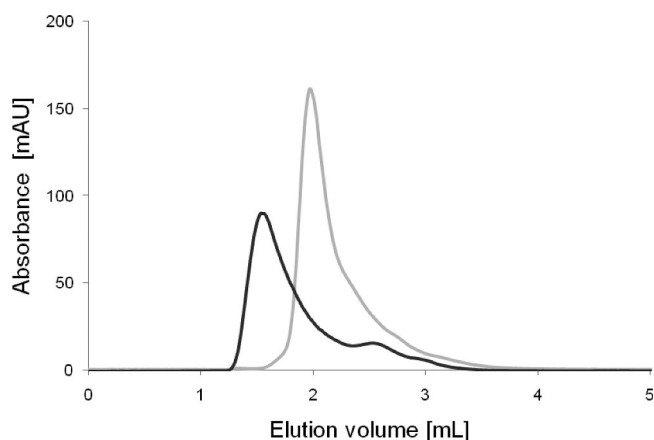


Figure 4. Gel filtration analysis for S218C mutant and the PEGylated derivative thereof. 50 μL of PEGylated (full dark gray line) and unPEGylated forms (full light gray line) of the S218C mutant (3 mg/mL) were loaded on a Superdex 200 column (GE Healthcare Life Sciences) and eluted isocratically at 25 $^{\circ}\text{C}$ with 50 mM potassium phosphate buffer, pH 7.0, containing 150 mM NaCl. The flow rate was 0.5 mL/min, and detection was at 280 nm. mAU, arbitrary units.

mPEG-mal 5000, we carried out a steady-state kinetic characterization of the S218C mutant in both unmodified and PEGylated forms. Table 2 summarizes the results, showing

Table 2. Kinetic Characterization of PEGylated and Unmodified forms of S218C for Reaction with L-(+)-Lactic Acid^a

enzyme	specific activity [U/mg]	k_{cat} [s^{-1}]	K_{M} [mM]	$k_{\text{cat}}/K_{\text{M}}$ [$[(\text{s mM})^{-1}]$]
Wild-type LOX	204 (± 10)	140 (± 1)	0.83 (± 0.03)	167
S218C mutant	90 (± 5)	62 (± 2)	1.0 (± 0.10)	61
PEGylated S218C	62 (± 4)	43 (± 3)	1.0 (± 0.10)	42

^a k_{cat} ($=V_{\text{max}}/E$) was calculated from maximum initial rates (V_{max}) with the molar enzyme concentration (E) used. Standard deviation on specific activity is from five independent experiments. Standard deviations on kinetic parameters are from nonlinear fits of data with the Michaelis-Menten equation.

kinetic parameters for the two preparations of the mutant along with kinetic parameters for the wild-type enzyme. Experimental data are shown in Figures S3 of Supporting Information. The mutation resulted in a 2.7-fold loss in catalytic efficiency for reaction with L-lactate ($k_{\text{cat}}/K_{\text{M}}$). This loss can be ascribed almost exclusively to a decrease in turnover number (k_{cat}) caused by the mutation. Apparent substrate binding (K_{M}) was only slightly affected in the mutant as compared to WT. When compared to its unmodified counterpart, the PEGylated mutant displayed a relatively small loss in $k_{\text{cat}}/K_{\text{M}}$ (by about 30%), again resulting from a corresponding decrease in k_{cat} . The PEGylated mutant was about one-fourth as efficient ($k_{\text{cat}}/K_{\text{M}}$) as the wild-type enzyme. Note: we determined that free PEG that might have remained in the PEGylated enzyme preparation due to incomplete removal of unreacted mPEG-mal 5000 after the modification is very unlikely to have affected the activity of PEGylated S218C mutant in any way. There was no significant ($\leq 2\%$) effect of added PEG4000 (12.5-fold molar excess over protein present) on the specific activity of WT and S218C mutant.

We further tested two other α -hydroxy acids (S-2-hydroxybutyric acid, S-2-hydroxyisocaproic acid) that serve as relatively slow alternative substrates of the wild-type LOX ($k_{\text{cat}} \leq 1.4 \text{ s}^{-1}$). Table S1 in Supporting Information shows the results. It is interesting that both unmodified (1.8 s^{-1}) and PEGylated S218C mutant (1.6 s^{-1}) displayed a higher k_{cat} for reaction with S-2-hydroxybutyric acid than wild-type LOX. However, the K_{M} for S-2-hydroxybutyric acid ($\sim 4 \text{ mM}$) was about 10 times higher in these enzymes as compared to the wild-type LOX. In $k_{\text{cat}}/K_{\text{M}}$ terms, therefore, the wild-type LOX ($3.2 \text{ mM}^{-1} \text{ s}^{-1}$) was still an 8-fold better catalyst for conversion of S-2-hydroxybutyric acid than the two forms of the S218C mutant. Using S-2-isocaproic acid as substrate, kinetic consequences of replacing Ser²¹⁸ by Cys and of modifying Cys²¹⁸ with mPEG-mal 5000 were markedly different from those observed in the reaction with S-2-hydroxybutyric acid. The k_{cat} of the mutated enzymes was decreased more substantially (up to 4-fold) than the K_{M} was increased in comparison to the wild-type enzyme ($k_{\text{cat}} = 1.1 \text{ s}^{-1}$; $K_{\text{M}} = 0.43 \text{ mM}$). The unmodified S218C mutant even showed a lower K_{M} for S-2-isocaproic acid (0.26 mM) than the wild-type enzyme. Substrate specificity of LOX was therefore changed somewhat as a result of both point mutation of Ser²¹⁸ and PEGylation of Cys²¹⁸.

We also examined the stability of the S218C mutant, unmodified and PEGylated, measuring irreversible loss of activity during incubation at 37 $^{\circ}\text{C}$. Figure 5 shows that the

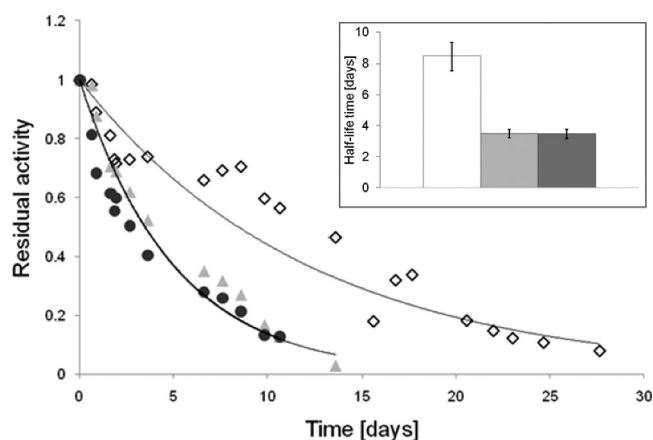


Figure 5. Inactivation time courses for S218C mutant (light gray triangles) and the PEGylated derivative (dark gray circles) thereof are shown in comparison to wild-type LOX (white diamonds). Residual activity is expressed as a fraction of the starting activity. The inset shows half-life times calculated from the data assuming pseudo-first-order decay of activity, shown as lines in the main panel. WT (white bar), S218C (light gray bar), PEGylated S218C (dark gray bar). Incubations were done in 40 mM HEPES buffer, pH 8.1, containing 150 mM NaCl. The temperature was 37 $^{\circ}\text{C}$. The enzyme concentration was 0.4 μM .

unmodified mutant was inactivated somewhat faster than the wild-type enzyme, manifested in a decrease in half-life time by a factor of about 2.5. Stability of the S218C mutant was unchanged after PEGylation, implying that the PEGylation itself did not deteriorate the stability of enzyme activity. This is worth remarking because it is quite difficult to predict the effect of PEGylation on the stability of a protein. In hemoglobin, for example, multiple-site PEGylation resulted in dissociation of the native protein homotetramer.⁴² Differential scanning

fluorimetry was used here to obtain a relevant parameter of overall conformational stability of the different LOX samples used. Unfolding of WT at high temperature was characterized by a T_i value of 69.5 ± 0.5 °C. The T_i values for S218C (70.0 ± 0.5 °C) and the PEGylated mutant (68.0 ± 0.5 °C) were very similar to the T_i of WT. PEGylated S218C may show a slightly reduced conformational stability as compared to the two unmodified proteins; however, any stability loss after PEGylation was clearly small. Lowering of the half-life time in S218C mutant as compared to WT was not reflected in the T_i values. However, it is not uncommon that different assays of stability give different results.

In conclusion, we have achieved the intended specific modification of LOX using a bioconjugation approach in solution that was based on introduction of a single Cys at position 218, identified through structure-guided selection, and Cys-directed modification with mPEG-mal 5000. Marked loss of activity and/or stability is a problem often encountered in the preparation of enzyme bioconjugates, especially when random multisite PEGylation is applied.^{1–4} Replacement of Ser²¹⁸ by Cys and PEGylation of Cys²¹⁸ also decreased the catalytic efficiency of LOX for reaction with L-lactate (4-fold overall) and abated resistance of the enzyme to inactivation at 37 °C (2.5-fold). However, the S218C mutant was still sufficiently active to be considered a useful biocatalyst. Importantly, the final PEGylation proceeded with very good yield in a selective modification reaction. The PEGylated form of the LOX could thus be an interesting new candidate enzyme for evaluation in lactate biosensors.^{8,25–27,30–33} It was shown for glucose oxidase that PEGylation brought about significant enhancement of the performance of the enzyme embedded in a carbon paste-based electrode.⁸ The availability of a defined PEG-LOX bioconjugate now enables similar questions to be addressed for LOX. Position Cys²¹⁸ presents an interesting site for further diversification of LOX bioconjugates (e.g., in situ polymerization⁴³) and optimization for the various known applications of the enzyme.^{34,35} Cys²¹⁸ could be used to attach redox mediators to the protein with the aim of facilitating direct (“wired”) electron transfer between the redox-active FMN cofactor and an electrode. The location of Cys²¹⁸ in the structure seems suitable for this purpose, and a recent study of glucose oxidase has elegantly demonstrated the use of gold nanoparticle conjugation to an engineered cysteine to achieve this effect.⁴⁴

■ ASSOCIATED CONTENT

● Supporting Information

Table S1 summarizes kinetic parameters of wild-type enzyme, the S218C mutant, and the PEGylated form of the mutant for α -hydroxyacid substrates other than L-lactate; Figure S1 shows determination of T_i values for temperature-dependent protein denaturation using differential scanning fluorimetry data. Figure S2 shows elution of the S218C mutant in hydrophobic interaction chromatography (panel A) and a SDS polyacrylamide gel documenting the different steps of the purification (panel B). Figure S3 shows Michaelis–Menten plots of data used for determination of kinetic parameters for reaction with L-lactate. Detailed protocol of LC-MS/MS analysis is provided. This material is available free of charge via the Internet at <http://pubs.acs.org>.

■ AUTHOR INFORMATION

Corresponding Author

*Telephone: +43-316-873-8400; fax: +43-316-873-8434; e-mail: bernd.nidetzky@tugraz.at.

Notes

The authors declare no competing financial interest.

■ ACKNOWLEDGMENTS

This work was supported by FFG, Land Steiermark, Steirische Wirtschaftsförderung (SFG) and Roche Diagnostics GmbH (Graz, Austria). We thank Dr. Bernhard Schaffar, Dr. Christoph Ritter and Dr. Thomas Meier (Roche Diagnostics) for helpful discussion. Assistance of Karin Longus and Daniela Rainer (Institute of Biotechnology and Biochemical Engineering) in the production of the S218C mutant is gratefully acknowledged.

■ ABBREVIATIONS

FMN, flavin mononucleotide; LOX, L-lactate oxidase; mPEG-mal 5000, methoxypoly(ethylene glycol) 5000; PEG, poly(ethylene glycol); WT, wild-type

■ REFERENCES

- (1) Pasut, G., and Veronese, F. M. (2012) State of the art in PEGylation: The great versatility after 40 years of research. *J. Controlled Release*, in press ([dx.doi.org/10.1016/j.jconrel.2011.10.037](https://doi.org/10.1016/j.jconrel.2011.10.037))
- (2) Jevsevar, S., Kunstelj, M., and Porekar, V. G. (2010) PEGylation of therapeutic proteins. *Biotechnol. J.* 5, 113–128.
- (3) Matsushima, A., Kodera, Y., Hiroto, M., Nishimura, H., and Inada, Y. (1996) Bioconjugates of proteins and polyethylene glycol: potent tools in biotechnological processes. *J. Mol. Cat. B: Enzymatic* 2, 1–17.
- (4) Fee, C. J., and Van Alstine, J. M. (2006) PEG-proteins: Reaction engineering and separation issues. *Chem. Eng. Sci.* 61, 924–939.
- (5) Veronese, F. M. (2011) Peptide and protein PEGylation: a review of problems and solutions. *Biomaterials* 22, 405–417.
- (6) Dattelbaum, A. M., Baker, G. A., Fox, J. M., Iyers, S., and Dattelbaum, J. D. (2009) PEGylation of a maltose biosensor promotes enhanced signal response when immobilised in a silica sol-gel. *Bioconjugate Chem.* 20, 2381–2384.
- (7) Doretto, L., Ferrara, D., Gattolin, P., Lora, S., Schiavon, F., and Veronese, F. M. (1998) PEG-modified glucose oxidase immobilized on a PVA cryogel membrane for amperometric biosensor applications. *Talanta* 45, 891–898.
- (8) Mizutani, F., Yabuki, S., and Iijima, S. (1995) Amperometric glucose-sensing electrode based on carbon paste containing poly(ethylene glycol)-modified glucose oxidase and cobalt octaethoxyphthalocyanine. *Anal. Chim. Acta* 300, 59–64.
- (9) Allard, L., Cheynet, V., Oriol, G., Gervasi, G., Imbert-Laurenceau, E., Mandrand, B., Delair, T., and Mallet, F. (2004) Antigenicity of recombinant proteins after regioselective immobilization onto polyanhydride-based copolymers. *Bioconjugate Chem.* 15, 458–466.
- (10) Rodriguez-Martinez, J. A., Rivera-Rivera, I., and Griebenow, K. (2011) Prevention of benzyl alcohol-induced aggregation of chymotrypsinogen by PEGylation. *J. Pharm. Pharmacol.* 63, 800–805.
- (11) Castillo, B., Sola, R. J., Ferrer, A., Barletta, G., and Griebenow, K. (2008) Effect of PEG modification on subtilisin Carlsberg activity, enantioselectivity, and structural dynamics in 1,4-dioxane. *Biotechnol. Bioeng.* 99, 9–17.
- (12) Lopez-Cruz, J. I., Viniegra-Gonzalez, G., and Hernandez-Arana, A. (2006) Thermostability of native and pegylated *Myceliophthora thermophila* laccase in aqueous and mixed solvents. *Bioconjugate Chem.* 17, 1093–1098.
- (13) Daly, S. M., Przybycien, T. M., and Tilton, R. M. (2007) Aggregation of lysozyme and poly(ethylene glycol)-modified lysozyme after adsorption to silica. *Colloids Surf., B: Biointerfaces* 57, 81–88.

- (14) Pai, S. S., Przybycien, T. M., and Tilton, R. M. (2010) Protein PEGylation attenuates adsorption and aggregation on a negatively charged and moderately hydrophobic polymer surface. *Langmuir* 26, 18231–18238.
- (15) Popp, M. W., Dougant, S. K., Chuang, T.-Y., Spooner, E., and Ploegh, H. L. (2011) Sortase-catalyzed transformation that improve the properties of cytokines. *Proc. Natl. Acad. Sci. U.S.A.* 108, 3169–3174.
- (16) Rossi, E. A., Goldenberg, D. M., and Chang, C.-H. K. (2011) The Dock-and-Lock method combines recombinant engineering with site-specific covalent conjugation to generate multifunctional structures. *Bioconjugate Chem.* 23, 309–323.
- (17) Veronese, F. M., Mero, A., Caboi, F., Sergi, M., Marongiu, C., and Pasut, G. (2007) Site-specific pegylation of G-CSF by reversible denaturation. *Bioconjugate Chem.* 18, 1824–1830.
- (18) Manujula, B. N., Tsai, A., Upadhyay, R., Perumalsamy, K., Smith, P. K., Malavalli, A., Vandegriff, K., Winslow, R. M., Intaglietta, M., Prabhakaran, M., Friedman, J. M., and Acharya, A. S. (2003) Site-specific PEGylation of hemoglobin at Cys-93(β): correlation between the colligative properties of the PEGylated protein and the length of the conjugated PEG chain. *Bioconjugate Chem.* 14, 464–472.
- (19) Balan, S., Choi, J.-w., Godwin, A., Teo, I., Laborde, C. M., Heidelberger, S., Zloh, M., Shaunak, S., and Brocchini, S. (2007) Site-specific PEGylation of protein disulfide bonds using a three-carbon bridge. *Bioconjugate Chem.* 18, 61–76.
- (20) Slavica, A., Dib, I., and Nidetzky, B. (2007) Selective modification of surface-exposed thiol groups in *Trigonopsis variabilis* D-amino acid oxidase using poly(ethylene glycol) maleimide and its effect on activity and stability of the enzyme. *Biotechnol. Bioeng.* 96, 9–17.
- (21) Doherty, D. H., Rosendahl, M. S., Smith, D. J., Hughes, J. M., Chlipala, E. A., and Cox, G. N. (2005) Site-specific PEGylation of engineered cysteine analogues of recombinant human granulocyte-macrophage colony-stimulating factor. *Bioconjugate Chem.* 16, 1291–1298.
- (22) Hu, J., Duppatla, V., Harth, S., Schmitz, W., and Sebald, W. (2010) Site-specific PEGylation of bone morphogenetic protein-2 cysteine analogues. *Bioconjugate Chem.* 21, 1762–1772.
- (23) Lamppa, J. W., Ackerman, M. E., Lai, J. I., Scanlon, T. C., and Griswold, K. E. (2011) Genetically engineered alginate lyase-PEG conjugates exhibit enhanced catalytic function and reduced immunoreactivity. *PLoS ONE* 6, e17042.
- (24) Maeda-Yorita, K., Aki, K., Sagai, H., Misaki, H., and Massey, V. (1995) L-Lactate oxidase and L-lactate monooxygenase: mechanistic variations on a common structural theme. *Biochimie* 77, 631–642.
- (25) Minagawa, H., Nakayama, N., Matsumoto, T., and Ito, N. (1998) Development of long life lactate sensor using thermostable mutant lactate oxidase. *Biosens. Bioelectron.* 13, 313–318.
- (26) Wang, J., and Chen, Q. (1994) Enzyme microelectrode array strips for glucose and lactate. *Anal. Chem.* 66, 1007–1011.
- (27) Romero, M. R., Ahumada, F., Garay, F., and Baruzzi, A. M. (2010) Amperometric biosensor for direct blood lactate detection. *Anal. Chem.* 82, 5568–5572.
- (28) Furuichi, M., Suzuki, N., Dhakshnamoorthy, B., Minagawa, H., Yamagishi, R., Watanabe, Y., Goto, Y., Kaneko, H., Yoshida, Y., Yagi, H., Waga, I., Kumar, P. K., and Mizuno, H. (2008) X-ray structures of *Aerococcus viridans* lactate oxidase and its complex with D-lactate at pH 4.5 show an α -hydroxyacid oxidation mechanism. *J. Mol. Biol.* 378, 436–446.
- (29) Li, S. J., Umena, Y., Yorita, K., Matsuoka, T., Kita, A., Fukui, K., and Morimoto, Y. (2007) Crystallographic study on the interaction of L-lactate oxidase with pyruvate at 1.9 Å resolution. *Biochem. Biophys. Res. Commun.* 358, 1002–1007.
- (30) Patel, N. G., Erenkötter, A., Cammann, K., and Chemnitz, G.-C. (2000) Fabrication and characterization of disposable type lactate oxidase sensors for dairy products and clinical analysis. *Sens. Actuators, B: Chem.* 67, 134–141.
- (31) Zanina, V. P., López de Mishimaa, B., and Solís, V. (2010) An amperometric biosensor based on lactate oxidase immobilized in laponite–chitosan hydrogel on a glassy carbon electrode. Application to the analysis of L-lactate in food samples. *Sens. Actuators, B: Chem.* 155, 75–80.
- (32) Park, B. W., Yoon, D. Y., and Kim, D. S. (2010) Recent progress in bio-sensing techniques with encapsulated enzymes. *Biosens. Bioelectron.* 26, 1–10.
- (33) Romero, M. R., Garay, F., and Baruzzi, A. M. (2008) Design and optimization of a lactate amperometric biosensor based on lactate oxidase cross-linked with polymeric matrixes. *Sens. Actuators, B: Chem.* 131, 590–595.
- (34) Oikawa, T., Mukoyama, S., and Soda, K. (2001) Chemo-enzymatic D-enantiomerization of DL-lactate. *Biotechnol. Bioeng.* 73, 80–82.
- (35) Soda, K., Oikawa, T., and Yokoigawa, K. (2001) One-pot chemo-enzymatic enantiomerization of racemates. *J. Mol. Catal. B: Enzymatic* 11, 149–153.
- (36) Wang, W., and Malcom, B. A. (1999) Two-stage PCR protocol allowing introduction of multiple mutations, deletions and insertions using QuikChange Site-Directed Mutagenesis. *Biotechniques* 26, 680–682.
- (37) Munro, A. W., and Noble, M. A. (1999) Fluorescence analysis of flavoproteins. *Methods Mol. Biol.* (Chapman, S. K., and Reid, G. A., Eds.) pp 25–48, Vol. 131 Flavoprotein Protocols, Humana Press, Totowa, NJ.
- (38) Niesen, F. H., Berglund, H., and Vedadi, M. (2007) The use of differential scanning fluorimetry to detect ligand interactions that promote protein stability. *Nat. Protoc.* 2, 2212–21.
- (39) Cunane, L. M., Barton, J. D., Chen, Z. W., Diêp Lê, K. H., Amar, D., Lederer, F., and Mathews, F. S. (2005) Crystal structure analysis of recombinant rat kidney long chain hydroxy acid oxidase. *Biochemistry* 44, 1521–1531.
- (40) Xia, Z. X., and Mathews, F. S. (1990) Molecular structure of flavocytochrome b2 at 2.4 Å resolution. *J. Mol. Biol.* 212, 837–863.
- (41) Sukumar, N., Xu, Y., Gatti, D. L., Mitra, B., and Mathews, F. S. (2001) Structure of an active soluble mutant of the membrane-associated (S)-mandelate dehydrogenase. *Biochemistry* 40, 9870–9878.
- (42) Caccia, D., Ronda, L., Frassi, R., Perella, M., Del Favero, E., Bruno, S., Pioselli, B., Abbruzzetti, S., Viappiani, C., and Mozzarelli, A. (2009) PEGylation promotes hemoglobin tetramer dissociation. *Bioconjugate Chem.* 20, 1356–1366.
- (43) Heredia, K. L., Bontempo, D., Ly, T., Byers, J. T., Halstenberg, S., and Maynard, H. D. (2005) In situ preparation of protein-, “smart” polymer conjugates with retention of bioactivity. *J. Am. Chem. Soc.* 127, 16955–16960.
- (44) Holland, J. T., Lau, C., Brozik, S., Atanassov, P., and Banta, S. (2011) Engineering of glucose oxidase for direct electron transfer via site-specific gold nanoparticle conjugation. *J. Am. Chem. Soc.* 133, 19262–19265.

SUPPORTING INFORMATION

Engineering of *Aerococcus viridans* L-lactate oxidase for site-specific PEGylation: characterization and selective bioorthogonal modification of a S218C mutant

Birgit Unterweger[†], Thomas Stoisser[†], Stefan Leitgeb[†], Ruth Birner-Grünberger[‡], and Bernd Nidetzky^{†*}

[†] Research Center Pharmaceutical Engineering, and Institute of Biotechnology and Biochemical Engineering, Graz University of Technology, Petersgasse 12, A-8010 Graz, Austria

[‡] Institute of Pathology and Center for Medical Research, Medical University of Graz, Stiftingtalstraße 24, A-8010 Graz, Austria

Keywords: L-Lactate oxidase; site-specific PEGylation; cysteine-selective bioconjugation; biosensor; cysteine.

* Corresponding author

Telephone: +43-316-873-8400; fax: +43-316-873-8434; e-mail: bernd.nidetzky@tugraz.at

List of contents

Table S1 summarizing kinetic parameters of wild-type enzyme, the S218C mutant, and the PEGylated form of the mutant for α -hydroxyacid substrates other than L-lactate

Figure S1 showing unfolding of PEGylated and unmodified S218C mutant in a thermal-shift differential scanning fluorometry experiment.

Figure S2 showing elution of the S218C mutant in hydrophobic interaction chromatography (panel A) and a SDS polyacrylamide gel in which the different steps of the purification are documented (panel B).

Figure S3 showing Michaelis-Menten plots of data used for determination of kinetic parameters for enzymatic reactions with L-lactate.

Detailed description of methodology used for LC-MS/MS analysis

Table S1. Substrate specificity of PEGylated and unmodified S218C mutant as compared to wild-type LOX. Standard deviation on specific activity is from five independent experiments. Standard deviations on kinetic parameters are from non-linear fits of data with the Michaelis-Menten equation.

Enzyme	Substrate	Specific activity [U/mg]	k_{cat} [s ⁻¹]	K_M [mM]	k_{cat}/K_M [(s mM) ⁻¹]
Wild-type LOX	(S)-2-Hydroxybutyric acid	2.0 (± 0.05)	1.40 (± 0.01)	0.43 (± 0.05)	3.2
S218C mutant		2.5 (± 0.07)	1.80 (± 0.05)	4.0 (± 0.41)	0.45
PEGylated S218C		2.4 (± 0.10)	1.60 (± 0.04)	4.1 (± 0.41)	0.41
Wild-type LOX	(S)-2-Hydroxyisocaproic acid	1.6 (± 0.08)	1.10 (± 0.01)	0.43 (± 0.05)	2.5
S218C mutant		0.40 (± 0.01)	0.27 (± 0.01)	0.26 (± 0.02)	1.1
PEGylated S218C		0.50 (± 0.03)	0.35 (± 0.02)	0.82 (± 0.16)	0.4

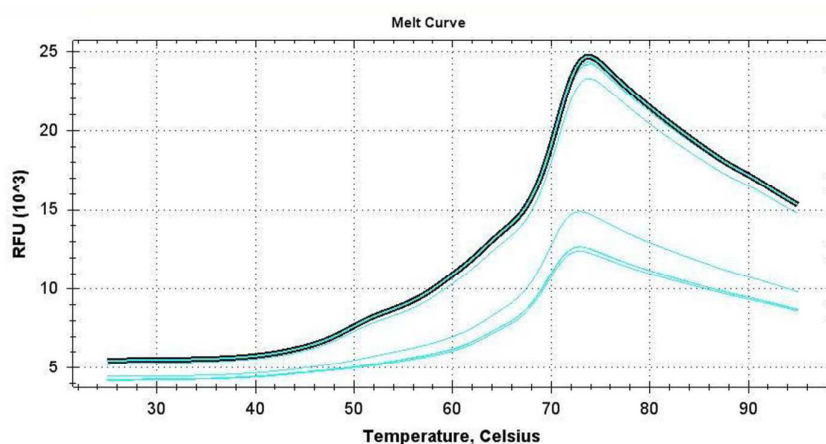
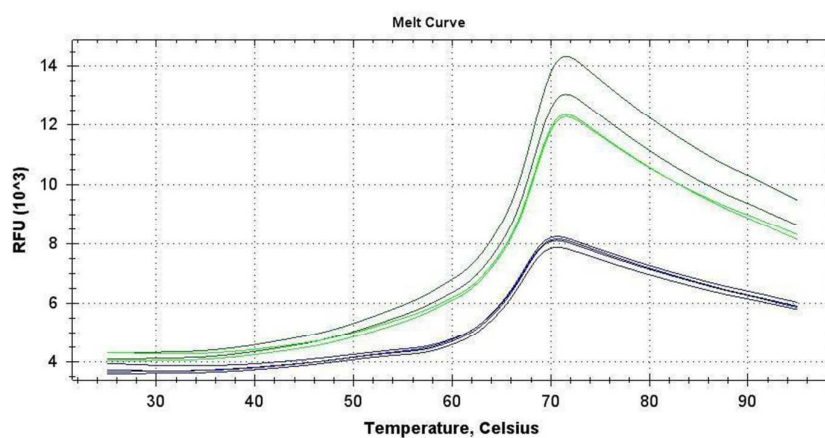
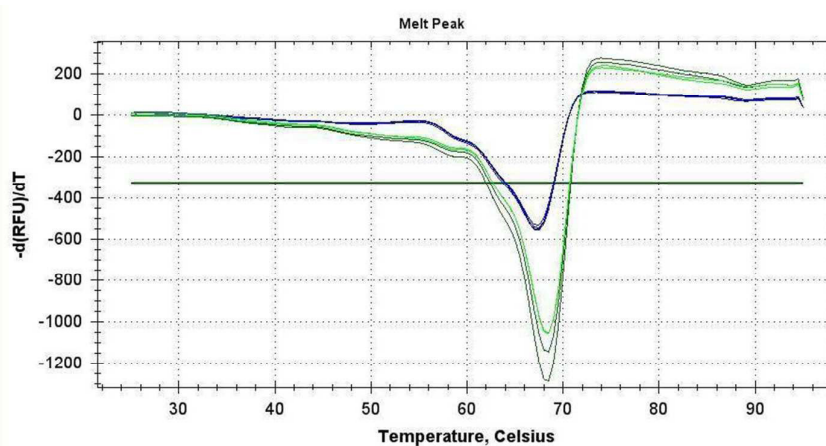
A**B****C**

Figure S1. Determination of protein conformational stability in differential scanning fluorimetry experiments. Temperature scans were performed in the presence of the probe SYPRO orange whose fluorescence intensity (relative fluorescence units, RFU) was recorded every 0.5 °C in dependence of the temperature in the range 25 – 95 °C. The scan rate was 0.5°C/min. Panels **A** and **B** show the “melt curves” for unPEGylated and PEGylated S218C mutant, respectively. In panel **A**, measurements were

done at an enzyme concentration of 5 μM and 10 μM (family of curves at higher fluorescence intensity). In panel B, the measurements were done at an enzyme concentration of 3 μM and 5 μM (family of curves at higher fluorescence intensity). Note: the decay of fluorescence intensity in the high-temperature range is due to aggregation of unfolded protein. Panel C shows determination of the T_i value (apparent melting point) for PEGylated S218C mutant. The requisite curve fitting was conducted with Bio-Rad CFX Manager software implemented in the Bio-Rad C1000 Thermocycler RT-PCR machine (CFX96 system) that was used for acquisition of the melt curves.

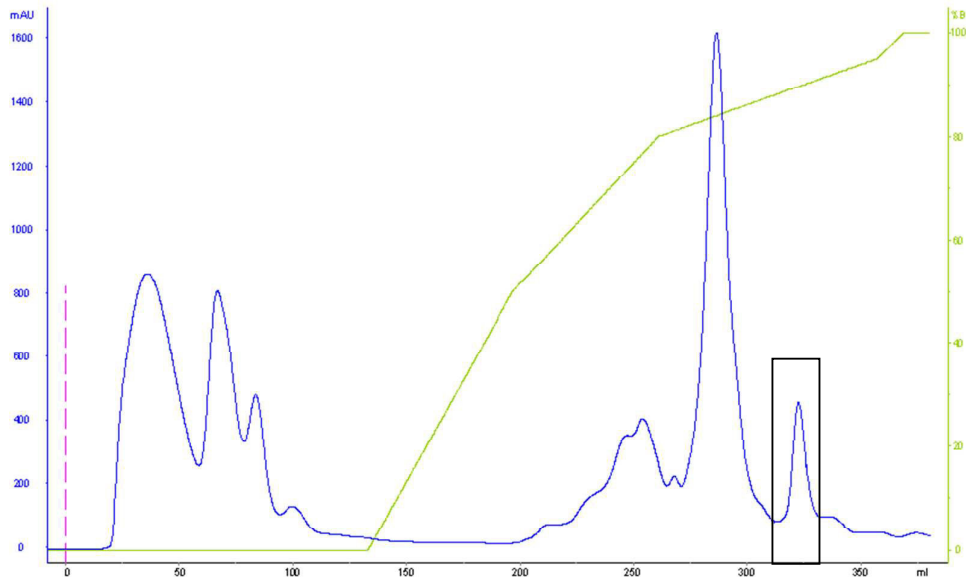


Figure S2A. Purification of the S218C mutant using hydrophobic interaction chromatography.

A Phenyl Sepharose 6 Fast Flow (High Sub) column (GE Healthcare Life Sciences; 64 mL) and the Äkta FPLC system (Amersham Biosciences) were used. The protein (about 100 mg in total) was loaded on the column equilibrated with buffer and eluted at 25 °C with a linearly decreasing gradient of $(\text{NH}_4)_2\text{SO}_4$ (green trace). The flow rate was 5 mL/min, and eluted protein (blue trace) was detected at 280 nm. All steps were performed using 50 mM potassium phosphate buffer, pH 7.0. The original buffer contained 1.5 M $(\text{NH}_4)_2\text{SO}_4$, the elution buffer (buffer B) contained no $(\text{NH}_4)_2\text{SO}_4$. The framed absorbance peak shows elution of LOX activity. The peak was divided into two fractions 1 and 2, where fraction 2 contained about two-thirds of the total protein eluted in the peak. The specific activity of protein present in fraction 2 was almost twice that contained in fraction 1. Purity determined by SDS PAGE was also higher for fraction 2 than fraction 1 (see panel 2B of this figure).

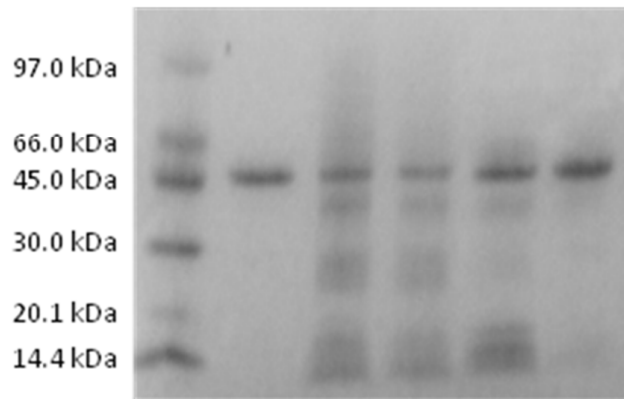


Figure S2B. Purification of S218C mutant documented by SDS PAGE. Lane 1 (from left), molecular mass marker; lane 2, Wild-type enzyme; lane 3, *E. coli* cell extract containing S218C mutant; lane 4, preparation after $(\text{NH}_4)_2\text{SO}_4$ precipitation; lanes 5 and 6, S218C mutant after HIC purification in fraction 1 (lane 5) and fraction 2 (lane 6).

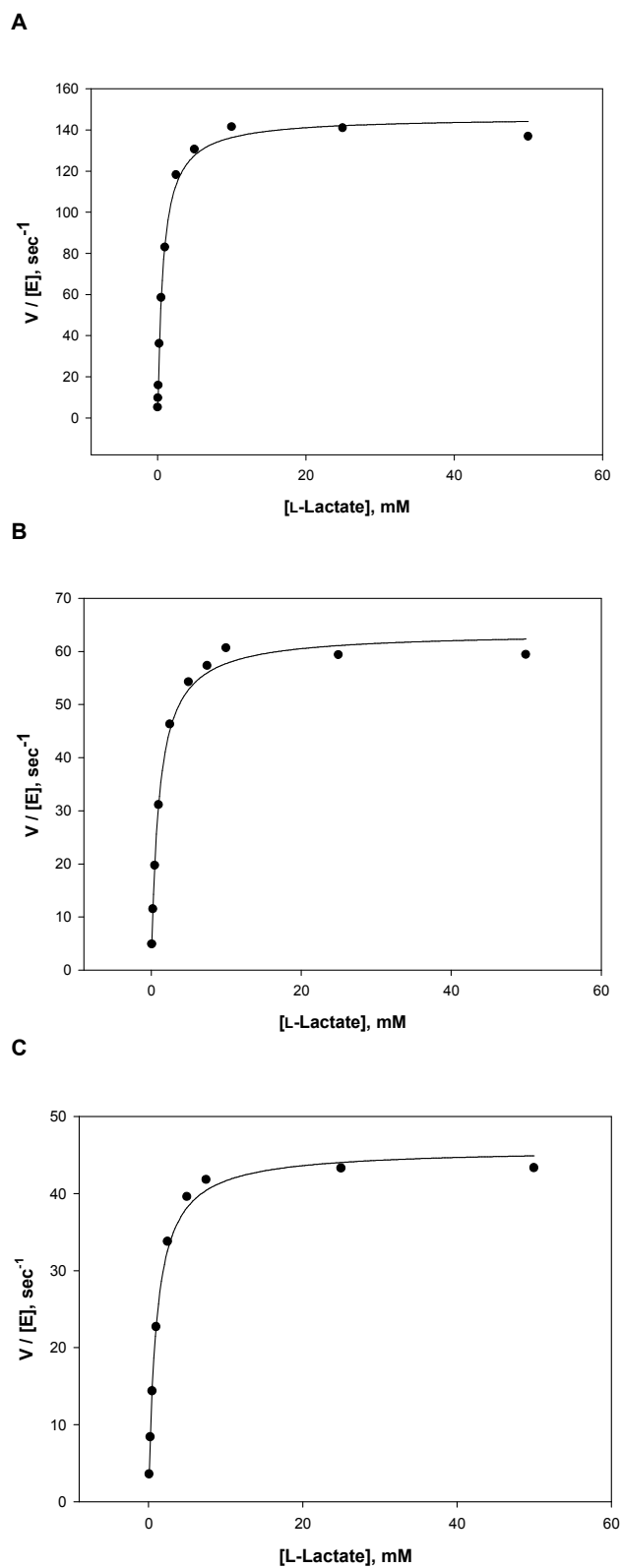


Figure S3. Michaelis-Menten plots of data applied in determination of kinetic parameters for reaction with with L-lactate. Reactions were performed at 37 °C. Panel **A**: wild-type LOX; **B**: S218C mutant; and **C**: PEGylated S218C mutant. Black circles are experimental data, and lines are results of the corresponding non-linear least squares fits.

Protocol of LC-MS/MS analysis

Internal sequence information of the PEGylated LOX, as confirmed by the detected mass shifts by MALDI-TOF analysis, was received from LC-MS/MS. Protein bands were excised from gels and digested with Promega modified trypsin according to the method of Shevchenko and colleagues (see the reference below) and/or with 0.5 µg chymotrypsin (Roche) in 50 mM ammonium bicarbonate containing 10 mM CaCl₂ with or without prior reduction and alkylation. Digests were separated by nano-HPLC (Agilent 1200 system; Vienna, Austria) equipped with a Zorbax 300SB-C18 enrichment column (5 µm, 5 × 0.3 mm) and a Zorbax 300SB-C18 nanocolumn (3.5 µm, 150 × 0.075 mm). 40 µL of sample were injected and concentrated on the enrichment column for 6 min using 0.1 % formic acid as isocratic solvent at a flow rate of 20 µL/min. The column was then switched in the nanoflow circuit, and the sample was loaded on the nanocolumn at a flow rate of 300 nL/min. Separation was carried out using the following gradient, where solvent A is 0.3 % formic acid in water and solvent B is a mixture of acetonitrile and water (4 : 1, by vol.) containing 0.3 % formic acid: 0-6min: 13 % B; 6-35 min: 13-28 % B; 35-47 min: 28-50 % B, 47-48 min: 50-100 % B; 48-58 min: 100 % B; 58-58,1 min: 100-13% B; 58,1-70 min: re-equilibration at 13 % B. The sample was ionized in the nanospray source equipped with nanospray tips (PicoTip™ Stock# FS360-75-15-D-20, Coating: 1P-4P, 15±1 µm Emitter, New Objective, Woburn, MA, USA). It was analyzed in a Thermo LTQ-FT mass spectrometer (Thermo Fisher Scientific, Waltham, MA, USA) operated in positive ion mode, applying alternating full scan MS (m/z 400 to 2000) in the ion cyclotron and MS/MS by collision induced dissociation of the 5 most intense peaks in the ion trap with dynamic exclusion enabled. The LC-MS/MS data were analyzed by searching the protein sequence of LOX of *Aerococcus viridans* (NCBI accession number ZP_06807595) with Mascot 2.2 (MatrixScience, London, UK). The database contained target protein and known contaminants such as the enzymes used for digestion and human keratins. PEGylation with 110 and 111 monomeric units (the two most abundant masses of PEG 5000) was included as variable modification at Cys or the protein N-terminus next to carbamidomethylation on Cys as variable modification. A maximum false discovery rate of 5% using decoy database search, an ion score cut off of 20 and a minimum of 2 identified peptides were chosen as identification criteria.

Shevchenko, A., Wilm, M., Vorm, O., Mann, M. (1996) Mass spectrometric sequencing of proteins silver-stained polyacrylamide gels. *Anal. Chem.* 68, 850-858

3 Probing the substrate specificity of L-lactate oxidase from *Aerococcus viridans*: analysis with different electron acceptors and crystallographic study of A95G mutant at 1.65 Angstrom resolution.

Thomas Stoisser[†], Daniela Rainer[†], Stefan Leitgeb[†], David K. Wilson[‡], and Bernd Nidetzky^{†*}

[†] Research Center Pharmaceutical Engineering, and Institute of Biotechnology and Biochemical Engineering, Graz University of Technology, Petersgasse 12, A-8010 Graz, Austria

[‡] Department of Molecular and Cellular Biology, University of California, One Shields Avenue, Davis, CA 95616

* Corresponding author

Institute of Biotechnology and Biochemical Engineering, Graz University of Technology, Petersgasse 12, A-8010 Graz, Austria

Telephone: +43-316-873-8400; fax: +43-316-873-8434; e-mail:

bernd.nidetzky@tugraz.at

ABBREVIATIONS

BSA: bovine serum albumin, DAO: D-amino acid oxidase, DCIP: 2,6 dichloroindophenol, FCB2: flavocytochrome *b*₂, FMN: flavomononucleotide, FPLC: fast protein liquid chromatography, GOD: glucose oxidase, GOX: glycolate oxidase, HIC: hydrophobic interaction chromatography, LCHAO: long chain hydroxy acid oxidase, LMO: L-lactate monooxygenase, LOX: L-lactate oxidase, MDH: L-mandelate dehydrogenase, PDB: protein data base, WT: wild-type

ABSTRACT

L-lactate oxidase (LOX) from *Aerococcus viridans* has been an enzyme in the focus of research and in industrial applications for decades. Nevertheless, there still remain open questions regarding substrate placement and electron transfer. We generated an A95G mutant enzyme, which was already reported earlier to display changed substrate specificity. The mutant enzyme was crystallized, and the structure was solved at 1.65 Å. Structural analysis revealed a change in the hydrogen network around the substrate binding site making it more accessible for larger substrates. A flipping residue is fixed by the mutation, which leads to a more rigid structure and facilitates substrate transfer into the active site of LOX.

Additionally, mechanistic aspects of the conversion of L-lactate into pyruvate and H₂O₂ reacts with alternative electron acceptors were addressed. For the use in lactate biosensors this might be of great interest, as oxygen is often limiting and can influence the LOX activity. Pre-steady state studies using O₂, 2,6-dichlorindophenol (DCIP) and certain quinones highlight differential behavior between wild-type LOX and A95G mutant. Bimolecular rate constants of the oxidative half-reaction indicated a 3-fold preferential usage of DCIP over O₂ for A95G LOX. Wild-type LOX, however, revealed a preference for molecular oxygen. Finally, time course analysis in concomitant presence of O₂ and DCIP reflected that the A95G mutant preferably uses DCIP over O₂, whereas for wild-type LOX the acceptor preference is switched vice versa.

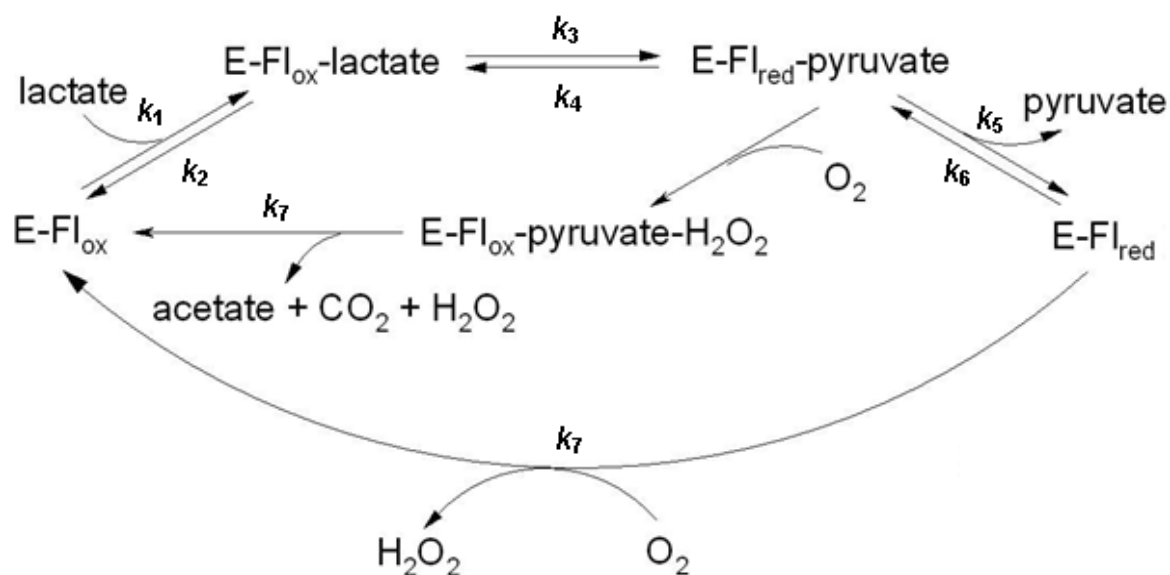
INTRODUCTION

Aerococcus viridans L-lactate oxidase (LOX) belongs to a group of in total six α -hydroxy oxidizing enzymes, consisting of L-lactate monooxygenase (LMO) from *Mycobacterium smegmatis* (**1, 2**) flavocytochrome b_2 (FCB2) from Baker's yeast (**3**), spinach glycolate oxidase (GOX) (**4**), L-mandelate dehydrogenase (MDH) from *Rhodotorula graminis* (**5**) and a long chain α -hydroxy acid oxidase (LCHAO) from rat kidney (**6**). The flavin mononucleotide (FMN) containing flavoprotein catalyzes the oxidation of L-lactate into pyruvate by transferring two electrons to O_2 as a terminal electron acceptor and forming H_2O_2 as a co-product. The formation of peroxide is the basis for the application of the oxidase in microelectrode array strips or in biosensors to test lactate levels of human blood samples (**7-9**).

The reaction mechanism of this flavoenzyme can be divided in two half-reactions with the flavin changing between an oxidized and reduced state (**10**). In the first (or reductive) half-reaction the substrate reduces FMN, whereas in the second (or oxidative) half-reaction, the cofactor is re-oxidized by an electron acceptor. This catalytic cycle follows a 'ping-pong mechanism' (**1**), a mechanism, which was also identified for glucose oxidase (**11**), cholesterol oxidase type II from *Brevibacterium sterolicum* (**12**) and spinach glycolate oxidase (**13**). However, other flavoproteins such as lactate monooxygenase (LMO) from *Mycobacterium smegmatis* (**1, 14**), vanilyl-alcohol oxidase from *Penicillium simplicissimum* (**15**) or cytokinin dehydrogenase (**16**) follow a ternary complex mechanism. In this ternary complex mechanism an electron acceptor (e.g. dioxygen) reacts with the enzyme-product complex, whereas in the ping pong mechanism product is released prior to the reaction of the electron acceptor with the enzyme (**1**). Both, LOX and LMO oxidize L-

lactate, but generate different products due to this fact that the dissociation constants of the ternary complex are significantly altered.

For a better understanding, **Scheme 1** explains the difference between LOX and LMO in more detail: after the conversion of L-lactate into pyruvate the product rapidly dissociates from the active site, and molecular oxygen reacts with the enzyme producing H_2O_2 . In contrast, (the preliminary product) pyruvate doesn't dissociate from the enzyme, and O_2 reacts rapidly with the $\text{E-FMN}_{\text{red}}$ -pyruvate complex resulting in the products acetate, CO_2 and H_2O . The presence of this intermediate has been proven by photometric studies of LOX indicating a biphasic behavior of the traces observed from 340 to 550 nm (17). This species has been identified as a complex of reduced enzyme and pyruvate by titration of reduced enzyme with pyruvate and in stopped flow experiments by mixing different concentrations of pyruvate with the reduced enzyme (1).



Scheme 1. The reaction cycles of LOX (outer cycle) and LMO (inner cycle)

LOX from *Aerococcus viridans* has been the topic of research for 4 decades and the ongoing research indicates the industrial and scientific relevance of this enzyme. Crystal structures have been solved (**18**, **19**), and a large set of active site mutations has been generated to gain better understanding of the reaction mechanism (**20**). Two mechanisms are discussed in literature: a hydride transfer (**21**) or an alternative mechanism, which involves the abstraction of a proton from the substrate α -carbon by the catalytic base to form a carbanion and the subsequent transfer of two electrons to the FMN cofactor (**10**).

Ala-95 is reported to affect substrate binding affinity and is replaced by a glycine in LMO based on homology modeling. A mutant, in which Ala-95 was substituted by glycine (**17**), was generated to create a mimic of LMO, where the formed pyruvate-FMN_{red} complex dissociates into acetate, CO₂ and H₂O. However, A95G still retained LOX activity and followed the wild-type reaction mechanism. The smaller glycine residue failed to allow the product to be bound to the reduced enzyme, until the oxygen reacts with this ternary complex, and the decarboxylation occurs. Instead, this mutation offered several new features, in particular, altered substrate specificity. The mutant enzyme showed increased catalytic activity for longer and bulkier substrates than L-lactic acid, e.g. L- α -hydroxy acids like α -hydroxy-n-butyric acid, α -hydroxy-n-valeric acid and L-mandelic acid. The corresponding residue to Ala-95 in LMO is Gly-99, which is located on the *re*-face of FMN, with a hydrogen atom extended toward the methyl group of lactate that binds on the *si*-face of FMN (**17**). This interaction might explain why the decarboxylation occurs in LMO. An amino acid exchange in LMO of Gly-99 to Ala resulted in reversal of the reaction mechanism leading to an enzyme following the LOX pathway (**22**).

Substrates of flavoenzymes dock into the active site next to the *si*-face of the flavin, whereas the Ala-95 residue is positioned to the *re*-face of FMN. Residue Ala-95 considerably blocks the docking of larger side chains on the α -carbon, and this is removed by the mutation to glycine (**17**). Until now no crystal structure for LMO is present in literature, which allows a detailed comparison between the LMO and LOX system.

Recently, the crystal structures of LOX at pH 8.0 (PDB code 2DU2) and its complex with pyruvate at the same pH (PDB code 2E77) have been solved at 2.1 Å and 1.9 Å resolution, respectively (**18**). **Figure 1** shows an overlay of the active site of both structures. Tyr-191 and Ala-96 (in pink) are flexible residues. Worth

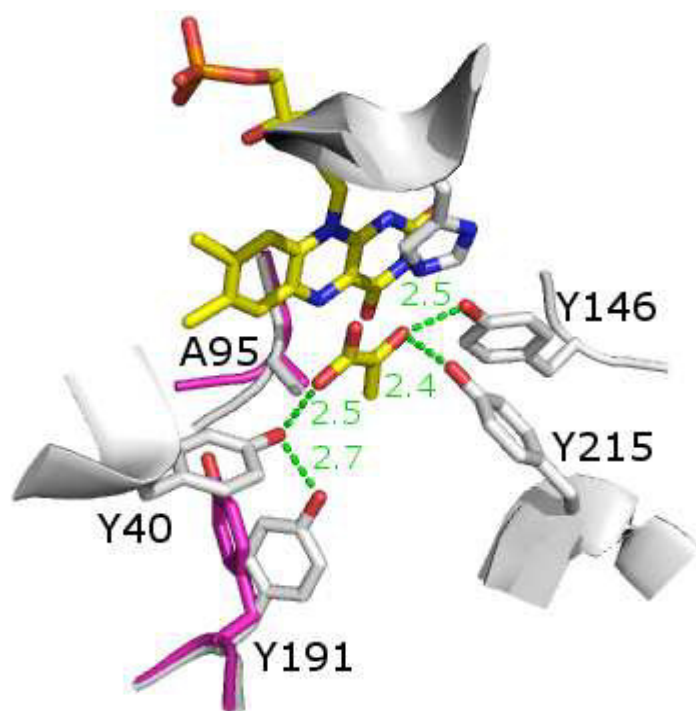


Figure 1

Active site of wild-type LOX

Overlay of wild-type LOX structures 2E77 and 2DU2. Residues in pink indicate flexible regions (residues) from 2DU2, which can switch to the orientation seen in 2E77

mentioning is the neighboring region around the conserved Ala-95. Ala-95 (as well as Ala-96) is positioned on loop 4. This loop has been proposed to play a prominent role for substrate binding as flexible region found in GOX, FCB2, MDH and LCHAO (**23-26**). For instance, loop 4 has been reported to influence the activity of LCHAO by possible interactions with the active site (**26**). For LOX, residue Ala-96 (not conserved) is also flexible and very likely the conformational change of loop 4 influences the vicinity of residue Tyr-191. Several publications have attempted to explain the altered substrate specificity for LOX A95G based on a putative enlarged binding pocket (**17, 27**). We present a detailed structural analysis of the crystal structure in this paper and additional steady state and pre-steady state experiments to shed light on the active site of this LOX mutant and illustrate the underlying mechanism of substrate binding. Previous work has revealed that the release of product from the binding pocket is supported by a rearrangement of three different amino acid residues, namely His-265, the proposed catalytic base, Asp-174 and Lys-221 generating a new hydrogen network (**21**). A comparison between crystal structures from wild-type LOX and A95G mutant enzyme allows new insights in the substrate binding step, which is the missing link to understand the reactivity of L-lactate oxidase completely.

Kinetic analysis of the A95G mutant enzyme revealed a significant effect of the amino acid exchange on the re-oxidation reaction with molecular oxygen. The LOX mutant reflects, in contrast to the wild-type, a ten-fold drop in oxygen acceptance. Applied biosensors based on oxygen or hydrogen peroxide (**28, 29**) often deal with the problem of sensitivity to O₂ concentration, whereas mediator based sensors can solve this circumstance (**30**). Such mediators as 2,6-dichlorindophenol (DCIP) and indophenols variants based on DCIP have been described for a LOX from

Pediococcus sp. and therefore are applied in lactate sensors (**30, 31**). Quinones such as hydroquinone (**32**) can also be the choice for supportive mediators for biosensors. Nevertheless, little is known about the behavior with mediators for LOX from *Aerococcus viridans*. Due to these issues our work analyzes the reaction of LOX with several electron acceptors other than O₂ including DCIP and three different quinones - a possible prospective for future applications in lactate sensing.

EXPERIMENTAL PROCEDURES

L-(+)-lactic acid (free acid, 98%, Aldrich), L-glycolic acid (free acid 97%, Fluka), L-(+) mandelic acid (free acid, 98%, Fluka), L-glyceric acid (sodium salt, 95%, Sigma), (S)-2-hydroxy-3-methylbutyric acid (free acid, 99%, Aldrich), (S)-2-hydroxybutyric acid (free acid, 97% Fluka), (S)-(-)-2-hydroxyisocaproic acid (free acid, 98%, Aldrich), D-(+)-glucose (99.5%, Sigma), 3,3-dimethylglutaric acid (free acid, 98%, Aldrich), 4-aminoantipyrine (98%, Fluka), peroxidase from horseradish (Type VI, Sigma), N,N-dimethylaniline (ReagentPlus[®], 99%, Aldrich), sodium dodecylbenzenesulfonic acid (technical grade, Aldrich), 2,6-dichlorophenolindophenol sodium salt hydrate (97%, Fluka), 2,5-dichloro-1,4-benzoquinone (98%, Aldrich), 2,5-dimethyl-1,4-benzoquinone (99%, Aldrich), 2-methyl-1,4-benzoquinone (98%, Aldrich). Lyophilized wild-type LOX (grade 1) from *Aerococcus viridans* (WT) and lyophilized GOD (glucose oxidase, grade 1) from *Aspergillus niger* were from Roche Diagnostics GmbH. Enzymes were stored at -20 °C until further use. The plasmid pLO-1, which harbored the LOX gene, was kindly provided by Dr. T. Meier (Roche).

Molecular cloning and site-directed mutagenesis

Site directed mutagenesis leading to substitution of Ala95 by Gly was introduced by a two-stage polymerase chain reaction, described previously (29). Therefore, two separate primer extension reactions were carried out, in which pLO-1 was used as the template and one of the two mutagenic oligonucleotide primers was also present. The two primers were 5`-CCAATTGGTGCCCATGGTTTAGCTCACGCTACTAAAGAAGCTGG-3` (termed A95Gfw; melting point: 61.3 °C), and 5`-AGCGTGAGCTAAACCATGGGCACCAATTGGGG-CCATGATGAATGG-3` (termed A95Grev; melting point: 61.3 °C). DNA was amplified by Pfu DNA Polymerase (Promega) setting up the following conditions: heat denaturation at 95 °C for 1 min; 4 elongation cycles, each consisting of 95 °C for 50 s, 59 °C for 50 s and 68 °C for 10 min; final extension at 68 °C for 7 min, and cooling at 4 °C. A second PCR was performed by combining the two separate PCR mixtures in a volume ratio of 1:1 under the same conditions mentioned above, but with a total repeat of 18 cycles. To ensure a higher transformation yield, template DNA was digested with *DpnI* at 37 °C for 1 h. Plasmid DNA was transformed into electrocompetent *E. coli* BL21 (DE3) cells, and the cells were cultured overnight at 37 °C on LB-amp plates (1% peptone, 0.5% yeast extract, 0.5% NaCl, 1.8% agar supplemented with 100 µg/mL ampicillin). For further steps, only transformants carrying plasmids with the mutation of interest verified by DNA sequencing were used.

Production of A95G mutant

Expression of LOX A95G in BL21 (DE3) was done in pre-culture over night containing 0.55% glucose monohydrate, 1% peptone, 0.5% yeast extract, 0.5%

NaCl, 1% NH₄Cl, 0.025% MgSO₄ * 7 H₂O, 100 μL/L poly(propylene glycol), 0.3% K₂HPO₄, 0.6% KH₂PO₄, 0.2*10⁻³% thiamine, 0.0115% ampicillin (Amp), 0.4*10⁻³% FeSO₄ * 7H₂O, 0.1*10⁻³% MnSO₄ * H₂O, 0.04*10⁻³% CuSO₄ * 5 H₂O, 0.01%*10⁻³% H₃BO₃, 0.02*10⁻³% ZnSO₄ * 7 H₂O, 0.02*10⁻³% Na₂MoO₄ * 2H₂O and 0.04*10⁻³% FeCl₃. The optical density (OD₆₀₀) of the pre-culture, grown over night at 37 °C, had a value about 5. The main culture (same ingredients as pre-culture except 2.2% glucose) was inoculated to an OD₆₀₀ of 0.5 directly to the fermenter. Temperature, pH, stirring and oxygen partial pressure in the B. Braun Biotech International Biostat®C, Type-CT5-2 fermenter were controlled and adjusted automatically during fermentation. The pH was balanced before start at pH 7.0 and pH 4.0 with a ready-to-use calibration solution. The pO₂ was fixed to a minimum of 40%. Temperature was set to 37 °C before induction and then reduced to 30 °C. Induction took place with 5 mL of isopropyl β-D-1-thiogalactopyranoside (IPTG) with a concentration of 250 μg/mL, which was a 1000-fold stock solution at an OD₆₀₀ of 2.4. 50 mg/mL Amp was added as well with the IPTG. Concurrent with the induction of the biomass the glucose level was measured continuously over time to determine the endpoint of fermentation with glucose strips (Diabur Test 5000, Roche Diagnostics). OD₆₀₀ was measured during the whole process of fermentation with a Beckman Coulter DU 800 UV/Vis Spectrophotometer. After all of the glucose was consumed, the fermentation was stopped and the cells were harvested by centrifugation. The cell pellet was suspended in 50 mM potassium phosphate buffer, pH 7.0, and stored at -20 °C.

Protein purification

All purification steps were performed in 50 mM potassium phosphate buffer, pH 7.0. Cells were first disrupted in a French press, and clarified cell lysate was obtained by centrifugation. Further, protein was precipitated in the presence of 1.5 M

$(\text{NH}_4)_2\text{SO}_4$ at 4 °C, and precipitate was removed by centrifugation. The supernatant was purified by hydrophobic interaction chromatography using a Phenyl Sepharose 6 Fast Flow (High sub) column (GE Healthcare Life Sciences; 64 mL) and the Äkta FPLC system (Amersham Biosciences) with a flow rate of 5 mL/min. Eluted LOX was detected at 280 nm. Purity of the fractions showing LOX activity was determined by SDS-PAGE with PhastGel™ Gradient 8-25 (GE Healthcare Life Sciences) gels and the Pharmacia High Speed Electrophoresis System (Pharmacia Biotech).

Finally, enzyme solution was desalted by repeated cycles of concentration and dilution using concentrator tubes (Vivaspin 20, 10 kDa cut-off, Vivascience AG) and stored in 50 mM potassium phosphate buffer, pH 7.0 at 25 °C until further use.

Assays

Protein concentrations were measured using the Bradford protein quantification assay (Roti®-Quant, Carl Roth GmbH + Co KG) using BSA as reference. Note: the commercial preparation of LOX was not used for calibration of the protein assay. The enzyme is a solid powder that contains various substances other than target enzyme. Calibration based on solid mass is therefore not possible.

For kinetic studies of LOX activity a peroxidase-coupled spectrophotometric assay (Sigma-Aldrich) was used, in which the H_2O_2 produced in the LOX reaction, is further reacting with peroxidase in the presence of 4-aminoantipyrine and N,N-dimethylaniline to give a quinonediimine dye that is detected spectrophotometrically. About 5 to 10 μL of enzyme appropriately diluted in 50 mM potassium phosphate buffer, pH 7.0, were added to a solution containing 40 mM 3,3-dimethylglutaric acid, 2.5 units peroxidase, 1.5 mM 4-aminoantipyrine, 50 mM L-(+)-lactic acid and 0.04% (v/v) N,N-dimethylaniline in a total volume of 0.5 mL. The pH of the solution was pH

6.5. After a reaction time of between 10 and 20 min at 37 °C, 1 mL of 0.25% (w/v) dodecylbenzenesulfonic acid was added to stop the reaction. The produced quinonediimine dye was measured spectrophotometrically at 565 nm with a Varian Cary® 50 Bio UV-Visible Spectrophotometer at 37 °C.

Activity of LOX was determined by using the aforementioned peroxidase-coupled assay or from direct measurements of the O₂ consumption during the analyzed reaction that was L-lactate + O₂ + H₂O → pyruvate + H₂O₂. Assays were performed at 37 °C for 10 minutes in a 4.5 mL glass vial (1500 µL reaction mixture) that was sealed with a septum and contained 50 mM air-saturated potassium phosphate buffer, pH 6.5, and different concentrations (0.1 - 50 mM) of L-lactate as substrate (to determine the *K_M*). Mixing was achieved with a magnetic stirrer (300 rpm) keeping the glass vial in a water bath. The reaction was started by adding 10 µL enzyme (10 mg/ml for wild-type LOX diluted 1:100 to 1:1000, same dilution used for peroxidase assay). Dilution was varied among the mutants regarding the rates to be between 5 and 50 µM/min. Rates of O₂ utilization were measured with a fiber-optic oxygen microoptode (PreSens GmbH, Regensburg, Germany) connected to a miniaturized lock-in amplifier (MICROX TX3, PreSens GmbH, Regensburg, Germany). Calibration of the electrode was performed according to instructions of the supplier. Only the values measured during the first 3 minutes after adding the enzyme were considered in the determination of the kinetic constants because for this time frame the temperature was assumed to be constant at 37 °C. Specific activities determined for wild-type LOX at 37 °C at saturated substrate concentration (pH 6.5, 50 mM L-lactate) were similar with 200 ± 10 U/mg (peroxidase assay) and 205 ± 8 U/mg (oxygen measurement).

Time course analysis: Oxygen versus DCIP

DCIP acts as an alternative electron acceptor for LOX. In a set-up the usage of DCIP was recorded simultaneously with the O₂-consumption during the reaction of LOX with L-lactate at 37 °C. The reaction mixture (490 µL, air-rated (200 µM oxygen), preheated at 37 °C in water bath) contained L-lactate (50 mM) and DCIP (200 µM), dissolved in potassium phosphate buffer, pH 6.5. Quartz cuvettes with a Teflon stopper were used. The reaction was initiated by adding 10 µL of LOX in the appropriate dilution (wild-type 5.5 mg/ml, diluted 1:1000), and the rate of DCIP reduction was monitored by the decrease in absorption at 600 nm using a Varian Cary® 50 Bio UV-Visible Spectrophotometer. The oxygen depletion (under conditions in which DCIP and oxygen were present at a time) was determined using a fiber-optic oxygen microoptode which was placed directly into the quartz cuvette through the Teflon stopper.

Absorbance spectroscopy

UV-visible absorbance spectra were recorded with a Varian Cary® 50 Bio UV-Visible Spectrophotometer in quartz cuvettes (Hellma® GmbH & Co. KG) of 10 mm light path. Based on the method of Massey (13) the extinction coefficient of LOX in 50 mM potassium phosphate, pH 7.0, was determined from the change in absorbance following the release of FMN by trichloroacetic acid (final concentration 5% v/v). The precipitated protein was spun down for 10 min at 13000g and the supernatant immediately neutralized with solid sodium carbonate. The extinction coefficient for LOX was calculated to be 12 500 M⁻¹ cm⁻¹.

Kinetic analysis

For steady state measurements at pH 6.5 and 37 °C, initial rates of the enzymatic oxidation of L-lactic acid or other hydroxy acids were determined, wherein the substrate concentration (10 measurements for concentrations of 0.1 - 50 mM) was varied. By using the mentioned peroxidase-coupled assay, these rates were determined. Kinetic constants (K_M , V_{max}) were obtained from nonlinear fit of the Michaelis-Menten equation (**equation 2.1** or **equation 2.2**) to the measured data using Sigma Plot®, and the k_{cat} was calculated with equation 2.3

Equation 1.1:
$$v = v_{max} * \frac{[S]}{K_M + [S]}$$

Equation 1.2:
$$k_{cat} = \frac{v_{max}}{[E]}$$

where v represents the reaction rate, v_{max} the maximum rate, $[S]$ the substrate concentration, K_M the Michaelis constant, K_{IS} the dissociation constant of the enzyme-inhibitor-substrate complex, k_{cat} the turnover number. $[E]$ corresponds to the molar concentration of the enzyme. E was determined from the protein concentration assuming a molecular mass of 41 kDa for the subunit of LOX.

Stopped flow

Pre-steady state measurements were conducted using an Applied Photophysics stopped flow apparatus, model SX17MV. A diode array detector was applied to collect spectral data between 280 and 700 nm. Several wavelengths were chosen from the collected spectra and single wavelength scans with a photomultiplier. The reductive half-reaction was monitored by collecting spectra with the diode array detector and by measuring the absorbance over time at 455 nm after anaerobically mixing 10 μ M enzyme with varying concentrations of substrate (L-lactic acid, L-

glycolic acid, DL-mandelic acid). The oxidative half-reaction was followed at 455 nm detector after mixing an anaerobical solution containing reduced enzyme (10 μ M) with a buffer solution containing different concentrations of dioxygen. The oxidative half-reaction was also determined with alternative electron acceptors (DCIP, 2,5-dichloro-1,4-benzoquinone, 2,5-dimethyl-1,4-benzoquinone, methyl-1,4-benzoquinone) respectively. Anaerobic conditions were created by the addition of 10 mM D-glucose to all solutions and flushing with nitrogen. Additionally, to remove all traces of residual oxygen, glucose oxidase (Roche) was added to a final concentration of 200 nM.

Traces obtained at 455nm were fitted to an exponential function

Equation 2.1:
$$A(t) = A + Cxe^{(-kt)}$$

where A describes the absorption, C is a constant, and k represents an observed rate constant. The observed rates for substrate concentration dependent reduction of LOX were fitted using the following equation

Equation 2.2:
$$k_{obs} = \frac{k_{red} \times S}{K_d + S}$$

where k_{obs} describes an observed rate constant, k_{red} is the reduction rate constant, S is the substrate concentration and K_d is the dissociation constant.

Oxidative half-reaction with molecular oxygen

The enzyme was reduced with 2 equivalents L-lactate to guarantee a completely reduced LOX. No Michaelis-Menten type complex is formed during this re-oxidation event with molecular oxygen; by varying oxygen concentration linear plots with the primary data were created in order to determine bimolecular rate constants for this

process. Bimolecular rate constants for the reaction of free reduced LOX with molecular oxygen were calculated from plotting the rates of re-oxidation [s^{-1}] versus the oxygen concentrations [M].

Oxidative Half-Reaction in presence of 2,6-Dichlorophenolindophenol (DCIP)

For the setup, DCIP was mixed with the reduced enzyme anaerobically in the stopped flow photometer. By detecting the whole spectra (between 280 and 700 nm) with a diode array, both the decrease of the typical absorbance maximum of DCIP (at 600 nm) and the increase of the FMN (at 455 nm) could be analyzed in one experiment. A complete re-oxidation of the reduced flavin cofactor could be achieved. Different DCIP concentrations were in the range between 20-50 μ M.

Oxidative half-reaction using quinones

In order to analyze the oxidative half-reaction, the reduced enzyme, achieved by 2 equivalents lactate, was mixed anaerobically in a stopped flow apparatus with various concentrations of quinones (2,5-dichloro-1,4-benzoquinone, 50 to 200 μ M; 2,5-dimethyl-1,4-benzoquinone, 50 to 400 μ M; 2-methyl-1,4-benzoquinone; 50 to 150 μ M, all concentrations are those after mixing) at 20 °C, pH 6.5, and the re-oxidation of flavin cofactor at 455 nm was monitored. LOX was fully reoxidized, no Michaelis-Menten type was formed. Kinetic traces were fit to two exponentials using Pro-Data software, (Applied Photophysics). Bimolecular rate constants were determined by fitting k_{obs} versus various quinone concentrations to a line.

Crystallization

Crystallization was carried out using hanging drop vapor diffusion in air atmosphere at 20 °C. 1 μ L of a protein solution at 10 mg/mL in 50 mM KH_2PO_4 buffer

(pH 7.0) was mixed with 1 μL of reservoir solution of 30% polyethylene glycol in 50 mM Tris-HCl buffer (pH 8.0) and addition of 0.05 M pyruvate. Crystals were harvested in well solution with 15% (v/v) ethylene glycol. X-ray measurements were done at the Stanford Synchrotron Radiation lab. **Table 1** summarizes the crystallographic data collection and refinement statistics.

Table 1. Crystallographic data collection and refinement statistics. Values in parentheses are for data in the high resolution bin.

<u>Data collection</u>	
Unit cell dimensions	
<i>a, b, c</i> (Å)	122.59 124.36 106.89
β (°)	124.29
Resolution range [Å]	50.00 - 1.65 (1.68 - 1.65)
Completeness (%)	98.2 (95.1)
R_{merge}	5.9% (37.1%)
Observations/unique reflections	581586 / 155981
Mean $I/\sigma(I)$	26.4 (4.1)
<u>Refinement statistics</u>	
R_{cryst} (%)	15.4
R_{free} (%)	18.0
R_{free} test set	7791
Deviations from ideal geometry	
Bond lengths [Å]	0.012
Bond angles [°]	1.97
<u>Average B values (Å²)</u>	
Main-chain atoms	12.136
Side-chain atoms	14.986
FMN	10.312
Water molecules (705)	17.757
All atoms	13.730
<u>Ramachandran Plot [%]</u>	
Most favoured	96.6
Additionally allowed	3.0
Outliers	0.4

Structure determination and refinement

Molecular replacement using PHASER (34) was done to determine rotation and translation using the LOX wild-type structure (PDB entry 2DU2). Appropriate changes in sequence were made manually to the structure, which was refined using REFMAC5 (35) to reach a final R of 15.4% and R_{free} of 18.0%. Iterations of refinement and manual refitting were used to identify and add waters, ethylene glycol and pyruvate molecules to the structure. PROCHECK analysis was done as implemented in CCP4i. WinCoot 07-pre 1 (36) was used for fitting and modeling.

RESULTS

Steady state kinetics

For all experiments we decided to use the commercially available (lyophilized) wild-type LOX. The determined k_{cat} (140 s^{-1}) was similar to our recombinant wild-type (117 s^{-1}).

The A95G mutant of LOX was first reported by Massey and coworkers in 1996. Literature data showed that the mutation did not influence the k_{cat} (17). In the present work the available mutant enzyme resulted in a 9-fold loss in catalytic efficiency ($k_{\text{cat}}/K_{\text{M}}$) for reaction with L-lactate (Figure 2). The loss mainly derives from a 6-fold decrease in turnover number (k_{cat}) caused by the mutation, whereas the substrate binding (K_{M}) is only slightly influenced in comparison with the WT. Further, we expanded the substrate spectrum to several other α -hydroxy acids for steady state kinetic characterization of the A95G mutant. Table 2 summarizes the results observed with a coupled peroxidase assay at 37 °C. Only the use of L-mandelic acid

was described previously (**17**, **37**). The A95G mutant (45, 2.2 and 1.6 s⁻¹) displayed significant higher k_{cat} values than WT for *S*-2-hydroxybutyric acid, L-mandelic acid and *S*-hydroxy-3-methylbutiric acid compared to wild-type LOX. On the other hand, the K_{M} values for the latter substrates are increased.

Interestingly, concerning substrate binding, A95G displays higher K_{M} values for six out of seven substrates, L-glyceric acid remains the exception. On the basis of previous findings (**17**), our data clearly indicate that the A95G mutant has an altered substrate specificity and decreased affinity for several substrates.

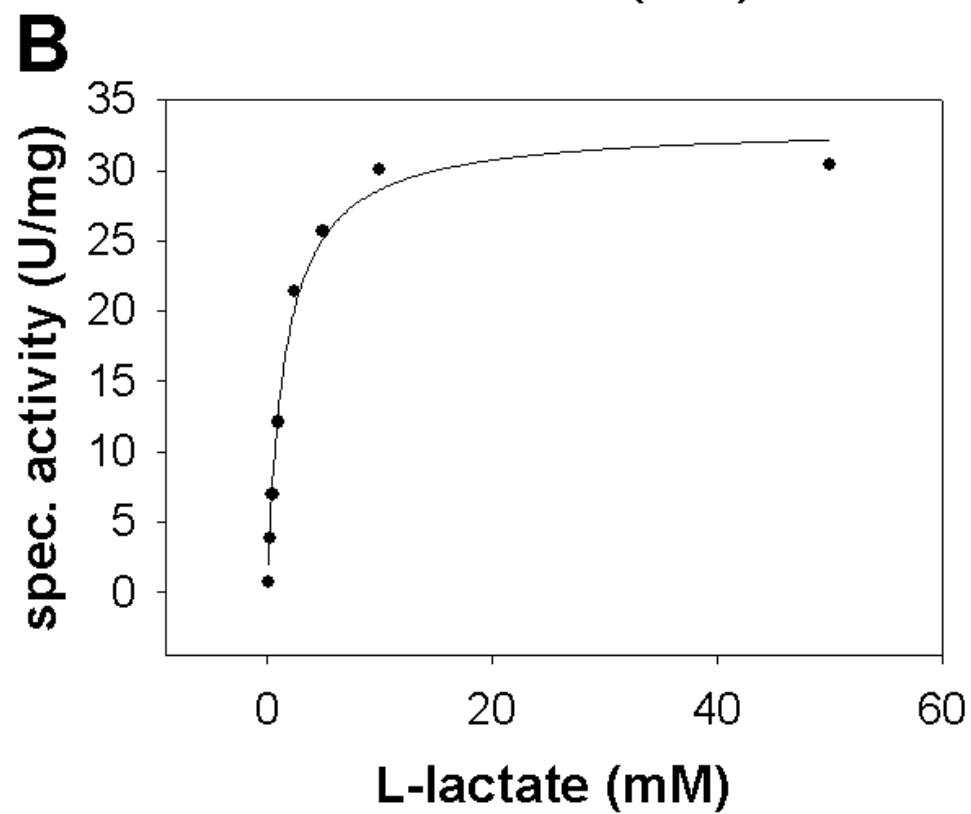
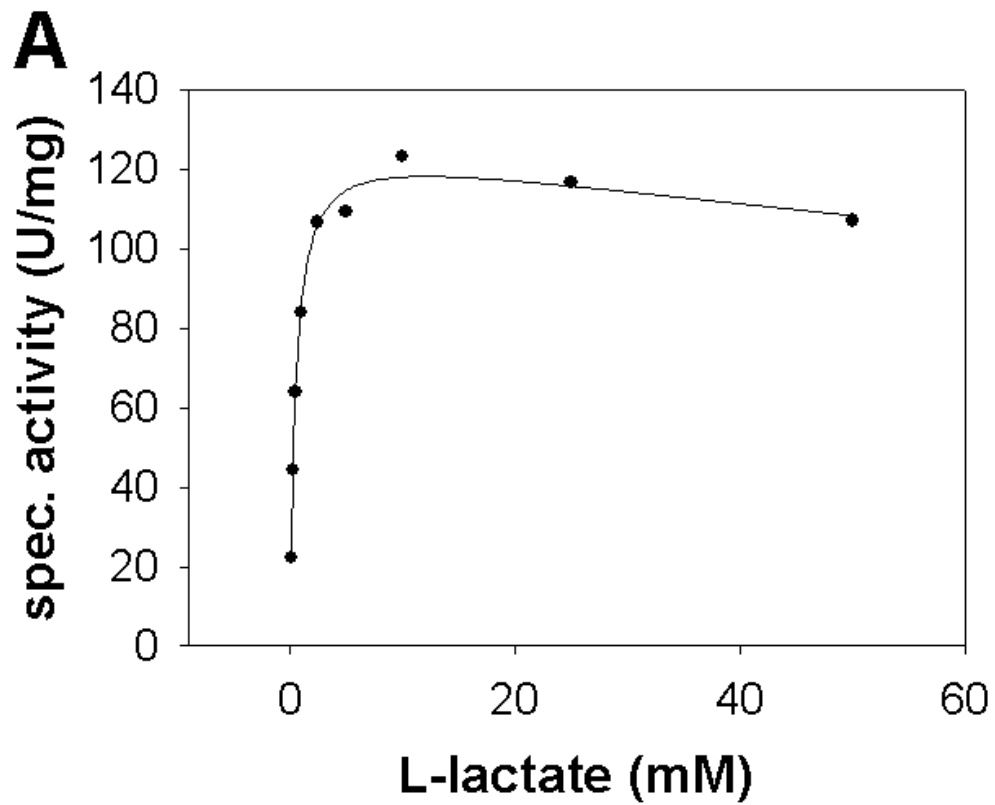
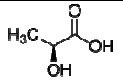
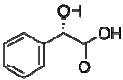
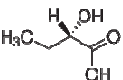
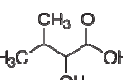
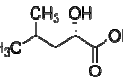
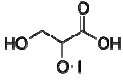
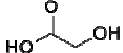


Figure 2

Steady state measurements of wild-type LOX (A) and A95G mutant (B) at different L-lactate concentrations determined by a coupled peroxidase assay at 20 °C. Wild-type LOX shows a substrate inhibition at higher substrate concentrations.

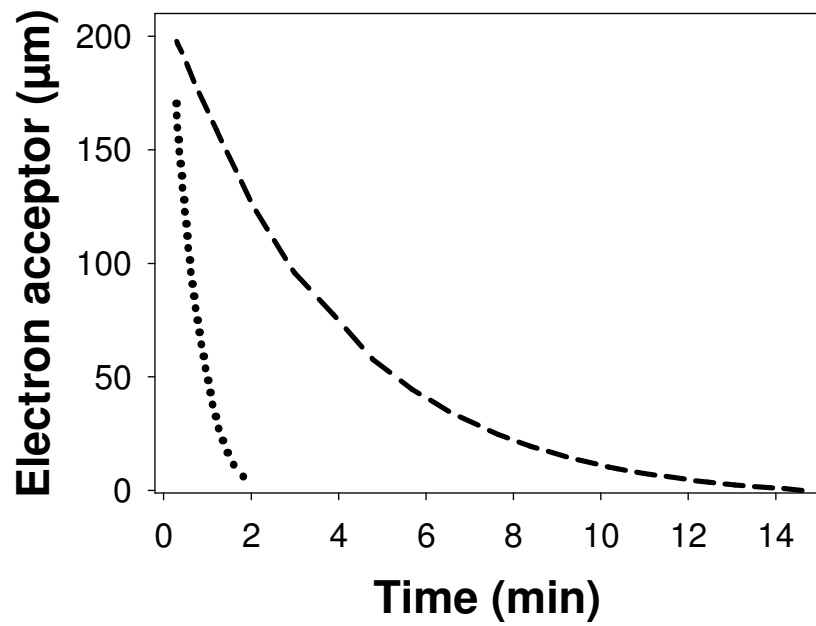
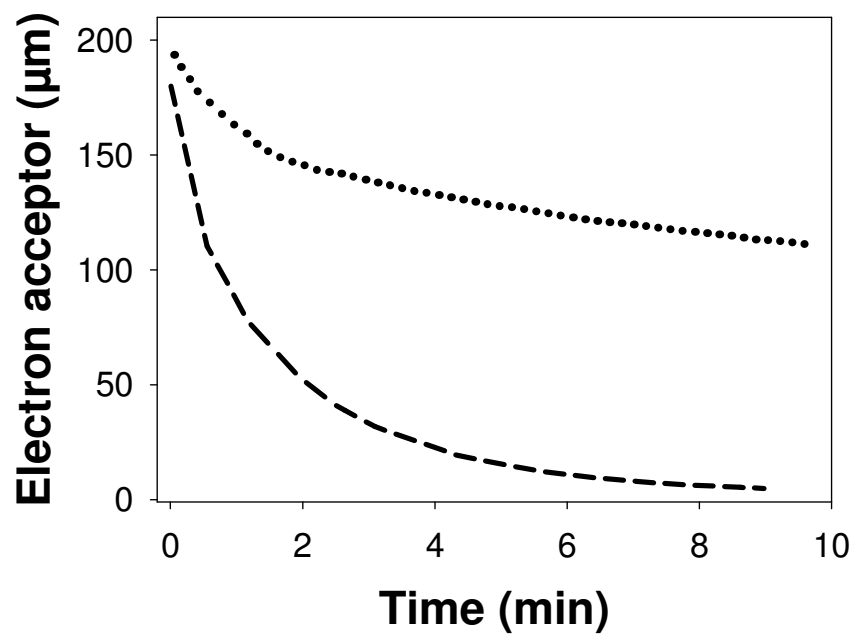
Table 2. Comparison of substrate specificity of wild-type LOX and A95G mutant

substrate		Wild-type LOX				A95G			
		k_{cat} (s ⁻¹)	K_{M} (mM)	$k_{\text{cat}}/K_{\text{M}}$ (mM ⁻¹ s ⁻¹)	K_{I} (mM)	k_{cat} (s ⁻¹)	K_{M} (mM)	$k_{\text{cat}}/K_{\text{M}}$ (mM ⁻¹ s ⁻¹)	K_{I} (mM)
L-(+)-lactic acid		140 ± 1	0.8 ± 0.03	167	-	23 ± 0.6	1.3 ± 0.1	18	-
L-mandelic acid		0.1 ± 0.002	0.5 ± 0.1	0.2	-	2.2 ± 0.1	2.8 ± 0.25	0.8	32
(S)-2-hydroxybutyric acid		1.4 ± 0.01	0.4 ± 0.05	3.2	-	45 ± 2.3	3.6 ± 0.3	12.5	50
(S)-hydroxy-3-methylbutyric acid		0.2 ± 0.01	3.3 ± 0.3	0.1	-	1.6 ± 0.1	15 ± 1.4	0.1	-
(S)-2-hydroxyisocaproic acid		1.1 ± 0.01	0.4 ± 0.05	2.5	-	0.2 ± 0.02	9 ± 1.5	0.03	-
L-(-)-glyceric acid		2.9 ± 0.1	8.6 ± 2.0	0.3	-	0.6 ± 0.05	1.3 ± 0.3	0.4	-
glycolic acid		0.98 ± 0.02	0.4 ± 0.06	2.2	116	0.6 ± 0.04	8 ± 0.05	0.07	-

^a Steady state measurements were performed at 37 °C with a coupled peroxidase assay. Standard deviations on kinetic parameters are from non-linear fits of data with the Michaelis-Menten equation.

Time course analysis

We analyzed the conversion of DCIP in a competing reaction with O₂ as electron acceptor when L-lactate is the chosen substrate. **Figure 3** shows a time course analysis for LOX wild-type and A95G mutant in the presence of molecular oxygen and DCIP, where in excess L-lactate is converted. In the presence of both acceptors, the oxygen concentration drops faster than that of DCIP for the wild-type enzyme. The A95G mutant showed an altered behavior contrary to the wild-type enzyme, as here DCIP was consumed faster than oxygen. The experiment additionally elucidated that DCIP seems to hinder the consumption of oxygen when the artificial acceptor is completely reduced, as the final concentration did not reach 0. However, the first linear depletion of DCIP has been used to determine the rates for the respective specific activities, which are listed in **Table 3**. Specific activities for L-lactate either determined with DCIP or the coupled peroxidase assay demonstrate changed behavior between wild-type and LOX A95G in terms of electron acceptors. LOX wild-type prefers O₂ 4-fold over DCIP as an electron acceptor. LOX S218C, a mutant previously described (**33**), resembles LOX wild-type properties with specific activities of 64 U/mg for O₂ and 16 U/mg with DCIP (**data not shown**). On the contrary, A95G indicates a significant preference (4-fold) for DCIP over molecular oxygen.

A**B****Figure 3****Time course analysis of LOX**

Panel A: Simultaneous consumption of DCIP (black dotted line) and molecular oxygen (medium dotted line) during the reaction of 25.6 nm wild-type LOX enzyme (**Panel A**) and 7.7 nm LOX A95G mutant (**Panel B**) with L-lactate (50 mM) at pH 6.5, 37 °C.

Table 3. Specific activity of LOX in excess L-lactate with O₂ and DCIP as electron acceptors

Specific activity	Wild-type LOX	A95G	WT : A95G
O ₂ assay (U/mg) ^a	200 ± 9	33 ± 3.5	6 : 1
DCIP assay (U/mg) ^b	46.2 ± 3.5	140 ± 7.5	1 : 3

^a determined in presence of 200 μM O₂ at 37 °C
^b determined in presence of 200 μM DCIP at 37 °C

We further measured the decay of free DCIP (in absence of oxygen) at 600 nm with several substrates for LOX A95G mutant at steady state conditions (potassium phosphate buffer, pH 6.5, 37 °C). **Table 4** compares the determined activities from the DCIP experiments with those evaluated by the coupled peroxidase assay. All results demonstrate that LOX A95G prefers the artificial electron acceptor (DCIP) 4- to 8-fold over molecular oxygen.

Table 4. Specific activities for various α-hydroxy acids determined for LOX A95G mutant at 37 °C

Substrate	DCIP assay (U/mg)	H ₂ O ₂ assay (U/mg)	DCIP : H ₂ O ₂
L-lactic acid	140	33	4.2 : 1
L-2-hydroxy-butyric acid	354	65	5.5 : 1
L-mandelate	9.3	1.1	8.2 : 1
Glycolate	3.4	0.8	4.2 : 1
2-fluro-mandelate	3.0	0.4	7.5 : 1

Pre-steady state experiments of the reductive half-reaction

In order to obtain pre-steady state kinetics of wild-type LOX and A95G mutant, we recorded spectral changes of the FMN cofactor by applying a stopped flow photometer using diode array detection for spectral scans and a photomultiplier for

single wavelengths. We analyzed the reductive and oxidative half-reaction separately to find a rate limiting-step in the reaction mechanism.

To monitor the reductive half-reaction, we mixed LOX anaerobically with various concentrations of L-lactic acid (0.05 -1 mM). The conversion from oxidized to reduced FMN at 20 °C was identified by one single phase, spectral scans show the typical reduced FMN spectrum; compared to the oxidized state FMN_{red} lacks both absorbance maxima at 373 and 455 nm. We followed the decay in absorbance by single wavelengths at 455 nm. The A95G mutant exhibits a slightly decreased reduction rate compared to wild-type LOX, whereas the determined k_{cat} for A95G (22.7 s⁻¹) is 4-fold slower than the wild-type k_{cat} (87.5 s⁻¹). **Figure 4** outlines how the k_{red} was determined for LOX, which was reduced with L-lactic acid. On the other hand, **Table 5** demonstrates the rate constants for L-lactic acid. We also tested the reductive half for the recombinant wild-type LOX (see **Figure S1B**) with _L-lactate at 20 °C ($k_{\text{red}} = 258 \pm 8 \text{ s}^{-1}$), and in comparison with the lyophilized wild-type no differences in k_{red} or K_{d} were detected.

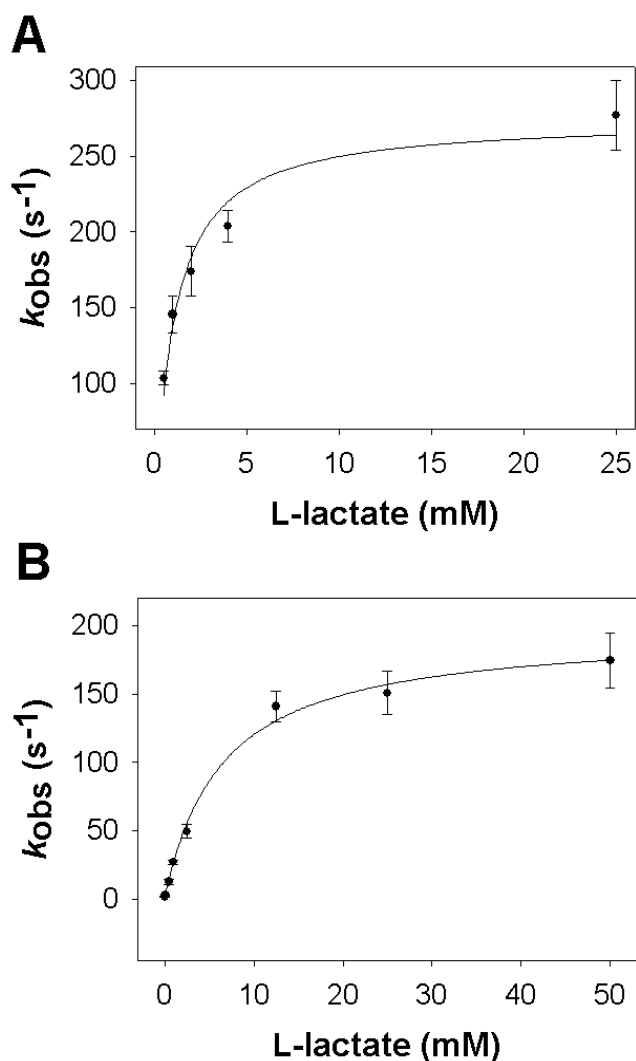


Figure 4

Determination of the reduction rate constant (k_{red}) and dissociation constant (K_d) for reaction of wild-type LOX (A) and A95G mutant (B) with L-lactate at 20 °C. Pseudo first order rate constants, k_{obs} from determined single traces at 455 nm are plotted versus L-lactate to yield k_{red} and K_d .

Table 5. Rate constants established for the reductive half-reaction for wild-type LOX and A95G^a

Substrate	Wild-type LOX			A95G		
	k_{red} (s ⁻¹)	K_d (mM)	k_{red}/K_d (s ⁻¹ mM ⁻¹)	k_{red} (s ⁻¹)	K_d (mM)	k_{red}/K_d (s ⁻¹ mM ⁻¹)
L-(+)-lactic acid	274 ± 11	1 ± 0.2	274	235 ± 13	7.4 ± 1.5	31.7
glycolic acid	0.2 ± 0.003	0.40 ± 0.04	0.5	n.d.	n.d.	n.d.
DL-mandelic acid	0.04 ± 0.001	0.9 ± 0.1	0.05	n.d.	n.d.	n.d.
L-mandelic acid	0.08 ± 0.001	n.d.	n.d.	5.3 ± 0.5	0.6 ± 0.24	9
(S)-2-hydroxy-	9 ± 0.5	0.9 ± 0.2	10	371 ± 0.1	2 ± 0.6	186

Furthermore, we examined the impact of several substrates on the reductive half-reaction. **Table 5** summarizes the rates of the reductive half-reaction of certain substrates for wild-type LOX and A95G mutant. For wild-type LOX, L-lactate (250 s^{-1}) represents the fastest reduction rate, whereas the highest rate for A95G was found with L-butyric acid (371 s^{-1}) (**compare Figure 5**). Reduction rate constants of wild-type LOX perfectly fit to steady state kinetics from **Table 2** (e.g. higher activity with L-lactate than L-hydroxy-butyric acid). Regarding the catalytic efficiency, the term $k_{\text{cat}}/K_{\text{M}}$ should be consistent with $k_{\text{red}}/K_{\text{d}}$ (**27**). When using L-lactate as substrate, the determined $k_{\text{cat}}/K_{\text{M}}$ ($176 \text{ mM}^{-1} \text{ s}^{-1}$) for wild-type LOX at 20 °C is almost half of the $k_{\text{red}}/K_{\text{d}}$ ($330 \text{ mM}^{-1} \text{ s}^{-1}$). The same is valid for the A95G mutant with a calculated $k_{\text{cat}}/K_{\text{M}}$ of $31.7 \text{ mM}^{-1} \text{ s}^{-1}$ and a $k_{\text{red}}/K_{\text{d}}$ of $14.2 \text{ mM}^{-1} \text{ s}^{-1}$. Therefore, the slower k_{cat} means that an additional limiting step for the reaction has to be present in the product formation.

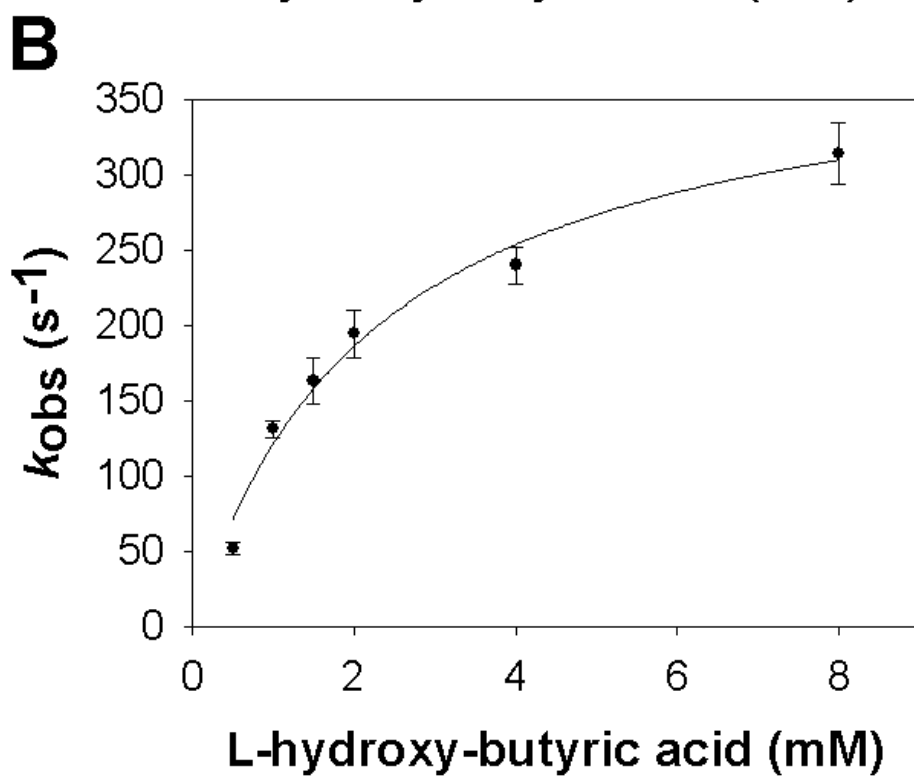
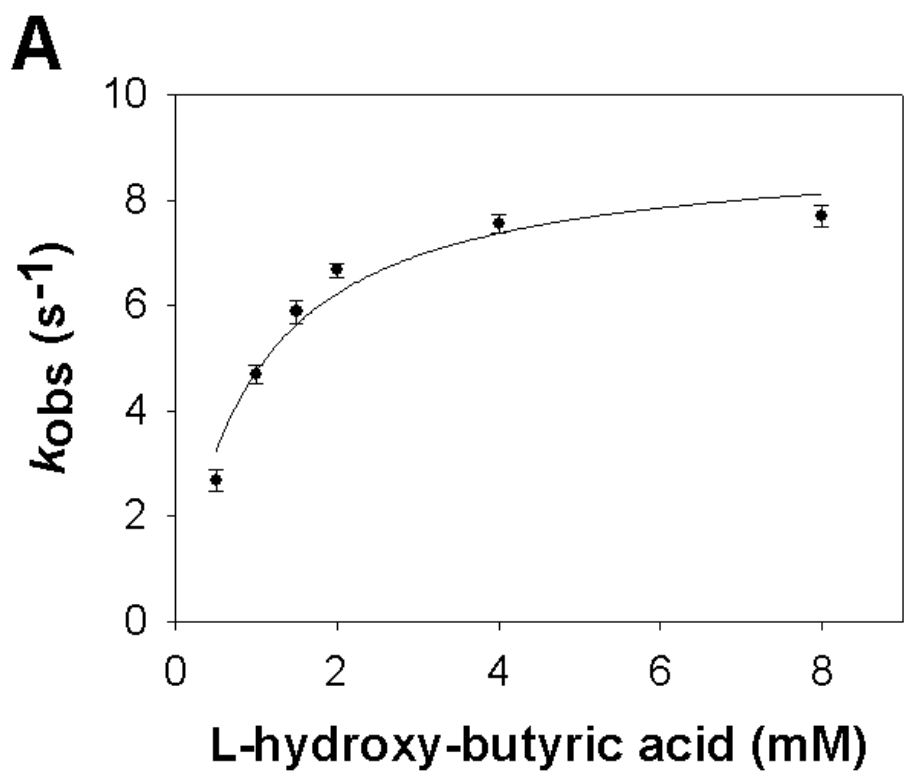


Figure 5

Determination of the reduction rate constant (k_{red}) and dissociation constant (K_d) for reaction of wild-type LOX (A) and A95G mutant (B) with L-hydroxy-butyric acid at 20 °C. Pseudo first order rate constants, k_{obs} from determined single traces at 455 nm are plotted versus L-hydroxy-butyric acid to yield k_{red} and K_d .

Differing reductive rates suggest that the rate limiting step is found in the first half-reaction, which includes the conversion of substrate and the release of the product, since the use of different substrates did not have an influence on the faster oxidative half-reaction. Additional stopped flow experiments proved that the re-oxidation rate with O₂ remained the same after reducing LOX with various hydroxy-acids (data not shown). Regardless of the substrate used in the experiment - L-lactate or L-glycolic acid - the FMN cofactor was fully reduced. However, with certain substrates the FMN cofactor is reduced differently. Steady state kinetics revealed a slow conversion of hydroxy-methyl butyric acid, in the pre-steady state analysis two separated phases occurred during the reductive half-reaction - a fast one within a few milliseconds, where the cofactor is reduced to one fifth up to one tenth of the fully reduced state depending on the used substrate concentration and a second slow phase, which needed several minutes. Data from the first phase could not be analyzed appropriately and are missing in **Table 5**. Nevertheless, the reductive half-reaction indicates that the substrate does not fit perfectly into the active site and subsequently displays low activity with wild-type LOX.

Pre-steady state experiments of the oxidative half-reaction

Besides the reductive half-reaction, we examined the oxidative half-reaction with O₂ and several alternative electron acceptors. **Figure 6** represents the determination of k_{ox} with O₂. Re-oxidation was followed by an increase in absorbance at 455 nm in a single exponential manner. The same has been observed when reduced LOX was mixed with an alternative electron acceptor in an anaerobic manner. **Figure 7** shows different LOX spectra in potassium phosphate buffer and DCIP. After reduction of L-lactate oxidase with dithionite the enzyme seems to form an equilibrium flavin N5 adduct with essentially complete loss of the typical flavin absorbance in the 350- to

500-nm region; a similar effect was achieved, when LOX was reacted with sulfite (1). For the re-oxidation experiments of a chemically reduced LOX with the alternative electron acceptor, we mixed LOX - after reducing it with dithionite - in a stopped flow experiment with low concentrations of DCIP (12.5, 25 μM). FMN was re-oxidized, and

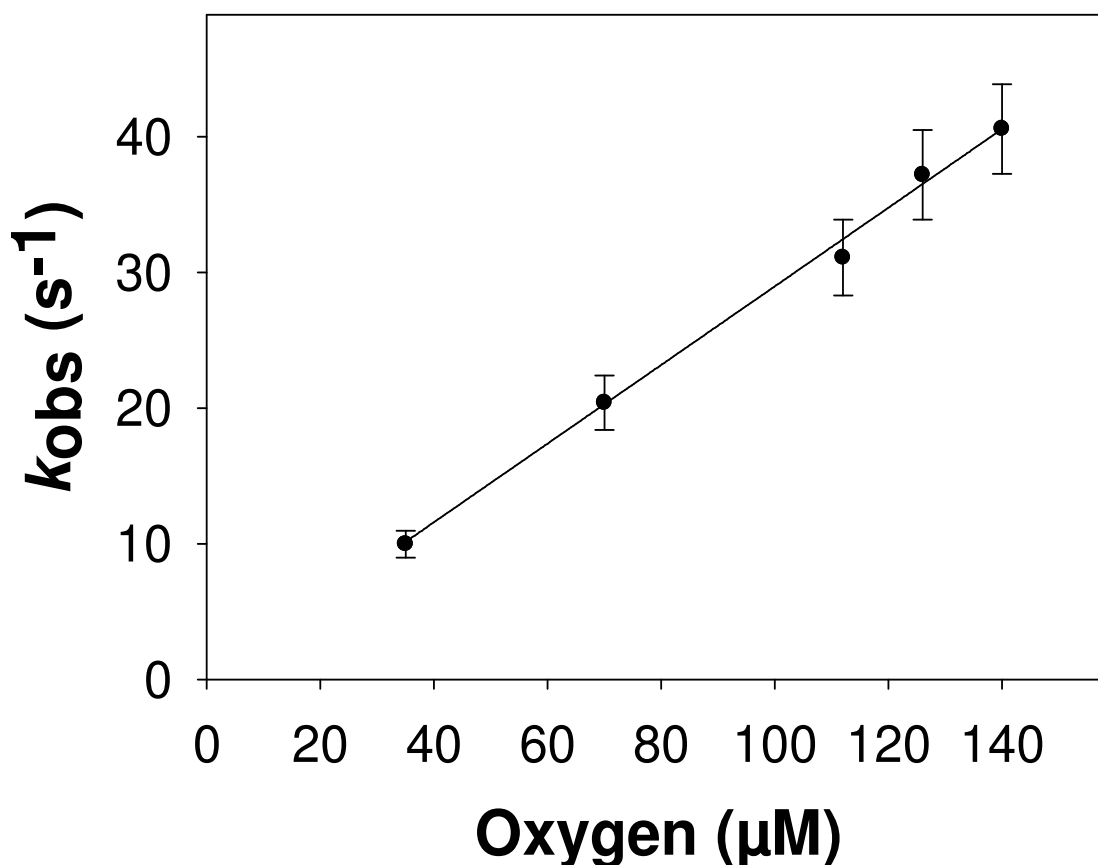


Figure 6

Re-oxidation of reduced LOX A95G with molecular oxygen in 50 mM potassium phosphate buffer, pH 6.5 (20 °C). Enzyme (10 μM after mixing) was reduced anaerobically by titrating with two equivalents of L-lactate. The reduced enzyme was mixed with aerobic buffer containing various concentrations of molecular oxygen (35, 70, 112, 126 and 140 μM) at pH 6.5, and the re-oxidation was monitored spectrophotometrically at 455 nm in a single exponential manner. The observed rate constants varied linearly with O_2 concentration, suggesting a bimolecular reaction with a rate constant of $2.8 \times 10^5 \text{ M}^{-1} \text{ s}^{-1}$.

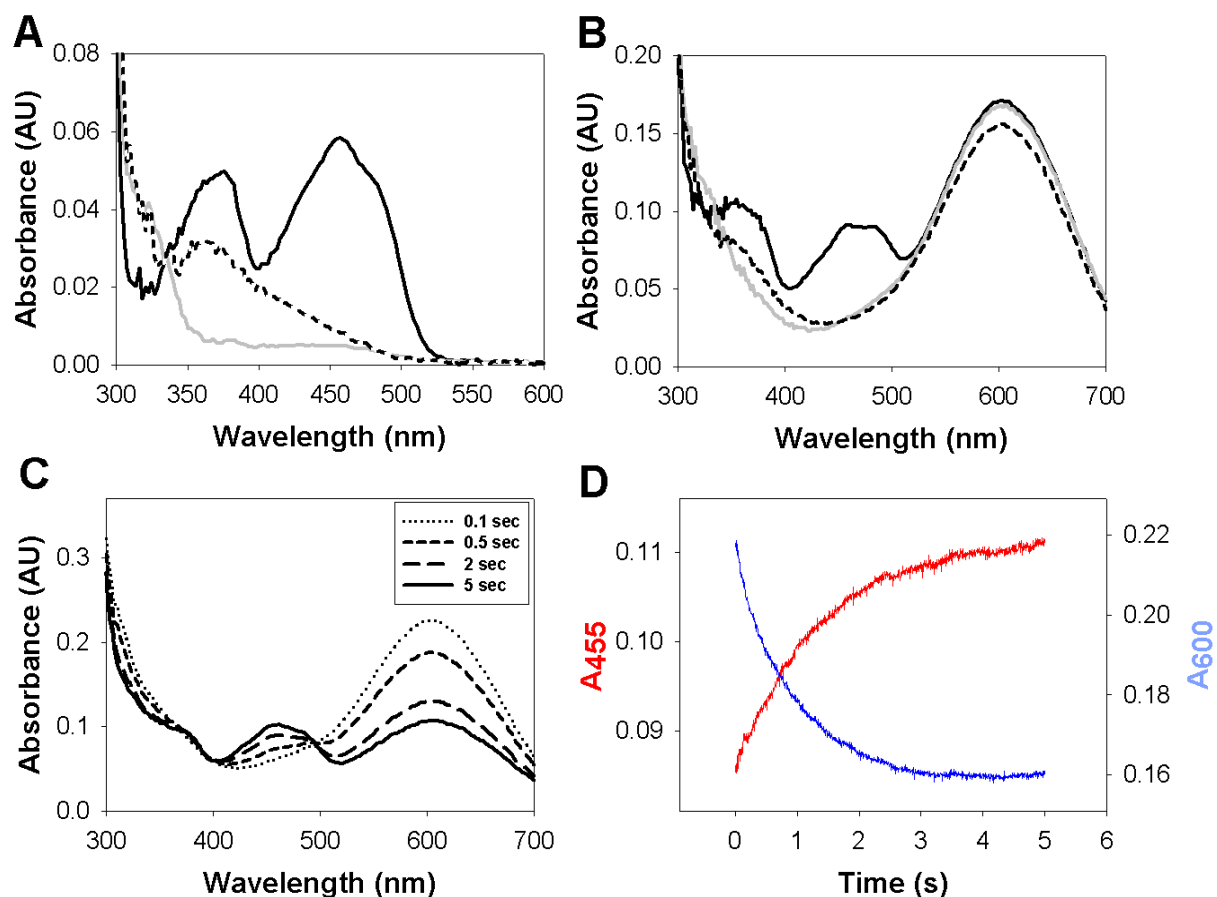


Figure 7

Different spectra of wild-type LOX from stopped flow experiments

Panel A: Spectrum of wild-type LOX ($5\ \mu\text{M}$) in 50 mM potassium phosphate buffer, pH 6.5. Enzyme in oxidized (**black line**) state, reduced state when 1 equivalent L-lactic acid is chosen as substrate (**black dotted**), and after chemical reduction with dithionite (**grey**).

Panel B: Spectrum of wild-type LOX ($5\ \mu\text{M}$) in 50 mM potassium phosphate buffer, pH 6.5 in presence of $25\ \mu\text{M}$ DCIP. Enzyme in oxidized (**black line**) state, reduced state (**black dotted**) when 1 equivalent L-lactic acid is chosen as substrate, and after chemical reduction (**grey**) with dithionite.

Panel C: Spectrum illustrating time resolved re-oxidation steps of $6\ \mu\text{M}$ LOX FMN_{red} with $30\ \mu\text{M}$ DCIP after 0.1, 0.5, 2 and 5 seconds.

Panel D: Single wavelength traces of LOX in presence of $25\ \mu\text{M}$ DCIP. Trace at 455 nm (**red**) follows re-oxidation of FMN cofactor; second trace at 600 nm (**blue**) demonstrates the reduction of DCIP during re-oxidation process.

DCIP was reduced simultaneously, though the re-oxidation process took around 500 seconds and was 100 times slower than under conditions, where L-lactic acid (5 s) was used to reduce FMN. Besides DCIP several quinones could fully re-oxidize the FMN cofactor after reduction with L-lactate. This result was verified for all different quinones and DCIP in absence of molecular oxygen by multi-wavelength scans at the

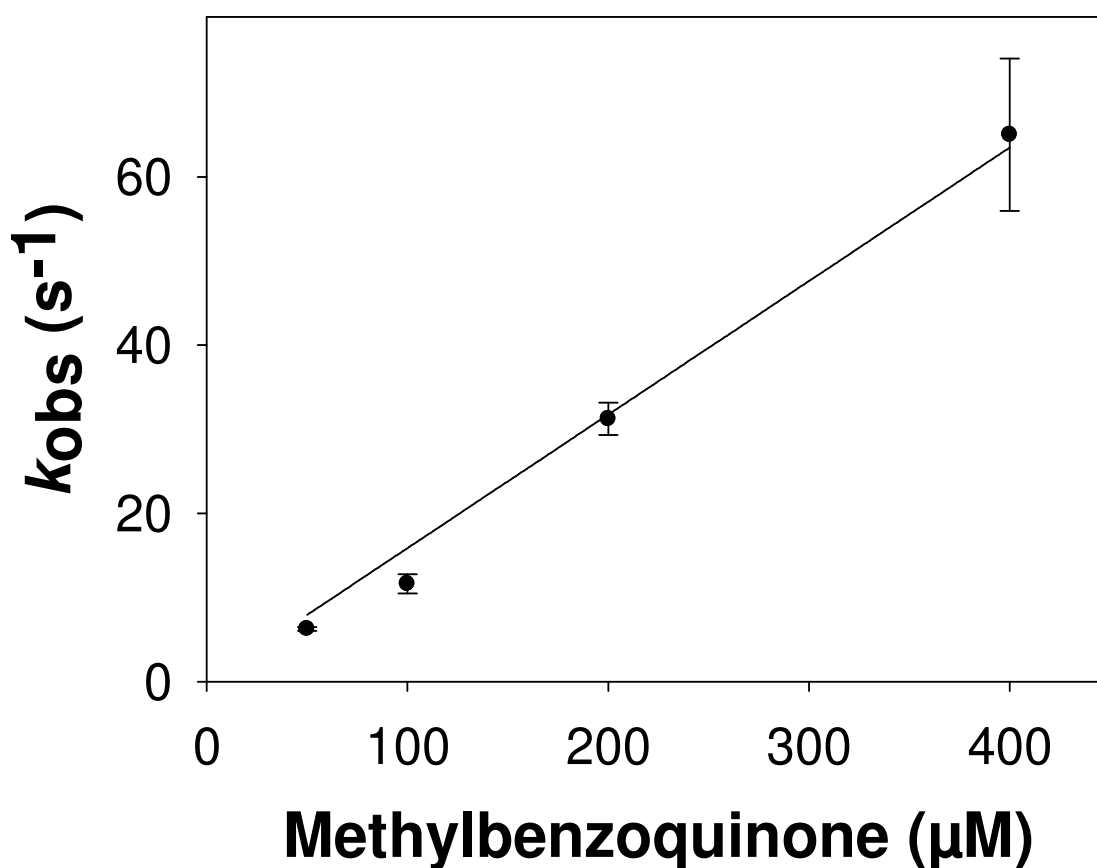


Figure 7

Oxidation of reduced LOX A95G with 2-methyl-1,4-benzoquinone in 50 mM potassium phosphate buffer, pH 6.5 (20 °C). Enzyme (10 μM after mixing) was reduced anaerobically by titrating with two equivalents of L-lactate. The reduced enzyme was mixed with various concentrations of methyl-*p*-benzoquinone (50, 100, 200 and 400 μM) at pH 6.5, and the re-oxidation was monitored in a single exponential manner at 455 nm. The observed rate constants varied linearly with quinone concentration, suggesting a bimolecular reaction with a rate constant of $1.6 \times 10^5 \text{ M}^{-1} \text{ s}^{-1}$.

typical absorbance maxima of LOX at 373 and 455 nm. (Note: An accurate re-oxidation rate could be determined at 455 nm; due to an overlay of the DCIP dye at 373 nm at higher substrate concentrations the determination was not possible). In agreement with the re-oxidation step of the FMN cofactor the DCIP dye is reduced simultaneously leading to the typical drop in absorbance at 600 nm. In addition, no further change, e.g. at 280 nm can be seen during this re-oxidation process. In detail, re-oxidation of the reduced A95G mutant was 3-fold faster with DCIP ($1.0 \times 10^6 \text{ M}^{-1}\text{s}^{-1}$) than with molecular oxygen.

Table 6. Re-oxidation rate constants of various electron acceptors for wild-type LOX and A95G^a

Electron acceptor	E_m (V)	wild-type LOX	A95G
		k_{ox} ($\text{M}^{-1} \text{s}^{-1}$)	k_{ox} ($\text{M}^{-1} \text{s}^{-1}$)
2,5-dichloro-1,4-benzoquinone	+0.310	$2.7 \pm 0.2 \times 10^4$	$8.9 \pm 0.5 \times 10^4$
2-methyl-1,4-benzoquinone	+0.240	$3.7 \pm 0.2 \times 10^4$	$1.6 \pm 0.1 \times 10^5$
2,6-dichlorophenolindophenole	+0.217	$1.3 \pm 0.1 \times 10^5$	$1.0 \pm 0.1 \times 10^6$
2,5-dimethyl-1,4-Benzoquinone	+0.176	$5.9 \pm 0.4 \times 10^4$	n.d.
O ₂		$1.8 \pm 0.1 \times 10^6$	$3.3 \pm 0.2 \times 10^5$

^a Pre-steady state experiments were performed in 50 mM potassium phosphate buffer, pH 6.5 at 20 °C
n.d. not determined

Several other electron acceptors used in this study reflected a similar effect as DCIP, however, the A95G mutant revealed an increased re-oxidation rate with the tested quinones compared to LOX wild-type. **Figure 8** exemplifies for methylbenzoquinone, how we determined the kinetic rate constant k_{ox} , which was similar to re-oxidation with O₂, DCIP and other quinones. For LOX, no Michaelis-Menten type complex is formed during the re-oxidation process with these electron acceptors. By varying the electron acceptor concentration, linear plots with the primary data (k_{obs}) were created, in order to determine bimolecular rate constants. **Table 6** lists the bimolecular rate constants for O₂, DCIP and 3 different quinones and demonstrates

the differences between wild-type LOX and A95G mutant. A drop in k_{ox} as determined for A95G mutant can also influence k_{cat} ($1/k_{cat} = 1/k_{red} + 1/k_{ox}$).

Structural analysis

As with the native enzyme, the LOX A95G mutant structure is tetrameric with an entire C_4 tetramer within the asymmetric unit. Disorder prevented the fitting of residue ranges in each subunit in the final refined model: A (1-5, 203-204), B (1-6, 199-204), C (1-7, 203-204) D (1-7, 203-204). FMNs and pyruvates were found in density consistent with the wild-type structure (PDB accession 2E77) (18). Unless stated otherwise, structural analysis will be done using subunit A as overall B-factors for each subunit (A: 13.6 Å²; B:14.9 Å²; C:14.5 Å²; D: 14.0 Å²) indicated the lowest disorder. These subunits are similar overall with r.m.s. deviations of C_α s from subunit A calculated to be 0.26 Å, 0.21 Å and 0.16 Å for subunits B, C and D respectively. The overall fold is a $(\beta/\alpha)_8$ barrel and the active site is found adjacent to the FMN cofactor at the C-terminal end of the inner β -barrel. In addition to the A95G mutation, this protein contains four other mutations, T102A, S163G, G232A and R255A. In most cases, these were well defined in the electron density. They are likely to be functionally inert as they are all on the periphery of the structure and >18 Å from the oxidized substrate carbon on the pyruvate in the active site. This pyruvate occupying the active site is completely sequestered from solvent by the loops connecting strands and helices as well as by two longer irregular excursions composed of amino acids 34-44 and 179-218. One or more of these loops must therefore move to allow substrate binding and product exit. We note B-factors trend higher for amino acids in this second loop, particularly in subunits B and C, suggesting that the mobility of some or all of these residues is important in access to the enzyme's active site.

Comparing the structure of the site of the A95G mutation with the pyruvate-bound wild-type enzyme (PDB accession number 2E77) reveals subtle changes in the active site in the case of subunits A, B and D. There is a slight change in the main chain conformational torsion angles of Gly-95 creating slightly more volume in the pyruvate methyl binding site. The missing methyl group in the wild-type alanine is replaced with a water molecule that hydrogen bonds with N5 of the isoalloxazine ring. In the case of subunit C, similar movements and the presence of the water molecule are found when comparing to the wild-type structure. On the other hand, substantial affecting other residues contacting the pyruvate were observed including significant (>1 Å) shifts in the backbone and side chains of Tyr-124, Tyr-146 and Tyr-215. There are little or no changes observed in other residues contacting the pyruvate including Tyr-40, Arg-181, His-265, Arg-268 or the FMN cofactor. Since subunit C in the wild-type structure has no substrate in the active site, this disorganization has previously been interpreted as a consequence of substrate binding (**18**).

DISCUSSION

In this work we have presented a mutant of L-lactate oxidase of *Aerococcus viridans*, which promotes an altered selectivity for electron acceptors, e.g. several quinones and DCIP. The prediction of the reactivity with oxygen in flavoproteins in re-oxidation reactions is still an unsolved challenge. Multiple 3D structures of oxidases and dehydrogenases highlighted that structural themes are missing to predict binding and reactivity of flavoenzymes (**42**). However, many structural and mutational studies of active-site residues provide mechanistic clues for future prospects (**43, 44**).

Crystal structure analysis

The enzyme's specificity for substituents at the 2 position in 2-hydroxy acids is believed to be governed by residues surrounding the methyl group in the lactate substrate, which includes Ala-95. The structure shows that the mutation of this residue to glycine increases the volume available at this position by removing the steric bulk of the alanine side chain and allowing the main chain to relax slightly away from the lactate binding site. This extra volume potentially allows the substrate to rotate slightly to permit a re-direction of the substituent at the 2 position. The ability to accommodate this explains the mutant enzyme's increased catalytic efficiency with 2-hydroxybutyric acid and slight improvement with the nearly-isosteric glyceric acid (**Table 2**). It also may account for the decreased activity with lactate as the substrate would have fewer structural constraints in binding and has the potential to bind in a more disordered fashion. Explanation of activity with the substrates with bulkier substituents described in **Table 2** is more difficult to explain using the static crystallographic model in both the wild-type and mutant enzymes. Modeling experiments indicate possible steric conflict between the groups at the 2 position and the side- and/or main-chain atoms of Tyr-124 and Tyr-191.

Kinetic analysis

Additionally to steady state experiments, we performed pre-steady state kinetic analysis of the reductive and oxidative half-reactions separately in order to see, if we could identify a rate-limiting step that would explain the lowered catalytic efficiency of A95G mutant compared to wild-type LOX. Whereas the reductive half-reaction of A95G had similar rates as the wild-type LOX, the lower rate of the oxidative half-reaction could explain the lower overall catalytic rate of A95G mutant.

Lowering the temperature explained even differences of the enzymes within the reductive half-reaction.

Spectral scans revealed the typical reduced FMN spectrum, where FMN_{red} lacks both absorbance maxima at 373 and 455 nm. Shown for wild-type LOX and A95G mutant at 4 °C, the conversion from the oxidized into the reduced FMN was identified in a biphasic manner. Besides a double exponential decay with a fast start and a slow phase at 455 nm resulting in $k_{\text{obs}1}$ and $k_{\text{obs}2}$, we observed the formation and the decay of an intermediate at 530 nm, which was previously described for wild-type LOX at temperatures below 5 °C (1) - to identify the formation of the intermediate for LOX wild-type, we repeated the stopped flow experiment at 4 °C. In contrast to a single exponential decay shown for LOX at 20 °C and resulting in a single constant termed k_{red} (expressed in s^{-1}), the reduction with lactate at 4 °C can be described by two different phases. The first phase ($k_{\text{red}1}$) of 455 nm reaches a maximum at $1.3 (1.4) \times 10^2 \text{ s}^{-1}$ for WT (A95G mutant), whereas the second phase ($k_{\text{red}2}$) reaches its maximum at $0.72 (0.27) \times 10^2 \text{ s}^{-1}$. The first phase of A_{455} is as fast as the increase at A_{530} , whereas the second phase of A_{455} is similar to A_{530} . To determine the overall k_{red} , k_{obs} ($1/k_{\text{obs}} = 1/k_{\text{obs}1} + 1/k_{\text{obs}2}$) was plotted against the lactate concentration.

Fitting and simulation of both traces were performed with software Berkeley Madonna (**compare Figures 9 and 10**). Studies by Massey and co-workers mainly identified an intermediate of LOX mutants at temperatures below 4 °C (17). In short, the 3 ms dead-time of the stopped flow instrument at higher temperatures was the virtual reason, which hindered the detection of the intermediate step. Consequently, we could only detect a decrease of the intermediate with both enzymes at 20 °C. **Scheme 2** represents the minimalistic reaction mechanism of LOX and explains the formation and the decay of the intermediate.

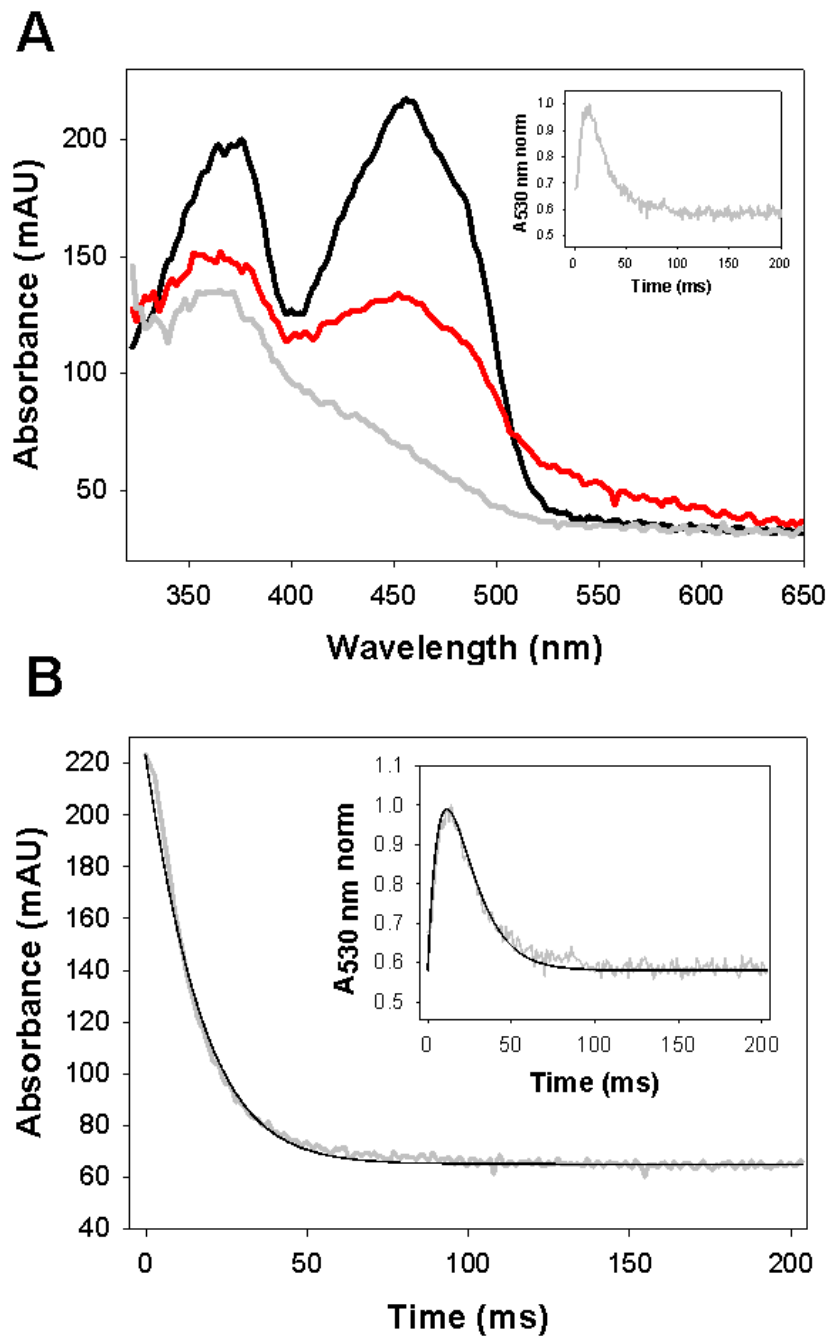
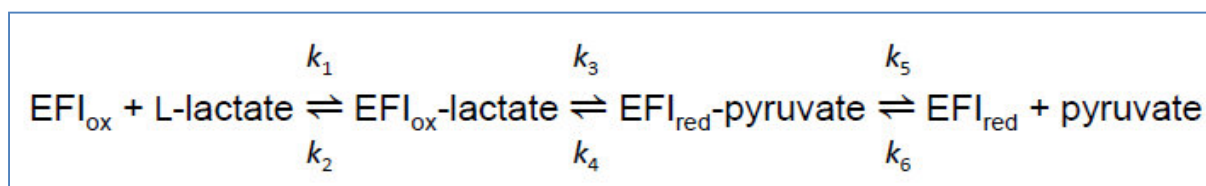


Figure 9

Spectral scans of wild-type LOX and fitting with Berkeley Madonna

Panel A: Spectral scans of wild-type LOX during the reductive half-reaction. 19.4 μM LOX were reduced with 10 mM L-lactate under anaerobic conditions in 50 mM potassium phosphate buffer, pH 6.5 at 4 °C. **Black** line: enzyme in oxidized state at start (0 ms); **red** line: reaction after 14 ms; **light grey** line: reaction after 200 ms. After 14 ms the maximum in absorbance at 530 nm is reached (compare dark **grey** trace for the whole reaction at inset), the amplitude decreases afterwards.

Panel B: Reductive half-reaction of wild-type LOX by L-lactate. 19.4 μM enzyme in 50 mM potassium phosphate buffer (pH 6.5) were reacted in the stopped flow photometer at 4 $^{\circ}\text{C}$ with 10 mM L-lactate. The grey line represents the reaction trace at 455 nm with two different phases (first phase = k_3 ; second phase = k_5) the inset reflects the trace at 530 nm in a biphasic manner. Black lines represent the fittings achieved with software Berkeley Madonna leading to the calculated kinetic constants in **Table 2**.



Scheme 2. Reaction mechanism of LOX

Simulation of the reductive half-reaction

The fitting of the traces of A_{455} and A_{530} was performed in two steps. First, since the only species absorbing at 530 nm is the complex EPyr, a normalized absorbance can be defined that could directly depend on the ratio of EPyr/EPyrmax (EPyrmax is the maximum concentration of EPyr reached during the reaction course). The experimental data for the intermediate (A_{530}) were normalized by dividing all data by the maximum value of the same data set. Normalized data were then fitted to a variable defined as R (=EPyr/EPyrmax plus Background absorbance). Different set of data were used for the fitting resulting in a calculated value for EPyrmax. Once EPyrmax was calculated, using the $A_{530\text{max}}$, the intrinsic absorbance of EPyr can be estimated. The consistency between different set of data was ensured, leading to a value of 6.7 (2.9) μM with a S.D. of 0.1 (0.2) μM for wild-type LOX (A95G mutant) when E= 19.5 (5) μM . This value was used to calculate the intrinsic absorbance (ϵ)

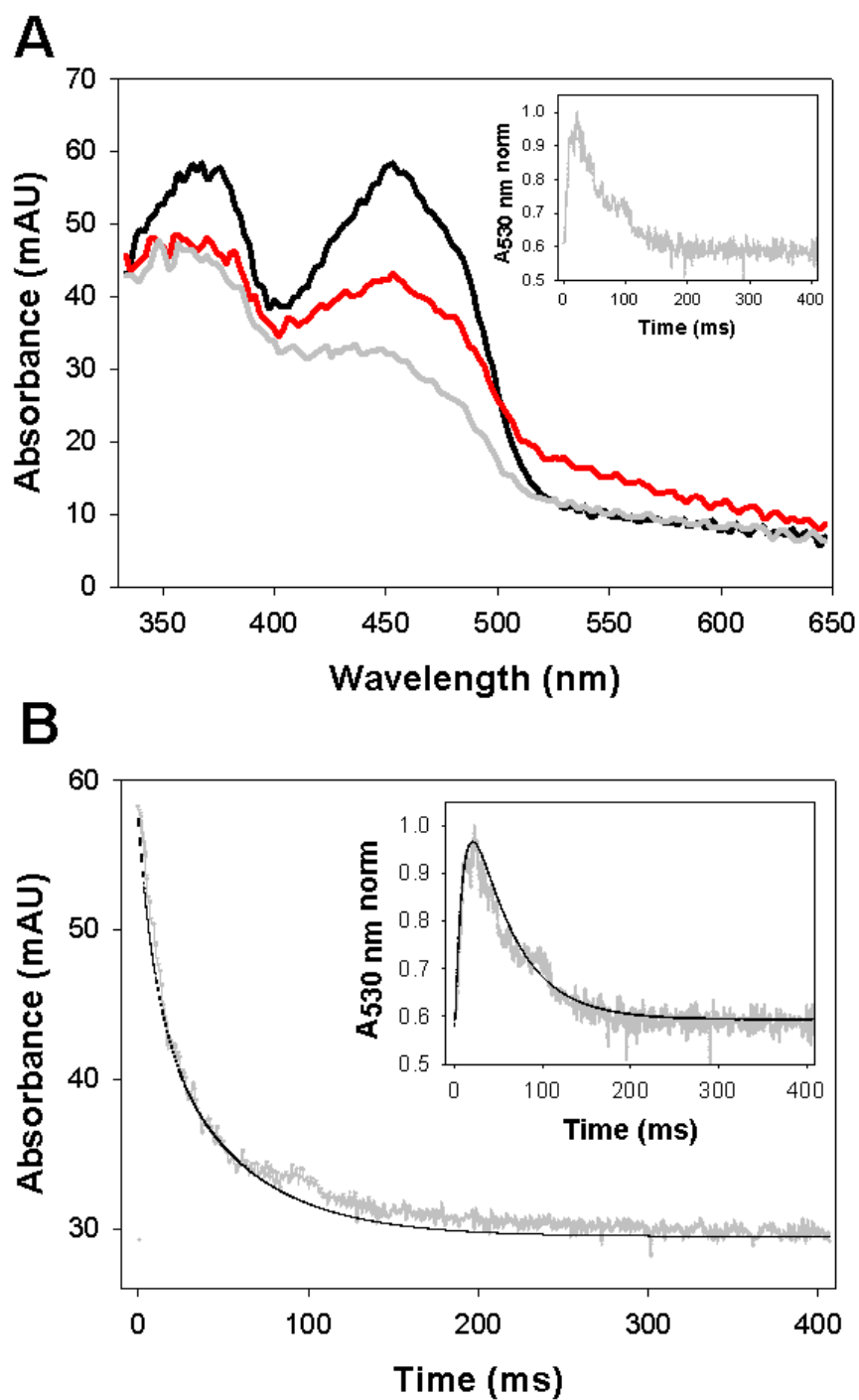


Figure 10

Spectral scans of LOX A95G mutant and fitting with Berkeley Madonna

Panel A: Spectral scans of LOX A95G mutant during the reductive half-reaction. 5 μM LOX were reduced with 8 mM L-lactate under anaerobic conditions in 50 mM potassium phosphate buffer, pH 6.5 at 4 $^{\circ}\text{C}$. **Black** line: enzyme in oxidized state at start (0 ms); **red** line: reaction after 18 ms; light **grey** line: reaction after 200 ms. After 18 ms the maximum in absorbance at 530 nm is reached (compare dark **grey** trace for the whole reaction at inset), the amplitude decreases afterwards.

Panel B: Reductive half-reaction of LOX A95G mutant by L-lactate. 5 μ M LOX in 50 mM potassium phosphate buffer (pH 6.5) were reacted in the stopped flow photometer at 4 °C with 8 mM L-lactate. The grey line represents the reaction trace at 455 nm with two different phases (first phase = k_3 ; second phase = k_5) the inset reflects the trace at 530 nm in a biphasic manner. Black lines represent the fittings achieved with software Berkeley Madonna leading to the calculated kinetic constants in **Table 2**.

for the formation of the intermediate by the formula $\epsilon = (A_{530\max} - A_{530\text{final}}) / C_{\text{EPyrmax}}$ resulting in a value of 2.8×10^3 (2.3×10^3) M^{-1} . Data of A_{455} were fitted to the variable defined as $C = E + \text{ELac} + \text{EPyr} \cdot A1 + \text{Ered} \cdot A2$. $A1$ and $A2$ are the relative contributions of the species EPyr and Ered to the absorbance at 455 nm. [$A1 (= A_{455\text{tx}}/A_{455\text{t0}})$ is the ratio between the absorbance (455 nm) at the point in time (tx), where EPyrmax is reached and the absorbance (455 nm) is at the start of the reaction (t0). $A2 = A_{455\text{final}}/A_{455\text{t0}}$.] On the other hand, the absorbance data of A_{530} were fitted to the variable $R (= \text{EPyr} \cdot \epsilon + A_{530\text{final}})$.

The simulated values of wild-type mutant for k_3 (88 s^{-1}) and k_5 (87 s^{-1}) are different to A95G mutant with $k_3 = 77 \text{ s}^{-1}$ and $k_5 = 23.5 \text{ s}^{-1}$ (**Table S2**). According to the fitting data we conclude that the rate limiting step can be found in k_5 for A95G mutant. We were able to identify the species EFl_{red} -pyruvate at 530 nm typical for LMO, but only at 4 °C, where we could detect the main difference between WT and mutant in k_5 .

Due to the active site mutation k_5 is lowered. We know from previous studies that the alanine to glycine mutant reflects an enlarged affinity for pyruvate (17). Taking all together, the proposed reaction includes the following steps: a substitution of alanine by glycine leads to a conformational change in the vicinity region and fixes

the Tyr-191 residue. As a consequence, enlarged α -hydroxy acids are able to enter the active site, as proven by steady state kinetics. Conversion of L-lactate into pyruvate is not altered, but the release of pyruvate is slowed down mainly due to the Tyr-191 residue, which is likely to fix the pyruvate. In literature only little is known about the pathway, how and where the pyruvate is released. Conformational hindrance caused by the mutation might as well play a role as the hydrogen bond network between Tyr-191 and Tyr-40. Worth mentioning is the fact that Tyr-40 is the residue, which is in close contact to the substrate/pyruvate.

The use of DCIP and quinones

2,6-dichlorindophenol (DCIP), an artificial two-electron acceptor, has been used in a mediator-based lactate sensor to serve as a mediator for LOX from *Pediococcus* sp. (31, 32). In contrast, oxygen or hydrogen peroxide (H_2O_2) based sensors applied in clinical analysis have disadvantages concerning the sensitivity to O_2 concentrations (38). Mediator based lactate sensors instead are capable to reduce the effects of O_2 interference by changing the redox potential and the efficiency of the mediator (39). Our intention therefore was to investigate, how the electron acceptors influence each other during catalysis in a time course analysis at the same time. For wild-type LOX, as well as for oxidases in general, oxygen is the main electron acceptor of choice during the conversion of L-lactate into pyruvate, which accepts both electrons from $FMNH_2$ and re-oxidizes it for a new reaction circle. In the presented time-course analysis we offered the enzyme two different electron acceptors at the same time during the reaction with L-lactate and found different results for wild-type LOX and A95G mutant. However, the simultaneous reduction of both compounds suggests two competing reactions. An earlier study showed for D-lactate oxidase that only after the complete consumption of oxygen the enzyme

switched to DCIP as an acceptor (40). In contrast to D-lactate oxidase, LOX does not show the strict preference of molecular oxygen over DCIP. Additionally, the data of time course analysis illustrate that DCIP does not directly influence the substrates - e.g. A95G mutant resembles an activity with L-hydroxybutyric acid (O_2 : 65 U/mg, DCIP: 354), which is ~2-fold higher than with L-lactate (O_2 : 33 U/mg; DCIP: 140 U/mg). Based on these findings, mainly the substrate affects the LOX reaction and causes the different activities. Pre-steady state experiments revealed that DCIP mainly influences the oxidative half-reaction, whereas the substrate is responsible for the reductive half-reaction.

In terms of oxygen reactivity, suppression in re-oxidation was achieved by product binding in cytokinin dehydrogenase. Due to a tight binding of product the flavin is preferentially re-oxidized by alternative electron acceptors such as quinones (41). Besides, LOX A95G features an 11-fold higher affinity to pyruvate (which means a tighter binding of product) compared to wild-type LOX (17). This might reflect, why the reactivity with certain quinones is increased, and the oxygen reactivity is decreased for the LOX mutant.

Analysis of the oxidative half-reaction revealed that both LOX variants were able to be re-oxidized by an alternative electron acceptor; this was proven for different substances like DCIP and various quinones (2-methyl-1,4-benzoquinone, 2,5-dimethyl-1,4-benzoquinone 2,5-dichloro-1,4-benzoquinone), which act as two electron acceptors (the same accounts for molecular oxygen). In detail, re-oxidation of the reduced A95G mutant was 3-fold faster with DCIP ($1.0 \times 10^6 \text{ M}^{-1}\text{s}^{-1}$) than with molecular oxygen. This leads us to the hypothesis that the region around the active site is enlarged for the docking of longer α -hydroxy acids, but on the other hand, the entry for oxygen seems to be hindered by the mutagenesis. As a consequence, the

re-oxidation rate of LOX A95G with O₂ compared to wild-type LOX is lowered more than 5-fold. Additionally, the changed/enlarged active site would also have more potential to allow a substantially larger alternative acceptor such as DCIP to function in the electron transfer. However, calculations for glucose sensors have shown that electrons can be transported across distances as large as 20 Å (see **Review 42**).

Behavior with O₂ matters

Yet to be discussed is the fact, why the re-oxidation with O₂ is changed for the A95G mutant. One rule is valid for every flavoprotein: the initial step of the oxidative half-reaction includes the transfer of one electron from the reduced flavin to O₂ leading to a caged radical pair, which is generated by a superoxide anion and flavin semiquinone (**45**). In the case of LOX, a second electron transfer causes the formation of hydrogen peroxide and the oxidation of the flavin. Though the rate limiting step lies in the first electron transfer step, where the semiquinone radical pair is formed (**46**). Mainly the electrostatic environment around C4a-N5 locus of the flavin is able to favor the oxidative reaction leading to this superoxide semiquinone radical pair. Protonation studies of a histidine side chain of glucose oxidase, which is located on the *si*-face of the C4a-N5, have proved that (**47**). Positively charged groups influence the reactivity; the exchange of Lys265 residues close to N5 of the isoalloxazine ring into a methionine shown for sarcosine oxidase decreased the re-oxidation rate 8000-fold (**43**). Further, 3D-structures of vanillyl-alcohol oxidase illustrated an anion-binding cavity on the flavin-side close to the substrate binding site, which might be the space, where oxygen binds (**48**). On the other hand, the proper positioning of a positive charge can play a crucial role in oxygen reactivity as seen for cholesterol oxidase type II (**49**). Here, Arg-477 either blocks or connects the

flavin with the protein like a “gate” by a conformational change and can therefore reduce or enhance oxygen reactivity.

It is not clear, if the re-oxidation needs a direct contact between dioxygen and the cofactor, and if there is a specific locus for the oxygen reaction (50). For instance, flavocytochrome b_2 represents a fully accessible flavin and reacts slowly with O_2 . In contrast, D-amino oxidase reacts fast, although the cofactor is shielded by active site amino acid residues (42). Molecular dynamic simulations revealed that O_2 approaches the flavin C4a position through multiple pathways (50). In oxidases, oxygens are thought to reach the flavin by ‘edge-on’ geometry, whereas in monooxygenases the face-on approach seems to be favored (Figure 7). Increase of hydrophobicity was found to guide and facilitate O_2 to re-oxidize the reduced enzyme (52). Additionally, several other mutations (51-55) highlight that changes in the environment of flavin N5-C4 drastically influence the reaction with molecular oxygen. Nevertheless, based on crystal structures, a specific oxygen-binding site seems to be missing in most cases.

On the other hand, the LOX structure at pH 4.5 displayed molecular oxygen in the active site (22). Mizuno and coworkers propose a reaction mechanism of LOX based on the flipping event of His-265, which acts as the active base/acid. In detail, when the substrate enters the active site, the hydride ion transfer occurs; FMN is reduced and the protonated His-265 flips out to form the hydrogen bond network consisting of His-265-Asp-174-Lys-221, and molecular oxygen approaches the *si*-face of FMN. (Note: due to the formation of the hydrogen bond network the entrance of O_2 and the release of pyruvate are possible.) After pyruvate is released, His-265 is flipped back, and O_2 enters the same position as the C^α and keto-oxygen atoms of the pyruvate molecule in the LOX-pyruvate complex. Hydrogen peroxide is produced,

FMN re-oxidized, and His-265 is re-oxidized for a new cycle. Therefore, hydrogen networks play a crucial role in LOX activity. A rearrangement of certain amino acid residues during the pyruvate release and the re-oxidation points out that the catalyzing enzyme is in permanent movement. However, a simple brake of such hydrogen bonds caused by single mutations can therefore seal the fate of LOX and lead to complete loss of activity, as substitution of Arg-174 and Lys-221 clearly evidenced. As mentioned before, this flipping event of His-265 enables molecular oxygen to enter this space. In contrast to the structure of pH 4.5, O₂ was reported to be missing in structures of LOX at pH 8.0, pH 7.5 and LOX-pyruvate at pH 8.0. Hence, these observations complicate a precise prediction for oxygen access as discussed previously (42).

Comparison with similar point mutations and conclusion

It is instructive to take a closer look at corresponding mutations in other flavoproteins, as they have different effects in the reductive and oxidative half-reaction. An alanine to glycine substitution in L-mandelate dehydrogenase for instance resulted in a significant decrease in catalytic activity and k_{red} with mandelate, whereas the oxidative half-reaction was increased (56, 57). On the other hand, G81A mutant of mandelate dehydrogenase highlighted increased specificity for smaller substrates (56). Similar effects for the oxidative half-reaction were obtained for G99A mutant in LMO, where the rates were increased and turned the enzyme into a lactate oxidase, while the mutation had no influence on the reductive half-reaction (58, 59). Modification of alanine by glycine in flavocytochrome b_2 led to a slight decrease in k_{red} , respectively (60). Taken together, all these findings make it obvious that even small changes in the active site can cause drastic changes in the reaction mechanism.

Remarkably, LOX, LMO, glycolate oxidase and flavocytochrome b_2 share highly conserved active sites, but represent different re-oxidation rate constants with oxygen ($1 \times 10^6 \text{ M}^{-1} \text{ s}^{-1}$ for LOX and LMO, $1 \times 10^4 \text{ M}^{-1} \text{ s}^{-1}$ for glycolate oxidase and almost zero for flavocytochrome b_2) (**1**, **61**, **62**). Substitution of Gly-99 by Ala (Ala-95 in LOX, Ala-198 in flavocytochrome b_2) showed that an alteration in stereochemistry reduces the reactivity with oxygen (**21**). Ala-95 of LOX in comparison also represents decreased reactivity with molecular oxygen. Another consequence of the mutation is the enhanced substrate specificity caused by another orientation of the side- and/or main-chain atoms of Tyr-124 and Tyr-191. Based on previous findings, we can assume that LOX A95G represents higher reactivity with quinones and DCIP due to a tight binding of pyruvate, though this might not be the only reason. An enlarged active site seems to guide quinones in closer position of the flavin N5. In terms of re-oxidation with O_2 , many recent works with flavoenzymes outlined that the environment around flavin N5-C4 in the active site plays a crucial role (**51**, **53**, **54**). Many crystal structures of LOX are lacking a distinct oxygen binding site, the possibility of multiple tunnels to diffuse oxygen for this enzyme remains unsolved. Re-oxidation with DCIP poses another question. Based on the available crystal structure, it has to be assumed that the molecule is too large to enter the active site. It seems that DCIP approaches the FMN cofactor by a different mechanism; as mentioned before electron transfer might be possible over 20 \AA . Such a transfer can only exist due to tunnel systems, which connect the molecule with the FMN cofactor. As a future prospective, our findings might be of interest for mediator based lactate sensors, which prefer indophenols over molecular oxygen.

REFERENCES

- 1 Maeda-Yorita K, Aki K, Sagai H, Misaki H, and Massey V (1995) L-lactate oxidase and L-lactate monooxygenase: mechanistic variations on a common structural theme. *Biochimie* **77**, 631-642.
- 2 Müh U, Massey V, Williams CH Jr. (1994) Lactate monooxygenase. I. Expression of the mycobacterial gene in *Escherichia coli* and site-directed mutagenesis of lysine 266. *The Journal of biological chemistry* **269**, 7982-7988.
- 3 Boubacar AK, Pethe S, Mahy JP, Lederer F (2007) Flavocytochrome b_2 : reactivity of its flavin with molecular oxygen. *Biochemistry* **46**, 13080-13088.
- 4 Stenberg K, Clausen T, Lindqvist Y, Macheroux P (1995) Involvement of Tyr24 and Trp108 in substrate binding and substrate specificity of glycolate oxidase. *European journal of biochemistry* **228**, 408-416.
- 5 Illias RM, Sinclair R, Robertson D, Neu A, Chapman SK, Reid GA (1998) L-mandelate dehydrogenase from *Rhodotorula graminis*: cloning, sequencing and kinetic characterization of the recombinant enzyme and its independently expressed flavin domain. *The Biochemical journal* **333**, 107-115.
- 6 Chen ZW, Vignaud C, Jaafar A, Lévy B, Guéritte F, Guénard D, Lederer F, Mathews FS (2012) High resolution crystal structure of rat long chain hydroxy acid oxidase in complex with the inhibitor 4-carboxy-5-[(4-chlorophenyl)sulfanyl]-1, 2, 3-thiadiazole. Implications for inhibitor specificity and drug design. *Biochimie* **94**, 1172-1179.
- 7 Minagawa H, Nakayama N, Matsumoto T, and Ito N (1998) Development of long life lactate sensor using thermostable mutant lactate oxidase. *Biosensors and Bioelectronics* **13**, 313-318.
- 8 Romero MR, Ahumada F, Garay F, and Baruzzi AM (2010) Amperometric biosensor for direct blood lactate detection. *Analytical Chemistry* **82**, 5568-5572.
- 9 Wang J, and Chen Q (1994) Enzyme microelectrode array strips for glucose and lactate. *Analytical Chemistry* **66**, 1007-1011.
- 10 Ghisla S and Massey V (1989) Mechanisms of flavoprotein-catalyzed reactions. *European journal of biochemistry* **181**, 1-17.
- 11 Roth JP, Klinman JP (2003) Catalysis of electron transfer during activation of O_2 by the flavoprotein glucose oxidase. *Proceedings of the National Academy of Sciences of the United States of America* **100**, 62-67.
- 12 Pollegioni L, Wels G, Pilone MS, Ghisla S (1999) Kinetic mechanisms of cholesterol oxidase from *Streptomyces hygroscopicus* and *Brevibacterium sterolicum*. *European journal of biochemistry*. **264**, 140-151.
- 13 Macheroux P, Massey V, Thiele DJ, Volokita M (1991) Expression of spinach glycolate oxidase in *Saccharomyces cerevisiae*: purification and characterization. *Biochemistry* **30**, 4612-4619.
- 14 Giegel DA, Williams CH Jr, Massey V. (1990). L-lactate 2-monooxygenase from *Mycobacterium smegmatis*. Cloning, nucleotide sequence, and primary structure homology within an enzyme family. *The Journal of biological chemistry* **265**, 6626-6632.
- 15 Fraaije MW, van Berkel WJ (1997) Catalytic mechanism of the oxidative demethylation of 4-(methoxymethyl)phenol by vanillyl-alcohol oxidase. Evidence for formation of a p-quinone methide intermediate. *The Journal of biological chemistry* **272**, 18111-18116.
16. Frébortová J, Fraaije, MW, Galuszka P, Sebela M, Pec P, Hrbác J, Novák O, Bilyeu KD, English JT, Frébort I (2004) Catalytic reaction of cytokinin dehydrogenase: preference for quinones as electron acceptors. *The Biochemical journal* **380**, 121-130.
- 17 Yorita K, Aki K, Ohkuma-Soyejima T, Kokubo T, Misaki H, Massey V (1996) Conversion of L-lactate oxidase to a long chain alpha-hydroxyacid oxidase by site-directed mutagenesis of alanine 95 to glycine. *The Journal of biological chemistry* **271**, 28300-28305.

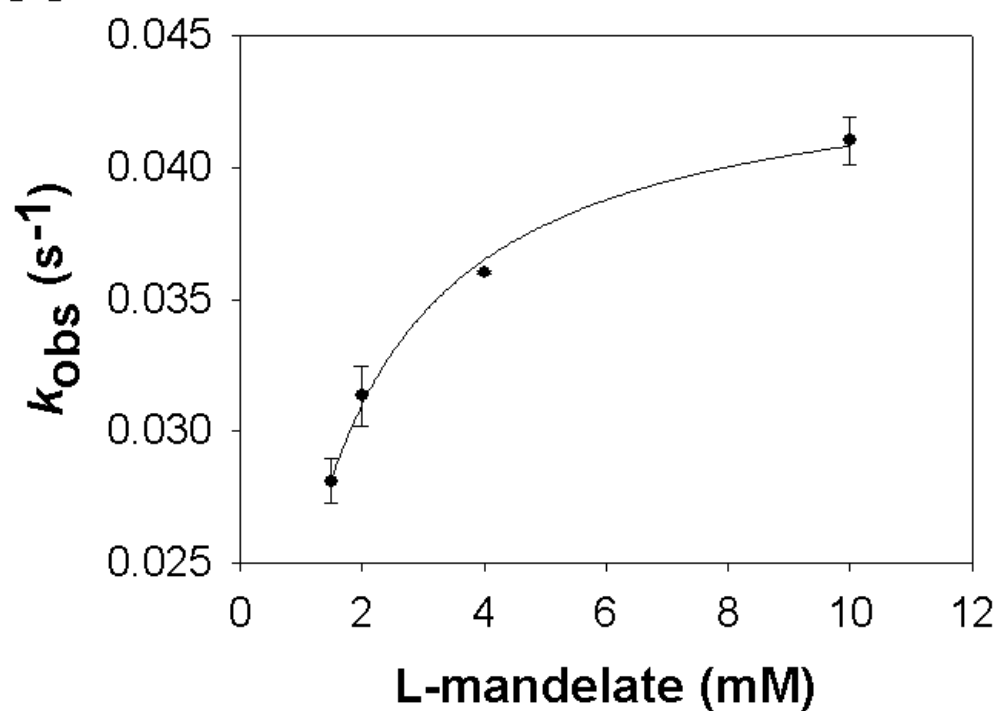
- 18 Li SJ, Umena Y, Yorita K, Matsuoka T, Kita A, Fukui K, Morimoto Y (2007) Crystallographic study on the interaction of L-lactate oxidase with pyruvate at 1.9 Angstrom resolution. *Biochemical and biophysical research communication* **358**, 1002-1007.
- 19 Umena Y, Yorita K, Matsuoka T, Kita A, Fukui K, Morimoto Y (2006) The crystal structure of L-lactate oxidase from *Aerococcus viridans* at 2.1Å resolution reveals the mechanism of strict substrate recognition. *Biochemical and biophysical research communication* **350**, 249-256.
- 20 Yorita K, Matsuoka T, Misaki, H, Massey V (2000) Interaction of two arginine residues in lactate oxidase with the enzyme flavin: conversion of FMN to 8-formyl-FMN. *Proceedings of the National Academy of Sciences of the United States of America* **97**, 13039-13044.
- 21 Furuichi M, Suzuki N, Dhakshnamoorthy B, Minagawa H, Yamagishi R, Watanabe Y, Goto Y, Kaneko H, Yoshida Y, Yagi H, Waga I, Kumar PK, Mizuno H (2008) X-ray structures of *Aerococcus viridans* lactate oxidase and its complex with D-lactate at pH 4.5 show an alpha-hydroxyacid oxidation mechanism. *Journal of molecular biology* **378**, 436-446.
- 22 Sun W, Williams CH Jr, Massey V (1996) Site-directed mutagenesis of glycine 99 to alanine in L-lactate monooxygenase from *Mycobacterium smegmatis*. *The Journal of biological chemistry* **271**, 17226-17233.
- 23 Lindqvist Y (1989) Refined Structure of, Spinach Glycolate Oxidase at 2 Å Resolution. *Journal of molecular biology* **209**, 151-166.
- 24 Sukumar, N, Xu Y, Gatti DL, Mitra B & Mathews FS (2001) Structure of an active soluble mutant of the membrane-associated (S)-mandelate dehydrogenase. *Biochemistry* **40**, 9870-9878.
- 25 Tegoni M, Begotti S, Cambillau C (1995) X-ray structure of two complexes of the Y143F flavocytochrome *b₂*: mutant crystallized in the presence of lactate or phenyl lactate. *Biochemistry* **34**, 9840-9850.
- 26 Belmouden A & Lederer F (1996) The role of a p barrel loop 4 extension in modulating the physical and functional properties of long-chain 2-hydroxy-acid oxidase isozymes. *European journal of biochemistry* **238**, 790-798.
- 27 Yorita K, Misaki H, Palfey BA, Massey V (2000) On the interpretation of quantitative structure-function activity relationship data for lactate oxidase. *Proceedings of the National Academy of Sciences of the United States of America* **97**, 2480-2485.
- 28 Nikolaus N, Strehlitz B (2007) Amperometric lactate biosensors and their application in (sports) medicine, for life quality and wellbeing. *Microchimica acta* **160**, 15-55.
- 29 Zimei R, Leitao E, Popplewell J, Alp B, Vadgama P (2008) Needle enzyme electrode for lactate measurement in vivo. *IEEE Sensors journal* **8**, 113-120.
- 30 Hirano K, Yamato H, Kunimoto K, Ohwa M (2001) Novel electron transfer mediators based on dichloroindophenol derivatives for lactate oxidase. *Journal of electroanalytical chemistry* **510**, 149-152.
- 31 Hirano K, Yamato H, Kunimoto K, Ohwa M (2002) Design of novel electron transfer mediators based on indophenol derivatives for lactate sensor. *Biosensors and bioelectronics* **17**, 315-322.
- 32 Taniguchi I, Miyamoto S, Tomimura S and Hawkrige M (1988) Mediated electron transfer of lactate oxidase and sarcosine oxidase with octacyanotungstate(IV) and octacyanomolybdate(IV). *Journal of electroanalytical chemistry* **240**, 333-339.
- 33 Unterweger B, Stoisser T, Leitgeb S, Birner-Grünberger R, Nidetzky B (2012) Engineering of *Aerococcus viridans* L-lactate oxidase for site-specific PEGylation: characterization and selective bioorthogonal modification of a S218C mutant. *Bioconjugate chemistry* **23**, 1406-1414.
- 34 Collaborative Computational Project 4, *Acta Crystallographica*. D50 (1994) 760-763.
- 35 Murshudov GN, Vagin AA, Dodson EJ (1997) Refinement of macromolecular structures by the maximum-likelihood method. *Acta crystallographica section D biological crystallography* **53**, 240-255.
- 36 Emsley P, Lohkamp B, Scott WG, Cowtan K (2010) Features and development of coot. *Acta crystallographica section D biological crystallography* **66**, 486-501.

- 37 Yorita K, Janko K, Aki K, Ghisla S, Palfey BA, Massey V (1997) On the reaction mechanism of L-lactate oxidase: quantitative structure-activity analysis of the reaction with para-substituted L-mandelates. *Proceedings of the National Academy of Sciences of the United States of America* **94**, 9590-9595.
- 38 Gorton L (1995) Carbon paste electrodes modified with enzymes and cells. *Electroanalysis* **7**, 23-41.
- 39 Serra B, Reviejo AJ, Parrado C, Pingarrón JM (1999) Graphite-TEFLON composite bi-enzyme electrodes for the determination of L-lactate: Application to food samples. *Biosensors and bioelectronics* **14**, 505-513.
- 40 Trampitsch C, Slavica A, Riethorst W, Nidetzky B (2005) Reaction of *Trigonopsis variabilis* D-amino acid oxidase with 2,6-dichloroindophenol: kinetic characterization and development of an oxygen-independent assay of the enzyme activity. *Journal of molecular catalysis B* **32**, 271-278.
- 41 Harper A, Anderson MR (2010) Electrochemical glucose sensors - developments using electrostatic assembly and carbon nanotubes for biosensors construction. *Sensors* **10**, 8248-8274.
- 42 Mattevi A (2006) To be or not to be an oxidase: challenging the oxygen reactivity of flavoenzymes. *Trends in biochemical sciences* **31**, 276-283.
- 43 Zhao G, Bruckner RC, Jorns MS (2008) Identification of the oxygen activation site in monomeric sarcosine oxidase: role of Lys265 in catalysis. *Biochemistry* **47**, 9124-9135.
- 44 Baron R, Riley C, Chenprakhon P, Thotsaporn K, Winter RT, Alfieri A, Forneris F, van Berkel WJ, Chaiyen P, Fraaije MW, Mattevi A, McCammon JA (2009) Multiple pathways guide oxygen diffusion into flavoenzyme active sites. *Proceedings of the National Academy of Sciences of the United States of America* **106**, 10603-10608.
- 45 Massey V (1994) Activation of molecular oxygen by flavins and flavoproteins. *The Journal of biological chemistry* **269**, 22459-22462.
- 46 Roth JP, Wincek R, Nodet G, Edmondson DE, McIntire WS, Klinman JP (2004) Oxygen isotope effects on electron transfer to O₂ probed using chemically modified flavins bound to glucose oxidase. *Journal of the American Chemical Society* **126**, 15120-15131.
- 47 Roth JP and Klinman JP (2003) Catalysis of electron transfer during activation of O₂ by the flavoprotein glucose oxidase. *Proceedings of the National Academy of Sciences of the United States of America* **100**, 62-67.
- 48 Mattevi A, Fraaije MW, Mozzarelli A, Olivi L, Coda A, van Berkel WJ (1997) Crystal structures and inhibitor binding in the octameric flavoenzyme vanillyl-alcohol oxidase: the shape of the active-site cavity controls substrate specificity. *Structure* **5**, 907-920.
- 49 Pollegioni L, Wels G, Pilone MS, Ghisla S (1999) Kinetic mechanisms of cholesterol oxidase from *Streptomyces hygroscopicus* and *Brevibacterium sterolicum*. *European journal of biochemistry* **264**, 140-151.
- 50 Chaiyen P, Fraaije MW, Mattevi A (2012) The enigmatic reaction of flavins with oxygen. *Trends in biochemical sciences* **37**, 373-380.
- 51 Baron R, McCammon JA, Mattevi A (2009) The oxygen-binding vs. oxygen-consuming paradigm in biocatalysis: structural biology and biomolecular simulation. *Current opinion in structural biology* **19**, 672-679.
- 52 Hernández-Ortega A, Lucas F, Ferreira P, Medina M, Guallar V, Martínez AT (2011) Modulating O₂ reactivity in a fungal flavoenzyme: involvement of aryl-alcohol oxidase Phe-501 contiguous to catalytic histidine. *The Journal of biological chemistry* **286**, 41105-41114.
- 53 Saam J, Rosini E, Molla G, Schulten K, Pollegioni L, Ghisla S (2010) O₂ reactivity of flavoproteins: dynamic access of dioxygen to the active site and role of a H⁺ relay system in D-amino acid oxidase. *The Journal of biological chemistry* **285**, 24439-24446.

- 54 Leferink NG, Fraaije MW, Joosten HJ, Schaap P J, Mattevi A, van Berkel WJ (2009) Identification of a gatekeeper residue that prevents dehydrogenases from acting as oxidases. *The Journal of biological chemistry* **284**, 4392-4397.
- 55 Finnegan S, Agniswamy J, Weber IT, Gadda G (2010) Role of valine 464 in the flavin oxidation reaction catalyzed by choline oxidase. *Biochemistry* **49**, 2952-2961.
- 56 Dewanti AR, Xu Y, Mitra (2004) B Role of glycine 81 in (S)-mandelate dehydrogenase from *Pseudomonas putida* in substrate specificity and oxidase activity. *Biochemistry* **43**, 10692-10700.
- 57 Sukumar N, Dewanti AR, Mitra B, Mathews FS (2004) High resolution structures of an oxidized and reduced flavoprotein. The water switch in a soluble form of (S)-mandelate dehydrogenase. *The Journal of biological chemistry* **279**, 3749-3757.
- 58 Sun W, Williams CH Jr, Massey V (1996) Site-directed mutagenesis of glycine 99 to alanine in L-lactate monooxygenase from *Mycobacterium smegmatis*. *The Journal of biological chemistry* **271**, 17226-17233.
- 59 Sun W, Williams CH Jr, Massey V (1997) The role of glycine 99 in L-lactate monooxygenase from *Mycobacterium smegmatis*. *The Journal of biological chemistry* **272**, 27065-27076.
- 60 Daff S, Manson FD, Reid GA, Chapman SK (1994) Strategic manipulation of the substrate specificity of *Saccharomyces cerevisiae* flavocytochrome b_2 . *Biochemical journal* **301**, 829-834.
- 61 Xia ZX, Mathews FS (1990) Molecular structure of flavocytochrome b_2 at 2.4 Å resolution. *Journal of molecular biology* **212**, 837-63.
- 62 Stenberg K, Lindqvist Y (1997) Three-dimensional structures of glycolate oxidase with bound active-site inhibitors. *Protein science* **6**, 1009-1015.

SUPPORTING INFORMATION

A



B

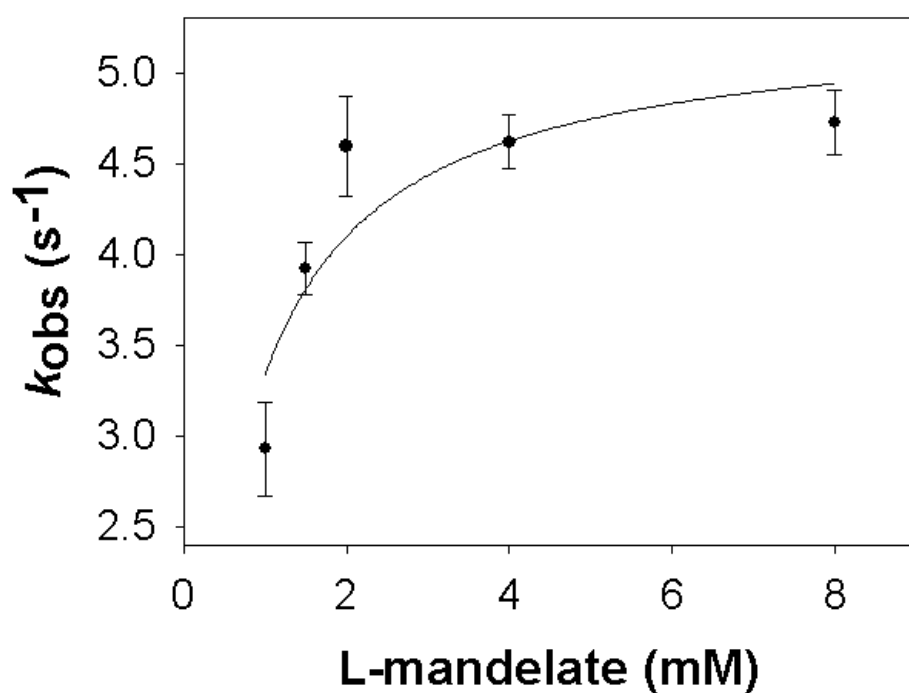


Figure S1A

Determination of the reduction rate constant (k_{red}) and dissociation constant (K_{d}) for reaction of wild-type LOX (A) and A95G mutant (B) with L-mandelate at 20 °C. Pseudo first order rate constants, k_{obs} from determined single traces at 455 nm are plotted versus L-mandelate to yield k_{red} and K_{d} .

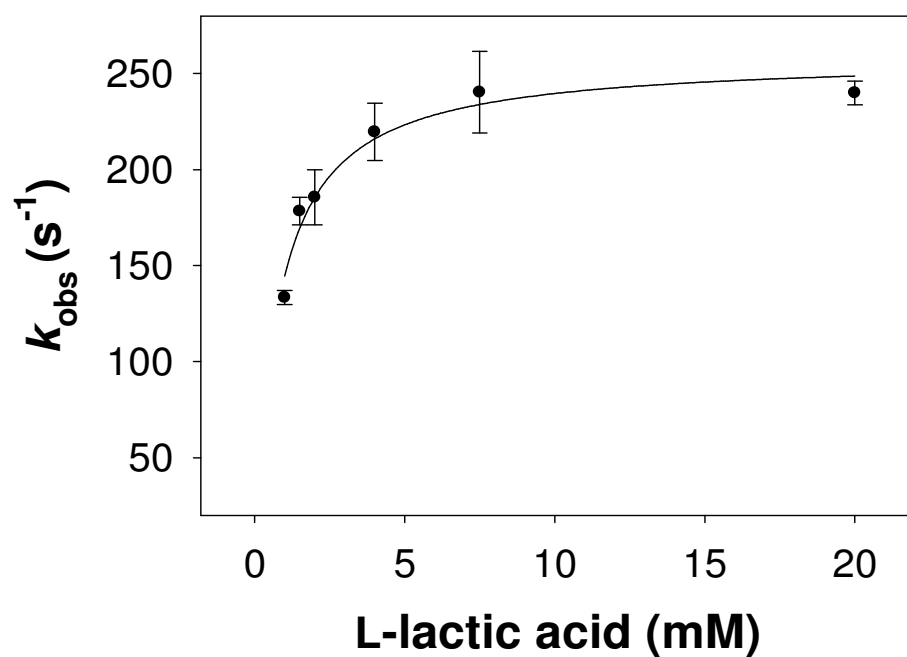
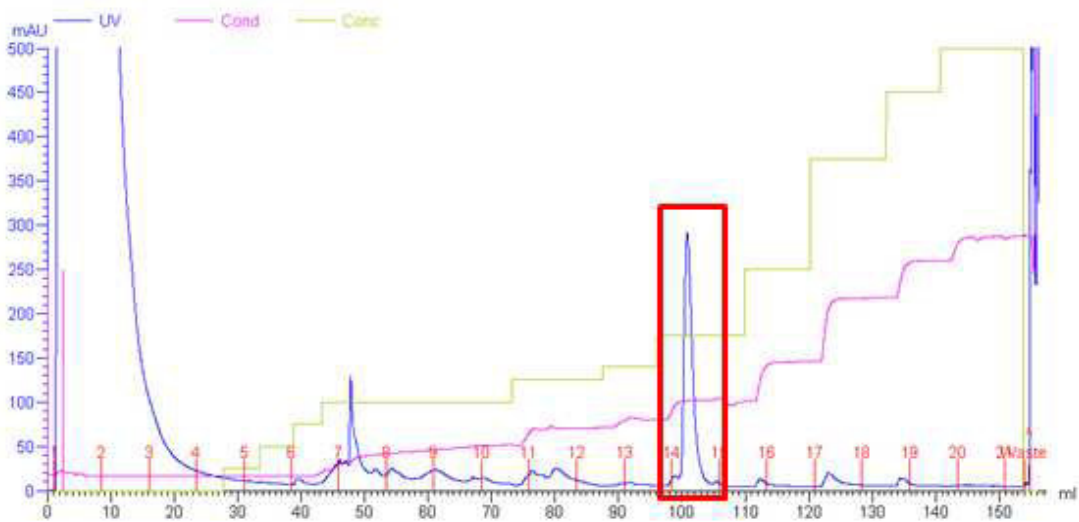
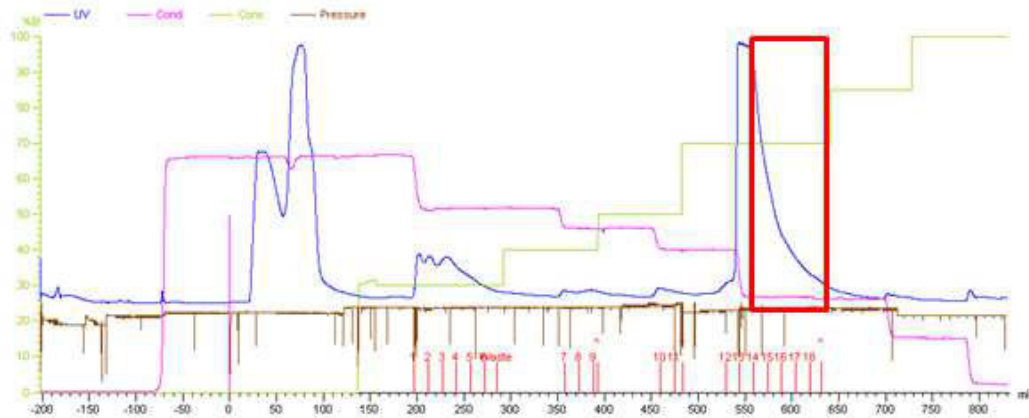


Figure S1B

Determination of the reduction rate constant (k_{red}) and dissociation constant (K_{d}) for reaction of wild-type LOX (recombinant) with L-lactate at 20 °C. Pseudo first order rate constants, k_{obs} from determined single traces at 455 nm are plotted versus **L-lactate** to yield k_{red} ($258 \pm 8 \text{ s}^{-1}$) and K_{d} ($0.8 \pm 0.1 \text{ mM}$).

A



B

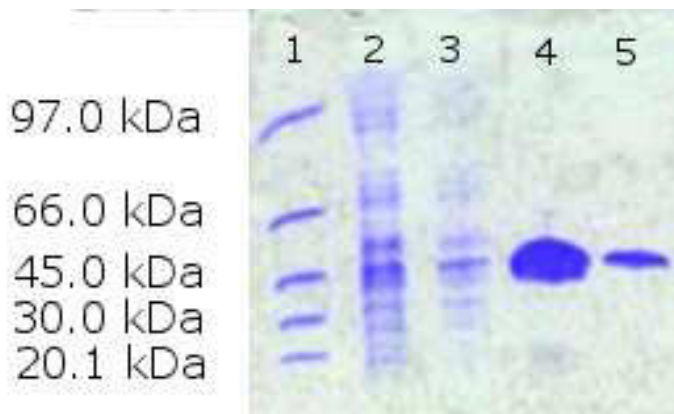


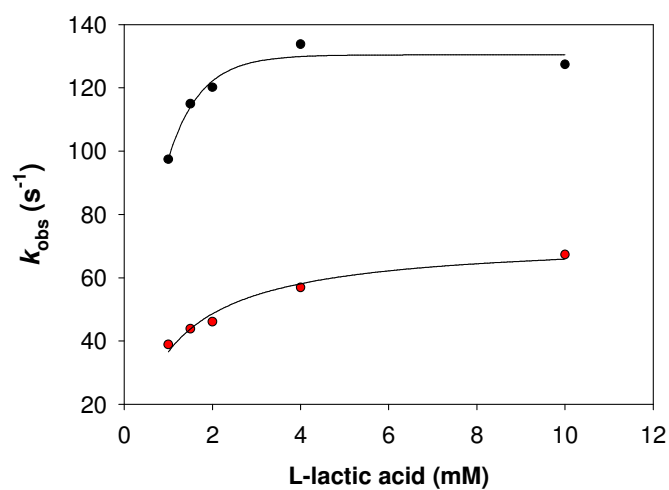
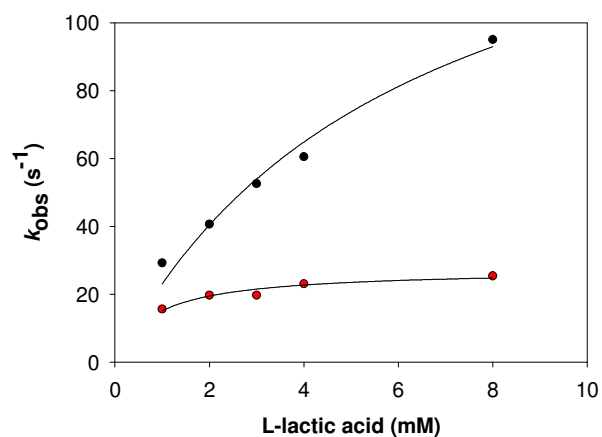
Figure S2
Purification of LOX A95G mutant

Panel A: *above:* Elution profile of the Phenyl-Sepharose FF HIC column
below: Elution profile of the MonoQ anion exchange column

Panel B: SDS polyacrylamide gel from LOX for different purification steps: CE: crude extract, 1.5M: ammonium sulfate precipitation supernatant, HIC: fraction after the hydrophobic interaction chromatography, MonoQ: pure protein after the ion exchange chromatography. As standard first row a Low molecular weight standard was chosen.

Table S1. Purification overview for the LOX A95G mutant

Purification step	Specific activity (U/mg)	Recovery (%)
Crude extract	1,8	100
1.5 M (NH ₄) ₂ SO ₄	2,1	90,6
HIC	13.4	9,9
MonoQ	23.7	1,7

A**B****Figure S3****Reductive half-reaction of wild-type LOX and A95G mutant at 4 °C**

Determination of the reduction rate constants k_3 (described by **black** dots) and k_5 (described by **red** dots) dissociation constants established for reaction of wild-type LOX (Panel **A**) and A95G mutant (Panel **B**) with L-lactate at 4 °C. Pseudo first order rate constants, k_{obs} from determined traces at 530 nm and 455 nm are plotted versus L-lactate to yield k_{red1} (k_3) and k_{red2} (k_5). k_{red1} was determined to be 128 (142) s^{-1} , k_{red2} 72 (27) s^{-1} for wild-type LOX (A95G mutant).

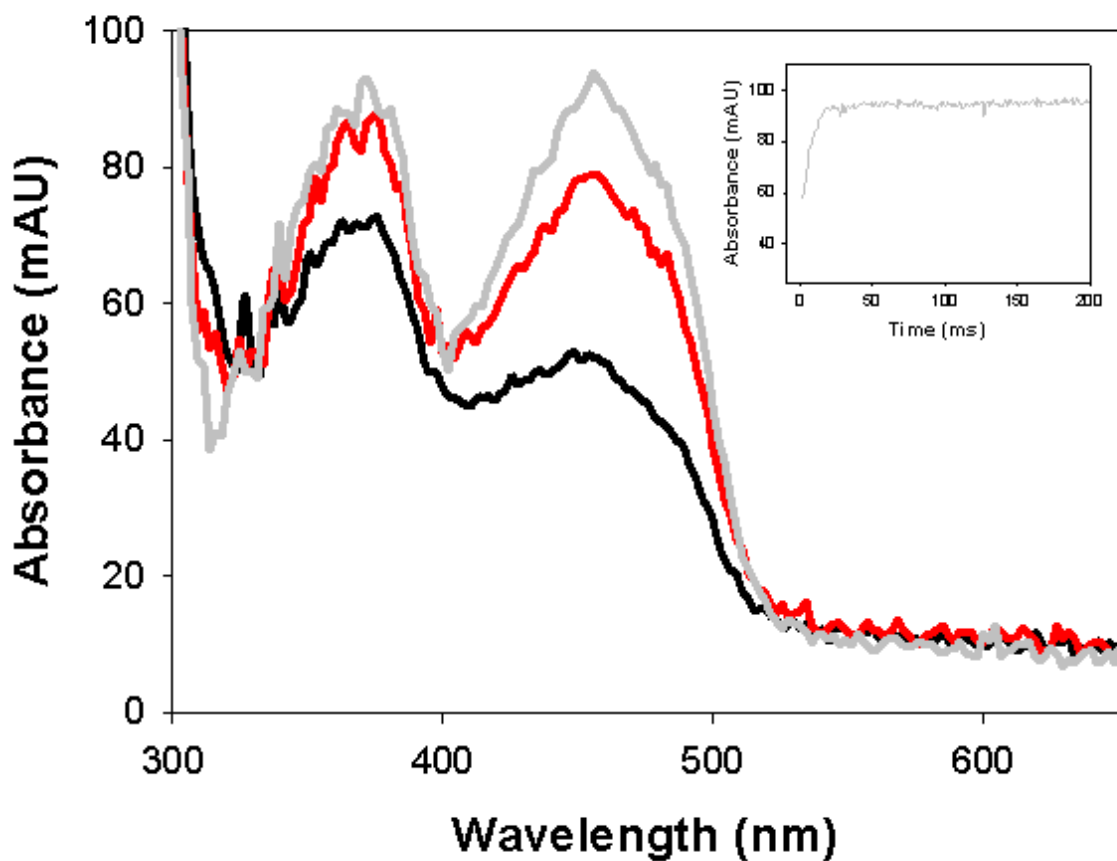


Figure S4

Spectral scans of wild-type LOX during the oxidative half-reaction.

8.1 μM LOX were reduced with 2 equivalent L-lactate under anaerobic conditions in 50 mM potassium phosphate buffer, pH 6.5 at 20 $^{\circ}\text{C}$ and reoxidized with 70 μM oxygen. **Black** line: enzyme in reduced state after 3 ms; **red** line: reaction after 8 ms; light **grey** line: reaction after 30 ms. Inset shows trace at 455 nm which was fitted in a single exponential manner as described in text ($k_{\text{obs}1} = 137 \text{ s}^{-1}$).

Table S2. List of kinetic rate constants and characteristics of FMN for wild-type LOX and A95G mutant with L-lactic acid as substrate determined at 4 °C in 50 mM potassium phosphate buffer, pH 6.5

		Wild-type LOX	A95G
$k_{\text{red1}}, [\text{s}^{-1}] = k_3$	(s^{-1})	128	142
$k_{\text{red2}}, [\text{s}^{-1}] = k_5$	(s^{-1})	72	27
K_{d1}	(mM)	1.4	4.9
K_{d2}	(mM)	1.0	0.8
FMN reduced	(%)	>99	>99
FMN re-oxidized	(%)	>90	>90
$\Delta A_{530\text{nm } 1}$		detected	Detected
$\Delta A_{530\text{nm } 2}$		detected	Detected
$\Delta A_{530\text{nm } 1}$	(s^{-1})	102*	92*
$\Delta A_{530\text{nm } 2}$	(s^{-1})	60.8*	25*
k_2/k_1 **	(mM)	1	6
k_3 **	(s^{-1})	88	77
k_4 **	(s^{-1})	0	0
k_5 **	(s^{-1})	87	23.5
k_6 **	($\text{mM}^{-1} \text{ s}^{-1}$)	10	10

$\Delta A_{530 \text{ 1}}$ describes an increase in absorbance, $\Delta A_{530 \text{ 2}}$ a decrease in absorbance

* Rates derive from linear fitting ($\Delta A_{530 \text{ 1}}$) and single exponential fitting ($\Delta A_{530 \text{ 1}}$) with start at highest absorbance of A_{530} (conditions: 10 mM L-lactate) and are estimations

** Description of fit with Berkeley Madonna in text. Numbering is based on **Scheme 1**

4 Characterization of *Aerococcus viridans* LOX mutants Y215F and Y215H

Thomas Stoisser[†], Stefan Leitgeb[†], David K. Wilson[‡], and Bernd Nidetzky^{†*}

[†] Research Center Pharmaceutical Engineering, and Institute of Biotechnology and Biochemical Engineering, Graz University of Technology, Petersgasse 12, A-8010 Graz, Austria

[‡] Department of Molecular and Cellular Biology, University of California, One Shields Avenue, Davis, CA 95616

* Corresponding author

Institute of Biotechnology and Biochemical Engineering, Graz University of Technology, Petersgasse 12, A-8010 Graz, Austria

Telephone: +43-316-873-8400; fax: +43-316-873-8434; e-mail:

bernd.nidetzky@tugraz.at

ABBREVIATIONS

AEC: anionic exchange chromatography, BSA: bovine serum albumin, DAO: D-amino acid oxidase, FCB2: flavocytochrome b_2 , FMN: flavomononucleotide, FPLC: Fast protein liquid chromatography, GOD: glucose oxidase, GOX: glycolate oxidase, HIC: hydrophobic interaction chromatography, LCHAO: long chain hydroxy acid oxidase, LMO: L-lactate monooxygenase, LOX: L-lactate oxidase, MDH: L-mandelate dehydrogenase, PDB: protein data base, WT: wild-type.

ABSTRACT

Flavoprotein L-lactate oxidase from *Aerococcus viridans* catalyzes the oxidation of L-lactate into pyruvate using oxygen and belongs to a huge family of α -hydroxyacid-oxidizing enzymes. Although L-lactate is its primary substrate, the enzyme is able to oxidize several other α -hydroxy acids. The crystal structure, where pyruvate is bound in the active site, was determined, and as a proposed stabilizer of the product residue Tyr-215 was found in the active site to be in close contact with the pyruvate. Further structural studies and sequence comparison with related members of the hydroxy acid oxidizing family revealed that this residue is not conserved. It is therefore very likely that this residue plays a key role in substrate specificity and catalysis. To elucidate this possibility, residue Tyr-215 was replaced by phenylalanine, which lacks the hydroxyl group and by histidine, which could stabilize the anionic form of the substrate. Steady state and pre-steady state measurements have been used to characterize the influence of these two mutants. Both mutations turned out not to alter the substrate specificity. The k_{cat} for L-lactate was very low for Y215H with an unchanged K_M . Moreover, Y215F showed an increased catalytic efficiency with L-lactate mainly due to a 10-fold lower K_M . On the other hand, the k_{cat} for the same mutant was 3-5 times lower resulting from a rate limiting step to be found in the reductive half-reaction. Additionally, steady state kinetics at different pH proofed Y215F not to be part of catalysis as been shown for Y254F in flavocytochrome b_2 .

INTRODUCTION

A special group of flavoproteins, the so called α -hydroxy acid oxidases, catalyze the oxidation of α -hydroxy acids to keto acids. The known members are L-lactate oxidase from *Aerococcus viridans*, L-lactate monooxygenase (LMO) from *Mycobacterium smegmatis* (1, 2, 3) flavocytochrome b_2 from Baker's yeast (4), spinach glycolate oxidase (GOX) (5), L-mandelate dehydrogenase from *Rhodotorula graminis* (MDH) (6) and a long chain α -hydroxy acid oxidase from rat kidney (HAO) (7). The crystal structures of these enzymes (with exception of LMO) have been determined by X-ray crystallography. All structures share a common feature: similar amino acid residues are found in the active site around the prosthetic group FMN. Moreover, the loops at the c-terminal end of the β -strands form the active site, which is quite usual for α/β TIM barrels (Li).

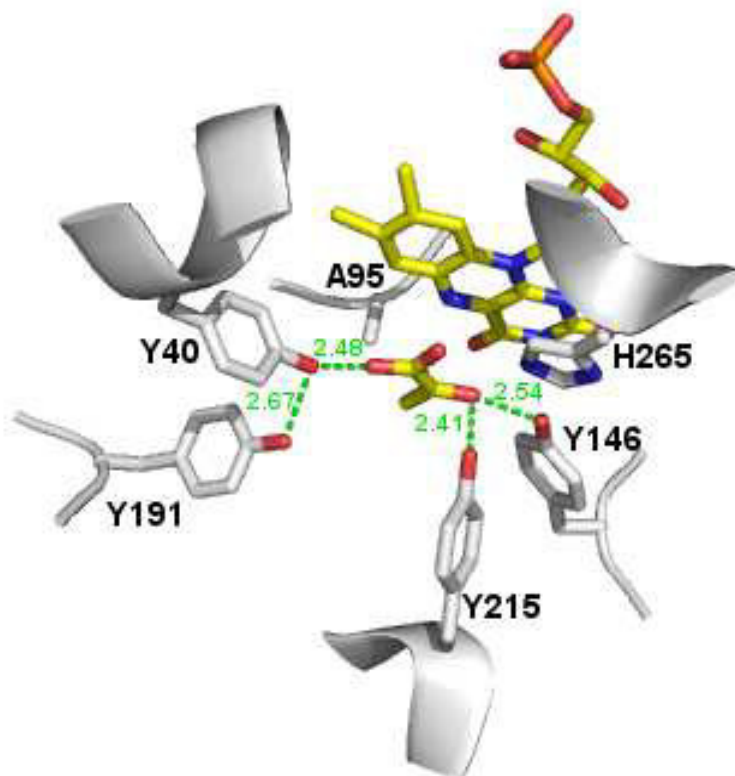


Figure 1

Look into active site of LOX. Structure from wild-type LOX from PDB 2E77.

Flavoprotein L-lactate oxidase (LOX) from *Aerococcus viridans* catalyzes the oxidation of L-lactate into pyruvate with H₂O₂ as a by-product (1). Besides many applications, the current LOX is mainly used in biosensors for the determination of L-lactate levels in medical and food analytics (8-11). These biosensors potentiometrically detect hydrogen peroxide in solution produced during the conversion of L-lactate to pyruvate. The crystal structures of LOX at pH 8.0 (PDB code 2DU2), at pH 7.5 (PDB code 2J6X), and in complex with pyruvate at pH 8.0 (PDB code 2E77) were solved at 2.1 Å, 2.1 Å and 1.9 Å resolution, respectively. Additionally, crystal structures of LOX at pH 4.5 and its complex with D-lactate at pH 4.5 were solved at 1.81 Å and 1.59 Å. LOX is a tetramer of 164,000 kDa (4 subunits of 41,000 kDa), and each subunit consists of eight α -helices and eight β -strands, which are arranged in a typical α/β -barrel also found in the aforementioned flavin α -hydroxyacid oxidases (12-15) and contains one FMN prosthetic group. The non-covalently bound FMN (flavomonocucleotide) plays a key role in catalysis and provides the enzyme its typical spectral properties at UV-Vis light. In LOX, the enzymatic reaction proceeds via a ping-pong mechanism (16).

The overall mechanism is split in two half-reactions (compare **Scheme 1**) (1). During the reductive half-reaction the α -hydroxy acid substrate is oxidized by the enzyme to form a keto acid as the product, and the flavin is reduced to the hydroquinone. In the oxidative half-reaction the reduced flavin is then re-oxidized by an electron acceptor, which is molecular oxygen for LOX resulting in the by-product H₂O₂. Whereas the oxidative half-reaction differs among several enzymes mainly due to different electron acceptors, the reductive half-reaction seems to follow a common reaction mechanism within the flavoprotein family. We picked **Scheme 1** to explain the important steps in catalysis: After the conversion of L-lactate into pyruvate the

product rapidly dissociates from the active site, and molecular oxygen reacts with the enzyme producing H_2O_2 ; when we look at LMO (the preliminary product), pyruvate doesn't dissociate from the enzyme, and O_2 reacts rapidly with the E-FMN_{red}-pyruvate complex resulting in the products acetate, CO_2 and H_2O . The presence of this intermediate has been proven for LOX and LMO by photometric studies of LOX indicating a biphasic behavior of the traces observed from 340 to 550 nm (**1**, **17**, **18**). This species has been identified as a complex of reduced enzyme and pyruvate by titration of reduced enzyme with pyruvate and in stopped flow experiments by mixing different concentrations of pyruvate with the reduced enzyme (**1**).

Within the last years the chemical mechanism has been investigated extensively: Consequently, still two proposed alternatives exist around the precise mechanism of L-lactate oxidation in LOX. Either a carbanion intermediate is formed by the deprotonation of the lactate-carbon by His-265, the active site base, prior to the oxidation of lactate (**10**). Or the α -hydrogen from lactate is transferred directly to the flavin as a hydride.

On the other hand, the active site arrangement leaves no doubt about a common substrate binding mechanism for the α -hydroxy acid oxidizing family. Structural comparison reveals that the active site of these hydroxyacid oxidases consists of six conserved amino acid residues (**12**). Only exception is a phenylalanine residue instead of a tyrosine (Tyr-40 in LOX) in long chain α -hydroxy acid oxidase (**1**). Every single conserved amino acid residue represents one important role. We know from crystallographic studies, where LOX was crystallized with pyruvate that certain amino acid residues are responsible for the stabilization of substrate (**13**). These are Tyr-40, Arg-181, His-265, Arg-268, Tyr-146 and Tyr-215. With the exception of Tyr-215, all other residues have been the topic of mutation studies and

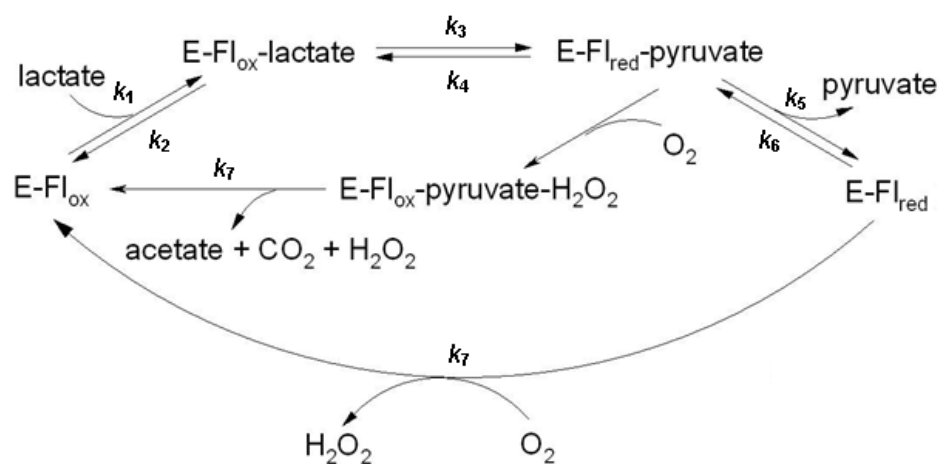
evidenced their importance in the LOX activity. Comparing the crystal structure of LOX with flavocytochrome b_2 and glycolate, four amino acid residues were identified (with exception of Tyr-215 and Arg-268) to interact with substrates. LCHAO has a very similar folding with LOX. A sequence alignment between those two enzymes identified the active site of LCHAO to be broader and more hydrophobic than that of LOX. Instead of a hydrophilic Tyr residue (Tyr-40 in LOX), it features a Phe-23 and has no hydrophilic residue tyrosine (Tyr-215 in LOX) surrounding the active site (13).

The hydroxyl group of Tyr-146 is close to the hydroxyl group of pyruvate (2.62 Å), whereas Tyr-215 is slightly closer (2.56 Å). Due to this short proximity Tyr-215 could be involved in substrate stabilization, and as shown for A95G, a mutation could influence the substrate specificity (17). Based on these facts, site-directed mutagenesis at Tyr-215 could help to illustrate the role of this active site residue. Furthermore, sequence comparison proved Tyr-215 residue to be unique in the α -hydroxy acid oxidizing family, a fact, which supports the idea that this residue is responsible for oxidase activity. A mutant form of LOX from *Aerococcus viridans*, in which Ala95 was replaced by glycine, was constructed as a mimic of L-lactate monooxygenase, but proved instead to be a mimic of long chain α -hydroxy acid oxidase from rat kidney (17). Due to these observations, the aim of the present work was to change substrate specificity of LOX, and gain insights in the mechanism of LOX by site-directed mutagenesis of an active site-residue.

Some amino acid residues are likely to change the orientation at different pH values, thus pH studies can help to identify such changes as already been illustrated by a previous work (15). Their crystal structure of wild-type LOX determined at pH 4.5 showed the catalytic His-265 to be flipped out during the reductive half-reaction. As proposed by the scientific group, the change mainly derives from the protonation of

His-265. Accordingly, the pK value of histidine is around 6, and therefore at pH 4.5 the histidine is likely to exist as the di-protonated form. A conformational change was also observed in crystal structure of LOX at pH 8.0. Here, His-265 remains closer to the substrate, whereas at pH 4.5 the histidine flips away from the substrate and is returned in its initial position during the oxidative half-reaction, i.e. the entrance of oxygen, to be deprotonated and to function as catalyst for FMN re-oxidation and the formation of hydrogen peroxide. Furuichi et al. did not perform any kinetic measurements in this context, but the facts of changing conformation of single active site residues by varying the pH are significant and could result in alteration of the reaction mechanism and kinetic parameters as well (15).

In this paper we have replaced Tyr-215 by the non-polar residue Phe, which lacks the hydroxyl group for hydrogen bond interaction with the substrate and by histidine, which could provide an alternative hydrogen bond and could stabilize the anionic form of the substrate. On the base of steady state measurements and pH studies, we tried to identify the role of Tyr-215 in catalysis.



Scheme 1. The reaction cycles of LOX (outer cycle) and LMO (inner cycle)

EXPERIMENTAL PROCEDURES

L-(+)-lactic acid (free acid, 98%, Aldrich), L-glycolic acid (free acid 97%, Fluka), L-(+) mandelic acid (free acid, 98%, Fluka), L-glyceric acid (sodium salt, 95%, Sigma), (S)-2-hydroxy-3-methylbutyric acid (free acid, 99%, Aldrich), (S)-2-hydroxybutyric acid (free acid, 97% Fluka), (S)-(-)-2-hydroxyisocaproic acid (free acid, 98%, Aldrich), D-(+)-glucose (99.5%, Sigma), 3,3-dimethylglutaric acid (free acid, 98%, Aldrich), 4-aminoantipyrine (98%, Fluka), peroxidase from horseradish (Type VI, Sigma), N,N-dimethylaniline (ReagentPlus[®], 99%, Aldrich), sodium dodecylbenzenesulfonic acid (technical grade, Aldrich). Lyophilized wild-type LOX (grade 1) from *Aerococcus viridans* (WT) and lyophilized GOD (glucose oxidase, grade 1) from *Aspergillus niger* were from Roche Diagnostics GmbH. Enzymes were stored at -20 °C until further use. The plasmid pLO-1, which harbored the LOX gene, was kindly provided by Dr. T. Meier (Roche).

Molecular cloning and site-directed mutagenesis

Site directed mutagenesis leading to substitution of Tyr-215 by Phe and by His was introduced by a two-stage polymerase chain reaction, utilizing a protocol from literature (36). Therefore, two separate primer extension reactions were carried out, in which pLO-1 was used as the template, and one of the two mutagenic oligonucleotide primers was also present. The two primers for Y215F were 5'-TATCTTCGGTGCTAGCAAACAAAAAATCTCACCAAGAG-3' (termed Y215Ffw; melting point: 62.3 °C), and 5'-GTTTGCTAGCACCGAAGATATTGTTTAATGACATACCTTCTGCTG-3' (termed Y215Frev; melting point: 63.8 °C). The two primers for Y215H were 5'-CAATATCCACGGTGCTAGCAAACAAAAAATCTCACCC-3' (termed Y215Hfw; melting

point: 62.2 °C), and 5'-GTTTGCTAGCACCGTGGATATTGTTTAATGACATACCTTCTG-3' (termed Y215Hrev; melting point: 63.1 °C). All primers are including a *NheI* restriction site. DNA was amplified by Pfu DNA Polymerase (Promega) setting up the following conditions: heat denaturation at 95 °C for 1 min; 4 elongation cycles, each consisting of 95 °C for 50 s, 59 °C for 50 s and 68 °C for 10 min; final extension at 68 °C for 7 min, and cooling at 4 °C. A second PCR was performed by combining the two separate PCR mixtures in a volume ratio of 1:1 under the same conditions mentioned above, but with a total repeat of 18 cycles. To ensure a higher transformation yield, template DNA was digested with *DpnI* at 37 °C for 1 h. Plasmid DNA was transformed into electrocompetent *E. coli* BL21 (DE3) cells, and the cells were cultured overnight at 37 °C on LB-amp plates (1% peptone, 0.5% yeast extract, 0.5% NaCl, 1.8% agar supplemented with 100 µg/mL ampicillin). For further steps, only transformants carrying plasmids with the mutation of interest verified by DNA sequencing were used.

Production of Y215F and Y215H mutants

Expression of the LOX mutants in BL21 (DE3) was done in pre culture over night containing 0.55% glucose monohydrate, 1% peptone, 0.5% yeast extract, 0.5% NaCl, 1% NH₄Cl, 0.025% MgSO₄ *7 H₂O, 100 µL/L poly(propylene glycol), 0.3% K₂HPO₄, 0.6% KH₂PO₄, 0.2*10⁻³% thiamine, 0.0115% ampicillin, 0.4*10⁻³% FeSo4 * 7H₂O, 0.1*10⁻³% MnSO₄ * H₂O, 0.04*10⁻³% CuSO₄ * 5 H₂O, 0.01%*10⁻³% H₃BO₃, 0.02*10⁻³% ZnSO₄ * 7 H₂O, 0.02*10⁻³% Na₂MoO₄ * 2H₂O and 0.04*10⁻³% FeCl₃. The optical density (OD₆₀₀) of the pre-culture, grown over night at 37 °C, had a value about 5. The main culture (same ingredients as pre-culture except 4 times higher glucose amount) was inoculated to an OD₆₀₀ of 0.5 directly to the fermenter.

Temperature, pH, stirring and oxygen partial pressure in the B. Braun Biotech International Biostat®C, Type-CT5-2 fermenter were controlled and adjusted automatically during fermentation. The pH was balanced before start at pH 7.0 and pH 4.0 with a ready-to-use calibration solution. The pO_2 was fixed to a minimum of 40%. Temperature was set to 37°C before induction and then reduced to 30 °C. Induction took place with 5 mL of isopropyl β -D-1-thiogalactopyranoside with a concentration of 250 μ g/mL, which was a 1000-fold stock solution at an OD_{600} of 2.4. 50 mg/mL Amp was added as well with the IPTG. Concurrent with the induction of the biomass, the glucose level was measured continuously over time to determine the endpoint of fermentation with glucose stripes (Diabur Test 5000, Roche Diagnostics). OD_{600} was measured during the whole process of fermentation with Beckman Coulter Photometer. After the whole consumption of glucose, the fermentation was stopped and the cells were harvested by centrifugation. The cell pellet was suspended in 50 mM potassium phosphate buffer, pH 7.0, and stored at -20 °C.

Protein purification

50 mM potassium phosphate buffer, pH 7.0 was used to perform the ongoing purification steps. First, cells were disrupted in a French press, and the crude extract was obtained by centrifugation. Further, protein was precipitated in the presence of 1.5 M $(NH_4)_2SO_4$ at 4 °C, and precipitate was removed by centrifugation. The supernatant was purified by hydrophobic interaction chromatography using a Phenyl Sepharose 6 Fast Flow (High Sub) column (GE Healthcare Life Sciences; 64 mL) and the Äkta FPLC system (Amersham Biosciences); the flow rate of the procedure was 5 mL/min, and eluted LOX was detected at 280 nm. Purity of the fractions showing LOX activity was controlled by SDS-PAGE with PhastGel™ Gradient 8-25

(GE Healthcare Life Sciences) gels and the Pharmacia High Speed Electrophoresis System (Pharmacia Biotech).

Finally, enzyme solution was desalted by repeated cycles of concentration and dilution using concentrator tubes (Vivaspin 20, 10 kDa cut-off, Vivascience AG) and stored in 50 mM potassium phosphate buffer, pH 7.0, at -25 °C until further use.

Assays

For kinetic studies of LOX activity, a peroxidase-coupled spectrophotometric assay (Sigma) was used, in which the H₂O₂ produced in the LOX reaction is further reacted with peroxidase in the presence of 4-aminoantipyrine and N,N-dimethylaniline to give a quinonediimine dye that is detected spectrophotometrically. About 5 to 10 μL of enzyme appropriately diluted in 50 mM potassium phosphate buffer, pH 7.0, were added to a solution containing 40 mM 3,3-dimethylglutaric acid, 2.5 units peroxidase, 1.5 mM 4-aminoantipyrine, 50 mM L-(+)-lactic acid and 0.04% (v/v) N,N-dimethylaniline in a total volume of 0.5 mL. The pH of the solution was pH 6.5. After a reaction time of between 10 and 20 min at 37 °C, 1 mL of 0.25% (w/v) dodecylbenzenesulfonic acid was added to stop the reaction. The produced quinonediimine dye was measured spectrophotometrically at 565 nm with a Varian Cary® 50 Bio UV-Visible Spectrophotometer at 37 °C. Specific activity was calculated with **Equation 1.1.** and **Equation 1.2.**

Equation 1.1:

$$v = \frac{A_{565\text{nm}} * V_{\text{assay}} * df}{\epsilon * c * f * t * V_{\text{enzyme}}}$$

where $A_{565\text{nm}}$ is the measured absorbance at 565 nm, V_{assay} the total volume of the assay, df the dilution factor of the enzyme, ϵ the millimolar extinction coefficient of quinonediimine (35.33 mM⁻¹ cm⁻¹), c of the conversion factor based on the fact that one

mole of H₂O₂ produces half a mole of quinonediimine, t the time of the assay and V_{enzyme} the volume of the enzyme. Specific activity was gained by considering the enzyme concentration (see **Equation 1.2**).

Equation 1.2:
$$\text{specific activity} = \frac{v}{c}$$

Protein concentrations were measured according to the Bradford protein quantification assay (Roti®-Quant, Carl Roth GmbH + Co KG) using BSA as reference. Note: the commercial preparation of LOX was not used for calibration of the protein assay. The enzyme is a solid powder that contains various substances other than target enzyme. Calibration based on solid mass is therefore not possible.

Absorbance spectroscopy

UV-visible absorbance spectra were recorded with a Varian Cary® 50 Bio UV-Visible Spectrophotometer in quartz cuvettes (Hellma® GmbH & Co. KG) of 10 mm light path. 100 µM of enzyme were scanned in 50 mM potassium phosphate buffer, pH 7.0, at 25 °C, and a molar extinction coefficient at 455 nm of 12500 was assumed by releasing the FMN cofactor, which was performed by treating the enzyme with trifluoroacetic acid.

Kinetic analysis

For steady state measurements at pH 6.5 and 37 °C, initial rates of the enzymatic oxidation of L-lactic acid or other hydroxy acids were determined, wherein the substrate concentration (10 measurements for concentrations of 0.1 - 50 mM) was varied. By using a peroxidase-coupled assay, these rates were determined. Kinetic constants (K_M , V_{max}) were obtained from nonlinear fit of the Michaelis-Menten

equation (**equation 2.1** or **equation 2.2**) to the measured data using Sigma Plot®, and the k_{cat} was calculated with equation 2.3

Equation 2.1:
$$v = v_{\text{max}} * \frac{[S]}{K_M + [S]}$$

Equation 2.2:
$$v = v_{\text{max}} * \frac{[S]}{K_M + [S] * (1 + \frac{[S]}{K_{IS}})}$$

Equation 2.3:
$$k_{\text{cat}} = \frac{v_{\text{max}}}{[E]}$$

where v represents the reaction rate, v_{max} the maximum rate, $[S]$ the substrate concentration, K_M the Michaelis constant, K_{IS} the dissociation constant of the enzyme-inhibitor-substrate complex, k_{cat} the turnover number. $[E]$ corresponds to the molar concentration of the enzyme. E was determined from the protein concentration assuming a molecular mass of 41 kDa for the subunit of LOX.

Enzyme kinetics for pH profile

10 μl LOX version appropriately diluted in 50 mM potassium phosphate buffer or H_2O were added to a coupled assay solution containing multiple-component buffer (20 mM MES, 20 mM HEPES and 40 mM ethanolamine) at various pH values (pH 5 - 10), 10 units peroxidase, 1.5 mM 4-aminoantipyrine, 0.04 v/v% N,N-dimethylaniline and L-lactate (up to ten various concentrations for compiling Michaelis-Menten kinetic) in a total volume of 0.5 mL reaction mixture. After reaction time of 10 minutes at 37 °C 1 mL 0.25 w/v % dodecylbenzenesulfonic acid solution was added to stop the reaction. The absorbance was measured spectrophotometrically at 565 nm with a Varian Cary 50® Bio UV-Visible Spectrophotometer at RT directly after addition of DBS. Specific activity was calculated with **Equation 1.1.** and **Equation 1.2.**

Data Analysis (pH-profile)

Determination of respective kinetic data k_{cat} and K_M at different pH values for the Y215F mutant, the Y215H mutant and the wild-type LOX occurred via SigmaPlot® (version 11.0) and by using **equation 2.1**, **equation 2.2** and **equation 2.3**.

The pH profiles of $\log(k_{\text{cat}})$ and $\log(k_{\text{cat}}/K_M)$ were non-linear fitted to **equation 3.1**. This equation was used because of curve characteristics, i.e. a “bell-shaped” curve with two observed p*K* values.

Equation 3.1:

$$\log Y = \log \left[\frac{C}{1 + \frac{[H^+]}{K_1} + \frac{K_2}{[H^+]}} \right]$$

where Y describes k_{cat} or k_{cat}/K_M , C is the pH independent value of Y at the optimal state of protonation, [H⁺] is the proton concentration and K_1 and K_2 are macroscopic dissociation constants (**20-22**).

Stopped flow

Pre-steady state measurements were conducted at 20 °C using an Applied Photophysics stopped flow apparatus, model SX17MV. A diode array detector was applied to collect spectral data between 280 and 700 nm. Several wavelengths were chosen from the collected spectra and single wavelength scans with a photomultiplier. The reductive half-reaction was monitored by collecting spectra with the diode array detector and by measuring the absorbance over time at 455 nm after anaerobically mixing 10 μM enzyme with varying concentrations of L-lactic acid. The oxidative half-reaction was followed at 455 nm after mixing an anaerobical solution containing reduced enzyme (10 μM) with a buffer solution containing different concentrations of dioxygen. Anaerobic conditions were created by the addition of 10

mM D-glucose to all solutions and flushing with nitrogen. Additionally, to remove all traces of residual oxygen, glucose oxidase (GOD) was added to a final concentration of 200 nM.

Traces obtained at 455nm were fitted to an exponential function:

Equation 4.1:
$$A(t) = A + Cxe^{(-kt)}$$

where A describes the absorption, C is a constant, and k represents an observed rate constant. The observed rates for substrate concentration dependent reduction of LOX were fitted using the following equation

Equation 4.2:
$$k_{obs} = \frac{k_{red}xS}{K_d+S}$$

where k_{obs} describes an observed rate constant, k_{red} is the reduction rate constant, S is the substrate concentration and K_d is the dissociation constant.

For the oxidative half-reaction the enzyme was reduced with 2 equivalents L-lactate to guarantee a completely reduced LOX. No Michaelis-Menten type complex is formed during the re-oxidation event with molecular oxygen; by varying oxygen concentration linear plots with the primary data were created in order to determine bimolecular rate constants for this process. Bimolecular rate constants for the reaction of free reduced LOX with molecular oxygen were calculated from plotting the rates of re-oxidation [s^{-1}] versus the oxygen concentrations [M].

RESULTS

Steady state kinetics

Kinetic characteristics for L-lactate and a range of other L- α -hydroxy acids, which were converted into the corresponded α -keto acid, are listed in **Table 1**. Measurements were performed at 37 °C using a peroxidase assay. The wild-type LOX was supplied by Roche Diagnostics.

A comparison with the wild-type points out that the specific activities of Y215F and Y215H mutants for L-lactate are lowered by a factor of 2.7 and approximately 15. Consequently, the lacking hydrogen bond for the stabilization of the anionic form of the substrate in Y215F might be the reason for the lower specific activity. Tyr-215 might not directly be involved in substrate conversion. A direct involvement of the mutant is very likely to result in a drastically lowered activity or to an inactive enzyme. Further, steric properties of the histidine residue in contrast to tyrosine might be responsible for the low specific activity for L-lactate in Y215H mutant. Contrariwise, the affinity for L-lactate was increased 9-fold in Y215F mutant expressed by a very low K_M . Possibly the lacking hydroxyl group could have a positive influence on the enzyme-substrate affinity. Although the k_{cat} of Y215F is lower compared to the wild-type, the low K_M value leads to a higher catalytic efficiency (k_{cat}/K_M) by a factor of 3.4 for Y215F. In addition substrate inhibition occurs at higher substrate concentrations in Y215F. Due to the removal of the hydroxyl group by the substitution of Y215 by phenylalanine a second substrate binding site might be induced, which further leads to the inhibition of substrate conversion (**19**).

Table 1. Steady state kinetic parameters of wild-type LOX, Y215F and Y215H mutant

		Wild-type	Y1215F	Y215H
L-(+)-lactic acid				
k_{cat}	(s ⁻¹)	140 ± 1	51.7 ± 1.2	9.1 ± 0.1
K_{M}	(mM)	0.8 ± 0.03	0.1 ± 0.01	0.85 ± 0.04
$k_{\text{cat}}/K_{\text{M}}$	(mM ⁻¹ s ⁻¹)	167	561	10.7
L-mandelic acid				
k_{cat}	(s ⁻¹)	0.1 ± 0.01	0.03 ± 0.001	n.d.
K_{M}	(mM)	0.5 ± 0.1	0.26 ± 0.02	n.d.
$k_{\text{cat}}/K_{\text{M}}$	(mM ⁻¹ s ⁻¹)	0.2	0.12	n.d.
(S)-2-hydroxy-butyrac acid				
k_{cat}	(s ⁻¹)	1.4 ± 0.01	7.72 ± 0.89	0.81 ± 0.02
K_{M}	(mM)	0.4 ± 0.05	1.47 ± 0.26	0.7 ± 0.07
$k_{\text{cat}}/K_{\text{M}}$	(mM ⁻¹ s ⁻¹)	3.2	5.4	1.2
(S)-hydroxy-3-methylbutyric acid				
k_{cat}	(s ⁻¹)	0.2 ± 0.01	0.02 ± 0.001	n.d.
K_{M}	(mM)	3.3 ± 0.3	1.3 ± 0.3	n.d.
$k_{\text{cat}}/K_{\text{M}}$	(mM ⁻¹ s ⁻¹)	0.1	0.012	n.d.
(S)-2-hydroxy-isocaproic acid				
k_{cat}	(s ⁻¹)	1.1 ± 0.01	2.56 ± 0.03	0.58 ± 0.02
K_{M}	(mM)	0.4 ± 0.05	0.71 ± 0.04	0.32 ± 0.07
$k_{\text{cat}}/K_{\text{M}}$	(mM ⁻¹ s ⁻¹)	2.5	4.8	1.8
L-(-)-glyceric acid				
k_{cat}	(s ⁻¹)	2.9 ± 0.1	5.5 ± 0.1	0.05 ± 0.01
K_{M}	(mM)	8.6 ± 2.0	3.7 ± 0.6	1.2 ± 0.2
$k_{\text{cat}}/K_{\text{M}}$	(mM ⁻¹ s ⁻¹)	0.3	1.5	0.04
glycolic acid				
k_{cat}	(s ⁻¹)	0.98 ± 0.02	0.19 ± 0.01	0.27 ± 0.01
K_{M}	(mM)	0.4 ± 0.06	0.22 ± 0.01	1.16 ± 0.33
$k_{\text{cat}}/K_{\text{M}}$	(mM ⁻¹ s ⁻¹)	2.2	0.6	0.2

α Steady state measurements were performed at 37 °C with a coupled peroxidase assay. Standard deviations on kinetic parameters are from non-linear fits of data with the Michaelis-Menten equation

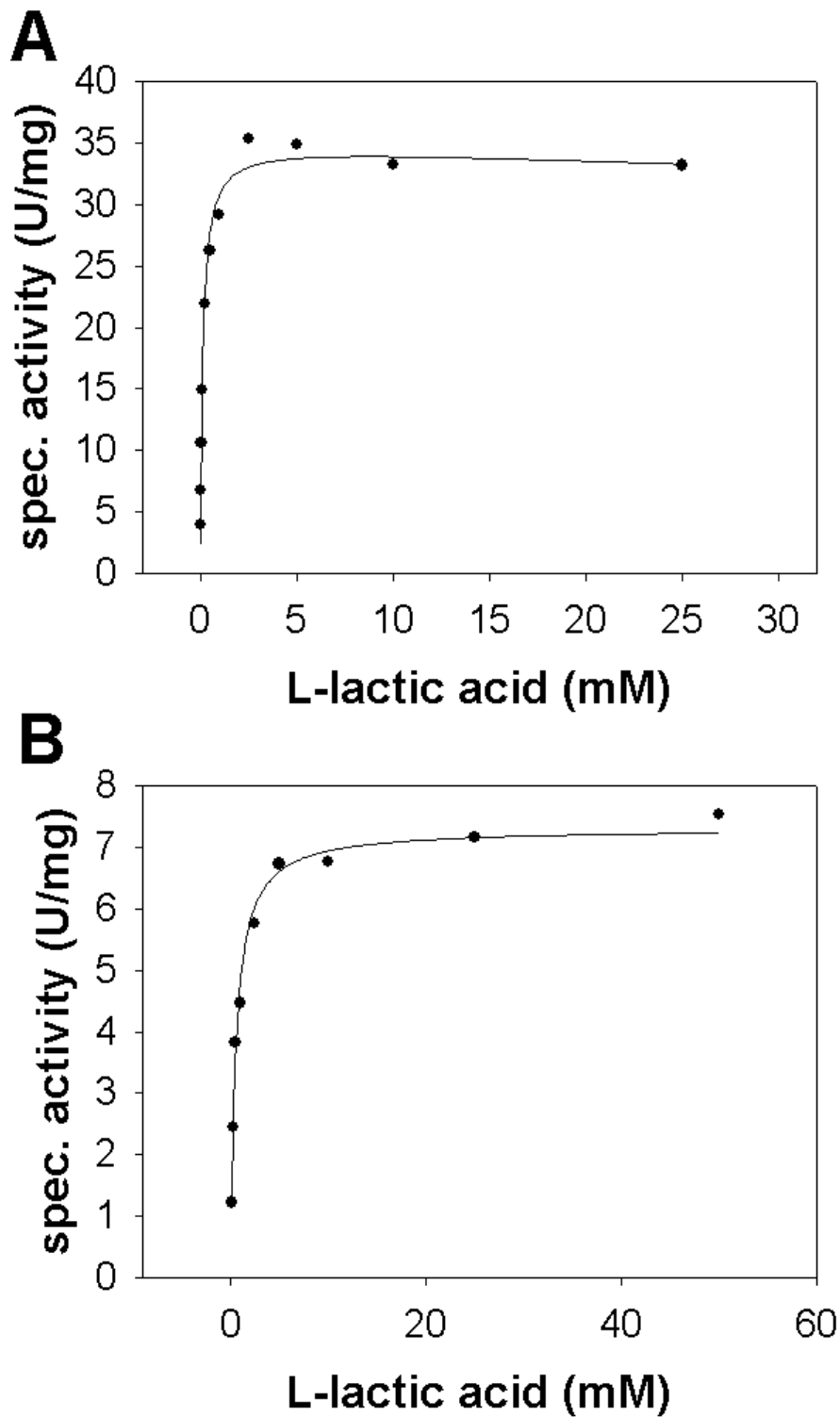


Figure 2

Steady state measurements of Y215F (Panel A) and Y215H mutant (Panel B) at different L-lactate concentrations determined by a coupled peroxidase assay at 20 °C.

In terms of k_{cat} , the activity of Y215H for glycolic acid is lowered by a factor of 3.5 compared to the wild-type and the K_M is increased, which could be considered a positive effect for the use of Y215H in biosensors used in medical diagnosis, without regard to the low specificity for L-lactate. Specific activity for glycolic acid is decreased in Y215F mutant, whereas the K_M is lowered by a factor of 2. Thus enzyme-substrate affinity for Y215F is higher compared to the wild-type. Furthermore, substrate inhibition at higher glycolic acid concentrations has been observed in Y215F as well as in the wild-type. That differs from Y215H, where no substrate inhibition at higher glycolic acid concentrations occurs, which might result from the steric properties of Y215H.

In terms of k_{cat} , it is also noticeable that Y215F mutant shows increased activities with L-hydroxy butyric acid (5.6-fold), L-hydroxy isocaproic acid (~2-fold) and L-glyceric acid (~2-fold) in contrast to wild-type. On the other hand, the affinity for L-hydroxy butyric acid and L-hydroxy isocaproic acid is decreased, which is the reason, why the catalytic efficiency for those two substrates is only slightly higher compared to wild-type LOX. Worth mentioning, a 10-fold lower K_M could only be observed for Y215F mutant when using L-lactate as substrate. With all chosen substrates determined Y215H mutant features similar or lower affinities (except L-glyceric acid with a 6-fold lower K_M) for each particular substrate compared to WT. In terms of k_{cat} (e.g. L-lactate 16-fold) and k_{cat}/K_M (e.g. L-glyceric acid 53-fold), the activities are always significantly lower than those ones of wild-type.

Specific activity, k_{cat} and K_M were changed by mutation at Tyr-215 for all determined substrates. Kinetic data of L-mandelic acid and L-2-hydroxy-3-methyl butyric acid for Y215H mutant could not be determined because values were below the detection limit. Specific activity for longer chain L- α -hydroxy acids, branched and

linear, is very low for the wild-type. This might result from the steric conditions in the active site. In our previous work and known from literature (2), a single mutation in the active site, namely the substitution of Ala-95 to glycine results in increased substrate specificity for longer L- α -hydroxy acids. Therefore, the change of steric properties in the active site caused by the mutations might also be a reason for the lowered specific activity of Y215F and Y215H for longer chain L- α -hydroxy acids.

In summary, substitution of Tyr-215 by phenylalanine has little influence on the substrate specificity. Unlike enhanced activities with longer α -hydroxy acids for A95G mutant (2), steady state experiments for Y215F and analysis of crystal structures for wild-type LOX clearly indicated that the residue is not responsible for the docking of the substrate. Obviously the hydroxyl group of Tyr-215 is not relevant for the conversion. Instead, the substitution by Phe and the consequential ameliorated hydrophobicity of the active site raised the affinity of L-lactate resulting in increased catalytic efficiency. Substitution of Tyr-215 by histidine leads to an active enzyme whose turnover numbers and catalytic efficiency with several substrates are far below the wild-type enzyme. Decreased activities can generally be described by the steric properties of the histidine residue.

pH studies

As already mentioned, two possible mechanism for the reductive half-reaction of the related L- α -hydroxy acid oxidizing flavoenzymes are postulated - on the one hand a mechanism, in which a carbanion is formed and on the other hand a hydride transfer mechanism. As illustrated in **Figure 1**, the orientation of the substrate is different for both supposed mechanisms. In case number one, the catalytic histidine (His-265 in LOX) abstracts the α -proton of the substrate to form a carbanion, the α -hydrogen points toward the histidine in the carbanion mechanism. In the case of a

hydride transfer mechanism, the proton of the α -hydroxyl group is abstracted by the base and the α -proton is directly transferred as a hydride to the cofactor (FMN). Consequently, the hydroxyl group points towards the histidine (15). Of particular interest for the present work are the considerations of Sobrado et al. (23). Flavocytochrome b_2 of *Saccharomyces cerevisiae* has been the most studied α -hydroxy acid oxidizing FMN-dependent enzyme. It catalyzes the oxidation of L-lactate to form pyruvate with a subsequent electron transfer to cytochrome c aided by FMN and heme b_2 cofactors. Residue Tyr-254 in flavocytochrome b_2 is a conserved amino acid within the enzyme family and correlates with Tyr-146 of LOX. Tyr-146 as well as Tyr-215 are in close distance to interfere with the hydroxyl group of the substrate (14, 23). According to Sobrado et al. (23), there are different considerations of the role of Tyr-254 in flavocytochrome b_2 , whether the carbanion or the hydride transfer mechanism occurs. If the carbanion mechanism occurred, the tyrosine would interact as a base to abstract hydrogen of substrate's α -carbon and it would have to be in the anionic form at physiological conditions to have the facility to interact as a base. In the hydride transfer the tyrosine would orient the substrate for hydride transfer by the formation of a hydrogen bond between the substrate and the phenol of the tyrosine, which would be most compatible with a neutral tyrosine. To this end, pH studies as well as solvent isotope effects and rapid reaction kinetics by stopped flow measurements with the flavocytochrome b_2 mutant Y254F supported the hydride transfer as mechanism of the reductive half-reaction of flavocytochrome b_2 and affirmed the role of Tyr-254 as stabilizer of the substrate (23, 24). Thus, pH studies for wild-type LOX and the aforementioned LOX Tyr-215 mutants could shed light on the substrate binding mechanisms and the reaction mechanism of LOX.

We conducted pH studies for wild-type LOX, Y215F and Y215H mutant in a three-component-buffer at 37 °C and used **equation 3.1** to yield data listed in **Table 3**. Both, **Figures 3-5** and **Table 3** point out wild-type LOX, Y215F and Y215H mutant to have two pK values. pK_1 shows the requirement for a group to be unprotonated for optimum enzyme activity and pK_2 shows the requirement for a group to be protonated. The “bell-shaped” curve of $\log(k_{\text{cat}})$ versus pH for wild-type LOX is well fitted and results in a pK_1 of 5.63 and pK_2 of 8.0, thus two ionisable groups are visible. $\log(k_{\text{cat}}/K_M)$ versus pH has a low R^2 and results in a pK_1 of 6.47, which differs significantly from the resulting pK_1 of $\log(k_{\text{cat}})$ versus pH, and a pK_2 of 8.17, which is similar to the pK_2 , resulting from $\log(k_{\text{cat}})$ versus pH. These results lead to the assumption that pK_1 is K_M dependent, whereas pK_2 is not. Similar findings were achieved for Y215H mutant. It is not exactly known, not even in literature, which active site residue leads to the determined pK values. pK_1 could derive from His-265. The imidazol ring of histidine has a pK of about 6 under physiological conditions (**25**).

Table 3. Apparent pK values for wild-type LOX, Y215F and Y215H mutant

LOX	Parameter	pK_1	pK_2	C	R^2
Wild-type	$\log(k_{\text{cat}})$	5.63	8.00	228 s ⁻¹	0.97
	$\log(k_{\text{cat}}/K_M)$	6.47	8.17	306 mM ⁻¹ s ⁻¹	0.95
Y215F	$\log(k_{\text{cat}})$	6.09	6.61	69.7 s ⁻¹	0.98
	$\log(k_{\text{cat}}/K_M)$	6.12	7.34	600 mM ⁻¹ s ⁻¹	0.95
Y215H	$\log(k_{\text{cat}})$	4.61	8.49	2.48 s ⁻¹	0.96
	$\log(k_{\text{cat}}/K_M)$	6.23	8.18	123 mM ⁻¹ s ⁻¹	0.99

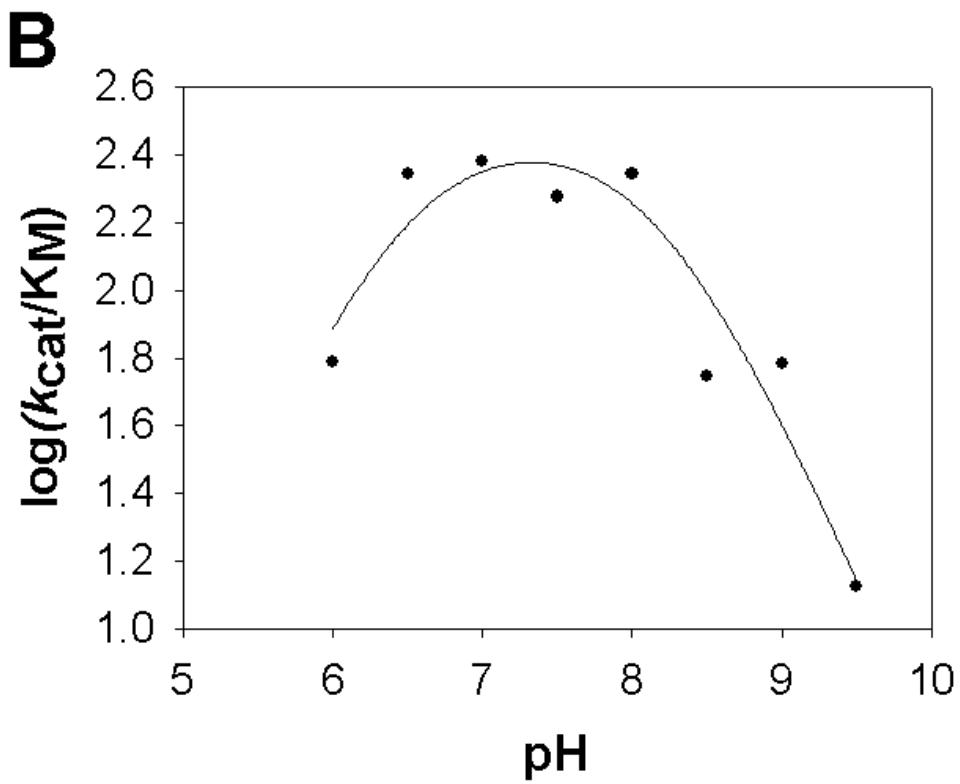
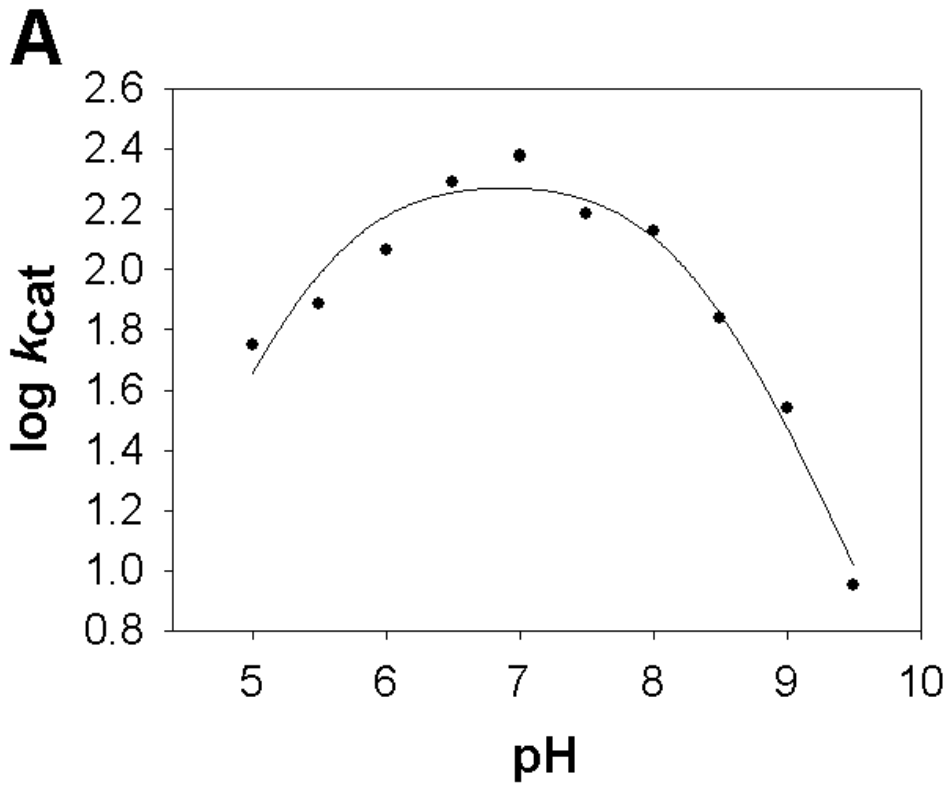


Figure 3

pH dependence of k_{cat} (Panel A) and k_{cat}/K_M (Panel B) for wild-type LOX

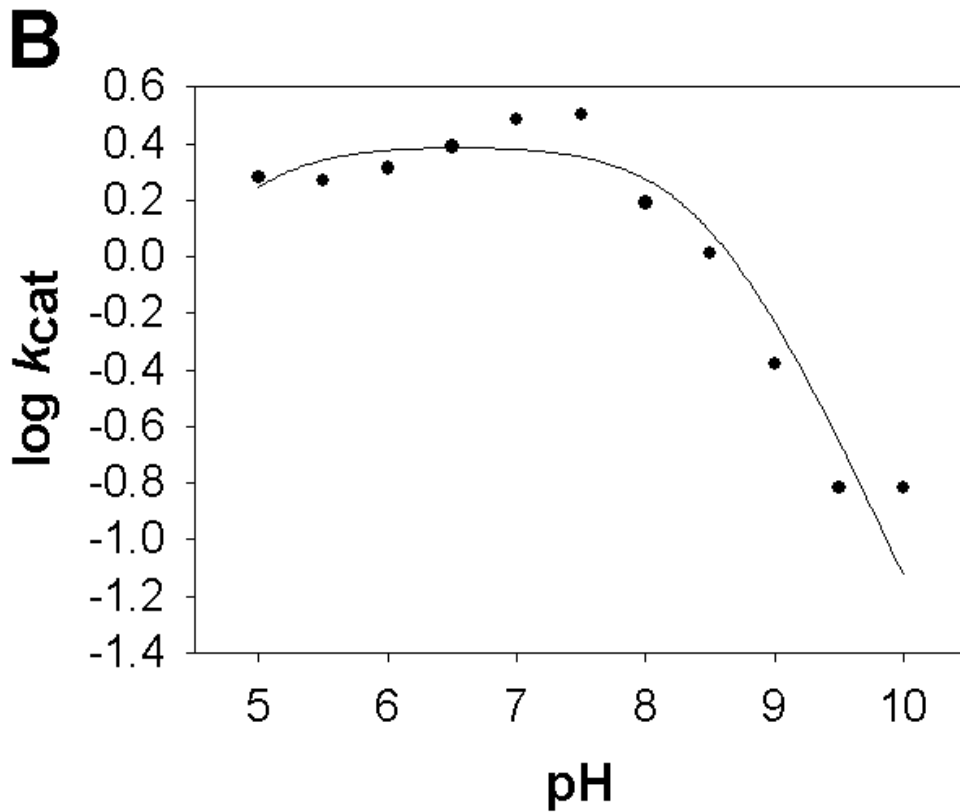
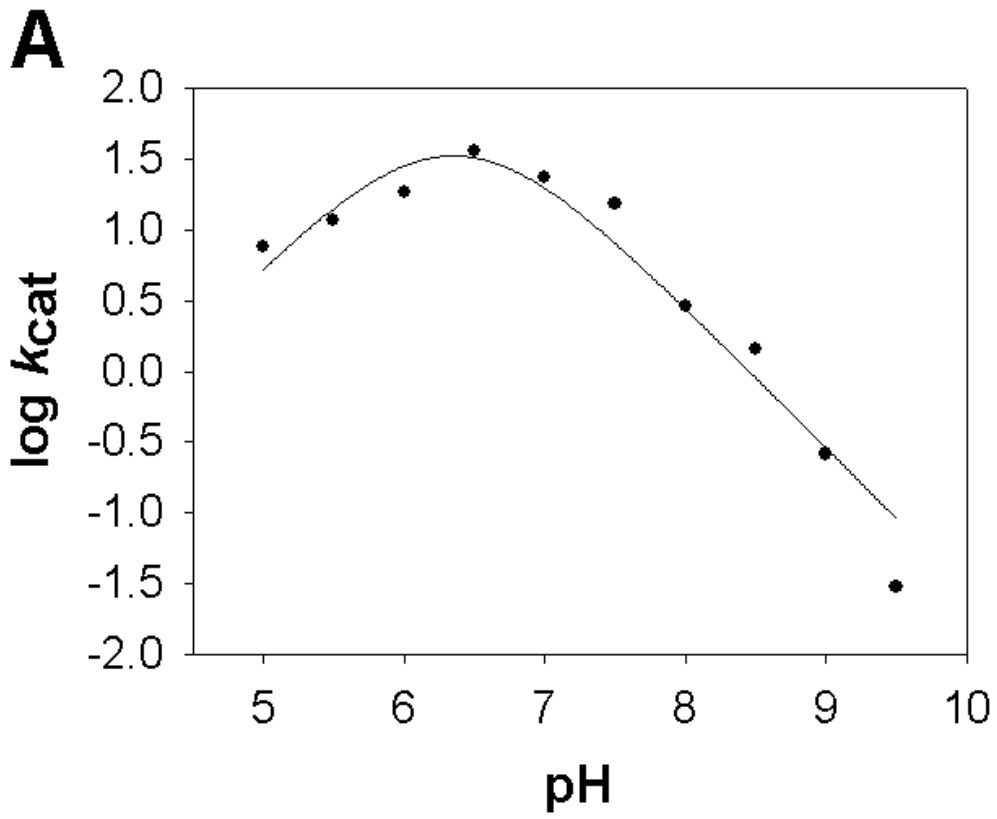


Figure 4

pH dependence of k_{cat} and k_{cat}/K_M for LOX Y215F (Panel A) and Y215H (Panel B) mutant

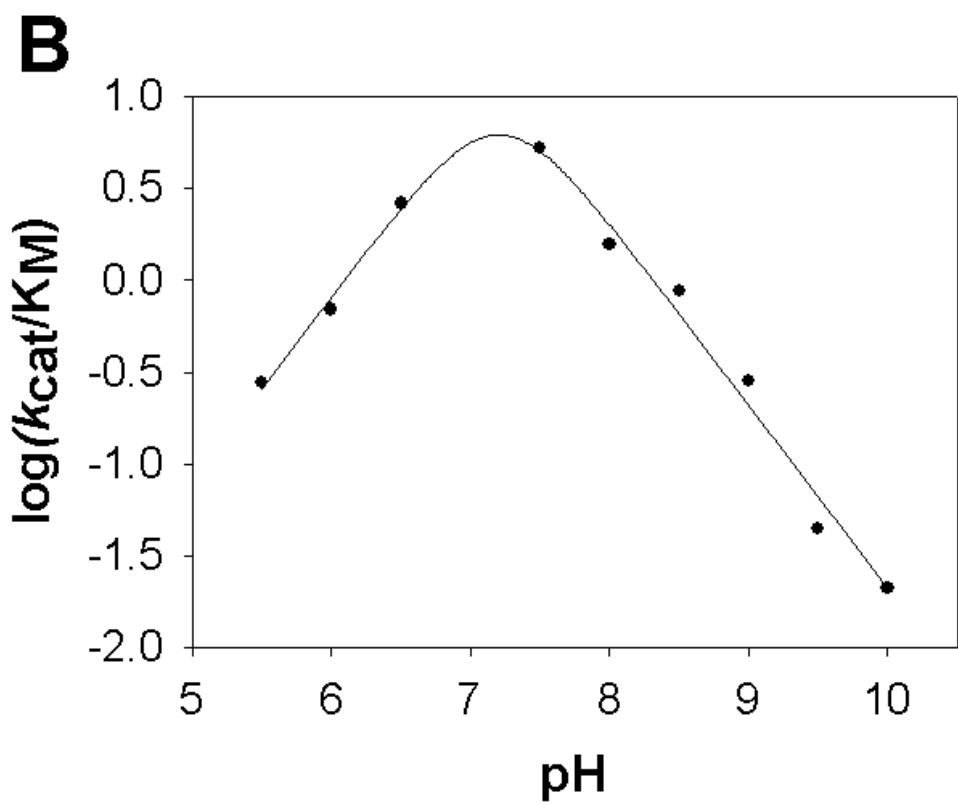
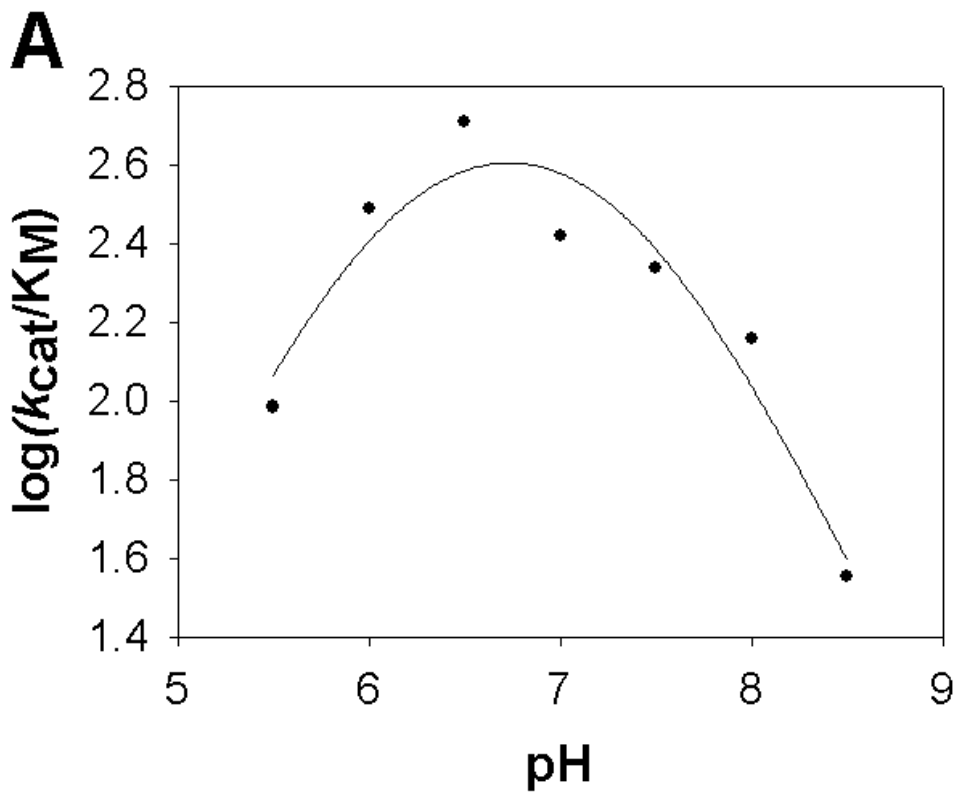


Figure 5

pH dependence of k_{cat}/K_M for LOX Y215F (Panel A) and Y215H (Panel B) mutant

For the Y215F mutant the apparent pK values resulting from $\log(k_{\text{cat}})$ versus pH are 6.09 for pK_1 and 6.61 for pK_2 . Thus, a remarkable change of the pK values due to mutation at Tyr-215 is only observed for pK_2 . pK_2 in Y215F is lowered by more than one pH unit compared to the wild-type. As the influence of the active site residues on the pK of the enzyme is not exactly understood, only assumptions to the change of pK_2 in Y215F can be made. Tyrosine has a pK of 10 under physiological conditions. It could influence the pK of other active site residues, the pK_2 respectively. Thus the removal of tyrosine in Y215F might cause the lowered pK_2 (25).

As influence of the substrate on the pK values can be excluded. L-lactate has a pK of 3.9 and in this pH range no kinetic measurements were conducted.

Reductive and oxidative half-reaction

In order to establish the rate limiting step of the LOX mutants, we conducted stopped flow experiments and investigated the reductive and the oxidative half-reaction separately. In terms of the reductive half-reaction, we mixed the enzyme anaerobically with different concentrations of L-lactate and recorded the decrease in absorbance at 455 nm ($A_{455\text{nm}}$) due to the instance that the reduced state of LOX loses its absorbance maximum at $A_{455\text{nm}}$. On the other hand, we followed the oxidative half-reaction by reducing LOX anaerobically with 1 equivalent of L-lactate and mixing with buffer containing different concentrations of O_2 . Here, the increase of $A_{455\text{nm}}$ was also followed spectrophotometrically leading to the re-oxidized enzyme with two absorbance maxima at 373 and 455 nm.

Regarding the reductive half-reaction, we observed no absorbance changes at any wavelength greater than 530 nm for wild-type LOX and Y215H mutant indicating that there is no (rate limiting) interaction with the product during the reductive half-

reaction. Following the reductive half-reaction, pseudo first order rates (k_{obs}) can be determined for different lactate concentrations at 455 nm (**Figure 6**). When the decrease in absorbance of 455 nm happens in a single exponential manner [$a \cdot \exp(-k \cdot x) + c$], k_{obs} (expressed in s^{-1}) describes the reduction rate at a certain substrate concentration. **Figure 6** shows the observed rates (k_{obs}) from single traces at 455 nm for LOX mutant Y215H, which are plotted to L-lactate to yield k_{red} (maximum rate of reductive half-reaction expressed in s^{-1}) and $K_d (= k_2/k_1)$ using **equation 4.2**:

The reduction of Y215F mutant (at 455 nm) can be described in a double exponential manner [$a_1 \cdot \exp(-k_1 \cdot x) + a_2 \cdot \exp(-k_2 \cdot x) + c$], with a fast phase at the beginning and we were also able to observe changes in absorbance greater than 530 nm (**Figure 7**). Here, the first phase in reduction is not influenced, but mainly the second phase.

In contrast to a single exponential decay shown for LOX wild-type and resulting in a single constant termed k_{red} (expressed in s^{-1}), the reduction of Y215F mutant can be described by two different phases; the first phase (described by k_{obs1}) is also increasing at higher substrate concentrations and reaches a maximum (termed as k_{red1} or k_3) of $1.2 \times 10^2 s^{-1}$, whereas the second phase (determined by k_{obs2}) reaches a maximum (termed as k_{red2} or k_5) of $20.3 s^{-1}$. To determine k_{red1} and k_{red2} , we plotted k_{obs1} and k_{obs2} against the lactate concentration (**Figure 7**) using **equation 4.3** and **equation 4.4**:

Equation 4.3:
$$k_{obs1} = \frac{k_{red1} \cdot S}{K_{d1} + S}$$

Equation 4.4:
$$k_{obs2} = \frac{k_{red2} \cdot S}{K_{d2} + S}$$

Interestingly, k_5 seems to be the rate limiting step (and is constant with the observed k_{cat} value from steady state experiments). Previous studies detected an absorbance change during the reductive half-reaction at 530 nm indicating a step, where the FMN_{red}-pyruvate complex is built and dissociates. In our experiments we were not able to detect such a change at 20 °C for the wild-type enzyme, but we clearly identified the formation and the decay of $A_{530\text{nm}}$ for the LOX mutant.

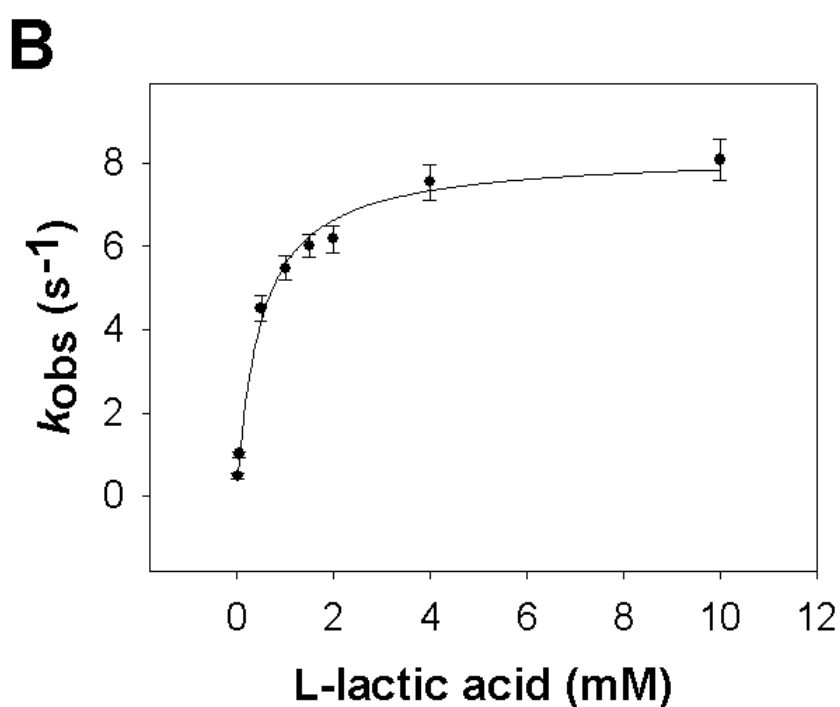
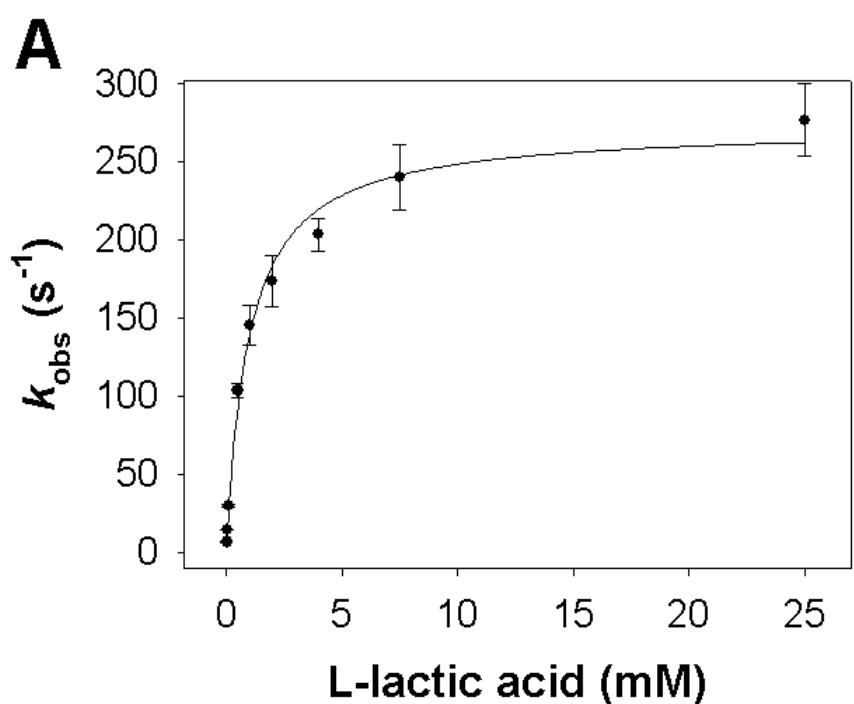


Figure 6

Determination of the reduction rate constant (k_{red}) and dissociation constant (K_{d}) for reaction of wild-type LOX (Panel A) and Y215H mutant (Panel B) with L-lactate at 20 °C. Pseudo first order rate constants, k_{obs} from determined traces at 455 nm are plotted to L-lactate to yield k_{red} and K_{d} .

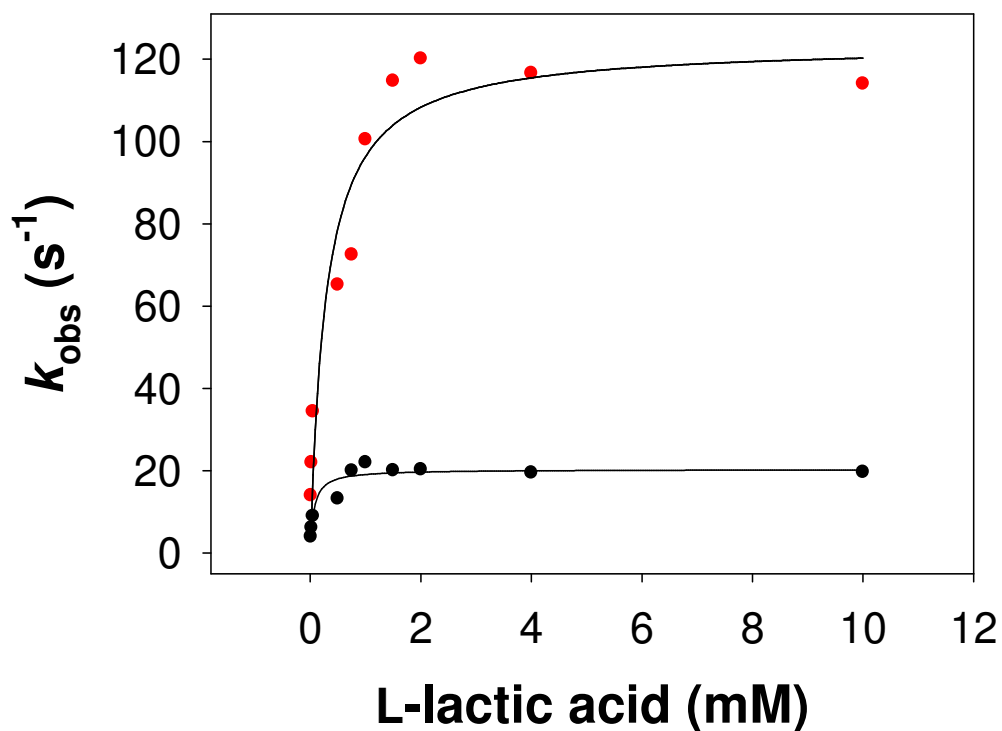


Figure 7

Determination of the reduction rate constant (k_{red1} and k_{red2}) for LOX Y215F mutant. The reaction is split into two phases leading to k_{obs1} (red) and k_{obs2} (black) at 455 nm (20 °C) for the different L-lactate concentrations. Fitting is described in the text. k_{red1} ($123.7 \pm 9.4 \text{ s}^{-1}$) is faster than k_{red2} ($20.3 \pm 0.9 \text{ s}^{-1}$), which is the rate limiting step in the reaction. $K_{\text{d1}} = 0.28 \pm 0.1 \text{ mM}$ and $K_{\text{d2}} = 0.06 \pm 0.02 \text{ mM}$.

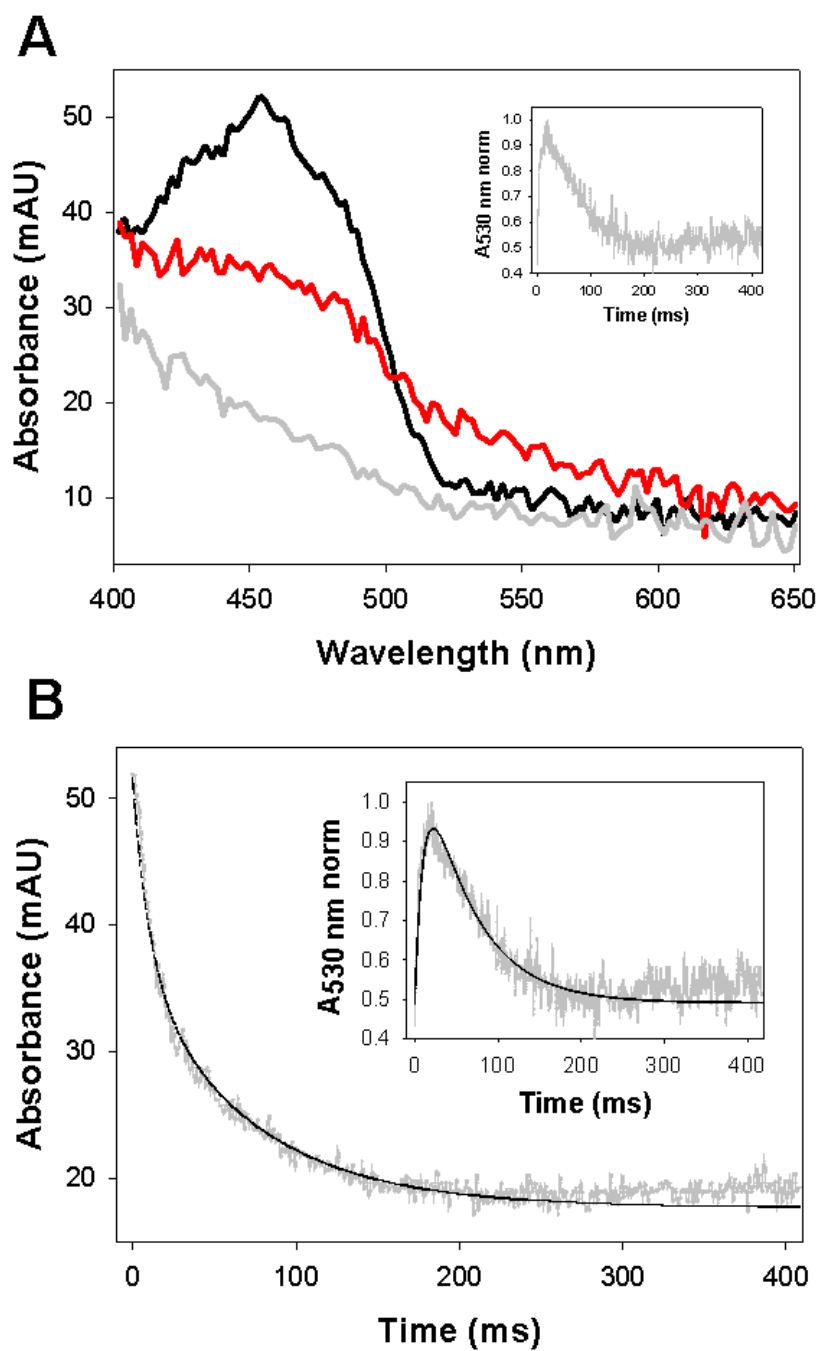


Figure 8

Spectral scans of LOX Y215F and fitting with Berkeley Madonna

Panel A: Spectral scans of LOX Y215F mutant during the reductive half-reaction. 4.3 μM LOX were reduced with 10 mM L-lactate under anaerobic conditions in 50 mM potassium phosphate buffer, pH 6.5 at 20 °C. **Black** line: enzyme in oxidized state at start (0 ms); **red** line: reaction after 20 ms; light

grey line: reaction after 200 ms. After 20 ms the maximum in absorbance at 530 nm is reached (compare dark **grey** trace for the whole reaction at inset), the amplitude decreases afterwards.

Panel B: Reductive half-reaction of LOX by L-lactate. 4.3 μM LOX Y215F mutant in 50 mM potassium phosphate buffer (pH 6.5) were reacted in the stopped flow photometer at 20 °C with 1 mM L-lactate. The grey line represents the reaction trace at 455 nm with two different phases (first phase = k_3 ; second phase = k_5) the inset reflects the trace at 530 nm in a biphasic manner. Black lines represent the fittings achieved with software Berkeley Madonna leading to the calculated kinetic constants in **Table 4**. The first phase ($k_3 = 90.7 \text{ s}^{-1}$) is faster than the second phase ($k_5 = 19.7 \text{ s}^{-1}$).

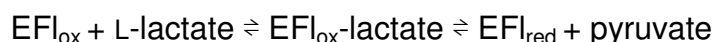
To point out the main difference observed during the reductive half-reaction between wild-type LOX and Y215F mutant, we generated **Figure 8**. It highlights spectral scans of Y215F mutant during the reduction with 10 mM L-lactate at 20 °C at different points in time and the concomitant change of the two mentioned traces ($\Delta A_{455\text{nm}}$ and $\Delta A_{530\text{nm}}$) during the same reaction. The figure demonstrates a biphasic manner of LOX previously pointed out for wild-type LOX at low temperatures (1). In principal, the spectral scan after 20 ms represents the point in time, where the max $A_{530\text{nm}}$ is reached. Additionally, we detected a biphasic manner for Y215F mutant at pH 5.5 and pH 9.5. On the other hand, wild-type LOX and Y215H mutant lack this behavior at pH 6.5 at 20 °C. Furthermore, only a decrease at $A_{530\text{nm}}$ was spotted for wild-type LOX. Interestingly, experiments at 4 °C reflected spectra of WT to be similar to those of Y215F mutant and prove that the reaction mechanism remains unchanged by the mutation, but results in a drop in k_{red} .

Table 4. List of kinetic parameters and characteristics of FMN for wild-type LOX and Y215F and Y215H mutant with L-lactic acid as substrate determined at 20 °C including pre-steady and steady states experiments and simulation of the fits.

		Wild-type LOX	Y215F	Y215H
Pre-steady state				
k_{red}	(s ⁻¹)	2.7 ± 0.1x10 ²	-	8.2 ± 0.3
K_d	(mM)	1 ± 0.1	-	0.55 ± 0.07
K_{d1}	(mM)	-	0.28 ± 0.1	-
K_{d2}	(mM)	-	6 ± 0.3x10 ⁻²	-
k_{red}/K_d	(mM ⁻¹ s ⁻¹)	2.7x10 ²	-	16
k_{ox}	(M ⁻¹ s ⁻¹)	1.8 ± 0.1x10 ⁶	7 ± 0.6x10 ⁵	1 ± 0.1x10 ⁵
k_{red1}	(s ⁻¹)	-	1.2 ± 0.1x10 ²	-
k_{red2}	(s ⁻¹)	-	24 ± 1	-
reduced FMN	(%)	>90	>95	>99
re-oxidized FMN	(%)	>90	>90	>90
$\Delta A_{530\ 1}$	(s ⁻¹)	-	99*	-
$\Delta A_{530\ 2}$	(s ⁻¹)	-	15.5*	-
Steady state				
k_{cat}	(s ⁻¹)	87.5 ± 2.2	22 ± 1.9	5 ± 0.3
K_M	(M)	0.5 ± 0.1	0.1 ± 0.01	0.5 ± 0.1
k_{cat}/K_M	(mM ⁻¹ s ⁻¹)	1.8 x10 ²	2.2 x 10 ²	10
k_{cat} calc	(s ⁻¹)	1.5 x10 ²	12.7	6.0
k_{cat} calc : k_{cat}		1.6:1	0.6 : 1	1.3 : 1
Berkeley Madonna **				
k_2/k_1	(M)	-	4.3 x 10 ⁻²	-
k_3	(s ⁻¹)	-	90.7	-
k_4	(s ⁻¹)	-	0	-
k_5	(s ⁻¹)	-	19.7	-
k_6	(M ⁻¹ s ⁻¹)	-	1 x 10 ⁴	-
$\Delta A_{530\ 1}$ describes an increase in absorbance, $\Delta A_{530\ 2}$ a decrease in absorbance				
* Rates derive from linear fitting ($\Delta A_{530\ 1}$) and single exponential fitting ($\Delta A_{530\ 1}$) with start at highest absorbance of A_{530} (conditions: 10 mM L-lactate)				
** Description of fit in text. Numbering is based on Scheme 1				

Worth mentioning, the rate of the formation of the complex ($\Delta A_{530\ 1}$) is as fast as the first phase of reducing the cofactor ($\Delta A_{455\ 1}$); moreover, the decay of the

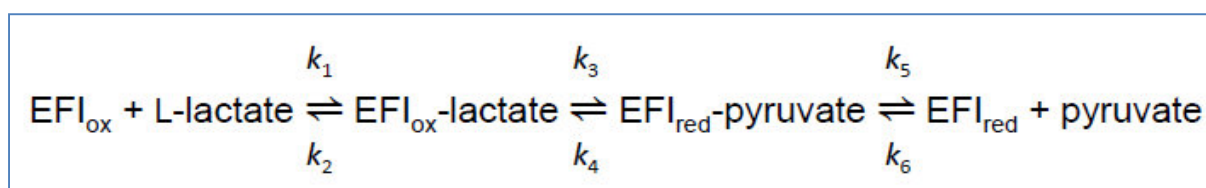
complex ($\Delta A_{530\ 2}$) corresponds to the second phase at 455 nm ($\Delta A_{455\ 2}$), which will be discussed in more detail later. In conclusion, $\Delta A_{455\ 1}$ ($= \Delta A_{530\ 1}$) describes k_3 and $\Delta A_{455\ 2}$ (and $\Delta A_{530\ 2}$) describe(s) k_5 of the reductive half-reaction. In contrast to Y215F (**Scheme 2**), the reductive half-reaction of wild-type LOX and Y215H is simplified to the reaction (where k_{red} includes k_3 and k_5):



The $K_{\text{d}2}$ of LOX Y215F mutant is in agreement with the K_{M} , though noticeable that it is more than 20 times lower than the one of LOX wild-type. On the other hand, both mutants and WT were re-oxidized by molecular oxygen in a single exponential manner and the observed rate constants were directly proportional to the oxygen concentration (**Figure 9**). Second order rate constants of Y215F and Y215H were $7.0 \times 10^5 \text{ s}^{-1} \text{ M}^{-1}$ and $1.1 \times 10^5 \text{ s}^{-1} \text{ M}^{-1}$ or 39% and 6% of that for wild-type enzyme (**Table 4**). A drop in k_{ox} can also influence k_{cat} ($1/k_{\text{cat}} = 1/k_{\text{red}} + 1/k_{\text{ox}}$).

Due to the instance that we detected differences in activity correlated to the pH, we carried out stopped flow experiments at pH 5.5 and 9.5 for wild-type LOX and Y215 mutants. Steady state experiments for Y215F mutant highlighted that k_{cat} and $k_{\text{cat}}/K_{\text{M}}$ were deteriorated by a factor of 2 at pH 5.5 in comparison to pH 6.5. Pre-steady state rates reveal that k_5 is 5 times lower than k_3 at pH 6.5. At pH 5.5 k_3 and k_5 differ by a factor of 7, but in general both rates are reduced compared to pH 6.5, which correlates with findings from the steady state. In contrast, we could only detect biphasic changes in absorbance at pH 5.5 and pH 9.5 for Y215H mutant. Best fits at pH 9.5 for Y215H mutant revealed that both the k_3 and $k_{\text{red}2}$ are changed by a factor of approximately 8 and 2 compared to Y215F mutant. In a nutshell, substitution of Y215 into Phe mainly yielded a k_5 to be much lower than k_3 , whereas mutation of

Y215 into His resulted in a decreased k_3 and k_5 (compare **Table S2**) Above all, the stopped flow results correlate with the diminished activities observed in steady state experiments. Additionally, we could not detect a noticeable change in the reductive half-reaction at pH 9.5 compared to pH 6.5. To this end we also investigated the oxidative half-reaction (**Table S2**) at pH 9.5. Wild-type LOX shows a k_{ox} of 6.0×10^5 , 33.3% of LOX at pH 6.5. This difference does not explain at all the low k_{cat} at pH 9.5.



Scheme 2: Minimalistic reaction mechanism of LOX Y215F mutant, whereas k_{red} of LOX wild-type includes the steps k_3 and k_5

DISCUSSION

Amino acid residue from Tyr-215 has been the main focus within this work. Crystal structures evidenced that Tyr-215 and Tyr-146 form strong H-bonds with the α -hydroxy function of pyruvate in LOX. Whereas Tyr-146 is strictly conserved within the alpha-hydroxy acid oxidizing family, which adopts a similar position and orientation in all structures, the residue Tyr-215, which is part of loop 4, is in a unique position in LOX (**13**). This loop has been proposed to play a prominent role for substrate binding as flexible region found in GOX, FCB2, MDH and LCHAO (**26-29**). For instance, loop 4 has been reported to influence the activity of LCHAO by possible interactions with the active site (**29**).

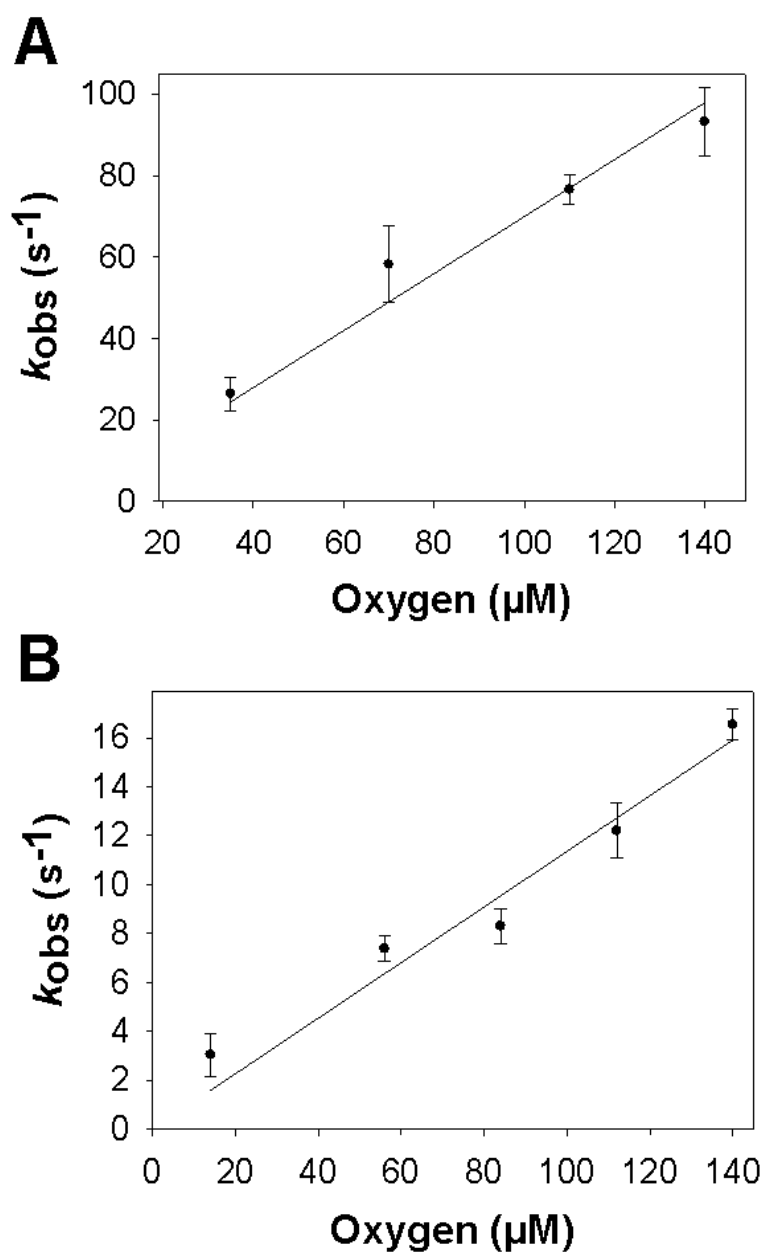


Figure 9

Re-oxidation of reduced LOX mutants Y215F (Panel A) and Y215H (Panel B) with molecular oxygen in 50 mM potassium phosphate buffer at pH 6.5 (20 °C). Enzyme (10 μM after mixing) was reduced anaerobically by titrating with two equivalents of L-lactate. The reduced enzyme was mixed with aerobic buffer containing various concentrations of molecular oxygen (35, 70, 112, 126 and 140 μM) at pH 6.5, and the re-oxidation was monitored spectrophotometrically at 455 nm in a single exponential manner. The observed rate constants varied linearly with O_2 concentration, suggesting a bimolecular reaction with a rate constant of $7.0 \times 10^5 \text{ M}^{-1} \text{ s}^{-1}$ for Y215F and $1.0 \times 10^5 \text{ M}^{-1}$ for Y215H.

Substitution of Tyr-215 by Phe and His led to decreased kinetic parameters of the enzyme. Especially the missing hydroxyl group in Y215F and Y215H lowers k_{cat} for lactate, which evidences the involvement of the Tyr-215 residue in stabilization processes in the active site in the wild-type. Furthermore, the low activity of Y215H mutant possibly derives from the change in steric properties in the active site compared to the wild-type. Considering the mutants not being inactive illustrates that Tyr-215 is not directly involved in substrate conversion. Kinetic data for other L- α -hydroxy acids showed that Tyr-215 mutants don't alter substrate specificity.

In literature, several methods are mentioned (23) to find out more about the mechanism of L- α -hydroxy acids and the involvement of active site residues. One of these opportunities was conducted, namely pH studies. Kinetic data at different pH values for Y215F mutant and the wild-type were compared. There is a slight difference between the pK values of the mutant and the wild-type in the basic range. This could bring out that the residue at position 215 in the enzyme influences active site residues, which are involved in substrate binding or conversion. Probably the residue itself is not involved in protonation or deprotonation of the substrate or the cofactor FMN. The lowered pK_2 in Y215F might result from the mutation. Tyr has a pK of 10 and might influence the pK values of other active site residues. In Y215F mutant tyrosine is replaced by phenylalanine and therefore the pK value of the enzyme is changed due to the missing influence of the tyrosine.

There is no remarkable change of the pK in the acid range of the profile for the mutant compared to the wild-type. pK_1 in Y215F and the wild-type is approximately 6. The crucial residue might be His-265.

Substrate inhibition could be observed in the wild-type as well as in Y215F at different pH values. Apart from pH 5.0 and pH 9.0, substrate inhibition is observed in Y215F mutant at every determined pH value. The mentioned exceptions could result either from measuring and sampling inaccuracy or it could describe the phenomenon that at pH 5.0 and pH 9.0 no second substrate binding site, which further leads to substrate inhibition, is found. As substrate inhibition at pH 9.0 is observed in the wild-type, it can be assumed that phenylalanine avoids substrate inhibition in Y215F at pH 9.0. In the wild-type substrate inhibition occurs in the basic range from pH 9.0 to pH 10.0. This might result from deprotonation of the tyrosine, which would mean that Tyr-215 has a pK lower than 9.0. That would coincide with the assumption made above based on the pH studies, where Tyr-215 influences the pK of the enzyme in the basic range.

Spectral scans at pH 5.5, 6.5 and 9.5 revealed the typical reduced FMN spectrum, where FMN_{red} lacks both absorbance maxima at 373 and 455 nm. Remarkably, the conversion from the oxidized into the reduced FMN was identified in a biphasic manner. Besides a second exponential decay with a fast start and a slow phase at A_{455nm} we observed the formation and the decay of an intermediate at A_{530nm} , which was previously described for wild-type LOX at temperatures below 5 °C (1) - to identify the formation of the intermediate for LOX wild-type we repeated the stopped flow experiment at 4 °C. Fitting and simulation of both traces were performed with software Pro-DataViewer (version 4.2.0) and Berkeley Madonna (version 8.3.18). Studies by Massey and Co-workers mainly identified an intermediate of LOX mutants at temperatures below 4 °C. In short, the 3 ms dead-time of the stopped flow instrument at higher temperatures was the virtual reason, which hindered the detection of the intermediate step. Consequently, we could only

detect a decrease of the intermediate with our wild-type LOX at 20 °C. However, Y215F mutant highlights another different behavior compared to wild-type during the reductive half-reaction. As previously described for another active site mutant at room temperature (30), Y215F mutant represented biphasic kinetic patterns, which were observed in pre-steady state experiments. Here, the fastest phase of reduction was associated with the major amplitude changes at 455 nm and 530 nm. Thus, the first and also faster phase of $\Delta A_{455\text{nm}}$ correlates with an increase at $A_{530\text{nm}}$ and the second phase of $\Delta A_{455\text{nm}}$ is very much alike the decrease of $A_{530\text{nm}}$. To this end, we were able to split the reductive half-reaction into two rates - the first is responsible for the formation (k_{red1} or k_3) and the second one for the decrease (k_{red2} or k_5) of the intermediate. As a consequence, the second phase is the rate limiting step of the whole reaction and can therefore be compared with the corresponding k_{cat} . In conclusion, k_{red1} is either equal or faster than k_{red2} , though shifting the temperature below 5 °C (demonstrated in this study for wild-type and in former publications for LOX WT and A95G mutant) results in decreased k_{red2} values. On the other hand, Y215H mutant inimitably indicated a lower k_{red} (possibly caused by the shift in pH). Results of both Tyrosine mutants are consistent with a modified ping-pong mechanism (displayed in **Scheme 2**) as illustrated for wild-type LOX (1, 2).

In conclusion, steady state and stopped flow analysis showed that the substitution of Tyr-215 into Phe has certain influences on the intermediate step in catalysis. Substrate inhibition possibly derives from a low K_M (and K_d). We propose that the affinity to pyruvate is changed and causes the slow rates of k_5 . In wild-type LOX and Y215H we were not able to detect k_3 and k_5 , here the K_M is much higher compared to Y215F. A95G mutant for instance also features a strong affinity to pyruvate, in a previous work we compared k_3 and k_5 (determined at 4 °C) with the

wild-type. k_5 was lower than k_3 for the mutant, but k_3 was similar to k_5 for wild-type LOX. This would implement that the affinity to pyruvate mainly influences k_5 .

Description of the Fitting

The fitting of the traces of A_{455} and A_{530} was performed in two steps. First, since the only species absorbing at A_{530} is the complex EPyr, a normalized absorbance can be defined that could directly depend on the ratio of EPyr/Epyrmax (Epyrmax is the maximum concentration of Epyr reached during the reaction course). The experimental data for the intermediate (A_{530}) were normalized by dividing all data by the maximum value of the same data set. Normalized data were then fitted to a variable defined as R (=EPyr/maxEPyr plus Background). Different set of data were used for the fitting resulting in a calculated value for EPyrmax. Once EPyrmax was calculated, using the A_{530max} , the intrinsic absorbance of EPyr can be estimated. The consistency between different set of data was ensured, leading to a value of 2.7 μM with a S.D. of 0.2 μM for LOX Y215F mutant (when E= 4 μM).

This value was used to calculate the intrinsic absorbance (ϵ) for the formation of the intermediate by the formula $\epsilon = (A_{530max} - A_{530final}) / c_{EPyrmax}$ resulting in a value of 3100 M^{-1} . Data of A_{455} were fitted to the variable defined as $C = E + E_{Lac} + EPyr \cdot A1 + E_{red} \cdot A2$. A1 and A2 are the relative contributions of the species EPyr and Ered to the absorbance at 455 nm. [A1 (= $A_{455 tx} / A_{455 t0}$) is the ratio between the absorbance (455 nm) at the point in time (tx) where EPyrmax is reached and the absorbance (455 nm) at the start of the reaction (t0). A2 = $A_{455final} / A_{455 t0}$.] On the other hand, the absorbance data of A_{530} were fitted to the variable R (=EPyr* ϵ + $A_{530final}$).

REFERENCES

- 1 Maeda-Yorita K, Aki K, Sagai H, Misaki H, and Massey V (1995) L-lactate oxidase and L-lactate monooxygenase: mechanistic variations on a common structural theme. *Biochimie* **77**, 631-642.
- 2 Sun W, Williams CH Jr, Massey V (1997) The role of glycine 99 in L-lactate monooxygenase from *Mycobacterium smegmatis*. *The journal of biological chemistry* **272**: 27065-27076.
- 3 Müh U, Massey V, Williams CH Jr. (1994) Lactate monooxygenase. I. Expression of the mycobacterial gene in *Escherichia coli* and site-directed mutagenesis of lysine 266. *The journal of biological chemistry* **269**, 7982-7988.
- 4 Boubacar AK, Pethe S, Mahy JP, Lederer F (2007) Flavocytochrome b_2 : reactivity of its flavin with molecular oxygen. *Biochemistry* **46**, 13080-13088.
- 5 Stenberg K, Clausen T, Lindqvist Y, Macheroux P (1995) Involvement of Tyr24 and Trp108 in substrate binding and substrate specificity of glycolate oxidase. *European journal of biochemistry* **228**, 408-416.
- 6 Illias RM, Sinclair R, Robertson D, Neu A, Chapman SK, Reid GA (1998) L-mandelate dehydrogenase from *Rhodotorula graminis*: cloning, sequencing and kinetic characterization of the recombinant enzyme and its independently expressed flavin domain. *Biochemical journal* **333**, 107-115.
- 7 Chen ZW, Vignaud C, Jaafar A, Lévy B, Guéritte F, Guénard D, Lederer F, Mathews FS (2012) High resolution crystal structure of rat long chain hydroxy acid oxidase in complex with the inhibitor 4-carboxy-5-[(4-chlorophenyl)sulfonyl]-1, 2, 3-thiadiazole. Implications for inhibitor specificity and drug design. *Biochimie* **94**, 1172-1179.
- 8 Minagawa H, Nakayama N, Matsumoto T, and Ito N (1998) Development of long life lactate sensor using thermostable mutant lactate oxidase. *Biosensors and bioelectronics* **13**, 313-318.
- 9 Romero MR, Ahumada F, Garay F, and Baruzzi AM (2010) Amperometric biosensor for direct blood lactate detection. *Analytical chemistry* **82**, 5568-5572.
- 10 Wang J, and Chen Q (1994) Enzyme microelectrode array strips for glucose and lactate. *Analytical chemistry* **66**, 1007-1011.
- 11 Frebel H, Chemnitiuss GC, Cammann K, Kakerow R, Rospert M and Mokwa W (1997) Multianalyte sensor for the simultaneous determination of glucose, L-lactate and uric acid based on microelectrode array. *Sensors and Actuators B. Chemical* **43**, 87-93.
- 12 Leiros I, Wang E, Rasmussen T, Oksanen, E, Repo, H, Petersen SB, Heikinheimo P, Hough E (2006) The 2.1 Å structure of *Aerococcus viridans* L-lactate oxidase (LOX). *Acta crystallographic sector F structural biology and crystallization communications* **62**, 1185-90.
- 13 Li SJ, Umena Y, Yorita K, Matsuoka T, Kita A, Fukui K, Morimoto Y (2007) Crystallographic study on the interaction of L-lactate oxidase with pyruvate at 1.9 Å resolution. *Biochemical and Biophysical Research Communications* **358**, 1002-1007.
- 14 Umena Y, Yorita K, Matsuoka T, Kita, A, Fukui, K, Morimoto Y (2006) The crystal structure of L-lactate oxidase from *Aerococcus viridans* at 2.1 Å resolution reveals the mechanism of strict substrate recognition. *Biochemical and Biophysical Research Communications* **350**, 249-256.
- 15 Furuichi M, Suzuki N, Dhakshnamoorthy B, Minagawa H, Yamagishi R, Watanabe Y, Goto Y, Kaneko H, Yoshida Y, Yagi H, Waga I, Kumar PK, Mizuno H (2008) X-ray structures of *Aerococcus viridans* lactate oxidase and its complex with D-lactate at pH 4.5 show an alpha-hydroxyacid oxidation mechanism. *Journal of molecular biology* **378**, 436-446.
- 16 Yorita K, Misaki H, Palfey BA, Massey V (2000) On the interpretation of quantitative structure-function activity relationship data for lactate oxidase. *Proceedings of the National Academy of Sciences of the United States of America* **97**, 2480-2485.
- 17 Yorita K, Aki K, Ohkuma-Soyejima T, Kokubo T, Misaki H, Massey V (1996) Conversion of L-lactate oxidase to a long chain alpha-hydroxyacid oxidase by site-directed mutagenesis of alanine 95 to glycine. *The journal of biological chemistry* **271**, 28300-28305.

- 18 Lockridge, O., Massey, V., Sullivan PA. (1972) Mechanism of action of the flavoenzyme lactate oxidase. *The journal of biological chemistry* **247**, 8097-8106.
- 19 Bisswanger, H. 2002. Substrate inhibition. *Enzyme kinetics - principles and methods*. Weinheim: Wiley-VCH Verlag GmbH, 2002, pp. 120-121.
- 20 Greene D, Das B and Fricker LD (1992) Regulation of carboxypeptidase. Effect of pH, temperature and Co^{2+} on kinetic parameters of substrate hydrolysis. *Biochemical journal* **285**, 613-618.
- 21 Schwarz A, Brecker L and Nidetzky B (2007) Acid base catalysis in *Leuconostoc mesenteroides* sucrose phosphorylase probed by site-directed mutagenesis and detailed kinetic comparison of wild-type and Glu237 --> Gln mutant enzymes. *Biochemical journal* **403**, 441-449.
- 22 Klimacek M and Nidetzky B (2010) The oxyanion hole of *Pseudomonas fluorescens* mannitol 2-dehydrogenase: a novel structural motif of electrostatic stabilization in alcohol dehydrogenase active sites. *Biochemical journal* **425**, 455-463.
- 23 Sobrado P, Fitzpatrick PF (2003) Solvent and primary deuterium isotope effects show that lactate CH and OH bond cleavages are concerted in Y254F flavocytochrome b_2 , consistent with a hydride transfer mechanism. *Biochemistry* **42**, 15208-15214.
- 24 Dubois J, Chapman SK, Mathews FS, Reid GA and Lederer F (1990) Substitution of Tyr 254 with Phe at the active site of flavocytochrome b_2 : consequences on catalysis of lactate dehydrogenation. *Biochemistry* **29**, 6393-6400.
- 25 Cleland WW (1982) The use of pH studies to determine chemical mechanisms of enzyme-catalyzed reactions. *Methods in enzymology* **87**, 390-405.
- 26 Lindqvist Y (1989) Refined structure of spinach glycolate oxidase at 2 Å resolution. *Journal of molecular biology* **209**, 151-166.
- 27 Sukumar N, Xu Y, Gatti DL, Mitra B & Mathews FS (2001) Structure of an active soluble mutant of the membrane-associated (S)-mandelate dehydrogenase. *Biochemistry* **40**, 9870-9878.
- 28 Tegoni M, Begotti S, Cambillau C (1995) X-ray structure of two complexes of the Y143F flavocytochrome b_2 mutant crystallized in the presence of lactate or phenyl lactate. *Biochemistry* **34**, 9840-9850.
- 29 Belmouden, A. & Lederer, F (1996) The role of a p barrel loop 4 extension in modulating the physical and functional properties of long-chain 2-hydroxy-acid oxidase isozymes. *European journal of biochemistry* **238**, 790-798.
- 30 Yorita K, Matsuoka T, Misaki H, Massey V (2000) Interaction of two arginine residues in lactate oxidase with the enzyme flavin: conversion of FMN to 8-formyl-FMN. *Proceedings of the National Academy of Sciences of the United States of America* **97**, 13039-13044.

SUPPORTING INFORMATION

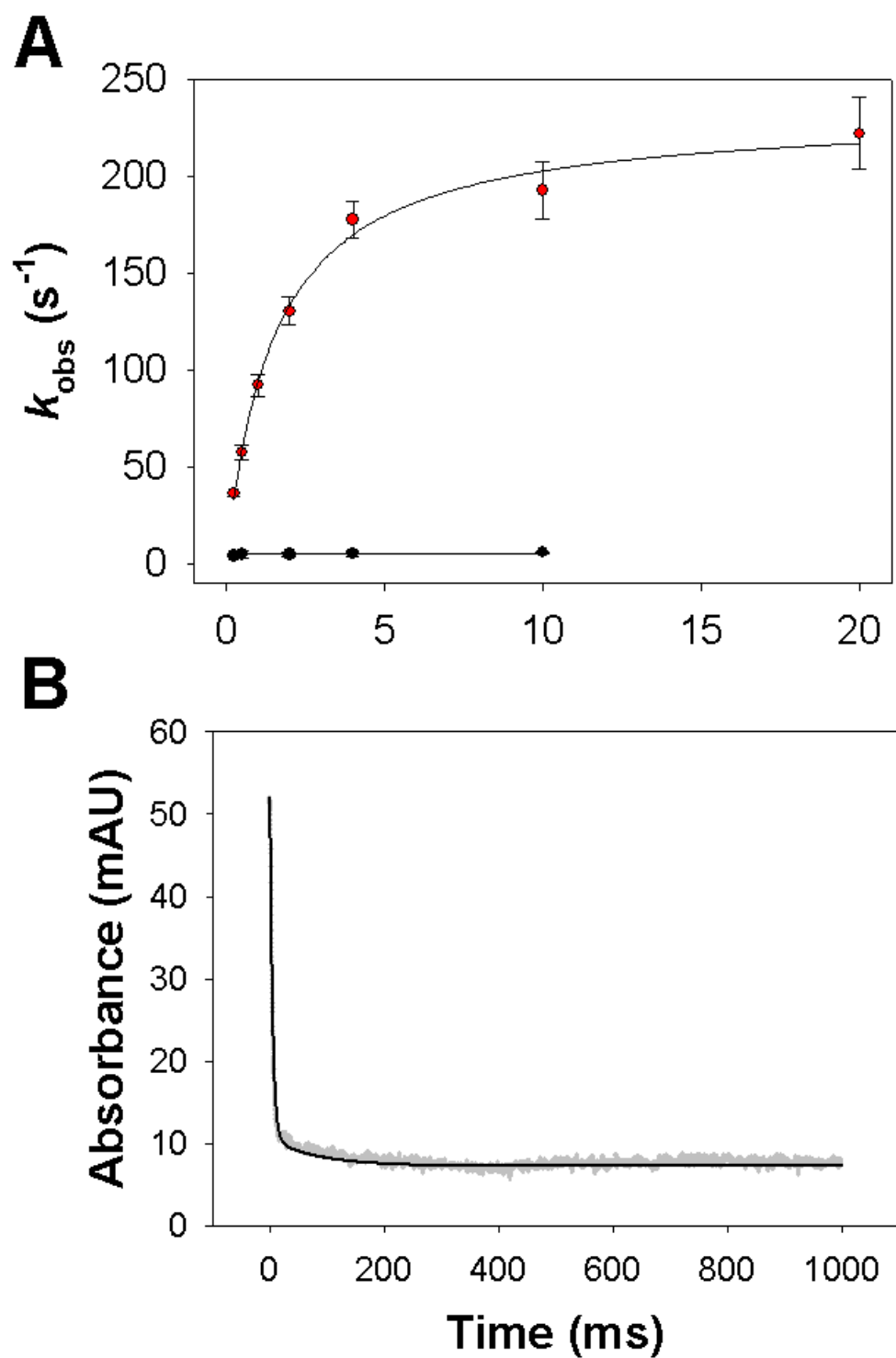


Figure S1

Determination of the reduction rate constants (k_{red1} , k_{red2}) and dissociation constants (K_{d1} , K_{d2}) for the reaction of wild-type LOX at pH 9.5 with L-lactate at 20 °C.

Panel **A**: The reductive half is split into two phases (description in text) expressed in $k_{\text{obs}1}$ and $k_{\text{obs}2}$ values, which lead to $k_{\text{red}1}$ and $k_{\text{red}2}$. **Red** dots indicate $k_{\text{obs}1}$ values, **black** dots illustrate $k_{\text{obs}2}$ values.

$k_{\text{red}1} = 233.4 \pm 6.2 \text{ s}^{-1}$ and $K_{\text{d}1} = 1.5 \pm 0.1 \text{ mM}$, $k_{\text{red}2} = 5.3 \pm 0.2 \text{ s}^{-1}$ and $K_{\text{d}2} = 0.1 \pm 0.03 \text{ mM}$.

Panel **B**: Reductive half-reaction of LOX by L-lactate. 4.5 μM wild-type LOX in 50 mM potassium phosphate buffer (pH 6.5) were reacted in the stopped flow photometer at 20 °C with 10 mM L-lactate. The reaction trace is shown at 455 nm with two different phases fitted in a double exponential manner, where the first phase ($k_{\text{obs}1} = 193 \text{ s}^{-1}$) is faster than the second phase ($k_{\text{obs}2} = 5.0 \text{ s}^{-1}$).

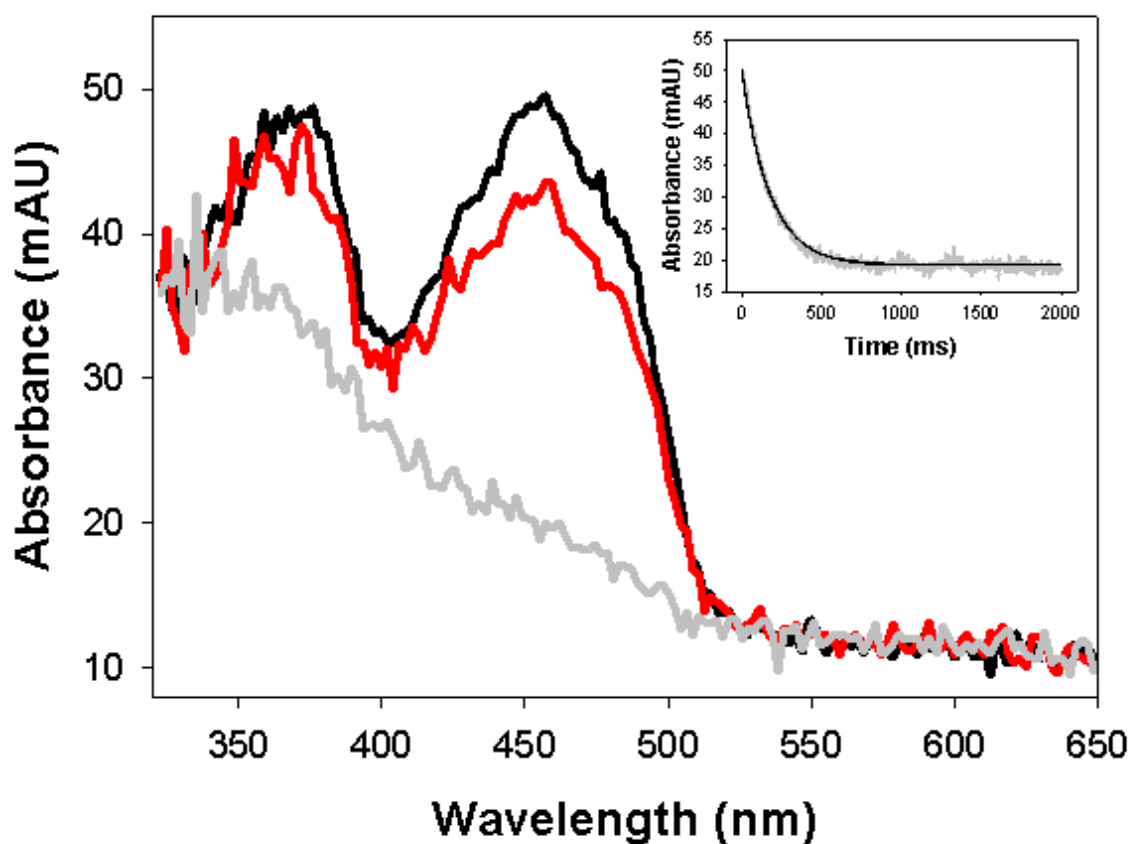


Figure S2

Spectral scans of LOX Y215H mutant during the reductive half-reaction.

4.3 μM LOX were reduced with 10 mM L-lactate under anaerobic conditions in 50 mM potassium phosphate buffer, pH 6.5 at 20 °C. **Black** line: enzyme in oxidized state at start (0 ms); **red** line: reaction after 20 ms; light **grey** line: reaction after 500 ms. No change in absorbance at 530 nm could be observed. Inset shows trace at 455 nm which was fitted in a single exponential manner as described in the text ($k_{\text{obs}} = 8 \text{ s}^{-1}$).

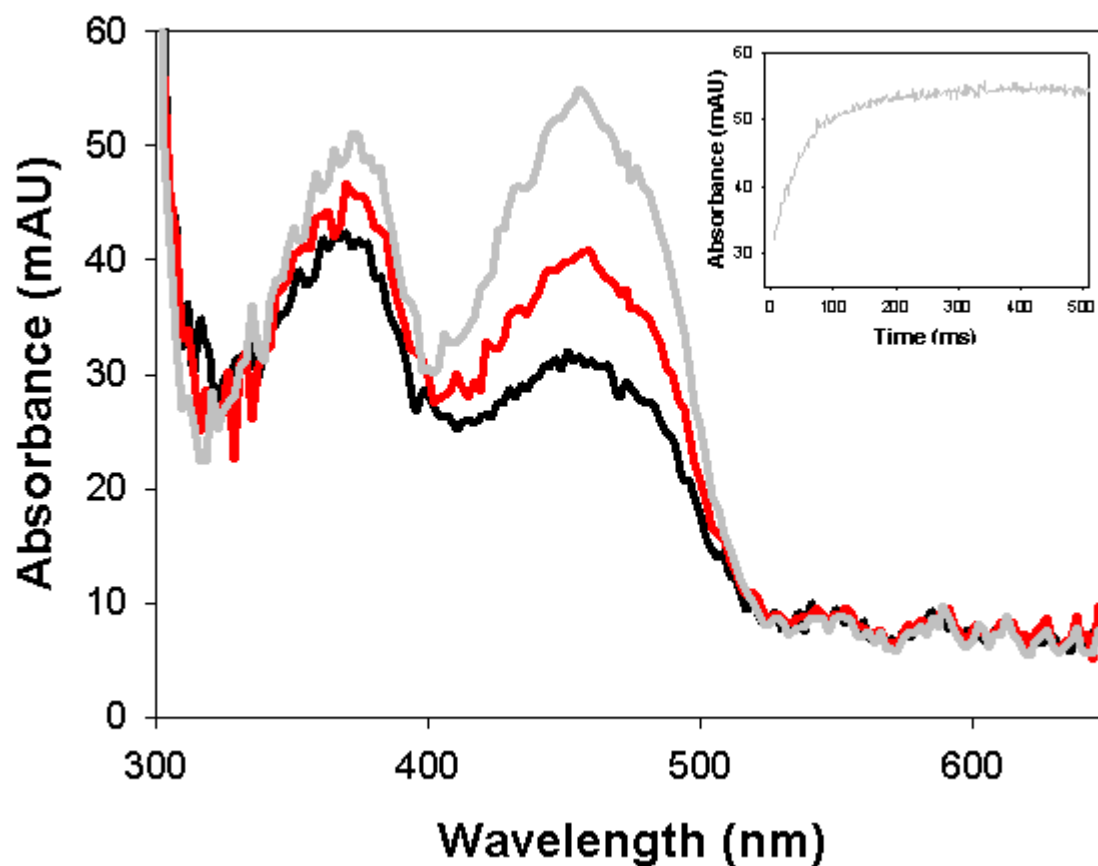


Figure S3

Spectral scans of LOX Y215H mutant during the oxidative half-reaction.

5.3 μM LOX were reduced with 2 equivalent L-lactate under anaerobic conditions in 50 mM potassium phosphate buffer, pH 6.5 at 20 $^{\circ}\text{C}$ and reoxidized with 140 μM oxygen. **Black** line: enzyme in reduced state after 3 ms; **red** line: reaction after 35 ms; light **grey** line: reaction after 300 ms. Inset shows trace at 455 nm which was fitted in a single exponential manner as described in text ($k_{\text{obs}1} = 14.5 \text{ s}^{-1}$).

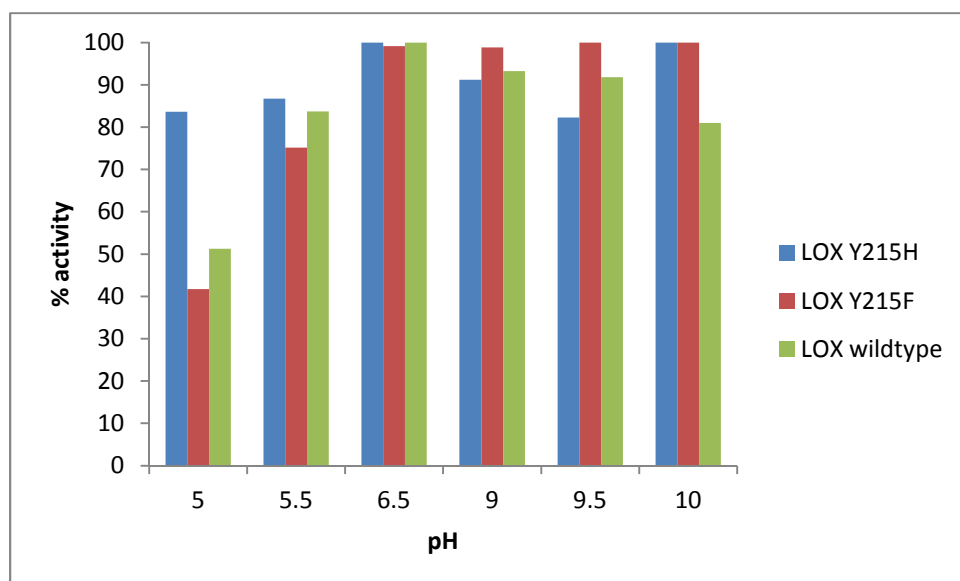


Figure S4

Stability of LOX at different pH values.

All enzymes were incubated at pH 5 to 10 and the activity with substrate was determined at pH 6.5.

Very often a loss of stability can falsify a pH profile. Therefore we adapted the coupled peroxidase assay by a single alteration. **Figure S1** illustrates the results of the control experiment where the stability of LOX (wild-type, Y215F and Y215H) was determined at various pH values. Each enzyme was incubated for 10 minutes at a certain pH (ranging from 5.0 to 10.0 in steps of 0.5) and the reaction with L-lactate was measured afterwards instantly at 37 °C for 5 to 10 minutes with the peroxidase coupled assay in a reaction mixture (containing solutions described in METHODS plus 50 mM L-lactate) at pH 6.5 (final concentration of enzyme 5-10 nm L⁻¹). Activities were then normalized to the highest activity (REMARK: not always at pH 6.5) and are given in '% activity'. Y215H mutant is the only protein among the chosen ones which stays stable at all selected pH-values and hardly loses its activity. Wild-type LOX and Y215F mutant remain their activity in the pH range from 5.5 to 10.0 (between 80 and 100 percent). On the other hand, they lose more than 50 % of their activity at pH 5.0; this pH value is missing for further pH studies. Furthermore, the stability of peroxidase was checked at pH 5.5 and pH 10.0 (same procedure as mentioned for LOX - peroxidase was incubated at different pH values (50 mM potassium phosphate buffer), and

activity of LOX wild-type was measured at pH 6.5 afterwards for 10 minutes), but in comparison to pH 6.5 no significant changes were observed, indicating that the coupled enzyme assay is also stable between pH 5.5 and 10.0. For this reason the pH-studies were conducted between pH 5.5 and 10.

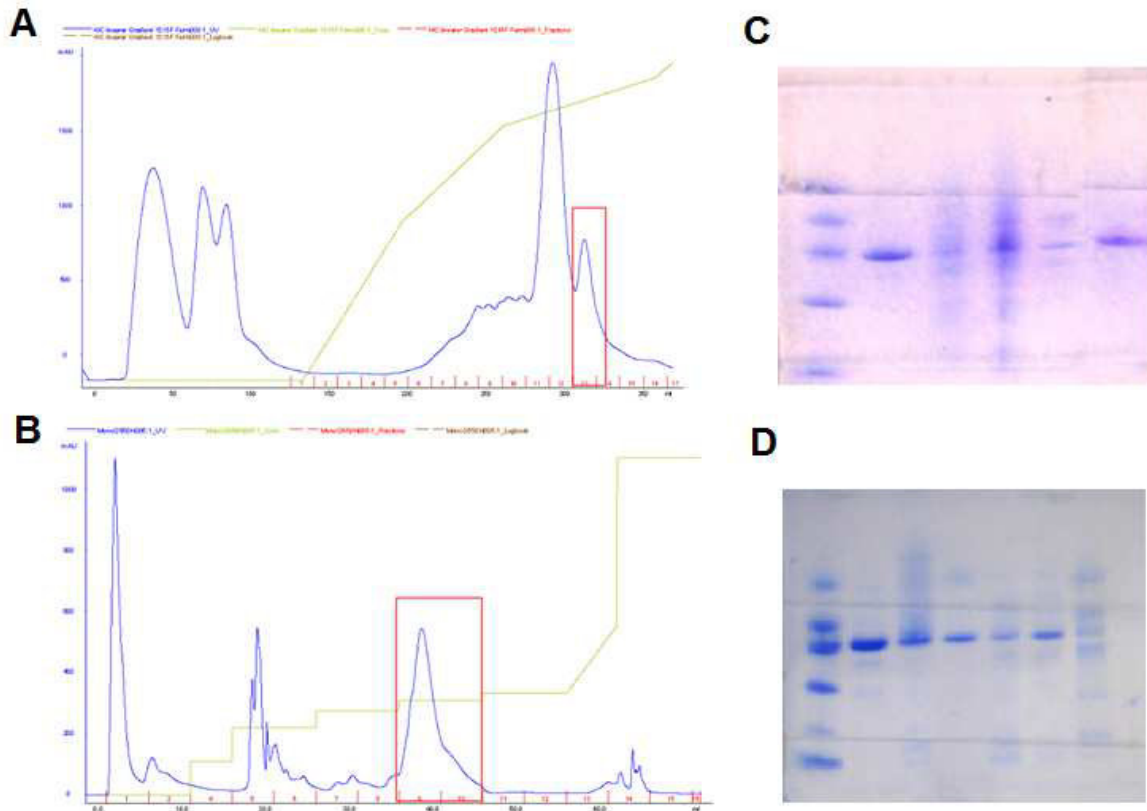


Figure S5

Purification of LOX Y215F mutant

Panel A: HIC purification with linear gradient of Y215F mutant, enzyme was found in the highlighted peak

Panel B: AEC purification run with stepwise gradient of Y215F mutant, LOX mutant was found in the highlighted fractions 9 and 10

Panel C: SDS Page of purified LOX wild-type and Y215F mutant; *lane 1:* low molecular weight marker, *lane 2:* LOX wild-type, *lane 3:* crude extract of Y215F (expressed in flasks), *lane 4:* after (NH₄)₂SO₄ precipitation of Y215F (expressed in flasks), *lane 5:* after HIC purification of Y215F (expressed in flasks), *lane 6:* after HIC purification of Y215F (expressed in fermenter)

Panel D: Purification of Y215H mutant documented by SDS-PAGE, highlighted lanes were used for further processing (from left to right: *lane 1*: low molecular weight marker, *lane 2*: WT, *lane 3 and 4*: Y215H after AEC, *lane 5-7*: Y215H after HIC)

Table S1. Purification of L-lactate oxidase mutants

LOX	Procedure	Specific activity (U/mg)	Recovery [%]
Y215F	Crude extract	0.30	100
	(NH ₄) ₂ SO ₄ precipitation	0.74	88
	HIC	30.1	43
	AEC	75.6	9
Y215H	Crude extract	0.25	100
	(NH ₄) ₂ SO ₄ precipitation	0.68	89
	HIC	1.77	42
	AEC	13.4	10

Table S2. List of kinetic rate constants and characteristics of FMN for wild-type LOX, Y215F and Y215H mutants with L-lactic acid as substrate determined at 20 °C including pre-steady and steady states experiments

	Wild-type LOX			Y215F			Y215H		
	pH 6.5	pH 5.5	pH 9.5	pH 6.5	pH 5.5	pH 9.5	pH 6.5	pH 5.5	pH 9.5
Pre-steady state									
k_{red} (s ⁻¹)	270	171	-	-	-	-	8.2	7.2	8.7
k_{red1} (s ⁻¹)			233	124	61.8	85.1		-	-
k_{red2} (s ⁻¹)			5.3	20.3	12	20		-	-
K_d (mM)	1	2.96	-	-	n.d.	n.d.	0.55	2.3	0.2
K_{d1} (mM)	-	-	1.5	0.28					
K_{d2} (mM)	-	-	0.1	0.06					
k_{red}/K_d	2.7×10^2	57.6	-	-	-	-	16.4		
k_{ox} (M ⁻¹ s ⁻¹)	1.8×10^6	1.1×10^6	6.0×10^5	7.0×10^5			1.0×10^5		
reduced FMN [%]	90	>95	>99	>95	75-80	>99	>99	90	90
re-oxidized FMN [%]	90	90	90	90	90	90	90	90	90
$\Delta A_{530\ 1}$ (s ⁻¹) *	n.v.	n.v.	n.v.	1.5×10^2	1.1×10^2	1.6×10^2	n.v.	-	27.8
$\Delta A_{530\ 2}$ (s ⁻¹) **	1.3×10^2	1.9×10^2	1.9×10^2	17.2	12.4	18.1	n.v.	4.5	10.3
Steady state									
k_{cat} (s ⁻¹)	87.5	36.6	4.1	22	11	0.03	5	3.8	0.5
K_M (mM)	0.5	13.1	0.7	0.13	0.1	5.5	0.5	6.3	3.4
k_{cat}/K_M (mM ⁻¹ s ⁻¹)	1.8×10^2	2.8	5.9	1.7×10^2	1.1×10^2	5×10^{-3}	10	0.6	0.1
Calculation									
k_{ox} 200μM (s ⁻¹)	3.6×10^2	2.2×10^2	1.2×10^2	1.4×10^2			22		
k_{cat} calc (s ⁻¹)	154	96.1	5.0	17.5			6.0		
k_{cat} calc : k_{cat}	1.8 : 1	3 : 1	1.2 : 1	0.9 : 1			1.3 : 1		

n.d. not determined, **n.v.** not visible

$\Delta A_{530\ 1}$ describes an increase in absorbance, $\Delta A_{530\ 2}$ a decrease in absorbance

* Rates derive from linear fitting, conditions: 10 mM L-lactate

** Rates from single exponential fitting (as 455 nm trace) with A_{530nm} as start (conditions: 10 mM L-lactate)

5 Clarifying the influence of a hydrogen bond network on the substrate binding in the active site of *Aerococcus viridans* L-lactate oxidase by substitution of residue Tyr 191

Thomas Stoisser[†], Stefan Leitgeb[†], David K. Wilson[‡], and Bernd Nidetzky^{†*}

[†] Research Center Pharmaceutical Engineering, and Institute of Biotechnology and Biochemical Engineering, Graz University of Technology, Petersgasse 12, A-8010 Graz, Austria

[‡] Department of Molecular and Cellular Biology, University of California, One Shields Avenue, Davis, CA 95616

* Corresponding author

Institute of Biotechnology and Biochemical Engineering, Graz University of Technology, Petersgasse 12, A-8010 Graz, Austria

Telephone: +43-316-873-8400; fax: +43-316-873-8434; e-mail:

bernd.nidetzky@tugraz.at

ABBREVIATIONS

BSA: bovine serum albumin, DAO: D-amino acid oxidase, FCB2: flavocytochrome *b*₂, FMN: flavomononucleotide, FPLC: fast protein liquid chromatography, GOD: glucose oxidase, GOX: glycolate oxidase, HIC: hydrophobic interaction chromatography, LCHAO: long chain hydroxy acid oxidase, LMO: L-lactate monooxygenase, LOX: L-lactate oxidase, MDH: L-mandelate dehydrogenase, PDB: protein data base, WT: wild-type.

ABSTRACT

L-lactate oxidase (LOX) from *Aerococcus viridans* catalyzes the oxidation of L-lactate to pyruvate and is a family member of 2-hydroxy acid-dependent flavoenzymes. Crystal structures of LOX have illustrated that Tyr-191 is located close to the substrate binding site. Its hydroxyl group is able to form a hydrogen bond to the active site residue Tyr-40, which is essential for the substrate binding. The role of Tyr-191 in the catalytic cycle of LOX has been investigated by replacing the residue with phenylalanine, leucine and alanine. To elucidate the function of the mutants in substrate binding and catalysis steady state and rapid reaction measurements have been carried out. LOX Y191F mutant showed 8- to 10-fold decrease in K_M and K_D with L-lactate, whereas for Y191L and Y191A mutants the K_M was similar or 20-fold higher, respectively, in comparison to wild-type LOX. However, the turnover number was decreased more than 1 order of magnitude for Y191A and Y191L mutants. On the other hand, Y191F mutant showed an increased catalytic efficiency mainly derived from the low K_M value. Moreover, stopped flow analysis evidenced that the rate of reduction and re-oxidation were affected by the deletion of the hydroxyl group. These findings suggest that the hydrogen bond between Tyr-40 and Tyr-191 is involved in substrate binding.

INTRODUCTION

The flavoprotein L-lactate oxidase (LOX) from *Aerococcus viridans* catalyzes the oxidation of L-lactate into pyruvate with H_2O_2 as a by-product (1). Besides many applications, LOX is mainly used in biosensors for the determination of L-lactate levels in medical and food analytics (2-5). These biosensors potentiometrically detect hydrogen peroxide.

LOX is a member of in total six α -hydroxy oxidizing enzymes whose active site consists of six conserved amino acid residues (1). Those enzymes are L-lactate monooxygenase (LMO) from *Mycobacterium smegmatis* (1, 5, 6) flavocytochrome b_2 (FCB2) from Baker's yeast (7), spinach glycolate oxidase (GOX) (8), L-mandelate dehydrogenase (MDH) from *Rhodotorula graminis* (9) and a long chain α -hydroxy acid oxidase from rat kidney (LCHAO) (10). One single exception is a tyrosine residue (Tyr-40) that is a phenylalanine in the case of LCHAO.

Within the last decade the crystal structure was solved (11-14), and a large set of active site mutants has been generated to gain a better understanding of the reaction mechanism (15-17). Its non-covalently bound FMN (flavomonocucleotide) plays a key role in catalysis and provides the enzyme its typical spectral properties in the UV-Vis region, e.g. during the oxidative and reductive half-reaction of LOX the cofactor is reduced or oxidized again concomitantly changing the absorbance spectrum of the enzyme completely. The interaction between FMN and the corresponding substrate and adjacent conserved amino acid residues in the active site are responsible for the substrate specificity and the reaction mechanism in α -hydroxy oxidizing enzymes (13).

Due to the proximity of the α -carbon of the pyruvate (3.13 Å) to the N5 atom of FMN, two mechanisms are discussed in literature. The mechanism could either be described by a hydride transfer or an alternative way, which involves the abstraction of a proton from the substrate α -carbon by the catalytic base to form a carbanion and the subsequent transfer of two electrons to the FMN cofactor (**11**). In general the reaction can be described as a ping-pong mechanism similar to the one of glucose oxidase (**8**). However, other flavoproteins like LMO from *Mycobacterium smegmatis* (**1**, **18**), vanilyl-alcohol oxidase from *Penicillium simplicissimum* (**19**) or cytokinin dehydrogenase (**20**) follow a ternary complex mechanism. In this ternary complex mechanism an electron acceptor (e.g. dioxygen) reacts with the enzyme-product complex, whereas in the ping-pong mechanism product is released prior to the reaction of the electron acceptor with the enzyme (**1**). Both, LOX and LMO oxidize L-lactate, but generate different products due to the fact that the dissociation constants of the ternary complex are significantly altered (compare **Scheme 1**).

Several amino acid residues in the active site were identified to play an auxiliary role in substrate binding and catalysis. Based on a crystal structure the carboxylate group of the pyruvate molecule interacts with amino acid residues Tyr-40, Arg-181, His-265 and Arg-268, whereas its keto-oxygen atom interacts with Tyr-146, Tyr-215 and His-265 (**12**). LOX is not only specific for L-lactate as the substrate; it was also shown to react with other L- α -hydroxy acids as well (**17**). Indeed, a previously published work describes enhanced substrate specificity for LOX generated by the substitution of Ala-95 into Gly, which is in the vicinity of the isoalloxazine ring and enlarges the active site (**17**).

Recently, the crystal structures of LOX at pH 8.0 (PDB code 2DU2) and its complex with pyruvate at the same pH (PDB code 2E77) have been solved at 2.1 Å

and 1.9 Å resolution, respectively (11). **Figure 1** shows an overlay of the active site of both structures. Of particular interest for this work is the conserved Tyr-40 residue (which has been found to bind to the carboxylate group of the substrate), though the residue is replaced by a phenylalanine in LCHAO (12). In LCHAO the Phe-23 was

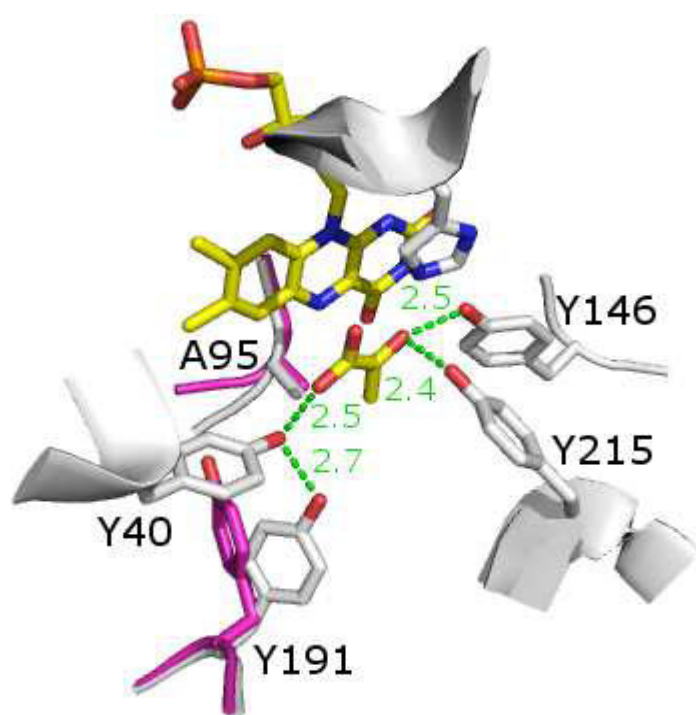


Figure 1

Active site of wild-type LOX

Overlay of wild-type LOX structures 2E77 and 2DU2. Residues in pink are different between the two structures and derive from 2DU2

altered by site-directed mutagenesis into Tyr and led to a ~10-fold reduced turnover for substrate mandelate in the mutant variant compared to the wild-type enzyme. On the other hand, the K_M was also 10-fold lower, so the k_{cat}/K_M was uninfluenced by the mutation (21). Mutation in GOX (Y24F) highlighted higher K_M values, but almost similar substrate specificities, e.g. a 10-fold higher K_M for glycolate with a 3-fold decrease in k_{cat} . As the rate of reduction of the flavin cofactor was hardly altered by

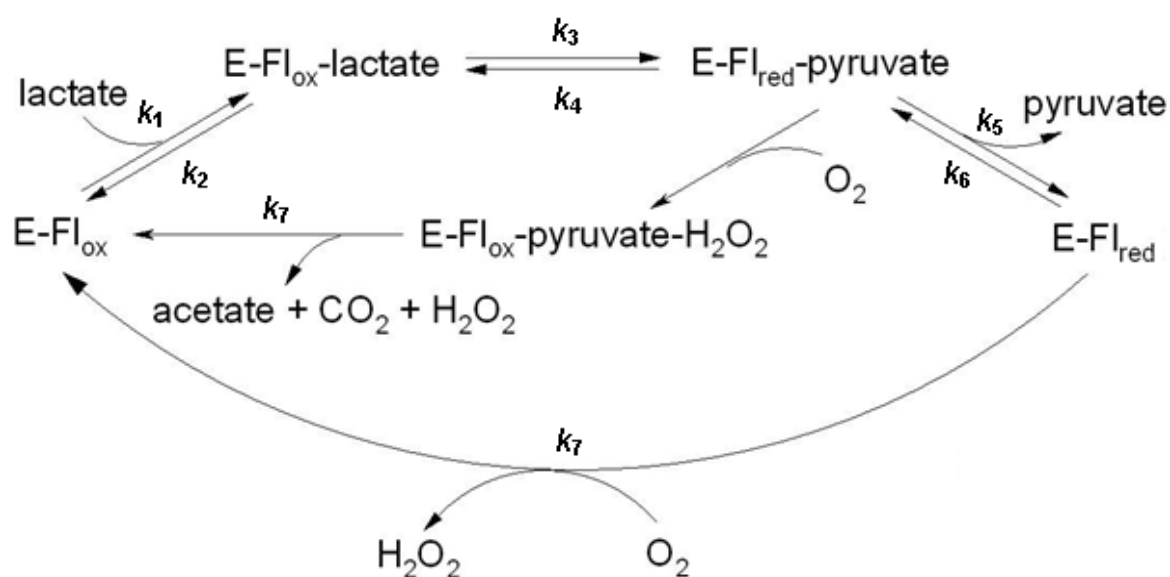
the mutation the main purpose of the tyrosine has been appointed to substrate binding and not to a catalytic step (8). The results obtained for the Y24F mutant are in full accordance with mutant enzymes from FCB2 (Y143F) and LMO (Y44F). Tyr-143 stabilizes the enzyme-substrate complex by forming a hydrogen bond to a substrate carboxylate, though the transition state was not stabilized by the residue (22). Furthermore, the LMO Y44F mutant represented a ~1000-fold reduction of k_{cat} and a ~50-fold lower K_M value for lactate. Interestingly, it was also proven that a significant amount of H_2O_2 was produced leading to the assumption that part of the reaction proceeds via the LOX-pathway (23).

Interestingly, the structure of PDB:2E77 reveals the side chain of Tyr-191 to be hydrogen bonded to the conserved Tyr-40 (2.7 Å), which, as described before, is crucial for substrate binding in the active site (12). However, the structure, which is lacking the product, indicates Tyr-191 to be flexible, as here it can either be close to Tyr-40 (equal to 2E77) or be flipped away (highlighted in pink) increasing the distance between Tyr-40 and Tyr-191 (~5 Å). Another effect worth mentioning is the neighboring region around the conserved Ala-95. Ala-95 (and Ala-96) is positioned on loop 4. This loop has been proposed to play a prominent role for substrate binding as flexible region found in GOX, FCB2, MDH and LCHAO (24-27). For instance, loop 4 has been reported to influence the activity of LCHAO by possible interactions with the active site (27). For LOX, residue Ala-96 (not conserved) is also flexible and very likely the conformational change of loop 4 influences the vicinity of residue Tyr-191.

From these results it would appear that Tyr-191 might play an important role in substrate binding as well. As already mentioned Tyr-40 is well known from previous publications for being involved in substrate binding and shows a distance of about 2.5 Å to pyruvate (12). LMO (Tyr-44) for instance is lacking an additional hydrogen

bond as the correspondent residue from Tyr-191 is Phe (based on a modelling where we overlaid the structure of LOX and LMO - compare **Figure S1**).

We hypothesize that the difference in the hydrogen network around Tyr-40 could play an important role for the differing reaction mechanisms. A sequence alignment assured Tyr-191 to be unique within the α -hydroxy acid oxidizing family. Another difference between the aforementioned LMO and LOX has been observed in an intermediate step during the oxidation of L-lactate. For a better understanding we picked **Scheme 1** to explain this difference in more detail: After the conversion of L-lactate into pyruvate the product rapidly dissociates from the active site and molecular oxygen reacts with the enzyme producing H_2O_2 ; in contrast (the preliminary product) pyruvate doesn't dissociate from the enzyme and O_2 reacts rapidly with the E-FMN_{red}-pyruvate complex resulting in the products acetate, CO_2 and H_2O . The presence of this intermediate has been proven by photometric studies of LOX indicating a biphasic behavior of the traces observed from 340 to 550 nm (17). This species has been identified as a complex of reduced enzyme and pyruvate by titration of reduced enzyme with pyruvate and in stopped flow experiments by mixing different concentrations of pyruvate with the reduced enzyme (1). Consequently, mutation of residue Tyr-191 could have an influence on the accumulation of this intermediate and alter the oxidase into a monooxygenase activity. Furthermore, such a mutation might break the mentioned hydrogen bond network, destabilize the pyruvate bonding, lead to a complete activity loss or have massive influences on the substrate specificity. In the present paper we thereof describe work, in which we have investigated the role of this residue by creating and characterizing mutant forms of LOX, in which Tyr-191 has been replaced by Phe, Ala and Leu.



Scheme 1. The reaction cycles of LOX (outer cycle) and LMO (inner cycle)

EXPERIMENTAL PROCEDURE

L-(+)-lactic acid (free acid, 98%, Aldrich), L-glycolic acid (free acid 97%, Fluka), L-(+) mandelic acid (free acid, 98%, Fluka), L-glyceric acid (sodium salt, 95%, Sigma), (S)-2-hydroxy-3-methylbutyric acid (free acid, 99%, Aldrich), (S)-2-hydroxybutyric acid (free acid, 97% Fluka), (S)-(-)-2-hydroxyisocaproic acid (free acid, 98%, Aldrich), D-(+)-glucose (99.5%, Sigma), 3,3-dimethylglutaric acid (free acid, 98%, Aldrich), 4-aminoantipyrine (98%, Fluka), peroxidase from horseradish (Type VI, Sigma), N,N-dimethylaniline (ReagentPlus[®], 99%, Aldrich), sodium dodecylbenzenesulfonic acid (technical grade, Aldrich). Lyophilized wild-type LOX (grade 1) from *Aerococcus viridans* (WT) and lyophilized GOD (glucose oxidase, grade 1) from *Aspergillus niger* were from Roche Diagnostics GmbH. Enzymes were stored at -20 °C until further use. The plasmid pLO-1, which harbored the LOX gene, was kindly provided by Dr. T. Meier (Roche).

Molecular cloning and site-directed mutagenesis

Site directed mutagenesis leading was introduced by a two-stage polymerase chain reaction, described previously (Unterweger et al). Therefore, two separate primer extension reactions were carried out, in which pLO-1 was used as the template and one of the two mutagenic oligonucleotide primers was also present.

For the substitution of Tyr-191 by Phe the oligonucleotides 5'-TCGTTTTC~~CC~~ATTTGGTATGCGATCGTTCAACGTTACTTACG-3' (termed Tyr191Phefw, melting point 65.8 °C; where TTC denotes the replacement of Tyr by Phe; *PvuI* site is underlined) and 5'-GAACGATCGGCATACCAAATGGGAAACGAATTTATTCTTCAC-3' (termed Tyr191Phefv, melting point 63.5 °C; GAA denotes the replacement of Tyr by Phe; *PvuI* site is underlined) were used.

Primers used for the substitution of Tyr-191 by Ala were 5'-TCGTTGCC~~CC~~ATTTGGTATGCCGATCGTTCAACGTTACTTACG-3' (termed Tyr191Afw, melting point 67.8 °C; where GCC denotes the replacement of Tyr by Ala) and 5'-GAACGATCGGCATACCAAATGGGGCAACGAATTTATTCTTCAC-3' (termed Tyr191Arev, melting point 65.5 °C; GGC denotes the replacement of Tyr by Ala).

Oligonucleotides for the substitution of Tyr-191 by Leu were 5'-TCGTTCTC~~CC~~ATTTGGTATGCCGATCGTTCAACGTTACTTACG-3' (termed Tyr191Lfw, melting point 66.4 °C; where CTC denotes the replacement of Tyr by Leu) and 5'-GAACGATCGGCATACCAAATGGGAGAACGAATTTATTCTTCAC-3' (termed Tyr191Lrev, melting point 64.1 °C; GAG denotes the replacement of Tyr by Leu).

DNA was amplified by Pfu DNA Polymerase (Promega) setting up the following conditions: heat denaturation at 95 °C for 1 min; 4 elongation cycles, each consisting of 95 °C for 50 s, 59 °C for 50 s and 68 °C for 10 min; final extension at 68 °C for 7 min, and cooling at 4 °C. A second PCR was performed by combining the two separate PCR mixtures in a volume ratio of 1:1 under the same conditions mentioned above, but with a total repeat of 18 cycles. To ensure a higher transformation yield, template DNA was digested with *DpnI* at 37 °C for 1 h. Plasmid DNA was transformed into electrocompetent *E. coli* BL21 (DE3) cells, and the cells were cultured overnight at 37 °C on LB-amp plates (% peptone, 0.5% yeast extract, 0.5% NaCl, 1.8% agar supplemented with 100 µg/mL ampicillin). For further steps only transformants carrying plasmids with the mutation of interest verified by DNA sequencing were used.

Production of LOX mutants

Expression of LOX A95G in BL21 (DE3) was done in pre culture over night containing 0.55% glucose monohydrate, 1% peptone, 0.5% yeast extract, 0.5% NaCl, 1% NH₄Cl, 0.025 MgSO₄ * 7 H₂O, 100 µL/L poly(propylene glycol), 0.3% K₂HPO₄, 0.6% KH₂PO₄, 0.2*10⁻³% thiamine, 0.0115% ampicillin, 0.4*10⁻³% FeSo4 * 7H₂O, 0.1*10⁻³% MnSO4 * H₂O, 0.04*10⁻³% CuSO4 * 5 H₂O, 0.01%*10⁻³% H₃BO₃, 0.02*10⁻³% ZnSO₄ * 7 H₂O, 0.02*10⁻³% Na₂MoO₄ * 2H₂O and 0.04*10⁻³% FeCl₃. The optical density (OD₆₀₀) of the pre-culture, grown over night at 37 °C, had a value about 5. The main culture (same ingredients as pre-culture except 4 times higher glucose amount) was inoculated to an OD₆₀₀ of 0.5 directly to the fermenter. Temperature, pH, stirring and oxygen partial pressure in the B. Braun Biotech International Biostat®C, Type-CT5-2 fermenter were controlled and adjusted automatically during fermentation. The pH was balanced before start at pH 7.0 and

pH 4.0 with a ready-to-use calibration solution. The pO_2 was fixed to a minimum of 40%. Temperature was set to 37 °C before induction and then reduced to 30 °C. Induction took place with 5 mL of isopropyl β -D-1-thiogalactopyranoside with a concentration of 250 μ g/mL, which was a 1000-fold stock solution at an OD_{600} of 2.4. 50 mg/mL Amp was added as well with the IPTG. Concurrent with the induction of the biomass the glucose level was measured continuously over time to determine the endpoint of fermentation with glucose stripes (Diabur Test 5000, Roche Diagnostics). OD_{600} was measured during the whole process of fermentation with a Beckman Coulter Photometer. After the whole consumption of glucose the fermentation was stopped and the cells were harvested by centrifugation. The cell pellet was suspended in 50 mM potassium phosphate buffer, pH 7.0, and stored at -20 °C.

Protein purification

50 mM potassium phosphate buffer, pH 7.0 was used to perform the ongoing purification steps. First, cells were disrupted in a French press, and the crude extract was obtained by centrifugation. Further, protein was precipitated in the presence of 1.5 M $(NH_4)_2SO_4$ at 4 °C, and precipitate was removed by centrifugation. The supernatant was purified by hydrophobic interaction chromatography using a Phenyl Sepharose 6 Fast Flow (High Sub) column (GE Healthcare Life Sciences; 64 mL) and the Äkta FPLC system (Amersham Biosciences); the flow rate of the procedure was 5 mL/min, and eluted LOX was detected at 280 nm. Purity of the fractions showing LOX activity was controlled by SDS-PAGE with PhastGel™ Gradient 8-25 (GE Healthcare Life Sciences) gels and the Pharmacia High Speed Electrophoresis System (Pharmacia Biotech).

Finally, enzyme solution was desalted by repeated cycles of concentration and dilution using concentrator tubes (Vivaspin 20, 10 kDa cut-off, Vivascience AG) and stored in 50 mM potassium phosphate buffer, pH 7.0, at -20 °C until further use.

Assays

For kinetic studies of LOX activity a peroxidase-coupled spectrophotometric assay (Sigma) was used, in which the H₂O₂ produced in the LOX reaction is further reacted with peroxidase in the presence of 4-aminoantipyrine and N,N-dimethylaniline to give a quinonediimine dye that is detected spectrophotometrically. About 5 to 10 µL of enzyme appropriately diluted in 50 mM potassium phosphate buffer, pH 7.0, was added to a solution containing 40 mM 3,3-dimethylglutaric acid, 2.5 units peroxidase, 1.5 mM 4-aminoantipyrine, 50 mM L-(+)-lactic acid and 0.04% (v/v) N,N-dimethylaniline in a total volume of 0.5 mL. The pH of the solution was pH 6.5. After a reaction time of between 10 and 20 min at 37 °C, 1 mL of 0.25% (w/v) dodecylbenzenesulfonic acid was added to stop the reaction. The produced quinonediimine dye was measured spectrophotometrically at 565 nm with a Varian Cary® 50 Bio UV-Visible Spectrophotometer at 37 °C.

Protein concentrations were measured according to the Bradford protein quantification assay (Roti®-Quant, Carl Roth GmbH + Co KG) using BSA as reference. Note: the commercial preparation of LOX was not used for calibration of the protein assay. The enzyme is a solid powder that contains various substances other than target enzyme. Calibration based on solid mass is therefore not possible.

Activity of LOX was also determined from direct measurements of the O₂ consumption during the analyzed reaction that was L-lactate + O₂ + H₂O → pyruvate + H₂O₂. Assays were performed at 37 °C for 10 minutes in a 4.5 mL glass vial (1500

μL reaction mixture) that was sealed with a septum and contained 50 mM air-saturated potassium phosphate buffer, pH 6.5, and different concentrations (0.1 - 50 mM) of L-lactate as substrate (to determine the K_M). Mixing was achieved with a magnetic stirrer (300 rpm) keeping the glass vial in a water bath. The reaction was started by adding 10 μL enzyme (10 mg/ml for wild-type LOX diluted 1:100 to 1:1000, same dilution used for peroxidase assay). Dilution was varied among the mutants regarding the rates to be between 5 and 50 μM/min. Rates of O₂ utilization were measured with a fiber-optic oxygen microoptode (PreSens GmbH, Regensburg, Germany) connected to a miniaturized lock-in amplifier (MICROX TX3, PreSens GmbH, Regensburg, Germany). Calibration of the electrode was performed according to instructions of the supplier. Specific activities determined for wild-type LOX at 37 °C at saturated substrate concentration (pH 6.5, 50 mM L-lactate) were similar with 200 ± 10 U/mg (peroxidase assay) and 205 ± 8 U/mg (oxygen measurement).

Absorbance spectroscopy

UV-visible absorbance spectra were recorded with a Varian Cary® 50 Bio UV-visible spectrophotometer in quartz cuvettes (Hellma® GmbH & Co. KG) of 10 mm light path. 100 μM enzyme was scanned in 50 mM potassium phosphate buffer, pH 7.0, at 25 °C and a molar extinction coefficient at 455 nm of 10.8 mM⁻¹ s⁻¹ was assumed by releasing the FMN cofactor, which was performed by treating the enzyme with trifluoroacetic acid.

Kinetic analysis

For steady state measurements at pH 6.5 and 37 °C, initial rates of the enzymatic oxidation of L-lactic acid or other hydroxy acids were determined, wherein

the substrate concentration (10 measurements for concentrations of 0.1 - 50 mM) was varied. By using a peroxidase-coupled assay, these rates were determined. Kinetic constants (K_M , V_{max}) were obtained from nonlinear fit of the Michaelis-Menten equation (**equation 1.1** or **equation 1.2**) to the measured data using Sigma Plot®, and the k_{cat} was calculated with **equation 1.3**

Equation 1.1:
$$v = v_{max} * \frac{[S]}{K_M + [S]}$$

Equation 1.2:
$$v = v_{max} * \frac{[S]}{K_M + [S] * (1 + \frac{[S]}{K_{IS}})}$$

Equation 1.3:
$$k_{cat} = \frac{v_{max}}{[E]}$$

where v represents the reaction rate, v_{max} the maximum rate, $[S]$ the substrate concentration, K_M the Michaelis constant, K_{IS} the dissociation constant of the enzyme-inhibitor-substrate complex, k_{cat} the turnover number. $[E]$ corresponds to the molar concentration of the enzyme. E was determined from the protein concentration assuming a molecular mass of 41 kDa for the subunit of LOX.

Stopped flow

Pre-steady state measurements were conducted at 20 °C using an Applied Photophysics stopped flow apparatus, model SX17MV. A diode array detector was applied to collect spectral data between 280 and 700 nm. Several wavelengths were chosen from the collected spectra and single wavelength scans with a photomultiplier. The reductive half-reaction was monitored by collecting spectra with the diode array detector and by measuring the absorbance over time at 455 nm after anaerobically mixing 10 μ M enzyme with varying concentrations of L-lactic acid. The oxidative half-reaction was followed at 455 nm after mixing an anaerobical solution

containing reduced enzyme (10 μM) with a buffer solution containing different concentrations of dioxygen. Anaerobic conditions were created by the addition of 10 mM D-glucose to all solutions and flushing with nitrogen. Additionally, to remove all traces of residual oxygen, glucose oxidase (Roche) was added to a final concentration of 200 nM.

Traces obtained at 455nm were fitted to an exponential function

Equation 2.1:
$$A(t) = A + Cxe^{(-kt)}$$

where A describes the absorption, C is a constant, and k represents an observed rate constant. The observed rates for substrate concentration dependent reduction of LOX were fitted using the following equation

Equation 2.2:
$$k_{obs} = \frac{k_{red}xS}{K_d+S}$$

where k_{obs} describes an observed rate constant, k_{red} is the reduction rate constant, S is the substrate concentration and K_d is the dissociation constant.

For the oxidative half-reaction the enzyme was reduced with 2 equivalents L-lactate to guarantee a completely reduced LOX. No Michaelis-Menten type complex is formed during the re-oxidation event with molecular oxygen; by varying oxygen concentration linear plots with the primary data were created in order to determine bimolecular rate constants for this process. Bimolecular rate constants for the reaction of free reduced LOX with molecular oxygen were calculated from plotting the rates of re-oxidation [s^{-1}] versus the oxygen concentrations [M].

RESULTS

Steady state kinetics

Mutations in the active site (Ala-95 to Gly) in the binding site influenced the substrate specificity massively (17). Due to this instance we focused our research on detailed characterization of LOX Y191F mutant enzyme with different substrates (Table 1). The Y191F mutant resulted in a 4-fold loss in turnover number (k_{cat}) for reaction with L-lactate compared to wild-type LOX. Consequently, the lack of the tyrosine is not crucial for the substrate conversion; otherwise the activity would drop significantly or lead to an inactive LOX. We also checked if LOX Y191 mutant was changed into LMO. Both, coupled (peroxidase) enzyme assay and measuring the O_2 consumption (with an oxygen electrode) during the reaction with L-lactate delivered similar rates. If the mutant was turned into a monooxygenase, it would appear that less (or no) H_2O_2 is produced than O_2 is consumed; this was clearly not the case, so Y191F remained an oxidase.

Table 1. Steady state kinetic parameters of wild-type LOX, Y191F, Y191L and Y191A mutants for several substrates

		Wild-type	Y191F	Y191L	Y191A
L-(+)-lactic acid					
k_{cat}	(s^{-1})	140 ± 1	32 ± 1.3	8.4 ± 0.4	5.3 ± 0.2
K_{M}	(mM)	0.8 ± 0.03	0.05 ± 0.005	0.9 ± 0.2	12.8 ± 1.3
$k_{\text{cat}}/K_{\text{M}}$	($\text{mM}^{-1} \text{s}^{-1}$)	167	952	9.4	0.4
L-mandelic acid					
		0.1 ± 0.01	0.1 ± 0.002	$0.03 \pm$	$0.03 \pm$
k_{cat}	(s^{-1})			0.001	0.001
K_{M}	(mM)	0.5 ± 0.1	0.5 ± 0.1	0.7 ± 0.04	0.5 ± 0.02
$k_{\text{cat}}/K_{\text{M}}$	($\text{mM}^{-1} \text{s}^{-1}$)	0.2	0.2	0.04	0.06
(S)-2-hydroxybutyric acid					
k_{cat}	(s^{-1})	1.4 ± 0.01	2.4 ± 0.08	0.8 ± 0.07	0.8 ± 0.07
K_{M}	(mM)	0.4 ± 0.05	0.98 ± 0.13	5.7 ± 1.3	5.9 ± 0.7
$k_{\text{cat}}/K_{\text{M}}$	($\text{mM}^{-1} \text{s}^{-1}$)	3.2	2.5	0.14	0.13
(S)-hydroxy-3-methylbutyric acid					
k_{cat}	(s^{-1})	0.2 ± 0.01	0.02 ± 0.002	n.d.	n.d.
K_{M}	(mM)	3.3 ± 0.3	1.5 ± 0.2	n.d.	n.d.
$k_{\text{cat}}/K_{\text{M}}$	($\text{mM}^{-1} \text{s}^{-1}$)	0.1	0.007		
(S)-2-hydroxyisocaproic acid					
k_{cat}	(s^{-1})	1.1 ± 0.01	1.3 ± 0.03	0.7 ± 0.01	1.3 ± 0.04
K_{M}	(mM)	0.4 ± 0.05	0.4 ± 0.04	4.4 ± 0.2	12.3 ± 1
$k_{\text{cat}}/K_{\text{M}}$	($\text{mM}^{-1} \text{s}^{-1}$)	2.5	3.1	0.17	0.1
L-(-)-glyceric acid					
k_{cat}	(s^{-1})	2.9 ± 0.1	3.3 ± 0.07	0.18 ± 0.04	n.d.
K_{M}	(mM)	8.6 ± 2.0	3.3 ± 0.2	4.5 ± 0.48	n.d.
$k_{\text{cat}}/K_{\text{M}}$	($\text{mM}^{-1} \text{s}^{-1}$)	0.3	0.99	0.04	
glycolic acid					
k_{cat}	(s^{-1})	0.98 ± 0.02	0.5 ± 0.02	0.7 ± 0.01	0.3 ± 0.01
K_{M}	(mM)	0.4 ± 0.06	0.1 ± 0.02	8.3 ± 0.8	50.2 ± 5.2
$k_{\text{cat}}/K_{\text{M}}$	($\text{mM}^{-1} \text{s}^{-1}$)	2.2	4.5	0.09	0.006

α Steady state measurements were performed at 37 °C with a coupled peroxidase assay. Standard deviations on kinetic parameters are from non-linear fits of data with the Michaelis-Menten equation

Changes in steric properties in the active site caused by the mutation might also be a reason for the lowered specific activity of Y191F for L-lactic acid. On the other hand, the catalytic efficiency (k_{cat}/K_M) was ameliorated 1.5- to 6-fold depending on the temperature. This primarily derives from a 6- up to 16-fold decrease in K_M meaning that phenylalanine has a positive effect on the substrate affinity. Another observation of interest is the substrate inhibition ($K_{\text{IS}} = 33.7 \pm 5.1$ mM) at higher substrate concentrations in Y191F (**Figure 2**). It seems that the removal of the hydroxyl group by the replacement of tyrosine with phenylalanine might induce a second substrate binding site, which further leads to the inhibition of substrate conversion (**28**).

In contrast to these observations, the mutants Y191L and Y191A reacted differently with the substrate L-lactate. Both k_{cat} values were more than 1 order of magnitude lower compared to the wild-type enzyme. Most significant change was observed for Y191A mutant, where the K_M for lactate increased 16- or 90-fold depending on the temperature and the catalytic efficiency (k_{cat}/K_M) was decreased by 3 orders of magnitude.

Further, we expanded the substrate spectrum to several other α -hydroxy acids (L-mandelic acid, S-2-hydroxybutyric acid, S-hydroxy-3-methylbutyric acid, S-2-hydroxyisocaproic acid, L-glyceric acid, and glycolic acid) for steady state kinetic characterization of the Y191F mutant. **Table 1** lists all kinetic characteristics for L-lactate and a range of other L- α -hydroxy acids, which were converted into the correspondent α -keto acid. Measurements were performed at 5 independent experiments at 37 °C utilizing a peroxidase assay. Y191F mutant displayed a 10-, 2- and 1.5-fold lower k_{cat} than wild-type LOX for S-hydroxy-3-methylbutyric acid, glycolic acid and L-mandelic acid, respectively.

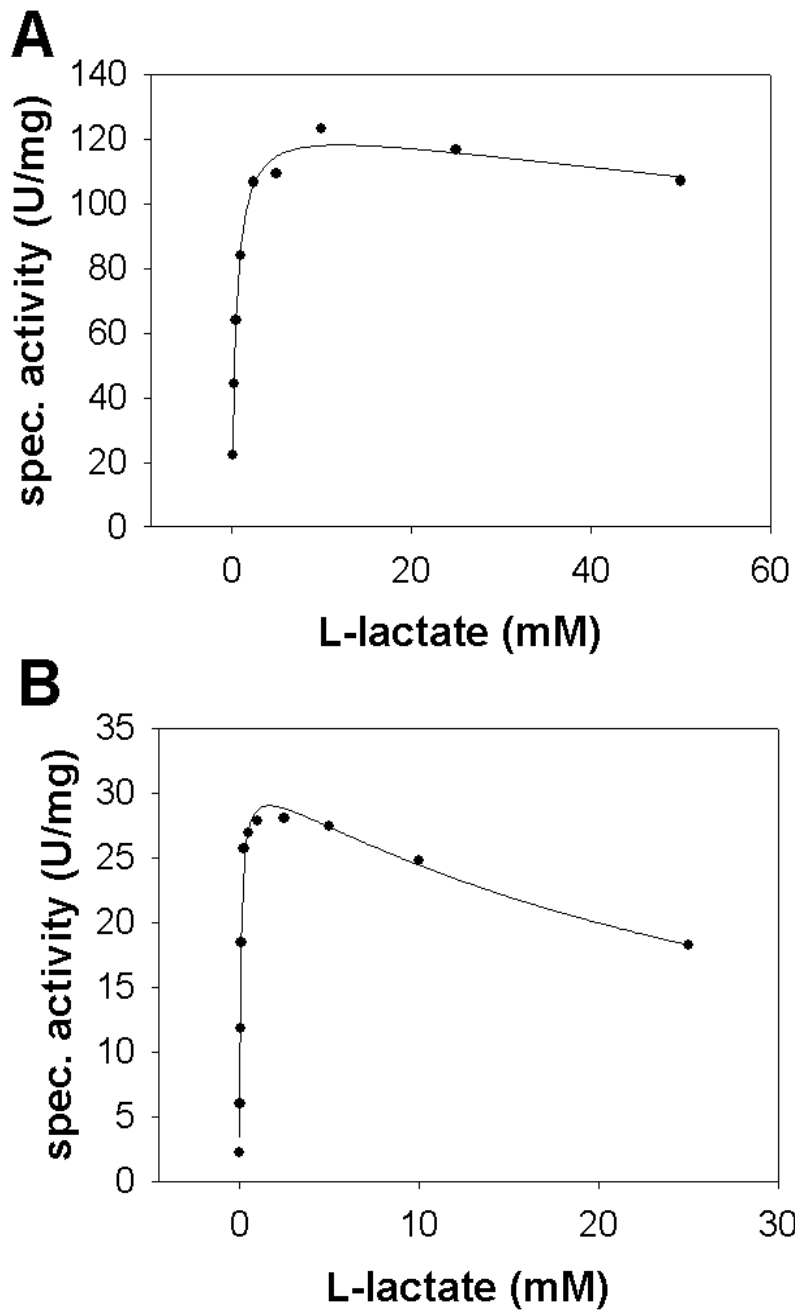


Figure 2

Steady state measurements of wild-type LOX (Panel A) and Y191F mutant (Panel B) at different L-lactate concentrations determined by a coupled peroxidase assay at 20 °C. Both enzymes show substrate inhibition at higher substrate concentrations

However, the k_{cat}/K_M value for LOX Y191F mutant was doubled, almost tripled and tripled compared to the wild-type LOX when converting glycolic acid/ S-2-hydroxybutyric acid, L-mandelic acid and L-glyceric acid. The higher catalytic

efficiency mostly derived from the lowered K_M . In only one case the k_{cat}/K_M was decreased more than 10-fold (S-hydroxy-3-methylbutyric acid). In short, the substrate specificity was not changed significantly, but the affinity for the substrates was increased 2- up to 16-fold with the exception of two substrates namely S-2-hydroxyisocaproic acid (equal) and S-2-hydroxybutyric acid (half). In terms of Y191L and Y191A mutants the k_{cat} values were generally lower; in some cases the absorbance changes for the produced peroxide were so low that we could not measure a reliable activity. Interestingly, referring to Y191A mutant, the affinity for several substrates was lower compared to the wild-type.

Pre-steady state experiments

In order to identify the influence of the generated mutations on the reaction mechanism, we conducted pre-steady state kinetics. Therefore we recorded spectral changes of the FMN cofactor by applying a stopped flow photometer using diode array detection for spectral scans and a photomultiplier for single wavelengths. By analyzing the reductive and oxidative half-reaction separately we could gather information and compared them with data from previous studies of wild-type LOX. In case of the reductive half-reaction the oxidized enzyme was mixed anaerobically with various concentrations of L-lactic acid (range: 0.01 - 10 mM). From literature we know that this includes the formation of a reduced enzyme-pyruvate complex and the release of the product from the active site without re-oxidation of the reduced flavin (1).

For wild-type LOX no absorbance changes at any wavelength greater than 530 nm could be detected, meaning that it shows no interaction with the product during

the reductive half-reaction. When anaerobically mixing L-lactate with the enzyme in a stopped flow photometer, pseudo first order rates (k_{obs}) can be determined for different substrate concentrations at 455 nm. When the decrease in absorbance of 455 nm happens in a single exponential manner [$a1 \cdot \exp(-k \cdot x) + c$], k_{obs} describes the whole reductive half-reaction at a certain substrate concentration. This is the case for wild-type LOX. **Figure 3A** shows the observed rates (k_{obs}) for WT LOX traces at 455 nm, which are plotted to L-lactate to yield k_{red} and K_d (listed in **Table 2**) using **equation 2**.

Contrary to wild-type LOX, the reduction of LOX Y191F mutant (at 455 nm) can be described in a double exponential manner [$a1 \cdot \exp(-k1 \cdot x) + a2 \cdot \exp(-k2 \cdot x) + c$], with a fast phase at the beginning, and worth mentioning, were also able to observe changes in absorbance greater than 530 nm. Furthermore, we identified inhibition at higher substrate concentrations during the reductive half-reaction (**Figure 3B**). Here, the first phase in reduction is not influenced, but mainly the second phase.

The reduction of Y191L and Y191A mutants happened in a double exponential manner leading to two different rates (k_{obs1} and k_{obs2}), which were used to determine k_{red1} and k_{red2} as well as K_{d1} and K_{d2} by the equations:

Equation 2.1:
$$k_{obs1} = \frac{k_{red1} \cdot S}{K_{d1} + S}$$

Equation 2.2:
$$k_{obs2} = \frac{k_{red2} \cdot S}{K_{d2} + S}$$

Noticeable, we could not record a change at 530 nm for Y191L and Y191A, a fact that was seen for LOX Y191F mutant. For Y191L (compare Panel **C**), k_{red2} was as high as the determined $k_{cat} = 7.5 \text{ s}^{-1}$. Similar results were investigated for Y191A (Panel **D**), where $k_{red2} = 3.8 \text{ s}^{-1}$ is similar to $k_{cat} = 5.1 \text{ s}^{-1}$.

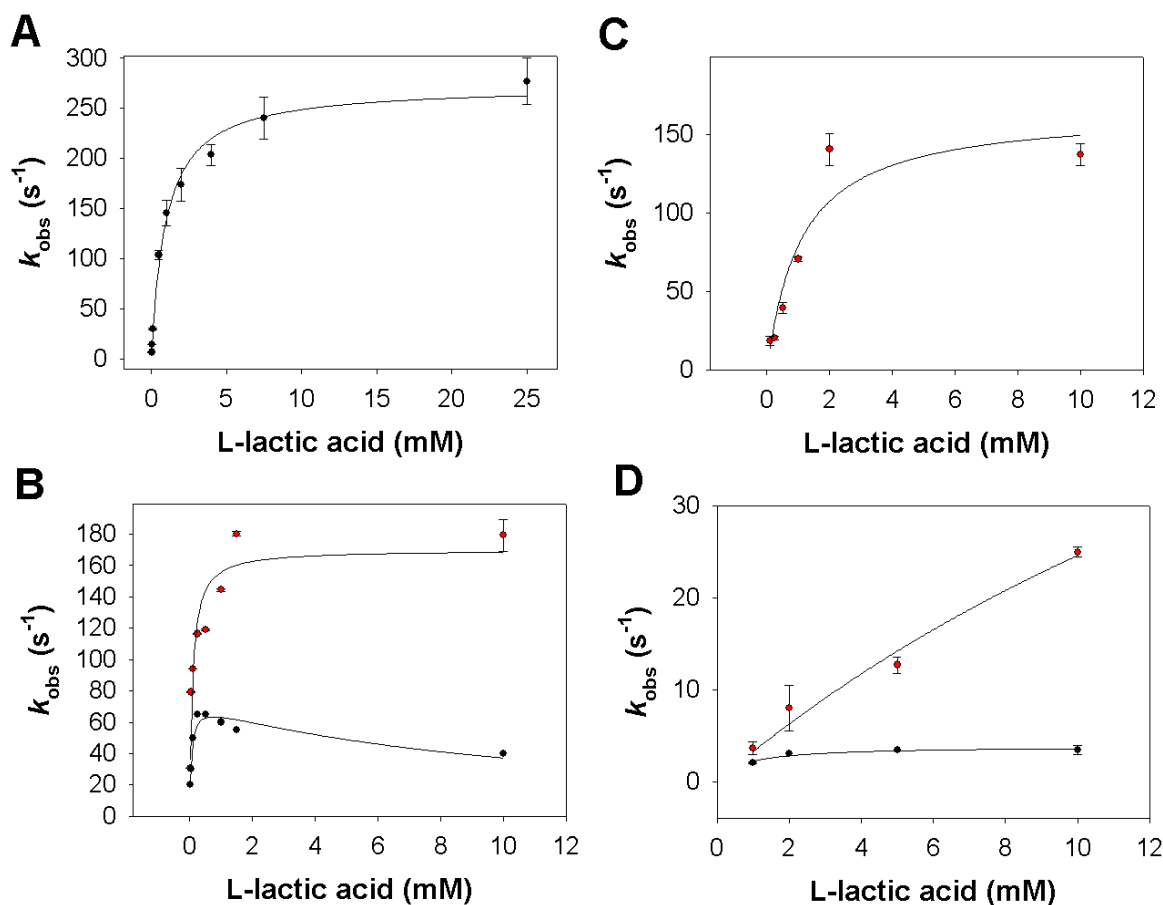


Figure 3

Determination of the reduction rate constants (k_{red} , k_{red1} , k_{red2}) and dissociation constant (K_d) for the reaction of wild-type LOX (Panel A) and Tyr-191 mutants (Panel B and C) with L-lactate at 20 °C.

Pseudo first order rate constants, k_{obs} values from determined single traces at 455 nm (Panel A) are plotted to L-lactate to yield k_{red} and K_d . In the case of the tyrosine mutants (Panel B, C, D) the reductive half is split into two phases (description in text) expressed in k_{obs1} and k_{obs2} values, which lead to k_{red1} and k_{red2} . Panel A: wild-type LOX with $k_{red} = 2.7 \pm 0.1 \times 10^2 \text{ s}^{-1}$ and $K_d = 1 \pm 0.1 \text{ mM}$. Panel B: Y191F mutant - **red** dots indicate k_{obs1} values, **black** dots illustrate k_{obs2} values. $k_{red1} = 169.9 \pm 10.8 \text{ s}^{-1}$ and $K_{d1} = 0.09 \pm 0.03 \text{ mM}$, $k_{red2} = 72.5 \pm 5.3 \text{ s}^{-1}$ and $K_{d2} = 0.05 \pm 0.01 \text{ mM}$, $K_{IS} = 10.6 \pm 4.0 \text{ mM}$. Panel C: Y191L mutant - **red** dots show k_{obs1} values, k_{obs2} was determined for all lactate concentrations to be 7.5 s^{-1} and is missing in the figure ($k_{obs2} = k_{red2}$). $k_{red1} = 165.4 \pm 26.0 \text{ s}^{-1}$ and $K_{d1} = 1.1 \pm 0.4 \text{ mM}$. Panel D: Y191A mutant - **red** dots indicate k_{obs1} values, **black** dots illustrate k_{obs2} values. $k_{red1} = 92.9 \pm 9.8 \text{ s}^{-1}$ and $K_{d1} = 27.7 \pm 3.3 \text{ mM}$, $k_{red2} = 3.8 \pm 0.2 \text{ s}^{-1}$ and $K_{d2} = 0.7 \pm 0.2 \text{ mM}$.

Table 2. List of kinetic parameters and characteristics of FMN for wild-type LOX, Y191F, Y191L and Y191A mutants with L-lactic acid as substrate determined at 20 °C including pre-steady and steady states experiments and simulation of the fits. Numbering is based on **Scheme 1**

		Wild-type	Y191F	Y191L	Y191A
Pre-steady state					
k_{red}	(s ⁻¹)	2.7 ± 0.1 x10 ²	-	-	-
K_d	(mM)	1 ± 0.1	-	-	-
K_{d1}	(mM)	-	0.09 ± 0.03	1.1 ± 0.4	27.7 ± 3.3
K_{d2}	(mM)	-	0.05 ± 0.01	-	0.7 ± 0.2
k_{red}/K_d	(mM ⁻¹ s ⁻¹)	2.7 x10 ²	-	-	-
k_{red1}	(s ⁻¹)	-	1.7 ± 1 x10 ²	1.7 ± 3 x 10 ²	92.9 ± 9.8
k_{red2}	(s ⁻¹)	-	72.5 ± 5.3	7.5 ***	3.8 ± 0.2
k_{ox}	(mM ⁻¹ s ⁻¹)	1.8 ± 0.1 x10 ³	7 ± 0.5 x10 ²	4.8 ± 0.4 x10 ²	2.9 ± 0.2 x10 ²
reduced FMN	(%)	>90	<75	>90	>90
re-oxidized FMN	(%)	>90	>90	>90	>90
$\Delta A_{530\ 1}$	(s ⁻¹)	n.v.	2.0 x10 ² **	n.v.	n.v.
$\Delta A_{530\ 2}$	(s ⁻¹)	1.3 x10 ² **	33 **	n.d.	n.d.
Steady state					
k_{cat}	(s ⁻¹)	87.5 ± 2.2	22 ± 0.6	7.5 ± 0.3	5.2 ± 0.9
K_M	(mM)	0.5 ± 0.1	0.08 ± 0.01	1.5 ± 0.2	46 ± 14
k_{cat}/K_M	(mM ⁻¹ s ⁻¹)	1.8 x 10 ²	2.7 x10 ²	5	0.13
k_{cat} calc	(s ⁻¹)	1.5 x 10 ²	39.2	6.7	3.4
k_{cat} calc : k_{cat}		1.6:1	1.8:1	0.9:1	0.7:1
Berkeley Madonna*					
k_2/k_1	(mM)	-	0.04	-	-
k_3	(s ⁻¹)	-	2 x10 ²	-	-
k_4	(s ⁻¹)	-	0	-	-
k_5	(s ⁻¹)	-	33	-	-
k_6	(mM ⁻¹ s ⁻¹)	-	10	-	-

$\Delta A_{530\ 1}$ describes an increase in absorbance, $\Delta A_{530\ 2}$ a decrease in absorbance

n.v. not visible; **n.d.** not detectable

* description of simulation in text

** data and fitting in **Figure 5** for Y191F; fitting for WT in single exponential manner, conditions: 10 μM enzyme, 10 mM L-lactate, 20 °C, pH 6.5

*** no dependence on the lactate concentration

In contrast to a single exponential decay detected for LOX wild-type and resulting in a single constant termed k_{red} (expressed in s^{-1}), the reduction of Y191F mutant can be described by two different phases (compare **Figure 3B**); the first phase is also increasing at higher substrate concentrations and reaches a maximum at $1.8 \times 10^2 s^{-1}$ (k_{obs1}), whereas the second phase (k_{obs2}) reaches its maximum at a lactate concentration of around 1 mM and is decreased at higher lactate concentrations. To determine k_{red1} and k_{red2} , we plotted k_{obs1} and k_{obs2} against the lactate concentration. Due to an inhibition shown for k_{obs2} we had to consider two different equations to determine k_{red1} and k_{red2} :

Equation 3.1:
$$k_{obs1} = \frac{k_{red1} \times S}{K_{d1} + S}$$

Equation 3.2:
$$k_{obs2} = \frac{k_{red2} \times S}{K_d + S \times (1 + \frac{S}{K_{IS}})}$$

To determine an overall k_{red} for LOX Y191F mutant, we calculated ($1/k_{red} = 1/k_{red1} + 1/k_{red2}$) (**Table 2**).

Interestingly, the second phase, termed k_5 , seems to be the rate limiting step (and is constant with the observed k_{cat} value from steady state experiments). Previous studies detected an absorbance change during the reductive half-reaction at 530 nm indicating a step, where the FMN_{red}-pyruvate complex is built and dissociates. In our experiments we were not able to detect such a change at 20 °C for the wild-type enzyme, but we clearly identified the formation and the decay of A_{530nm} for the LOX mutant (**Figure 5**).

Worth mentioning, the rate of the formation of the complex is as fast as the first phase of reducing the cofactor; moreover the decay of the complex corresponds to the second phase at 455 nm, which will be discussed in more detail later. K_{d1} is in

agreement with the K_M , though noticeable that it is more than 5 times lower than the one of LOX wild-type. Another difference between these two enzymes is the fact that the FMN cofactor is not reduced completely by L-lactic acid demonstrated for the Y191F mutant. In short, the cofactor is reduced between 75 and 90% (compare **Table 2**) depending mostly on the lactate concentration (data not shown). Starting at a range higher than 1 mM, the FMN cofactor is reduced less than 75%. On the other hand, all three mutants, where Tyr-191 was replaced by Ala, Phe or Leu were re-oxidized by molecular oxygen in a single exponential manner and the observed rate constants were directly proportional to the oxygen concentration (**Figure 4**). Second order rate constants of Y191F, Y191L and Y191A were $7.0 \times 10^5 \text{ s}^{-1} \text{ M}^{-1}$, $4.8 \times 10^5 \text{ s}^{-1} \text{ M}^{-1}$ and $2.9 \times 10^2 \text{ s}^{-1} \text{ M}^{-1}$, 39%, 27% and 16% of that for wild-type enzyme (**Table 2**). A drop in k_{ox} can also influence k_{cat} ($1/k_{cat} = 1/k_{red} + 1/k_{ox}$). Both, LOX wild-type and the mutant Y191F show substrate inhibition with L-lactic acid, though the K_I is almost 10 times higher for the LOX wild-type. We assume the high affinity of the LOX Y191F mutant for the L-lactic acid - expressed in K_M and K_{d1} - to be the cause for this inhibition; due to the higher affinity it's more likely for the lactate to bind the active site when the cofactor is still reduced and therefore blocks the conversion into pyruvate.

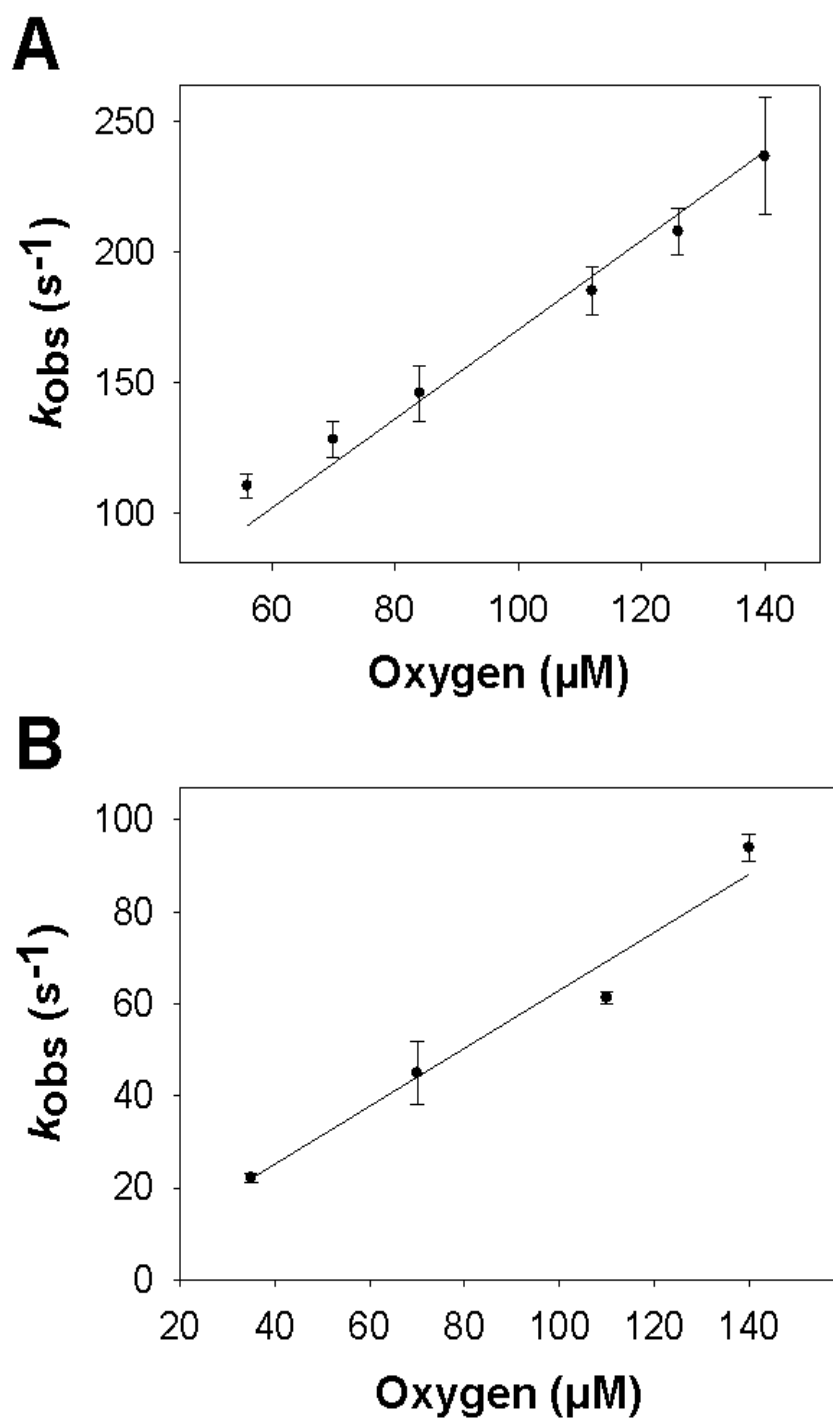


Figure 4

Determination of the oxidative rate constant (k_{ox}) for wild-type LOX (Panel A) and Y191F mutant (Panel B) at 20 °C. k_{obs} is plotted against oxygen.

DISCUSSION

From analysis of certain wild-type structures Tyr-191 was shown to have an orientation, where it forms a hydrogen bond to the Tyr-40 residue (**PDB code: 2E77**), which stabilizes the pyruvate. On the other hand, some wild-type structures, where pyruvate is lacking reveal Tyr-191 to be a mobile residue, which has the ability to flip away from Tyr-40. In brief, the overlay in **Figure 1** pointed out the conformational changes between monomer D of structure 2E77 and 2DU2. However, monomer C (picture not shown) of structure 2DU2 shows Tyr-191 being positioned in the same orientation like in structure 2E77. These findings clearly evidenced Tyr-191 being a flexible residue, which has the ability to switch away from Ala-96 enabling the entry of the substrate into the active site, though it is not clear if Ala-96 might be responsible for the switch of Tyr-191. Substitution of Tyr to Phe leads to a removal of the hydroxyl group, thereof breaks the hydrogen bond network to the Tyr-40 and increases the binding affinity for L-lactic acid. In a previous work, where we have solved the crystal structure of the A95G mutant (unpublished data), we evidenced Tyr-191 to act as a gatekeeper residue for different substrates, which was stuck in the vicinity of Tyr-40, even when no substrate is bound due to a conformational change of Ala-96. This means that Tyr-191 can only be positioned close to Tyr-40 and therefore the entering channel for several substrates is broadened, which was proven for A95G mutant by increased activities of the same chosen substrates listed in **Table S1** leaving the native L-lactate reactivity basically unaffected. Consequently for Y191F mutant the flipping to Ala-96 is still active and enables L-lactic acid to enter the binding site, but does not have an influence on longer α -hydroxy acids. Rate constants of several substrates are consistent with these findings (compare **Table 1**).

The active site mutant Y191F mainly influenced the kinetic parameters when converting L-lactic acid. The 4-fold decrease in k_{cat} for L-lactate observed for the mutant compared to the wild-type underlines the putative involvement of the Tyr-191 residue in stabilization processes in the active site. The Tyr-191 hydroxyl group and its hydrogen bond network to Tyr-40 and the substrate are therefore of importance during the conversion. As already mentioned, the lack of this hydroxyl group destabilizes the process of conversion on the one hand, but also increases the affinity for L-lactic acid on the other hand. Another explanation for the ameliorated binding affinity could be the fact that Phe is a hydrophobic amino acid residue, which turns the active site into a more hydrophobic core of the enzyme and stabilizes its environment. Substitution of Tyr-191 by Leu, another hydrophobic residue had similar effects on k_{cat} , but minimal consequences in terms of K_{M} for lactate. Investigating the reductive half-reaction of Y191A and Y191L mutants it turned out that the k_{red} was decreased 3- and 4-fold compared to wild-type LOX implicating that the mutation of this residue influences the conversion. Especially Y191A mutant illustrated an increased K_{M} for lactate indicating that the Tyr-191 is of relevance for the substrate binding. Regarding the mutant form of GOX, where Tyr-24 (equivalent to Tyr-40 in LOX) was substituted by Phe, a higher K_{M} with similar substrate specificities and a lower k_{cat} (for the main substrate) leads to the conclusion that in LOX alteration of Tyr-191 mainly influences the substrate binding and partly the catalytic step. Overall, the fact that the observed K_{d} for lactate is similar to K_{M} for the Tyr-191 mutants is in full agreement with the aforementioned role on the substrate affinity.

Detailed pre-steady state kinetics of Y191F mutant revealed that a step in the reductive half-reaction is rate limiting in overall catalysis; the reductive half-reaction includes the conversion of substrate and the release of the product. The whole

reductive half-reaction of Y191F mutant ($1/k_{\text{red}} = 1/k_{\text{red1}} + 1/k_{\text{red2}}$) was slower than shown for wild-type LOX and confirmed the decreased k_{cat} of the steady state kinetics (**Table 2**). Additionally, the re-oxidation rate with O_2 was 3-fold higher for wild-type LOX compared to the Y191F mutant. Besides the low K_{d} for lactate two main differences were observed for the Y191F mutant compared to wild-type, Y191A and Y191L mutants: On the one hand we identified lower reduction rates at higher lactate concentrations during the reductive half-reaction, which is in accordance with the observed substrate inhibition from steady state analysis. On the other hand, we clearly elucidated a species, which is a complex of EFl_{red} and pyruvate and is a characteristic for LMO. Worth mentioning, in previous works this species from LMO could only be identified in anaerobic stopped flow experiments (**1**) due to the instance that molecular oxygen reacts so fast with this species that an additional species ($\text{EFl}_{\text{ox}}\text{-Pyr}$) is formed. In LMO, the $\text{EFl}_{\text{red}}\text{-Pyr}$ species stays stable during the half-reaction for several seconds indicating a strong affinity of the enzyme for pyruvate.

Spectral scans of Y191F mutant revealed the typical reduced FMN spectrum, where FMN_{red} lacks both absorbance maxima at 373 and 455 nm. Remarkably, the conversion from oxidized to reduced FMN was identified in a biphasic manner (**Figure 5, Figure S2**) when mentioning the absorbance band at 530 nm (species of LMO). Besides an exponential decay at 455 nm we observed the formation and the decay of an intermediate step at 530 nm, which was previously described for wild-type LOX at low temperatures (**1, 16**). Studies by Massey and co-workers were not able to identify an intermediate of LOX mutants at temperatures above 4 °C. The reason was mainly because the first step, where the intermediate is formed cannot be detected accurately within the 3 ms dead time of the stopped flow instrument at higher temperatures. We were confronted with similar problems when using wild-type

LOX at 20 °C. We proved the formation of the intermediate with LOX wild-type at 4 °C in a single stopped flow experiment (compare **Supporting Information Figure S2**).

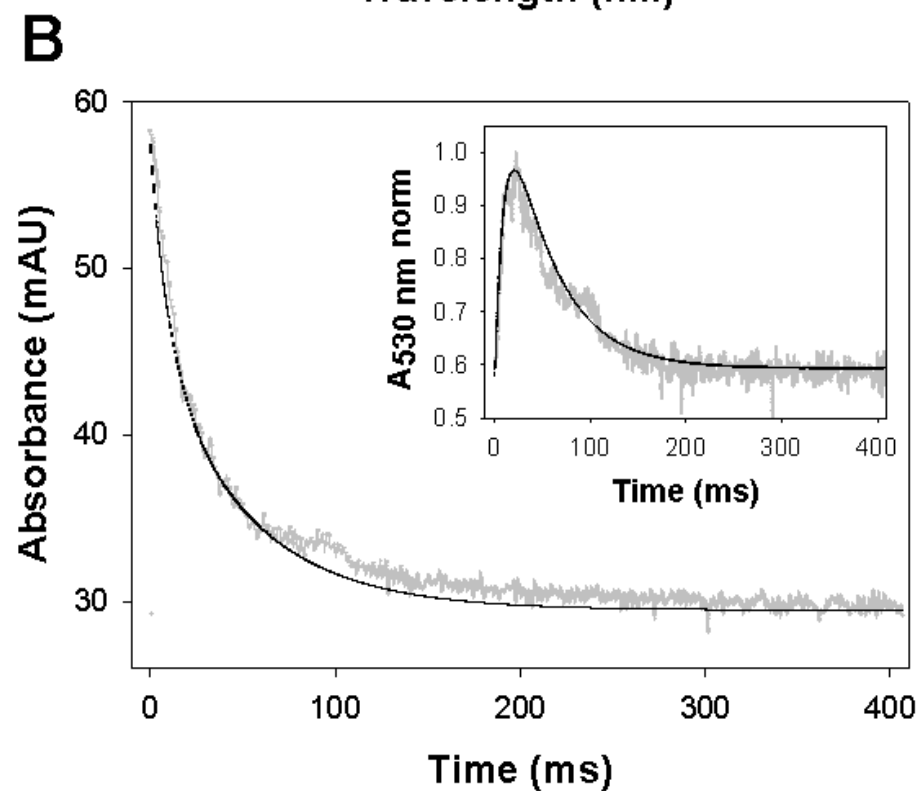
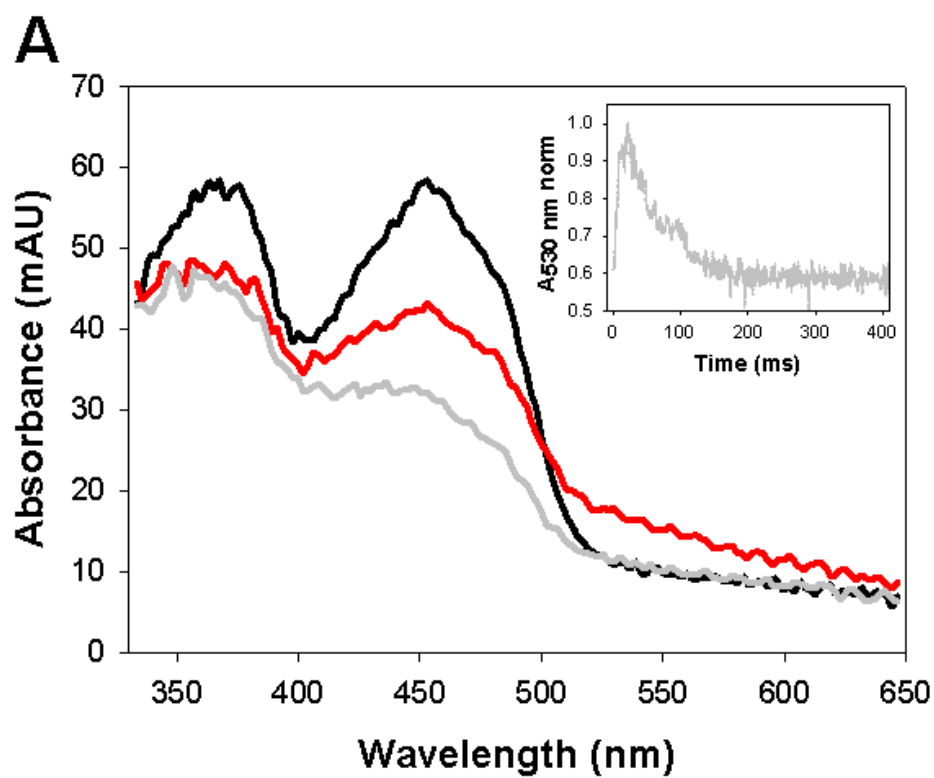


Figure 5

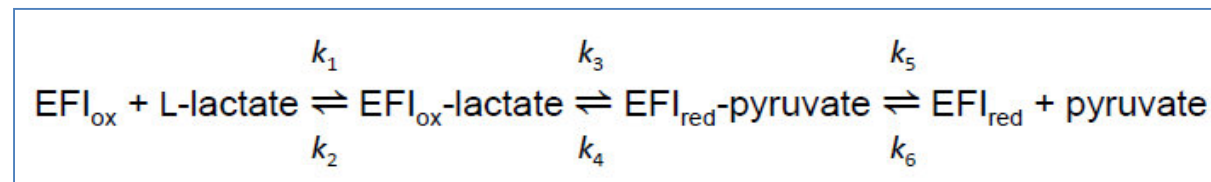
Spectral scans of LOX Y191F and fitting with Berkeley Madonna

Panel A: Spectral scans of LOX Y191F mutant during the reductive half-reaction. 4.0 μM LOX were reduced with 1 mM L-lactate under anaerobic conditions in 1 mM potassium phosphate buffer, pH 6.5 at 20 °C. **Black** line: enzyme in oxidized state at start (0 ms); **red** line: reaction after 9 ms; light **grey** line: reaction after 200 ms. After 9 ms the maximum in absorbance at 530 nm is reached (compare dark **grey** trace for the whole reaction at inset), the amplitude decreases afterwards.

Panel B: Reductive half-reaction of LOX by L-lactate. 4.0 μM LOX Y191F mutant in 50 mM potassium phosphate buffer (pH 6.5) were reacted in the stopped flow photometer at 20 °C with 1 mM L-lactate. The grey line represents the reaction trace at 455 nm with two different phases (first phase = k_3 ; second phase = k_5) the inset effects the trace at 530 nm in a biphasic manner. Black lines represent the fittings achieved with software Berkeley Madonna (Description in text) leading to the calculated kinetic constants k_3 (200 s^{-1}) and k_5 (33 s^{-1}).

However, the Y191F mutant highlights another different behavior compared to wild-type during the reductive half-reaction. As previously described for an active site mutant (**16**) the Y191F mutant displayed biphasic kinetic patterns, which were observed in pre-steady state experiments. Here, the fastest phase of reduction was associated with the major amplitude changes at 455 nm and 530 nm. Unlike the wild-type LOX the fast phase of absorbance decrease at 455 nm correlates with an increase at $A_{530\text{nm}}$ and the second phase of absorbance at 455 nm is similar to the decrease of $A_{530\text{nm}}$. To this end we could split the reductive half into two kinetic rates - the first is responsible for the formation (k_{red1} or k_3) and the second one for the decrease (k_{red2} or k_5) of the intermediate species. Due to the instance that the second phase is the rate limiting step of the reaction it can be compared with the k_{cat} . The results of Y191F mutant are consistent with a modified ping-pong mechanism (displayed in **Scheme 2**) as established for wild-type LOX (**1**).

Fitting and simulation of both traces was performed with software Berkeley Madonna.



Scheme 2: Minimalistic reaction mechanism of LOX Y191F mutant, whereas k_{red} of LOX wild-type includes the steps k_3 and k_5

Simulation of the reductive half-reaction

The fitting of the traces of A_{455} and A_{530} was performed in two steps. First, since the only species absorbing at 530 nm is the complex EPyr, a normalized absorbance can be defined that could directly depend on the ratio of EPyr/EPyrmax (EPyrmax is the maximum concentration of EPyr reached during the reaction course). The experimental data for the intermediate (A_{530}) were normalized by dividing all data by the maximum value of the same data set. Normalized data were then fitted to a variable defined as R (=EPyr/EPyrmax plus background absorbance). Different sets of data were used for the fitting resulting in a calculated value for EPyrmax. Once EPyrmax was calculated, using the $A_{530\text{max}}$, the intrinsic absorbance of EPyr can be estimated. The consistency between different set of data was ensured, leading to a value of 3.1 μM with a S.D. of 0.2 μM for LOX Y191F mutant (when $E = 5 \mu\text{M}$). This value was used to calculate the intrinsic absorbance (ϵ) for the formation of the intermediate by the formula $\epsilon = (A_{530\text{max}} - A_{530\text{final}}) / C_{\text{EPyrmax}}$ resulting in a value of $1.5 \times 10^3 \text{ M}^{-1}$. Data of A_{455} were fitted to the variable defined as $C = E + \text{ELac} + \text{EPyr} \cdot A1 + \text{Ered} \cdot A2$. A1 and A2 are the relative contributions of the species EPyr and Ered to the absorbance at 455 nm. [A1 (= $A_{455 \text{ tx}} / A_{455 \text{ t0}}$) is the ratio between the absorbance (455 nm) at the point in time (tx), where EPyrmax is reached and the

absorbance (455 nm) at the start of the reaction (t_0). $A_2 = A_{455\text{final}}/A_{455\ t_0}$.] On the other hand, the absorbance data of A_{530} were fitted to the variable $R (= \text{EPyr}^* \epsilon + A_{530\text{final}})$.

Table 2 also shows the data of the simulation for LOX. The simulated values of Y191F mutant for k_3 ($2.0 \times 10^2 \text{ s}^{-1}$) and k_5 (33 s^{-1}) are comparable with the aforementioned rate constants k_{obs1} ($1.8 \times 10^2 \text{ s}^{-1}$) and k_{obs2} (54 s^{-1}). According to the fitting data we conclude that the rate limiting step can be found in k_5 . Generally spoken we can conclude that the substitution of Tyr-191 by Phe did not change the LOX into a monooxygenase, though we were able to identify the species EFl_{red} -pyruvate at 530 nm typical for LMO. If the mutant was changed to monooxygenase it would not produce hydrogen peroxide and would have a stabilized species; here the species was too unstable to be able to react with molecular oxygen.

REFERENCES

- 1 Maeda-Yorita K, Aki K., Sagai H, Misaki H, and Massey V (1995) L-lactate oxidase and L-lactate monooxygenase: mechanistic variations on a common structural theme. *Biochimie* **77**, 631-642.
- 2 Minagawa H, Nakayama N, Matsumoto T, and Ito, N (1998) Development of long life lactate sensor using thermostable mutant lactate oxidase. *Biosensors and bioelectronics* **13**, 313-318.
- 3 Romero MR, Ahumada F, Garay F, and Baruzzi AM (2010) Amperometric biosensor for direct blood lactate detection. *Analytical chemistry* **82**, 5568-5572.
- 4 Wang J, and Chen Q (1994) Enzyme microelectrode array strips for glucose and lactate. *Analytical chemistry* **66**, 1007-1011.
- 5 Ghisla S and Massey V (1989) Mechanisms of flavoprotein-catalyzed reactions. *European journal of biochemistry* **181**, 1-17.
- 6 Müh U, Massey V, Williams CH Jr (1994) Lactate monooxygenase. I. Expression of the mycobacterial gene in *Escherichia coli* and site-directed mutagenesis of lysine 266. *The Journal of biological chemistry* **269**, 7982-7988.
- 7 Boubacar AK, Pethe S, Mahy JP, Lederer F (2007) Flavocytochrome b_2 : reactivity of its flavin with molecular oxygen. *Biochemistry* **46**, 13080-13088.
- 8 Stenberg K, Clausen T, Lindqvist Y, Macheroux P (1995) Involvement of Tyr24 and Trp108 in substrate binding and substrate specificity of glycolate oxidase. *European journal of biochemistry* **228**, 408-416.
- 9 Illias RM, Sinclair R, Robertson D, Neu A, Chapman SK, Reid GA (1998) L-mandelate dehydrogenase from *Rhodotorula graminis*: cloning, sequencing and kinetic characterization of the recombinant enzyme and its independently expressed flavin domain. *Biochemical journal* **333**, 107-115.
- 10 Chen ZW, Vignaud C, Jaafar A, Lévy B, Guéritte F, Guénard D, Lederer F, Mathews FS (2012) High resolution crystal structure of rat long chain hydroxy acid oxidase in complex with the inhibitor 4-carboxy-5-[(4-chlorophenyl)sulfanyl]-1, 2, 3-thiadiazole. Implications for inhibitor specificity and drug design. *Biochimie* **94**, 1172-1179.
- 11 Furuichi M, Suzuki N, Dhakshnamoorthy B, Minagawa H, Yamagishi R, Watanabe Y, Goto Y, Kaneko H, Yoshida Y, Yagi H, Waga I, Kumar PK, Mizuno H (2008) X-ray structures of *Aerococcus viridans* lactate oxidase and its complex with D-lactate at pH 4.5 show an alpha-hydroxyacid oxidation mechanism. *Journal of molecular biology* **378**, 436-446.
- 12 Li SJ, Umena Y, Yorita K, Matsuoka T, Kita A, Fukui K, Morimoto Y (2007) Crystallographic study on the interaction of L-lactate oxidase with pyruvate at 1.9 Angstrom resolution. *Biochemical and Biophysical Research Communications* **358**, 1002-1007.
- 13 Umena Y, Yorita K, Matsuoka T, Kita A, Fukui K, Morimoto Y (2006) The crystal structure of L-lactate oxidase from *Aerococcus viridans* at 2.1 Å resolution reveals the mechanism of strict substrate recognition. *Biochemical and Biophysical Research Communications* **350**, 249-256.
- 14 Leiros I, Wang E, Rasmussen T, Oksanen E, Repo H, Petersen SB, Heikinheimo P, Hough E (2006) The 2.1 Å structure of *Aerococcus viridans* L-lactate oxidase (LOX). *Acta crystallographica section F structural biology and crystallization communications* **62**, 1185-90.
- 15 Umena Y, Yorita K, Matsuoka T, Abe M, Kita A, Fukui K, Tsukihara T, Morimoto Y (2005) Crystallization and preliminary X-ray diffraction study of L-lactate oxidase (LOX), 181M mutant, from *Aerococcus viridans*. *Acta crystallographica section F structural biology and crystallization communications* **61**, 439-441.
- 16 Yorita K, Matsuoka T, Misaki H, Massey V (2000) Interaction of two arginine residues in lactate oxidase with the enzyme flavin: conversion of FMN to 8-formyl-FMN. *Proceedings of the National Academy of Sciences of the United States of America* **97**, 13039-13044.
- 17 Yorita K, Aki K, Ohkuma-Soyejima T, Kokubo T, Misaki H, Massey V (1996) Conversion of L-lactate oxidase to a long chain alpha-hydroxyacid oxidase by site-directed mutagenesis of alanine 95 to glycine. *The Journal of biological chemistry* **271**, 28300-28305.

- 18 Giegel DA, Williams CH Jr, Massey V (1990). L-lactate 2-monooxygenase from *Mycobacterium smegmatis*. Cloning, nucleotide sequence, and primary structure homology within an enzyme family. *The Journal of biological chemistry* **265**, 6626-6632.
- 19 Fraaije MW, van Berkel WJ (1997) Catalytic mechanism of the oxidative demethylation of 4-(methoxymethyl)phenol by vanillyl-alcohol oxidase. Evidence for formation of a p-quinone methide intermediate. *The Journal of biological chemistry* **272**, 18111-18116.
- 20 Frébortová J, Fraaije MW, Galuszka P, Sebela M, Pec P, Hrbáč J, Novák O, Bilyeu KD, English JT, Frébort I (2004) Catalytic reaction of cytokinin dehydrogenase: preference for quinones as electron acceptors. *Biochemical journal* **380**, 121-130.
- 21 Filipe A, Belmouden A, Lacombe J & Lederer F (1997) Long-chain α -hydroxy acid oxidase: Substitution of the active site Phe23 with tyrosine. In *Flavins and Flavoproteins 1996* (Stevenson L, Massey V, & Williams C), pp. 559-562. University of Calgary Press, Calgary.
- 22 Miles CS, Rouvière-Fourmy CS, Lederer F, Mathews FS, Reid GA, Black MT & Chapman SK (1992) Tyr 143 facilitates interdomain electron transfer in flavocytochrome b_2 . *Biochemistry* **285**, 187-192.
- 23 Müh U, Williams CH & MASSEY V (1994) Lactate Monooxygenase: III Additive contributions of active site residues to catalytic efficiency and stabilization of an anionic transition state. *The Journal of biological chemistry* **97**, 7994-8000.
- 24 Lindqvist Y (1989) Refined structure of, spinach glycolate oxidase at 2 Å Resolution. *Journal of molecular biology* **209**, 151-166.
- 25 Sukumar N, Xu Y, Gatti DL, Mitra B & Mathews FS (2001) Structure of an active soluble mutant of the membrane-associated (S)-mandelate dehydrogenase. *Biochemistry* **40**, 9870-9878.
- 26 Tegoni M, Begotti S, Cambillau C (1995) X-ray structure of two complexes of the Y143F flavocytochrome b_2 mutant crystallized in the presence of lactate or phenyl lactate. *Biochemistry* **34**, 9840-9850.
- 27 Belmouden A & Lederer F. (1996) The role of a p barrel loop 4 extension in modulating the physical and functional properties of long-chain 2-hydroxy-acid oxidase isozymes. *European journal of biochemistry* **238**, 790-798.
- 28 Bisswanger H. 2002. Substrate inhibition. *Enzyme kinetics - principles and methods*. Weinheim: Wiley-VCH Verlag GmbH, 2002, pp. 120-121.

SUPPORTING INFORMATION

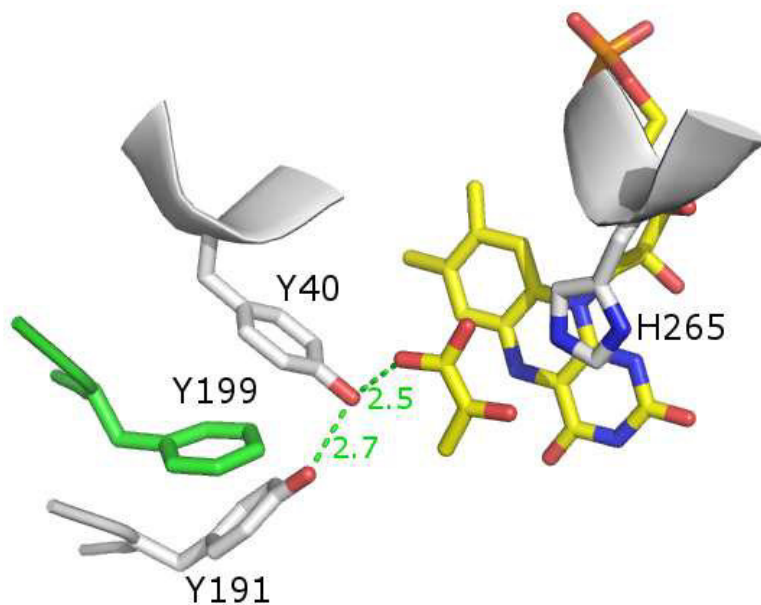


Figure S1

Comparison of LOX and LMO. Y191 is Y199 (shown in green) in LMO.

Table S2. Purification of LOX Y191F mutant

Procedure	Specific activity	
	(U/mg)	Recovery [%]
Crude extract	1.2	100
(NH ₄) ₂ SO ₄ precipitation	1.4	92
HIC	11	27
AEC	47	3

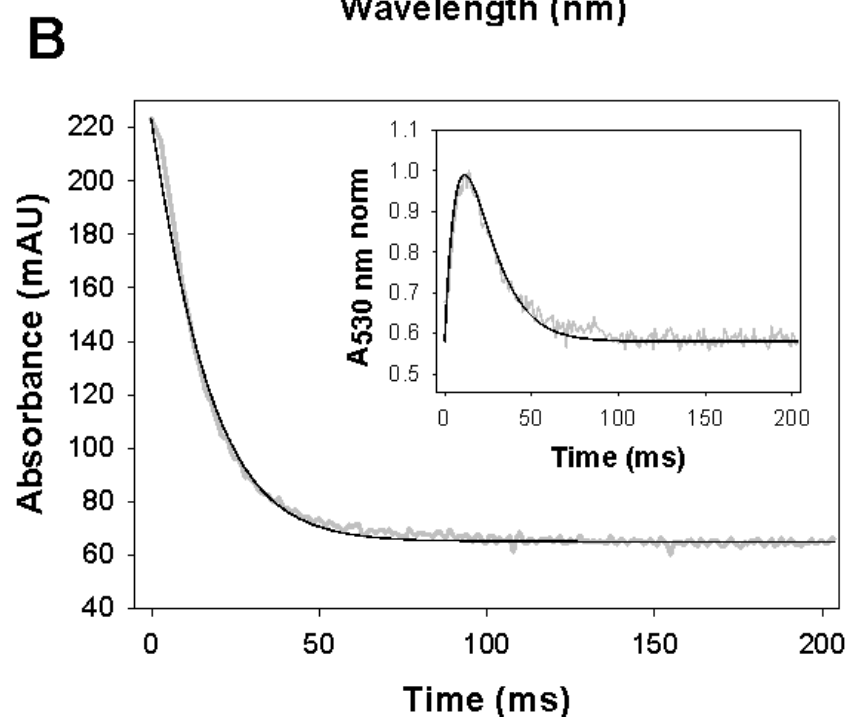
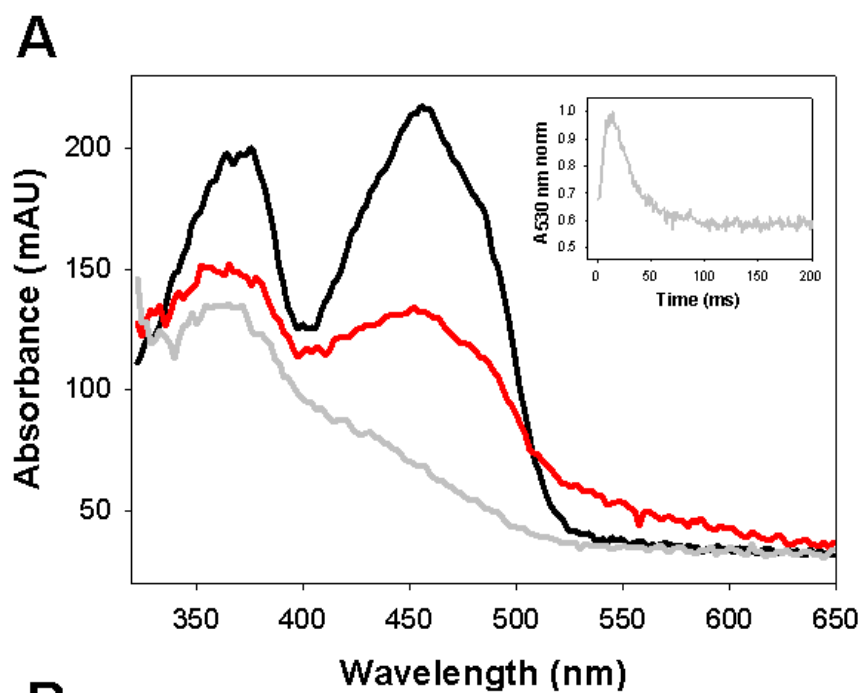


Figure S2

Spectral scans of wild-type LOX and fitting with Berkeley Madonna

Panel A: Spectral scans of wild-type LOX during the reductive half-reaction. 19.4 μM LOX were reduced with 10 mM L-lactate under anaerobic conditions in 50 mM potassium phosphate buffer, pH 6.5 at 4 $^{\circ}\text{C}$. **Black** line: enzyme in oxidized state at start (0 ms); **red** line: reaction after 14 ms; light **grey** line: reaction after 200 ms. After 14 ms the maximum in absorbance at 530 nm is reached (compare dark **grey** trace for the whole reaction at inset), the amplitude decreases afterwards.

Panel B: Reductive half-reaction of wild-type LOX by L-lactate. 19.4 μM enzyme in 50 mM potassium phosphate buffer (pH 6.5) were reacted in the stopped flow photometer at 4 $^{\circ}\text{C}$ with 10 mM L-lactate. The grey line represents the reaction trace at 455 nm with two different phases (first phase = k_3 ; second phase = k_5) the inset reflects the trace at 530 nm in a biphasic manner. Black lines represent the fittings achieved with software Berkeley Madonna leading to the calculated kinetic constants in **Table 2**. Black lines represent the fittings achieved with software Berkeley Madonna (Description in text) leading to the calculated kinetic constants with k_3 (88 s^{-1}) and k_5 (87 s^{-1}).

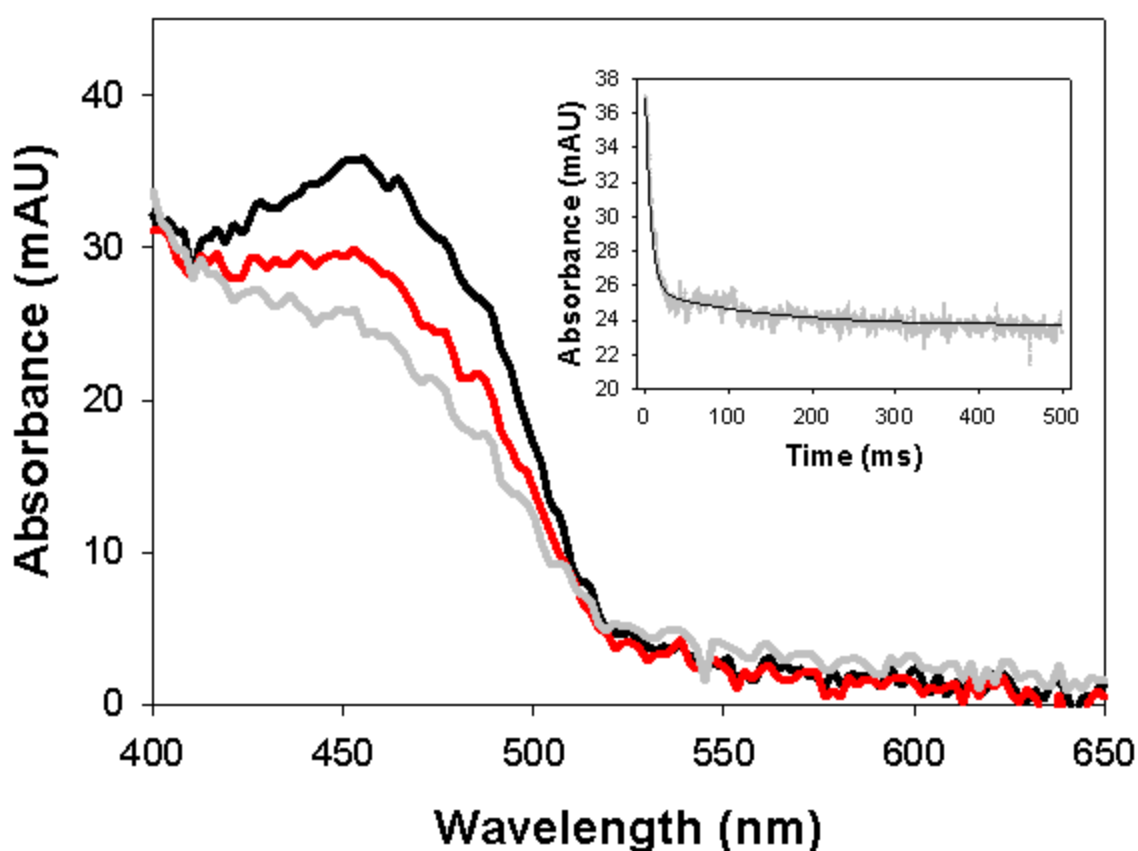


Figure S3

Spectral scans of LOX Y191L mutant during the reductive half-reaction.

3.3 μM LOX were reduced with 10 mM L-lactate under anaerobic conditions in 50 mM potassium phosphate buffer, pH 6.5 at 20 $^{\circ}\text{C}$. **Black** line: enzyme in oxidized state at start (0 ms); **red** line: reaction after 10 ms; light **grey** line: reaction after 90 ms. No change in absorbance at 530 nm could be observed. Inset shows trace at 455 nm which was fitted in a double exponential manner as described in the text ($k_{\text{obs}1} = 150 \text{ s}^{-1}$, $k_{\text{obs}2} = 7.5 \text{ s}^{-1}$).

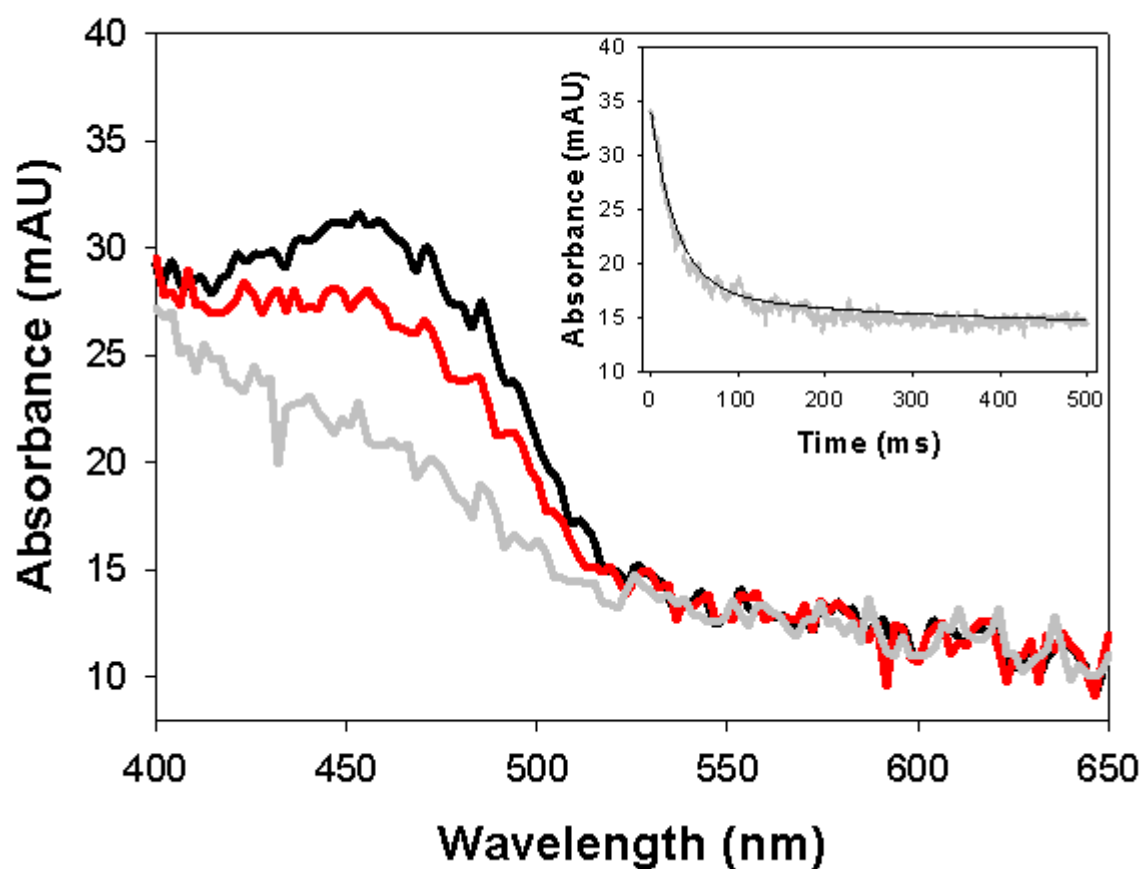


Figure S4

Spectral scans of LOX Y191A mutant during the reductive half-reaction.

3.0 μM LOX were reduced with 10 mM L-lactate under anaerobic conditions in 50 mM potassium phosphate buffer, pH 6.5 at 20 $^{\circ}\text{C}$. **Black** line: enzyme in oxidized state at start (0 ms); **red** line: reaction after 10 ms; light **grey** line: reaction after 60 ms. No change in absorbance at 530 nm could be observed. Inset shows trace at 455 nm which was fitted in a double exponential manner as described in the text ($k_{\text{obs}1} = 29 \text{ s}^{-1}$, $k_{\text{obs}2} = 3.8 \text{ s}^{-1}$).

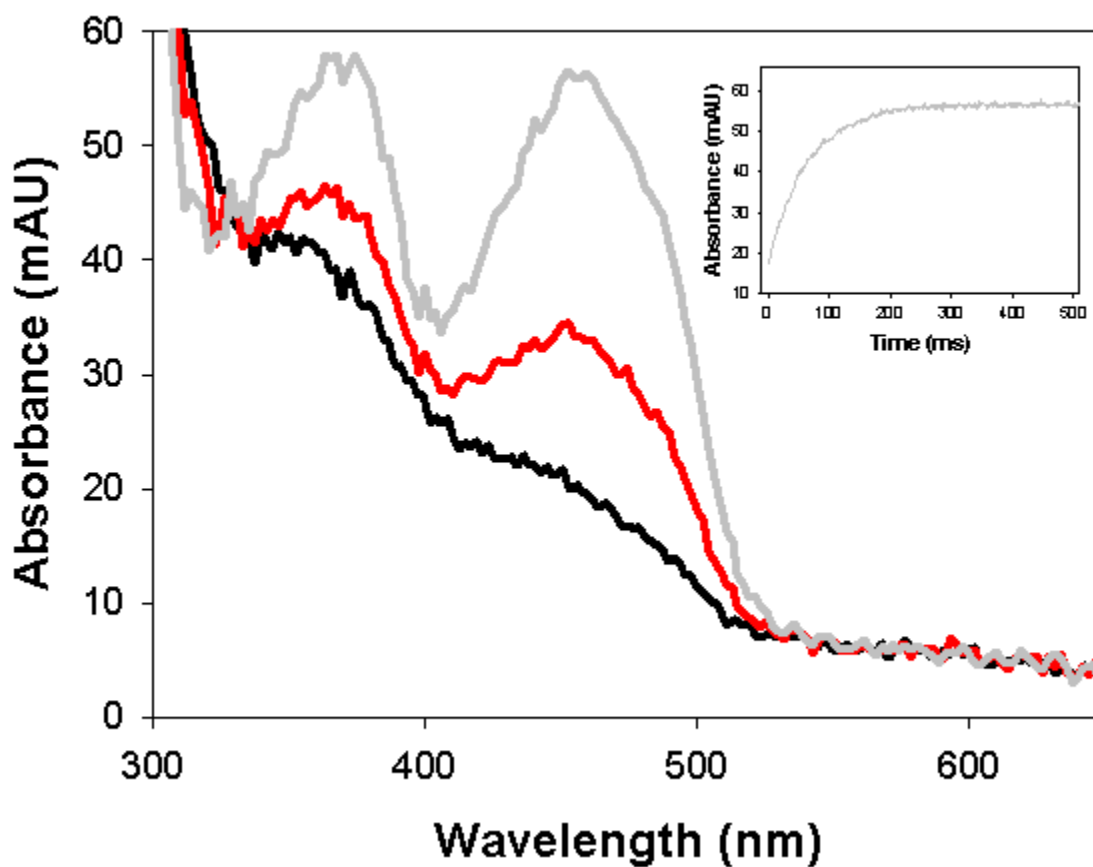


Figure S5

Spectral scans of LOX Y191A mutant during the oxidative half-reaction.

5.4 μM LOX were reduced with 2 equivalent L-lactate under anaerobic conditions in 50 mM potassium phosphate buffer, pH 6.5 at 20 $^{\circ}\text{C}$ and reoxidized with 14 μM oxygen. **Black** line: enzyme in reduced state at start (0 ms); **red** line: reaction after 35 ms; light **grey** line: reaction after 300 ms. Inset shows trace at 455 nm which was fitted in a single exponential manner as described in text ($k_{\text{obs}1} = 13.8 \text{ s}^{-1}$).

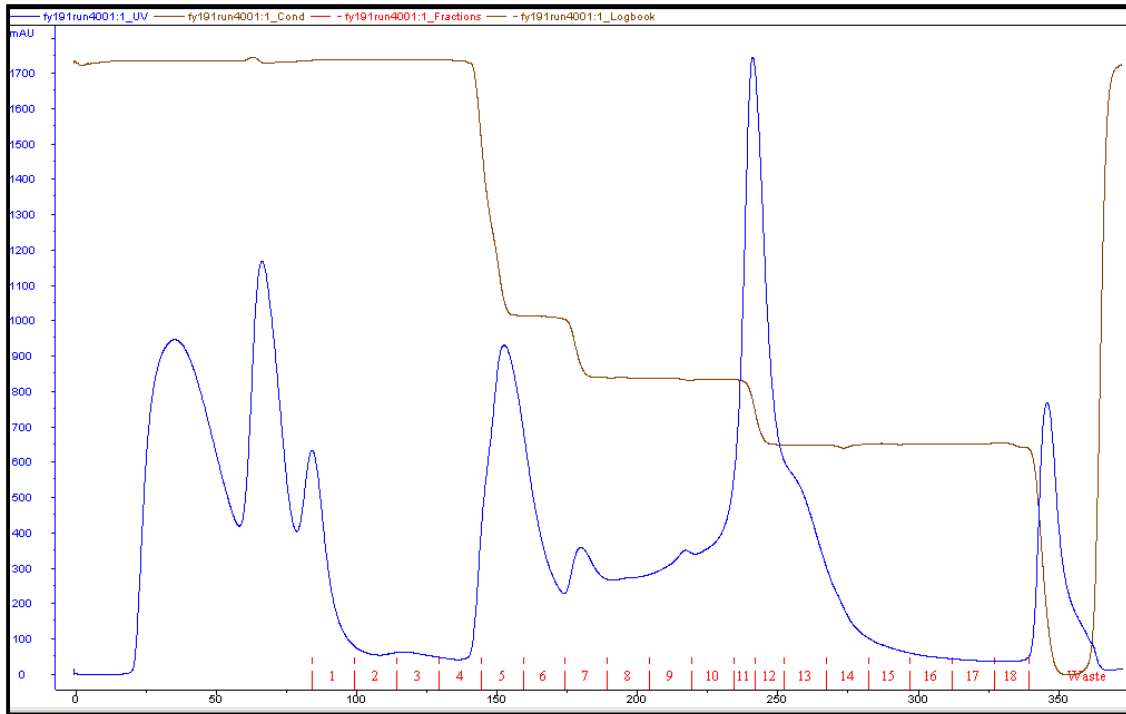


Figure S6

HIC purification of LOX Y191F mutant.

HIC purification run with stepwise gradient of Y191F. LOX mutant was found in area 13-14

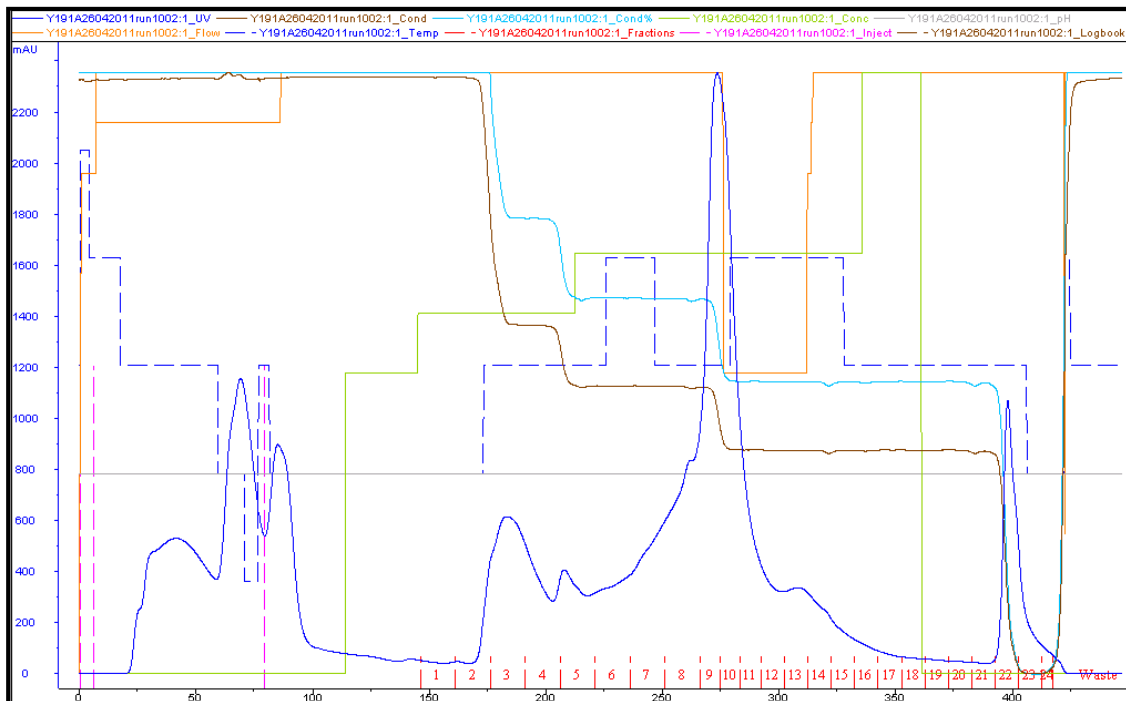


Figure S7

HIC purification of LOX Y191A mutant.

HIC purification run with stepwise gradient of Y191A, LOX mutant was found in area 13-14

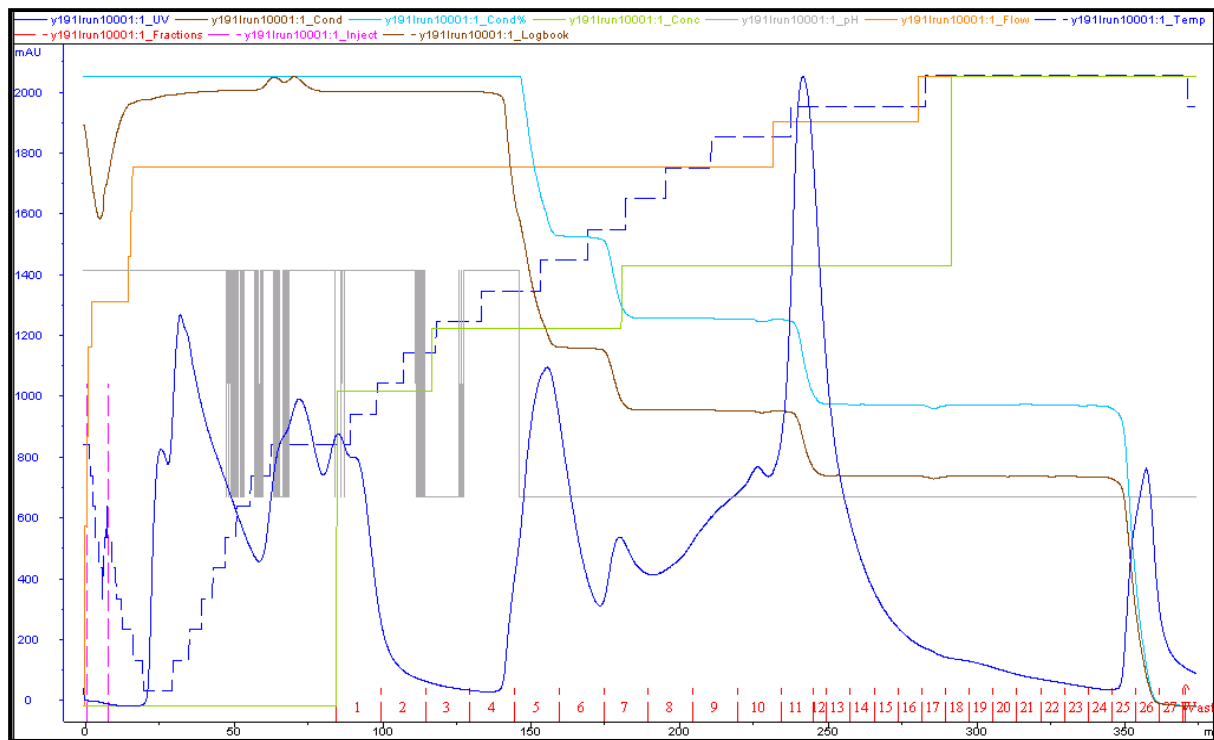


Figure S8

HIC purification of LOX Y191L mutant

HIC purification run with stepwise gradient of Y191L, LOX mutant was found in area 13-14

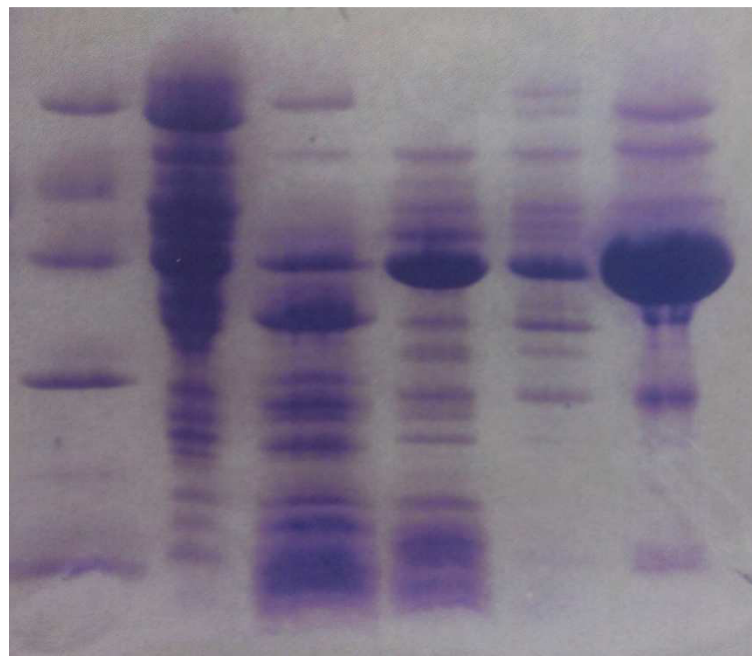


Figure S9

SDS Page of purified LOX wild-type and Y191A and Y191L mutants; *lane 1:* low molecular weight marker, crude extract (*lane 2*) and $(\text{NH}_4)_2\text{SO}_4$ precipitation (*lane 3*) of Y191A mutant, *lane 4:* after HIC purification of Y191A mutant, *lane 5:* after HIC purification of Y191L, *lane 6:* LOX wild-type.

6 APPENDIX

LOX is used in biosensors to determine the lactate level in human's blood. The protein is inactivated within several days. Thereof, one goal of this work was to investigate the inactivation mechanism of LOX and on the other hand, to create a mutant, which has an enlarged stability.

Stability assays of Tyr191 mutants

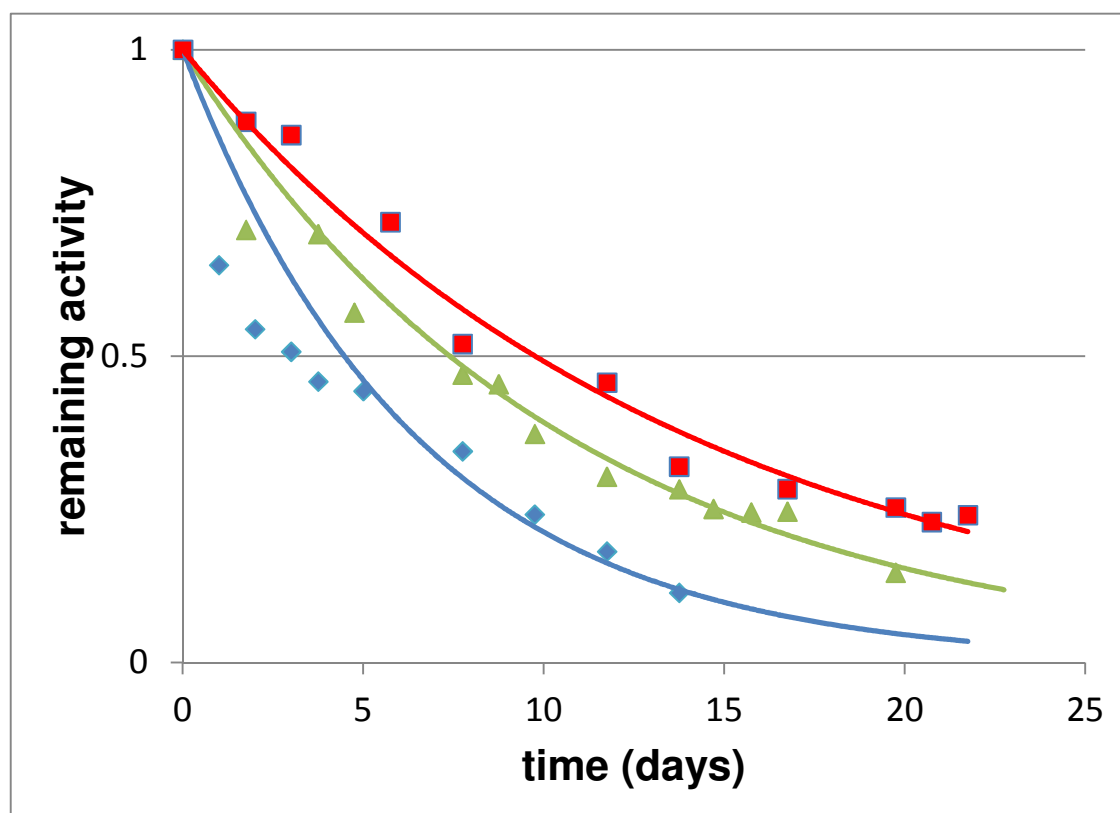


Figure 1

Stability assay of LOX wild-type (diamonds, blue), Y191F (squares, red) and Y191L (triangles, green). The activity was normalized to the starting value. Conditions: 40 mM HEPES, pH 8.1, 150 mM NaCl, 20 mM NaHCO₃, 37 °C.

We have measured the activity of wild-type LOX, Y191F and Y191L mutants for over 20 days at standard conditions (40 mM HEPES, pH 8.1, 150 mM NaCl, 20

mM NaHCO₃, 37 °C.). The Tyr mutants showed increased half-lives compared to wild-type LOX (compare **Table 1**). **Figure 1** shows the stability assay for both mutants.

Table 1. Half-lives of wild-type LOX, Y191A, Y191F and Y191L mutants at 37 °C. Activity was measured for more than 20 days in buffer with or without NaHCO₃. Buffer conditions were 40 mM HEPES, pH 8.1, 150 mM NaCl, (20 mM NaHCO₃)

	0 mM NaHCO ₃	20 mM NaHCO ₃
Wild-type	7.1	4.6
Y191F	20.5	9.8
Y191A	4.8	3.9
Y191L	12.6	7.4

Inactivation mechanism

First, we analyzed the influence of the protein concentration on the inactivation speed, which was really low. **Table 2** provides an overview of the inactivation results. High protein concentrations (10 mg/mL) are stabilizing in contrast to lower concentrations (0.05 and 0.1 mg/mL). A similar effect was achieved at different buffer concentrations. Here, the enzyme reflects a 1.5 times higher half-life in 83 mM HEPES buffer than in the standard buffer. Standard conditions for the stability experiments were 40 mM HEPES, pH 8.1, 150 mM NaCl, 500 mM NaHCO₃ and 37 °C. The half-life lies between 33 hours (0.1 mg/mL) and 33 hours (0.1 mg/mL) 71 hours (10 mg/mL).

We also wanted to know how the temperature and the pH affect LOX (**Table 2**). The half-time was lowered (compare **Figure 2**) to 5.3 hours when using 50 °C,

which correlates with a 10-fold faster inactivation, and was lowered to 9.3 hours at pH 9.0.

Table 2. Inactivation study from LOX on different protein and buffer concentration.

Standard conditions: 40 mM HEPES, pH 8.1, 150 mM NaCl, 500 mM NaHCO₃, 37 °C.

Conditions	t _{1/2} (hours)
10 mg/mL LOX	71,2
2 mg/mL LOX	53,1
0,5 mg/mL LOX	39,0
0,1 mg/mL LOX	33,5
0,05 mg/mL LOX	47,2
0,05 mg/mL LOX, 83 mM HEPES	67,9

Table 3. Influence of Temperature and pH on the stability of LOX. Standard conditions:

40 mM HEPES, pH 8.1, 150 mM NaCl, 500 mM NaHCO₃, 37 °C and 0.05 mg/mL protein.

Conditions	t _{1/2} (hours)
Standard	66.6
44 °C	11.1
50 °C	5.3
pH 8,5, 40 mM Tris	28.7
pH 9,0, 40 mM Tris	9.3

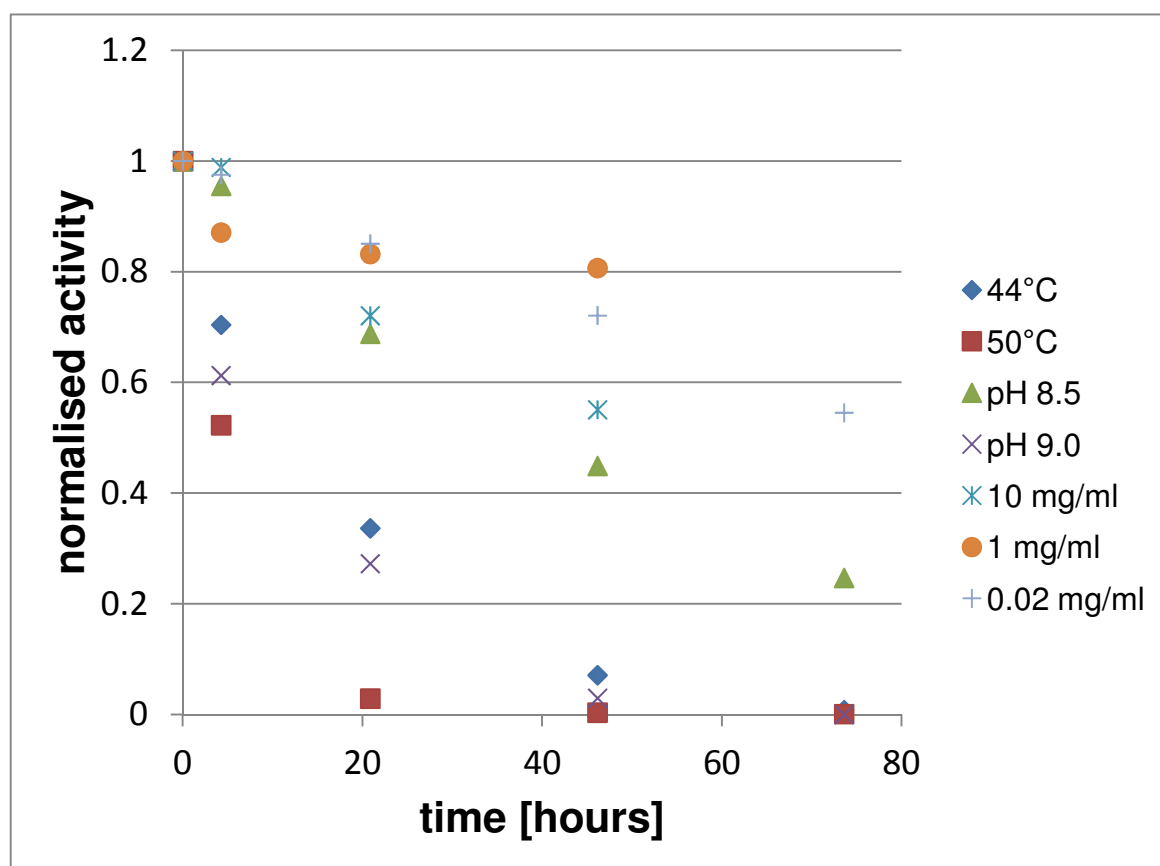


Figure 2

Stability assays of LOX at different conditions. Half-lives listed in Table 1 and 2.

Fluorescence measurements with 8-Anilino-1-naphtalenesulfonic acid (ANSA) were performed (Figure 3) to determine unfolding reactions in LOX. Stability assays were performed at standard conditions and at different temperatures (44 °C, 50 °C) and pH (8.5, 9.0) for about 170 hours. With ANSA an increase in fluorescence could be observed, which correlates with the inactivation of LOX. Conditions leading to the fastest inactivation also showed a higher increase in fluorescence meaning a faster unfolding. Worth mentioning, even when activity was completely lost, the fluorescence intensity still increased. That leads us to the conclusion that the unfolding must reach a certain level until the biological activity is lost, whereas the unfolding process is still going on; and further, that the unfolding plays a main role in

the inactivation, but still it cannot be excluded that other unknown processes might influence the inactivation of LOX.

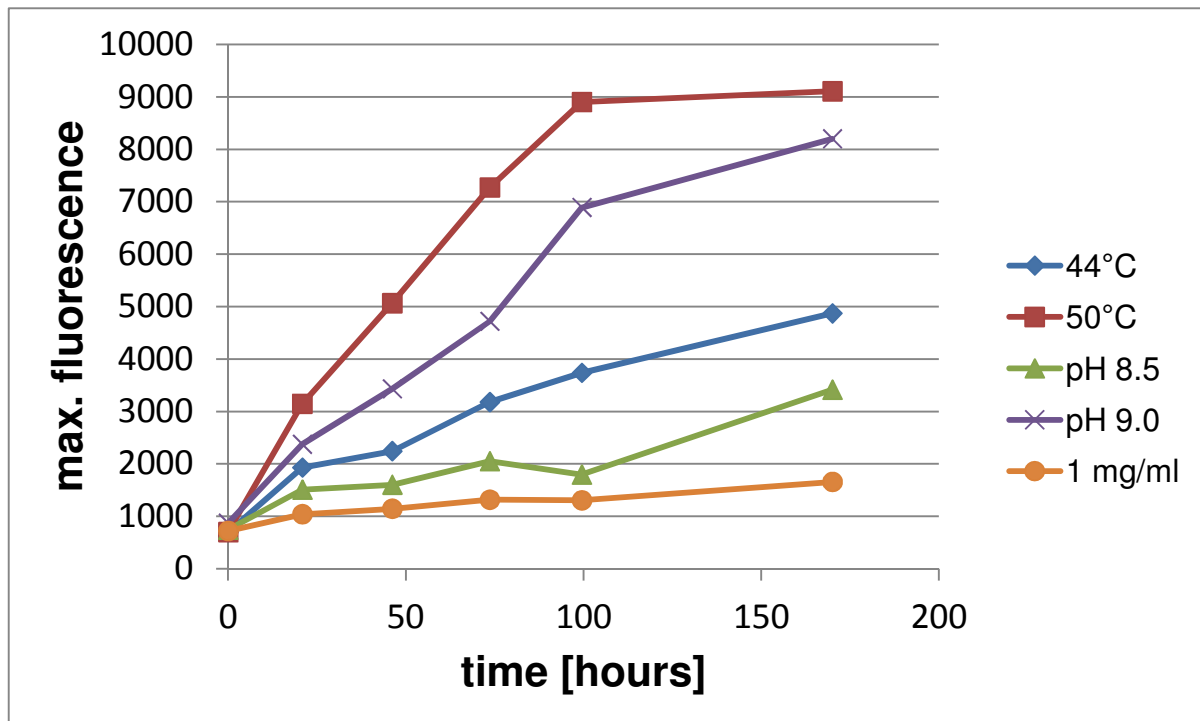


Figure 3

Progress of ANSA-fluorescence over time. Conditions are shown in Table 1.

We figured out that during the inactivation the protein is partly unfolded, which leads to a change in the tertiary structure. By using circular dichroism (CD) and gel filtration we wanted to investigate putative changes in the secondary and quaternary structure. Figure 4 shows CD-spectra at different points in time during an inactivation experiment (Conditions: 40 mM HEPES, pH 8.1, 500 mM NaHCO₃, 150 mM NaCl). The spectra illustrate differences in the intensity, which might derive from different protein concentrations, the spectra look very similar. From the spectra we calculated the amount of α -helices and β -sheets (Table 4), which did not alter during the inactivation meaning that the secondary structure was not changed significantly.

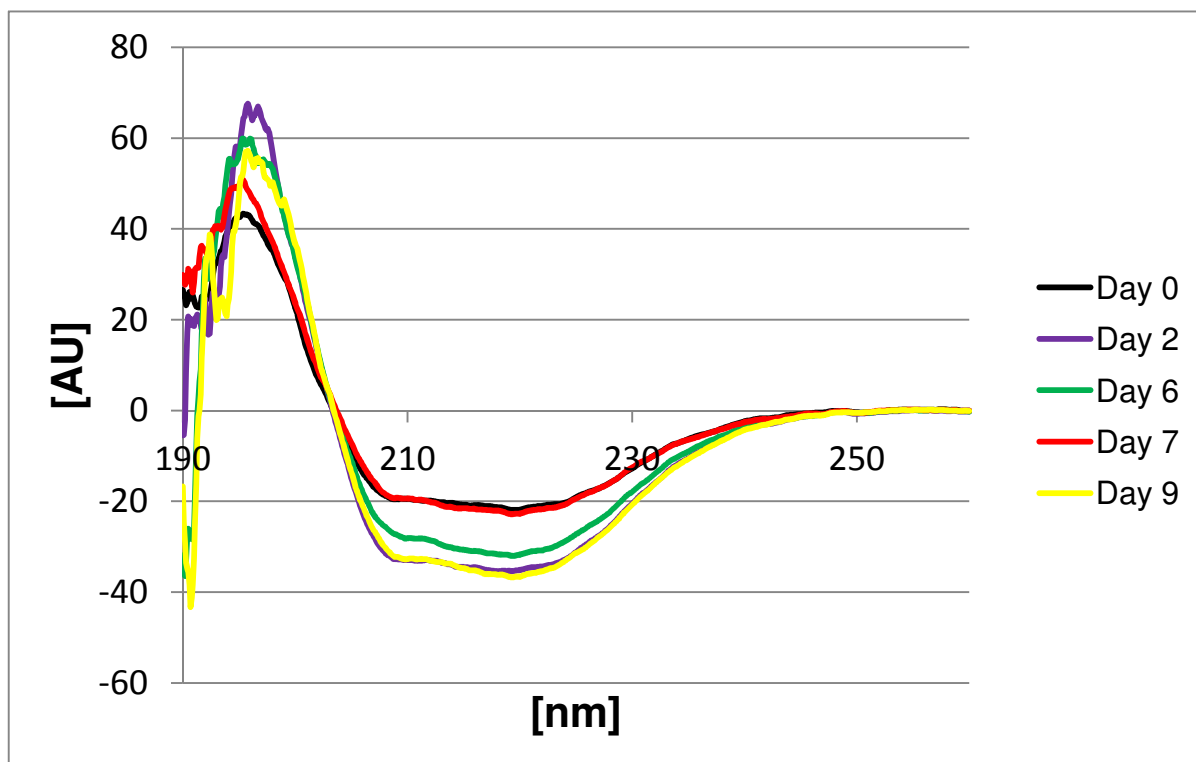


Figure 4
CD spectra of LOX during the inactivation

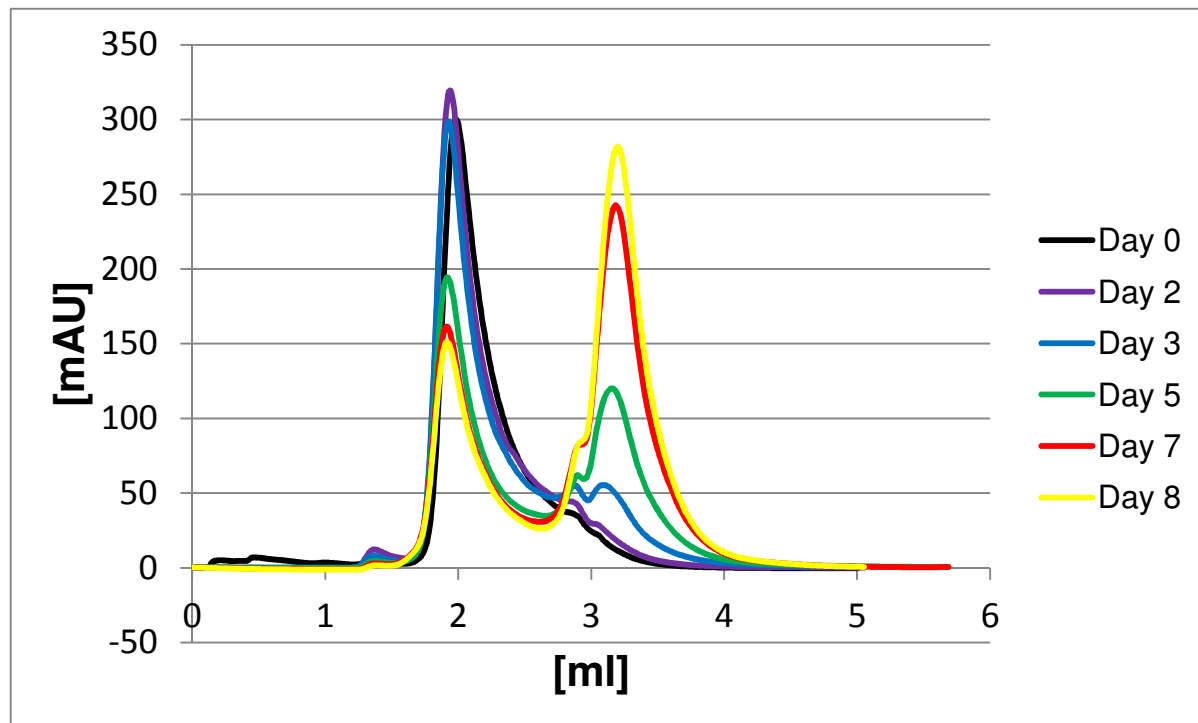
Table 4. Amount of helices and sheets at different time points during the inactivation of LOX determined by CD-spectroscopy.

Day	α -Helix (%)	β -Sheet (%)
0	46	27
2	42	30
6	42	30
9	43	29

The gel filtration showed a defined peak (eluted at ~2 mL) for LOX in the active form, which describes the tetramer (**Figure 5**). During the stability assay the ‘tetramer-peak’ decreases and two new peaks arise (~2.9 und 3.1 mL). A correlation between log MW of tetramer, dimer and monomer and the elution volume show a linear dependency, which leads to the conclusion that the tetramer decays into a dimer, which collapses fast into the monomers. This can be seen because the peak

for the dimer stays small during the whole time period, but the amount on dimers increases.

A



B

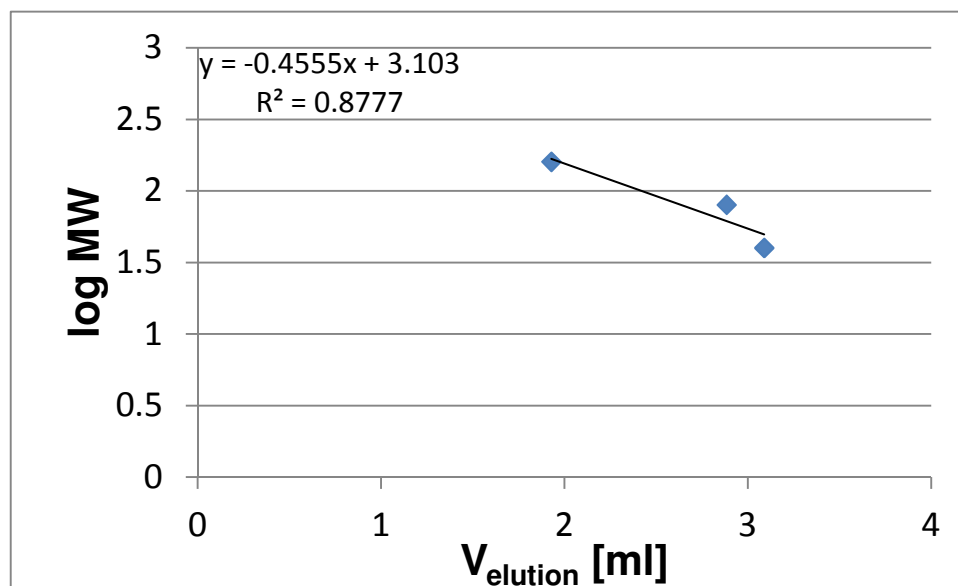


Figure 5

Gel filtration of LOX (Panel A) at different time points during an inactivation experiment. Panel B shows the correlation between the MW of tetramer, dimer and monomer and the elution volume.

Figure 6 compares activity loss, unfolding (measured via ANSA) and the dissociation into the subunits with each other. It is noticeable that the activity loss correlates with the unfolding of the enzyme, but the change of the quaternary structure happens time-delayed. This means that the dissociation of the subunits is not the reason for the inactivation, but a consequence of it.

From the observed data we propose the following inactivation mechanism: starting with the active enzyme, which is a tetramer, the first step, which shows a decrease in activity leads to (partial) unfolding. Here, the enzyme is still a tetramer. In the next step, the dissociation into the monomers happens. The last step is the complete unfolding of the protein. For the first step in inactivation we could determine an inactivation rate of $k = 0.0177 \text{ h}^{-1}$.

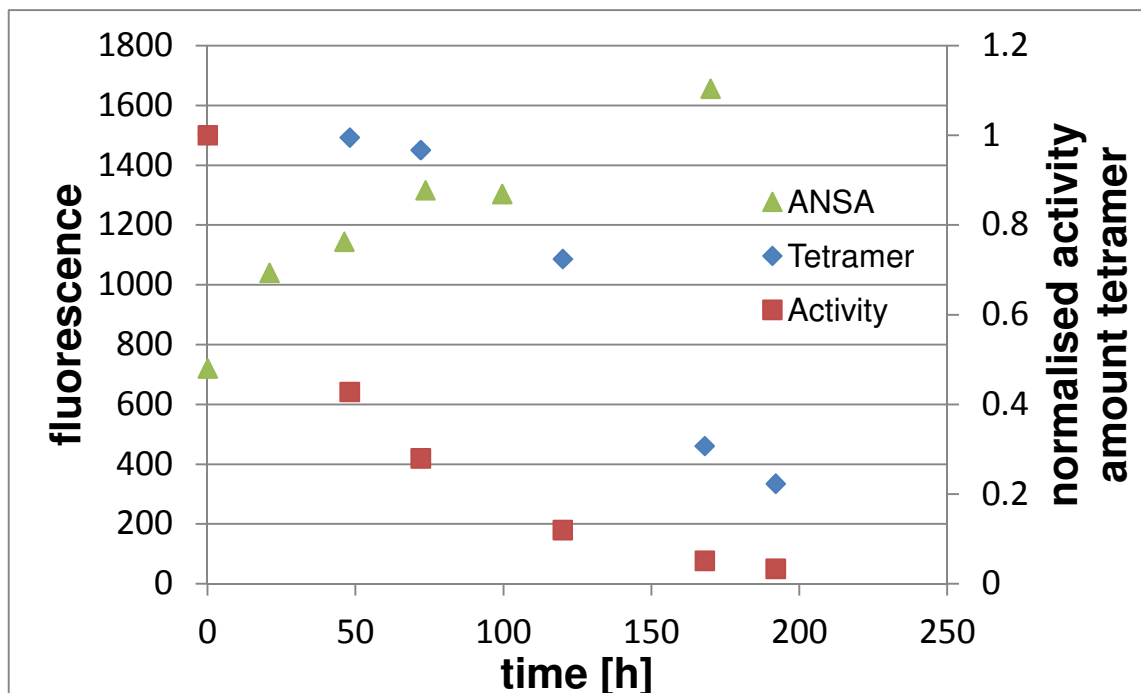


Figure 6

Correlation between activity, (partial) unfolding and the amount of tetramers during a stability assay. Activity was normalized to the starting value. Activity and amount of tetramer on y-axis (right), ANSA-fluorescence on y-axis on the left.

Protocol ANSA Fluorescence

1.) Preparation of solutions:

- 1 mM ANSA (dissolve 3,2 mg 8-Anilinonaphtalene-1-sulfonic acid NH^{4+} -salt in 10 mL H_2O)
 - LOX solution (10 μM)
- Store all solutions at 4 °C.

2.) Procedure:

- Use the fluorescence cuvette for the fluorescence spectrophotometer
- Measure at room temperature
- Set the excitation wavelength to 388 nm and record the emission spectrum from 400 - 650 nm
- Mix 500 μL LOX-solution with 50 μL ANSA solution
- Incubate for 2 minutes in the cuvette
- Record spectra (5 replications)
- Record peak wavelength and peak intensity

3.) Analysis:

- If the assay is used during stability measurements plot the maximal intensity against the time.